Fracturing Fluid Effects on Young's Modulus and Embedment in the Niobrara Formation — Source link ⧉

Hakan Corapcioglu

Institutions: Colorado School of Mines

Published on: 27 Oct 2014

Topics: Hydraulic fracturing and Embedment

Related papers:

- The Effects of Fracturing Fluids on Shale Rock Mechanical Properties and Proppant Embedment

- Experimental and numerical studies of reduced fracture conductivity due to proppant embedment in the shale reservoir

- Fracture Width and Embedment Testing in Soft Reservoir Sandstone

- Proppant Embedment And Conductivity of Hydraulic Fractures In Shales

- The effect of proppant embedment upon the long-term conductivity of fractures

`

FRACTURING FLUID EFFECTS ON YOUNG'S MODULUS AND EMBEDMENT IN THE
NIOBRARA FORMATION

By

Hakan Corapcioglu

`

A thesis submitted to the Faculty and the Board of Trustees of the Colorado School of Mines in partial fulfillment of the requirements for the degree of Master of Science (Petroleum Engineering).

Golden, Colorado

Date _____

Signed: _____
Hakan Corapcioglu

Signed: _____
Dr. Jennifer L. Miskimins
Thesis Advisor

Signed: _____
Dr. Manika Prasad
Thesis Co-Advisor

Golden, Colorado

Date _____

Signed: _____
Dr. William W. Fleckenstein
Professor and Head
Department of Petroleum Engineering

ABSTRACT

New discoveries of shale plays and their abundant resources have directed the petroleum industry towards their development. Production from shale reservoirs has grown significantly in the past few decades spurred by successful development of plays such as the Barnett and Bakken Shales. Due to their low permeability, hydraulic fracturing is a necessity for economic production in these reservoirs, and the success of these reservoirs is dependent on optimizing hydraulic fracturing designs which are in turn dictated by an understanding of the mechanical properties of these reservoirs. The geometric growth and conductivity of fractures in these reservoirs are influenced by many factors. Young's modulus reduction, which essentially means weakening of the formation, is one of these factors. This reduction damages the reservoir and makes embedment of proppants into the fracture face a detrimental effect on fracturing success. The goal of this research project is to focus on how different fracturing fluids change the Young's modulus of the Niobrara shale and how this change affect the proppant embedment and conductivity when commonly used proppants are subjected to pressure tests in the effected Niobrara shale samples.

A series of tests and associated methodology were developed and applied to investigate how the Niobrara shale's Young's modulus is affected by various fracturing fluids and to quantify associated proppant embedment. In order to achieve this, core samples at various depths from the same well were selected from the cores. The selection was made based on mineralogy data. Samples containing the highest, lowest, and median calcite percentage and porosity were selected to be imaged with QEMSCAN in order to understand the mineralogy of the samples being used. Eight selected samples were then saturated with four fracturing fluids (freshwater, KCl, KCl+friction reducer, and freshwater+KCl substitute). Four of these samples were the "expansion" samples to see if the results were more dependent on the fluid selections. Two additional samples were heated with freshwater and KCl at 180°F for five days to investigate the heat effect on Young's modulus and embedment in comparison to room

temperature experiments. In order to compare in-situ saturated Young's modulus values to dry Young's modulus values of cores obtained by nanoindenter, the Gassmann fluid substitution equation was used. This method showed significant Young's modulus difference between in-situ saturated and dry core values.

The saturated/room temperature and saturated/heated cores were then subjected to 3030 psi for one hour while selected proppants were placed in between them. Four different proppant types (16/30 Brady, 20/40 Ottawa, 20/40 Ceramic, and 20/40 RCS) were used in this research. Various combinations of cores affected by fluids and proppants were made in order to simulate actual treatment designs. The cores were also scanned by scanning acoustic microscope (SAM) before and after they were subjected to pressure with proppants, so that a comparison could be made and embedment profiles could be observed. The very last method was to quantify the proppant embedment caused by proppants for cores that were treated by fracturing fluids. A profilometer was used in order to achieve this.

In addition to developing the study methodology, experiments showed that Young's modulus decreased with fluid exposure regardless of the fracturing fluid type and also increased after some time of saturation. The magnitude of decrease in Young's modulus values was dependent on fluid type and saturation time and very significant reaching up to approximately 80%. The Young's modulus reduction is believed to be happening due to calcite minerals dissolving in the fluids. Higher reductions experienced by KCl based fluids are believed to be due to KCl causing a detrimental chemical reaction with the calcite minerals in the samples, or possibly due to the nanoindenter measuring salt precipitates and friction reducer residue on samples. Results also showed proppant embedment and crushing are inevitable under the tested circumstances and are related to stress contact effect as well as proppant type and fluid exposure.

TABLE OF CONTENTS

LIST OF FIGURES

LIST OF TABLES

ACKOWLEDGEMENTS

Corapcioglu, and Aylin Corapcioglu for always loving me and making me a better man. I would also like to thank Danielle Tomasetti for supporting me and being beside me and loving me for the last two years during my study at Colorado School of Mines.

I would like to thank all my fellow graduate students at Colorado School of Mines, for all their support, friendship and valuable information on my thesis work. A special thanks to Ezgi Karasozen, Mehmet Ali Torcuk, Caglar Komurcu, Murat Yuksel Kaya, and Maxwell Willis for their tremendous help in completing my thesis. I would also like to thank to countless friends I made and crossed paths with throughout my journey here in the United States; they each have given me great memories and made my time here an impeccable experience.

This thesis is dedicated to my grandfather Selahattin Bilgic, who had been with me since my birth and

dedicated his life to make me a valuable and noble man for the world.

Your teachings and impact on me will never fade away.

May you rest in peace and sleep comfortably above the clouds.

CHAPTER 1

INTRODUCTION

Over the last few decades, natural gas and oil production from unconventional shales has increased significantly. These reservoirs are essential parts of the present and future of the oil and gas industry. Throughout the last 40 years, the petroleum industry has progressed from conventional gas reservoirs, to tight gas reservoirs, to ultra-low matrix permeability unconventional shale-gas reservoirs (Kundert & Mullen, 2009). Shale reservoirs are becoming increasingly important day-by-day due to the production success and abundance of shale plays. The petroleum industry across the globe is now paying attention and trying to utilize this valuable resource since there is a vast amount of it, and it is now technically and economically feasible to produce. The Energy Information Agency has shale resource estimates of 335 billion bbl of oil and 7,795 tcf of gas for the world and 58 billion bbl of oil and 665 tcf of gas for the United States (Energy Information Agency, 2013). The significance of these numbers, and with conventional reservoirs depleting, unconventional reservoirs across the globe will have to supply the world with energy and meet the high demands of hydrocarbon usage. For unconventional reservoirs to satisfy the world energy demand, their reservoir properties must be carefully studied and new technological developments should be utilized to achieve economically optimized production levels.

There are many definitions for shale reservoirs. The Niobrara shale play in this work is a current unconventional reservoir that is producing in many areas. Some shale plays have numerous things in common such as mineralogy, rock mechanics, and geomechanics. However these properties can also vary by a great margin. Most shale plays are actually fine-grained clastics and not necessarily shales (Britt and Schoeffler, 2009). In the case of this research, the Niobrara shale is mostly referred to as a limestone formation interbedded with shale beds. Water-frac treatments are the common stimulation choice for most of the producing shale plays (Britt and Schoeffler, 2009). These formations also require optimized proppant selection.

Evolving technology and demand in fossil fuels have made shales, which are the source, the seal, and reservoir all in one, unique when compared to conventional hydrocarbon reservoirs, which are sourced by shales. Although shales are known for their low permeability, low porosity, and heterogeneous geomechanical characteristics, advancing technology in hydraulic fracturing has overcome most of these production issues and placed shale plays in a very important spot for the industry. Hydraulic fracturing is a necessity for shale reservoirs in order for them to be productive and profitable. Very simply put, hydraulic fracturing is the most frequently used stimulation technique that aims to increase the effective producing volume of a given well and increase the hydrocarbon flow between the reservoir and wellbore by creating highly connected and conductive network of fractures. Hydraulic fractures in the formation are established by pumping large amounts of fluids (usually water) into the zone of interest. Since the stresses and pressures in the formation force the fracture to close, proppants are pumped simultaneously with the fluid to keep the fractures open and conductive which create a conductive flowing system.

There are many factors controlling the success of a fracturing treatment. Two important factors are the selection of the fracturing fluid and the proppant, since these components will dictate the initiation of the fracture and how conductive it will be. There is a wide range of fracturing fluids available for hydraulic fracturing. Water is the most common fracturing fluid. It is preferred due to its simple and non-complex nature as well as its cost. However, other fracturing fluids (discussed later in this thesis) may be used because certain formations will react negatively with freshwater or other fluids. Clay swelling, changes in mechanical properties and flow back to the wellbore are common problems that can be caused by fracturing fluids. These issues also effect the proppant selection for the fracturing job.

Proppants are the main component in maintaining the fractures conductivity to allow hydrocarbon flow. It is vital to select the appropriate proppant type to use. Selection is very dependent on the formation characteristics and geomechanical properties of the reservoir. The right proppant will directly affect the productivity of the well. Proppants may embed into the fracture face, they may settle too close to the

wellbore, or they may travel too far into the formation and be inefficient. These are very common issues with proppants and cause inevitable damage up to a certain level. Frequently, companies assume if a certain fluid and proppant combination was successful for a fracturing job in one area that it will succeed anywhere else. However, efforts and research should be put into understanding the specific mechanical and chemical properties of individual reservoirs. Each formation has different geomechanical characteristics and each will require a different fluid and proppant combination for optimized ultimate recovery. This research aims to emphasize the significance of the uniqueness of formation mechanical properties and how they are affected by various fluids and proppants.

1.1 Research Motivation

Establishing sufficiently conductive fractures is the main component to a successful hydraulic fracturing job. The goal of hydraulic fracturing is to utilize these highly conductive fractures in order to increase and enhance production from tight unconventional reservoirs to reach a maximum level of profit. This project aims to investigate proppant embedment in a carbonate-rich shale system by understanding the mechanical properties of the formation and how they change under various conditions. Based on this investigation, hydraulic fracturing treatments can be optimized and designed for maximum profit.

It is essential to understand the importance of mechanical properties of formations before designing a fracturing treatment. Young's modulus and hardness are properties that have a large effect on formations and the success of hydraulic fracturing jobs. Young's modulus represents the elastic stiffness of a rock; and it can be defined as the ratio of the tensile stress over tensile strain. Young's modulus and alteration in its values are highly dependent on mineralogy of the rocks; therefore, knowledge of mineralogy of formations is critical. Figure 1.1 shows QEMSCAN images from Phase 1 of this research project. It is very visible that the shales studied in Phase 1 have varying mineralogies.
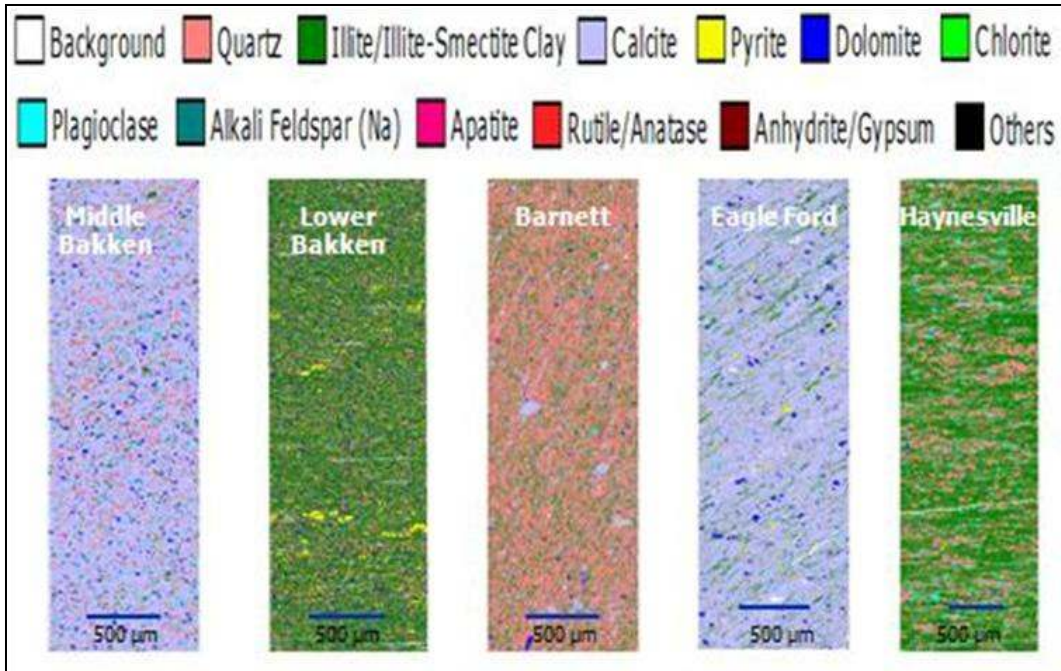
Figure 1.1: QEMSCAN image from Phase1. Image shows the different mineralogy in formations that were studied (Akrad et al., 2011).

When rocks are exposed to water or any kind of fracturing fluid, the mechanical properties can show a significant amount of reduction and the rock frame gets weaker. This weakening process is a factor of how fluids react with the minerals in the rock. Nanoindentation results from Phase 1 of this project indicated that calcite-rich formations (Middle Bakken and Eagle Ford) had the highest reduction in Young's modulus of the studied samples (Akrad et al., 2011). Due to the relationship between Young's modulus and proppant embedment, such results are the main motivational factor for this continued phase of the project. A lower Young's modulus means proppants will embed into the fracture face easier and more rapidly due to physical weakening of the rock (Cipolla et al., 2008). Thus the conductivity will drastically decrease to a level where production may not be feasible. Figure 1.2 shows theoretical work done by Walsh (Walsh, 1981) and indicates that, at the same stress, rocks with lower Young's modulus can result in less conductivity (Cipolla et al., 2008). As seen in the figure, lower Young's moduli rocks have lower initial conductivity even under lower stresses.
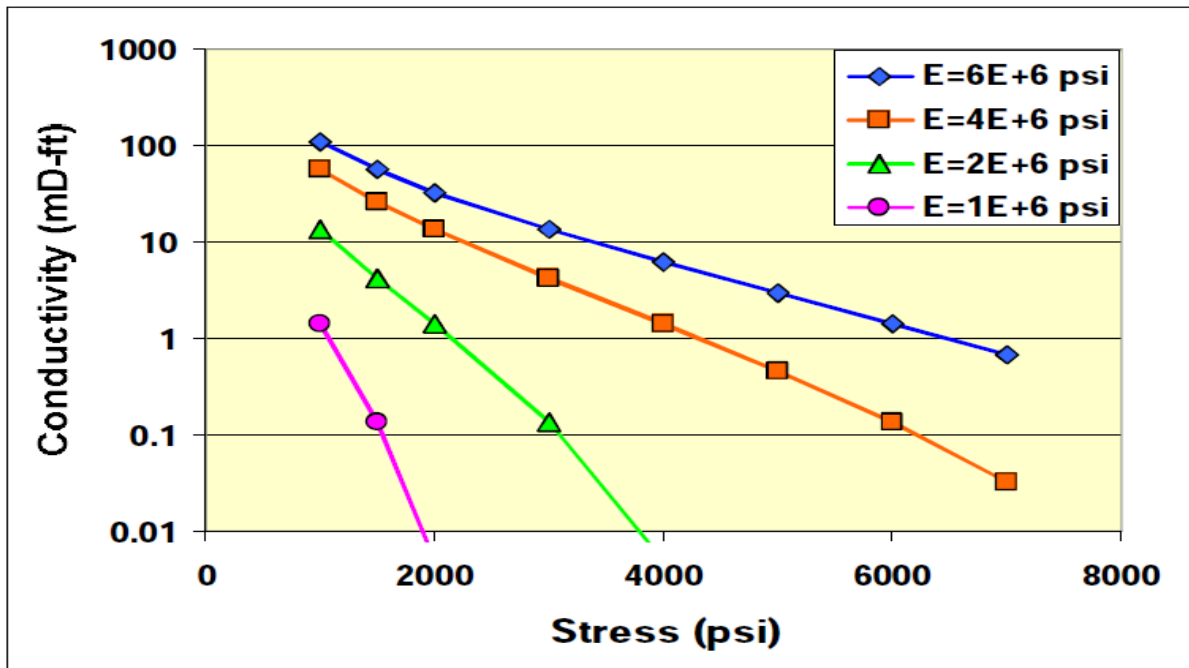
Figure 1.2: Plot represents conductivity versus stress for different Young's modulus values. There are not any proppants used to generate the conductivity shown in this plot. It is very evident that lower Young's modulus can be associated with lower initial conductivity, it also notable that as stress increases, conductivity decreases regardless of the Young's modulus values (Cipolla et al., 2008).

1.2 Results of Phase 1

Phase 1 of this project is discussed in Akrad et al., (2011) and produced many beneficial results regarding proppant embedment and mechanical properties of shales. Results obtained showed how much of an effect mineralogy variation can have on mechanical properties of shales when they come in contact with fracturing fluids. These results were obtained by utilizing QEMSCAN, nanoindentation and imaging tools. Results from Phase 1 are listed as follows:

- Young's modulus decreases after rocks are exposed to fracturing fluids, therefore, decreasing the expected conductivity which should be accounted for when designing for required conductivity;

- Calcite-rich, quartz-rich, and clay rich formations had different modulus reductions. Calcite-rich had the most decrease with 30-50%. Quartz-rich had 10-30%, and clay-rich had 3-30% decreases in their Young's modulus values;

- Precipitation of carbonate minerals in calcite rich formations could be the reason for high Young's modulus reduction, therefore, overdesigning the conductivity could be useful in these formations;

- Young's modulus decreases in both soft and hard minerals. This causes the rock frame to weaken and is a major factor of embedment in the fracture face;

- Rocks fracture in regions that have differences in acoustic impedance, this region is also where most embedment occurs and is concentrated more at lower impedance regions;

- Young's modulus decrease causes more embedment in fracture face, thus conductivity and permeability decrease accordingly which could be as high as 40%;

- Young's modulus values decreased more at higher temperatures than room temperature, which makes embedment a major issue for high temperature formations. Clay-rich formations turn out to be less sensitive to temperature;

- No significant correlations were found between organic content and decreases in Young's modulus; and,

- KCl prevents clay swelling and Young's Modulus decrease in clay-rich formations.

1.3 Thesis Objectives

This research project, a continuation of Akrad's work and called Project #16 Phase2, is a lab based project. The project focuses on fracturing fluid effects on mechanical properties and proppant embedment issues in the Niobrara shale formation which is located in the Denver-Julesberg Basin (discussed later in this thesis). Objectives for this research consist of experimenting with the Niobrara shale formation cores for a better understanding of fracturing fluid exposure and weakening in mechanical properties and their effects proppant embedment issue. The specific objectives and steps taken in order to accomplish this project are as follow:

- Utilize QEMSCAN to identify and the specific mineralogy content of samples;

- Measure hardness (H) and Young's modulus (E) of Niobrara shale samples using nanoindentation;

- Apply four different fracturing fluids (freshwater, slickwater (2% KCl), slickwater (2% KCl+friction reducer), slickwater (freshwater+KCl substitute) then re-measure mechanical properties of selected samples;

- Place four different proppants (16/30 Brady, 20/40 Ottawa, 20/40 Ceramic, 20/40 RCP) in cores and apply high stress (3030 psi);

- Capture embedment behavior using Scanning Acoustic Microscope (SAM);

- Quantify proppant embedment using a profilometer;

- Analyze how different fracturing fluids effect the mechanical properties of Niobrara shale; and,

- Analyze how different proppant types and sizes effect proppant embedment in Niobrara shale.

All tools and technologies used in this project are unique and had specific roles in completion of the project. Nanoindentation was utilized before and after saturating the samples to measure and compare the Young's modulus changes due to fracturing fluid exposure. Nanoindentation was also picked due to its availability, user friendly and non-damaging nature on samples. Although the samples arrived with identified mineralogy, QEMSCAN was used to double-check and validate the samples in hand to obtain more decisive and creditable results. The high pressure equipment was used to pressure the cores up to 3030 psi that were cut in half after placing proppants in them. This tool was used due to its ability to represent in-situ pressures by applying up to 3030 psi on cores filled with proppants. SAM (Scanning Acoustic Microscope) was used to capture the embedment behavior of proppants in the selected shale samples. SAM has high resolution and magnification (200X) which helped capture mechanical changes that the proppants went through and their final image after the pressuring process was over. These imaging tools were very beneficial, because they give image representations of actual proppant behavior

in hydraulic fracturing treatments. The profilometer was used to quantify and measure the proppant embedment occurrence on the core surfaces.

1.4 Research Applications and Benefits/Contributions to Industry

Hydraulic fracturing is a stimulation technique that all operating companies use. Its importance to industry is vital and it is an irreplaceable technique for producing more hydrocarbons and reaching higher recovery. It has many benefits that include; increasing not only production amount but also production rate, improving and healing connectivity between wellbore and formation, establishing vertical connectivity by eliminating barriers to vertical fluid movement, increasing areal drainage by reaching out and tapping into isolated discontinuous hydrocarbon pockets, and increasing the recovery rate and efficiency. Through understanding of fracturing fluid and proppant behavior in reservoirs due to their mechanical properties is a key for taking advantage of all the benefits. Thus, this project was proposed to expand and improve the results obtained during Phase 1 in an attempt to provide the industry with more realistic and in-situ representative understanding of proppant embedment behavior. The Niobrara formation was picked because of the development and success of new fields due to hydraulic fracturing treatments and its importance to the industry from a prospective production and economical standpoint. Completion of the objectives listed in previous Section 1.3 for the Niobrara shale formation provided a great understanding of general shale properties and their contribution in hydraulic fracturing designs. The more detailed and specified contributions of this project to the industry and to fracturing success of Niobrara are listed as follows:

- Improved and better understanding of the mechanical properties of the Niobrara shale samples and the relationship between the changes in these properties with various fracturing fluids;
- Understanding of the proppant type effect on proppant embedment issue when the Niobrara shale samples are exposed to widely used fracturing fluids;

- Quantifying the proppant embedment and permeability loss of certain proppant types when they are pressured in the Niobrara shale samples; and,

- Observing proppant behaviors via utilizing high pressuring equipment and imaging tools, gaining more knowledge on how proppant embedment occurs and what causes it.

All the new and improved knowledge and information listed above will provide the industry with many ways of designing better, more efficient, more optimized and most importantly more profitable hydraulic fracturing treatments. Observing and obtaining the relationship between fracturing fluids used along with mineralogy of shales and their mechanical properties and how this relationship effects the proppant embedment and conductivity of the fractures will be a significant improvement for selecting the appropriate proppant and fluid combination for a given shale mineralogy and a specific shale formation. Selecting the appropriate combination for the desired formation will optimize the treatment design. This appropriate selection will also help create fractures that are highly conductive and more efficient by staying open for a much longer time. Knowing the right proppants and fluids to use for the Niobrara formation will make the fractures more optimized and efficient so it can also lead to reducing the number of treatment stages required for a successful fracture. The optimization and efficiency achieved can also possibly eliminate re-fracturing which will help companies save a great amount of money by not using extra proppants and fluids. The information gained from this project can also help the fracturing industry to get more use out of unconventional reservoirs by extending depletion and lifespan with optimized fracture designs. To sum it up, it would be fair to say that results of this project will aid industry in designing optimized, more efficient and more conductive fractures in shale formations.

CHAPTER 2

BACKGROUND INFORMATION AND LITERATURE REVIEW

Unconventional reservoirs are explained very simply as accumulations that are pervasive throughout a large area and not significantly affected by hydrodynamic influences (Etherington and Ritter, 2007). The emergence of unconventional reservoirs as critical sources of oil and natural-gas production has forced engineers and geoscientists to view field development in new ways (Miskimins, 2009). In the past shales were not considered for development because they were considered only as source rocks and were uneconomical even if firms tried to produce them. With drastically increasing demand on fossil fuels throughout the world and evolving technology, shales are now considered source, seal and also the reservoir. Through this evolution, production from unconventional shale reservoirs has increased and become an essential part of the oil and gas industry in the past few decades through the exploration, drilling, and production success of shale plays such as the Barnett, Bakken, Haynesville, Fayetteville, and Marcellus systems.

Shale reservoirs usually have nanodarcy range permeability and very low porosity in addition to their very complex mechanical properties that requires stimulation technologies for efficient production (Warpinski, et al., 2009). These mechanical properties and the behavior of shale formations under reservoir conditions are very highly dependent on their mineralogical content. Shales can contain a wide range of minerals. Calcite, quartz and clay are among the most abundant minerals in shales. The success of shale plays can be linked directly to the success of Barnett Shale that was first developed in 1980's. As the Barnett Shale play has matured, producers have been extrapolating the lessons learned in the Barnett to the other shale formations present across the U.S and Canada (Arthur et al., 2009). Although the Barnett Shale has been the role model and the facilitator in discovering and producing from other shale plays, the uniqueness and heterogeneous nature of shale plays cannot be disregarded. As much as shale plays seem similar, they all have very distinctively differentiating characteristics and properties. The

following sections discuss more in depth about the geology of the selected formations and the associated hydraulic fracturing treatments.

2.1 Hydraulic Fracturing in Shales

Production from shale formations has been and still is increasing to accommodate the tremendous rise in hydrocarbon energy demand. Shales have become more and more important as the industry has progressed from conventional reservoirs, to tight reservoir, to ultra-low matrix permeability unconventional reservoirs (Kundert and Mullen, 2009). As the type of producing reservoirs changed so did the characteristics of these producible reservoirs.

The matrix permeability of the reservoir of interest has gone from milidarcies (conventional), to microdarcies (tight), to nanodarcies (shale) (Kundert and Mullen, 2009). Shale reservoirs that are in the zone of interest for oil and gas companies usually have nanodarcy range permeability, very low porosity and also very complex mechanical and geological properties which make completions and production very challenging. In order to efficiently produce the maximum amount of hydrocarbons and reach a high recovery factor to optimize the profit out of these so called uneconomical reservoirs, all the geological and hydrodynamical challenges should be overcome with certain stimulation techniques, mainly hydraulic fracturing.

Hydraulic fracturing has progressed significantly since its establishment roughly 60 years ago. A government study found that up to 80% of natural gas wells drilled in the next decade will require hydraulic fracturing (www.api.org/oil-and-natural-gas-overview/exploration-and-production/hydraulic-fracturing/hydraulic-fracturing-qa.aspx). Hydraulic fracturing is the best and most efficient way to produce from tight unconventional formations in order for operations to be both economically and technically successful. Fractures via hydraulic fracturing are initiated by injecting vast amounts of solid-free gel (usually water) at high enough pressures and injection rates to create a pressure higher than the formation fracture pressure. The solids-free fluid (water) is then followed by the injection of a fluid slurry

that is mostly composed of intensifying concentrations of spherical solids or so called "proppants". The achieved pressure difference via the fracturing fluid and slurry causes the formation to break and creates conductive fractures to enhance hydrocarbon flow into the wellbore.

2.2 Fluid and Proppant Selection

Due to the low permeability in shale systems, it is critical that they are not damaged and the permeability decreased even more when it is trying to be stimulated. Thus, it is important to select fluids that are mechanically and chemically least damaging to the formation and also the right type, size and concentration of proppant that will compliment the selected fracturing fluid in order to create an optimum conductive fracture network. Fracturing fluid and proppant selection dictate the quality and success of a hydraulic fracturing treatment. Behind the selection of these ingredients stands the motivation to create a conductive and productive fracture network that can also withstand the possible mechanical property effects of formations.

2.2.1 Fracturing Fluid Selection

Fracturing fluid is the initial component of a hydraulic fracturing treatment. Selection of fracturing fluid has many criteria, requirements and specific selection details in terms preventing damage on other phases of hydraulic fracturing and achieving compatibility with formation, proppants, wellbore design (metal corrosion), etc. Fracturing fluids are the main ingredients of a hydraulic fracturing design, however with all the requirements they have to satisfy, these fluids can also be very damaging to the hydrocarbon production process. Some of big issues fracturing fluids can cause are (Anderson et al., 1982):

- Metal Corrosion: Most tanks are cleaned via steam before fluids are pumped, however corrosion products used can yield a surprising volume of gelatinuous iron oxide.

- Gel-residue: There maybe vast amount of solid content left over from the gelling agent of fluids depending on time.

- Fluid compatibility: Fracturing fluids picked should be compatible with the formation and formation fluids.

- Matrix Compatibility: Fracturing fluids should not be damaging to matrix minerals.

- Fluid Leak-off: The fracturing fluid should be able to optimize the leak-off during the treatment so the process is more efficient and desired fractures are created but also cleaned up.

- Fluid flowback: Fluid recovery from hydraulic fracturing is very important. Picking the right fluid can increase the recovery efficiency.

It is very clear that selecting the fracturing fluid is complicated due to all the requirements listed above. In addition to water and proppant, there are additives that can be essential to meet all these requirements and successfully accomplish the fracturing treatment. The most commonly used additives are corrosion inhibitor to prevent the corrosion of tubings, casings and tanks; biocides to minimize the bacterial corrosion which can also be found in health care products; potassium chloride to overcome the clay swelling and stabilize the clay-water reaction; and breaker to decrease the viscosity in order for better proppant settlement and more efficient fluid flowback. Flowback is probably one of the most fiercely contested considerations made in unconventional-reservoir completions (Miskimins, 2011). The use of some of these additives and their effect on embedment is part of this research.

Along with the increasing development of unconventional reservoirs, the use of slickwater fracturing has become popular for stimulating the tight gas sands and shale gas systems. The main advantages of slickwater fracturing treatments are the economics and adequate conductivity they can place in low permeability reservoirs (Wang and Miskimins, 2010). Additionally, it is possible for slickwater treatments to create long, complex fractures which enhance the well's "stimulated reservoir volume" (Mayerhofer et al., 2008). Therefore some slickwater fracturing fluids were used in this study.

2.2.2 Proppant Selection

Proppants are one of the essential parts of a hydraulic fracturing treatment; their selection can single-handedly affect overall economics of the job, treatment size and ultimate productivity of the well. Annual usage in U.S has gone up from 3 billion lbs to 20 billion lbs between the years of 1999 and 2009. Proppants are granular, angular sand or industrially made ceramic particles. Proppants were introduced to the industry with the first fracture job in 1947 with 20,000 lbs of uncoated fracture sand (http://momentivefracline.com/a-brief-history-of-proppants), but were not being widely used in the 1940's and early 1950's. These unpropped fractures were closing rapidly and were not successfully providing the conductivity therefore the production goals were not being met. The 1950's brought the discovery of several types white and brown natural fracture sands that are still being used today.

Figure 2.1 illustrates the difference between Ottawa (White) and Brady (Brown) sands. Along with the color variation, differences in sphericity and angularity are also present. Just like the grains of rocks contributing to permeability the rounder and more spherical the sand pieces are the more proppant pack conductivity will be achieved.
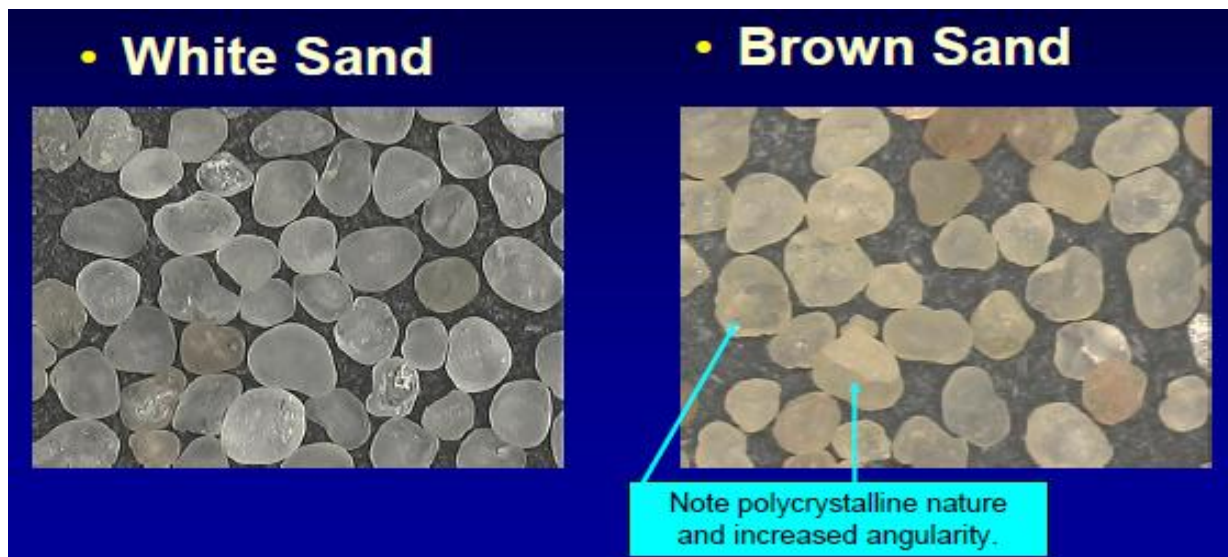
Figure 2.1: Figure showing bunch of White (Ottawa) and Brown (Brady) sands. The color variation is very evident. (http://images.sdsmt.edu/learn/speakerpresentations/Kullman.pdf).

Figure 2.2 shows how various proppant types may look like from a roundness and sphericity standpoint. The permeability of any proppant pack is dependent on its packing arrangement which is not always the same, for the same material. As closure stress increases, the packing geometry changes. The conductivity is also dependent on the grain packing and grain size distribution which is dependent on the roundness and sphericity of the proppants (Barree et al., 2003).
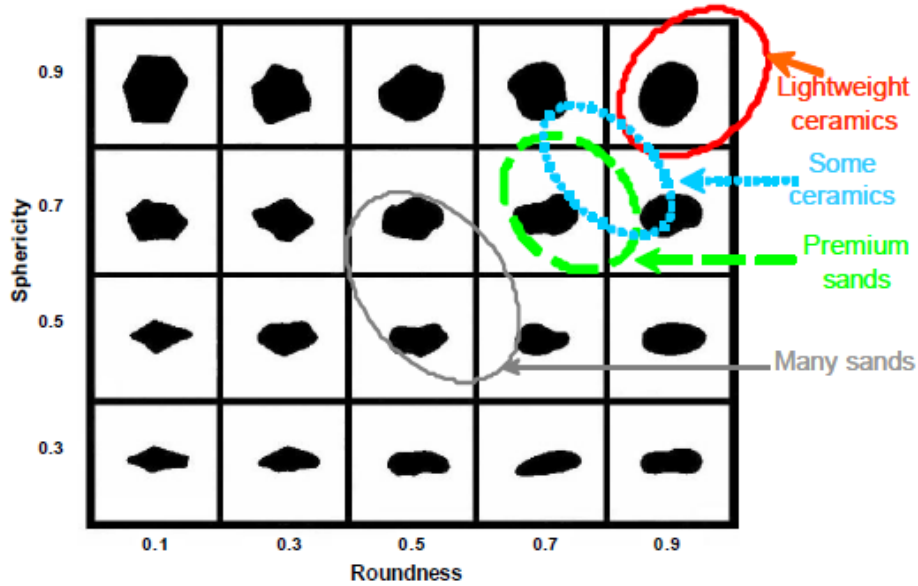
Figure 2.2: Figure showing variation of roundness and sphericity depending on the proppant type. (Vincent et al., 2004).

Higher strength and better shaped proppants will improve fracture conductivity (Cipolla et al., 2008). Based on work by Darin and Huitt (1960) and others using a Hertz cap model and quoted by Cipolla 2008: "It can be observed that for the same proppant concentration in the fracture, smaller particles will be more resistant to crushing due to having more individual grains per surface area and more contact points to distribute the applied load which also reduces the proppant embedment issue". The biggest dilemma industries are facing in choosing sand proppants is deciding on using the cheaper and more available Brady sand or choosing the stronger, rounder, more efficient but much more expensive Ottawa sand.

RCP (Resin Coated Proppants) and ceramic proppants are two very popular man–made proppants used instead of sand proppants. Ceramics are accepted in the industry as stronger proppants that can withstand higher closer stresses over the years by laboratory experiments. RCP's are generally considered to control fines migration, diagenesis, and degredation and prevent proppant flowback. Some suggest that resin coated proppants have been proven to help with the embedment issue because of the thin dielectic polymer film that coats the proppant (Weaver et al., 2005). Out of these man-made proppants some are argued to be more efficient and better than others. Terracina et al., (2010) suggests that CRCS (Curable Resin Coated Sand) provides a higher downhole fracture conductivity which then will lead to more production from that treatment. However the same argument can be made for other man-made proppants. The critical part is to be aware of the mechanical properties of the subject formation and to identify the causes of fracture conductivity loss (high pressure, temperature, flow rate, clay swelling, etc.) and select the appropriate proppant type to be used.

Although proppants come in different materials, shapes, sizes, characteristics, and costs; at the end of the day they all serve for the same goal, that is keeping created fractures open so the connectivity between wellbore and formation increases which then results in (hopefully) ultimate recovery rates and values. An overall explanation of how proppants work was stated by Nguyen et al., (1998) as follows: "During hydraulic fracturing treatments, proppant grains suspended in a viscous fluid are pumped into fractures that the fluid itself created. When the pumping pressure is released, the proppant remains in the fractures, holding them open and forming a conduit for fluid flow into the wellbore. If the proppant flows back into the wellbore, the width of the fracture channels will decrease; the loss of proppant in the fracture limits the flow-channel conductivity, impairing the effectiveness of the fracture treatment". Upon this definition it is very fair to say that conductivity of the proppant pack is the main concern for the proppant selection and success of the fracturing treatment. Other factors contributing to damaged conductivity and general effectiveness of proppants can be (Terracina, et al., 2010):

- Proppant fines generation and migration in the fracture;

- Proppant resistance to cyclic stress changes;

- Proppant embedment in the fracture face;

- Proppant flowback and pack rearrangement in the fracture; and,

- Downhole proppant scaling.

2.3 Proppant Transport

Accurately modeling and simulating the transportation and distribution behavior of proppants when fracture is propagating is a very difficult task. Figure 2.3 shows the various possible cases for proppant transport in fractures; three different cases of distribution mechanisms are considered to represent how proppants actually behave in fractures (Cipolla, et al., 2008); these are:

- Case1: Proppants are evenly distributed throughout complex fracture system;

- Case2: Proppants are concentrated in a dominant planar fracture with an unpropped complex fracture system accepting fluid only; and,

- Case3: Proppants settle and form pillars.
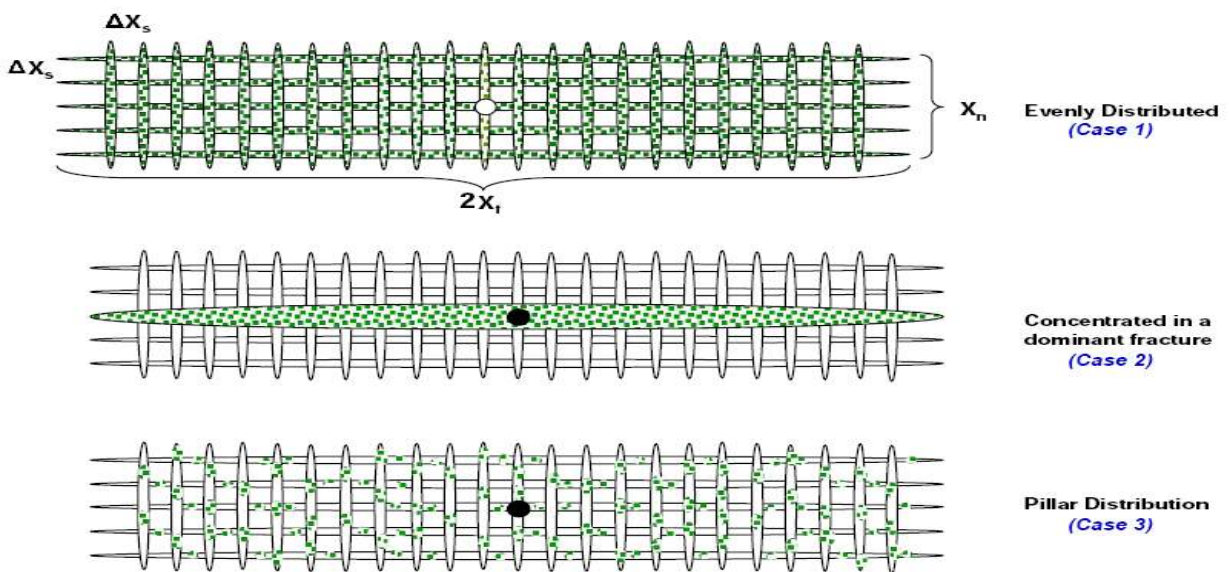
Figure 2.3:Various proppant transportation and distribution scenarios in complex fracture systems from a plan view; dot in the middle represents a vertical well (Cipolla et al., 2008).

17

Figure 2.3 shows the possible proppant distribution among fracture systems. The shale system used in this research project and other are very heterogeneous shales and also contain natural fractures in them. Figure 2.3 is a possible representation of proppant distribution in shales. It is almost impossible to get actual figures like this from actual fracturing treatments because the diagnostics are not available and realistically the spacing will not be this even. Along with physical and formation properties; fluid specific gravity, fluid viscosity, proppant size, proppant specific gravity, and pumping rate control proppant distribution. Figure 2.4 shows the proppant distribution in planar and complex fracture systems.
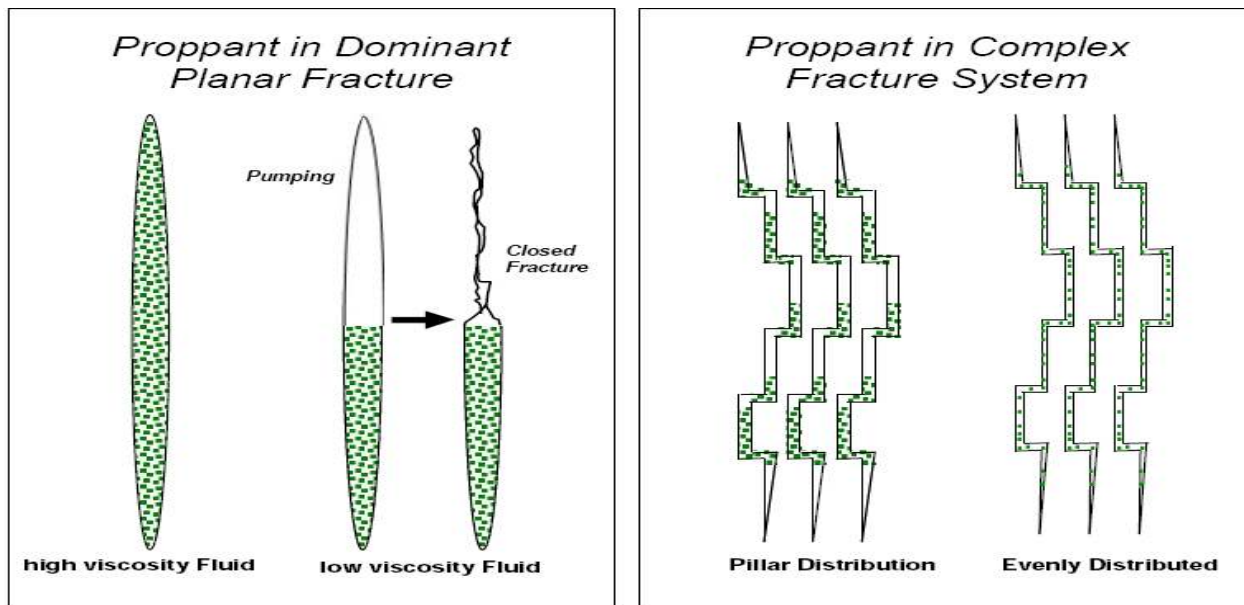
Figure 2.4:Various proppant transportation and distribution scenarios in planar and complex vertical fracture systems from a side view (Cipolla et al., 2008).

As visible on the planar fracture system on the left side of Figure 2.4, gravity plays a big role in distribution of proppants. Presence of low viscosity fluid in the fracture does not support the proppants and decreases the frictional forces, thus making proppants more vulnerable to gravitational forces. This event can also be called proppant settling. Low viscosity or sometimes high viscosity fluids may be lost and have high leak-off. When this issue combines with proppants developing packs and settling due to gravity; a significant amount of the created fractures may close and decrease the conductivity for production just like shown on the left side of Figure 2.4. Gravity will have more a significant effect on vertically induced or natural fractures which could make vertical fractures being less effective due to the

closure of the upper portions. Complexity in vertical fractures just like stated before can be beneficial or detrimental to the conductivity via the distribution of proppants. On the right side of Figure 2.4, pillar distribution looks like it is in contact with a high volume of reservoir, but the proppants are banking and creating packs in certain parts of the fractures, this may allow fracture closure in certain parts and block the fluid flow. When the proppants are more evenly distributed, they help the fracture to stay open in most parts. In most cases since fractures have an irregular and a rough surface, proppants can move randomly and they can build packs due to tensile and shear fracturing (Daneshy, 2005). In cases where fractures are horizontal or a more complex fracture system exist, the flowrate of proppants is very critical. A threshold flowrate should be obtained and maintained for proppants to get properly distributed in horizontal fractures or turn the corners in more complex systems (Sahai and Miskimins, 2012). Not being able to reaching this rate could cause some proppants to develop packs and/or beds also due to gravity and some of the proppants may be loosely scattered and free to move.

The distribution of randomly loose scattered and packed proppants can be referred to as a "multilayer" distribution. When proppants get distributed with a multilayer structure, they do not hold any consistent pattern or uniformity on how they are scattered along the fracture face. Multilayer distribution can also indicate that proppants are placed on top of each other, thus having more than one layer of proppant in between the fracture surfaces. Multilayer distribution could be beneficial or detrimental to conductivity and production. When multilayer of proppants is present in the fracture, the stresses from formations can be distributed better among the proppants since there are more proppants in the fracture, which can result in a lower embedment effect. However at the same time, presence of multiple layers of proppants means the proppants are stacked on top of each other, mechanically this distribution may cause proppants to be crushed against each other and reduce the permeability and pack conductivity.

Proppants can also be distributed in a single layer (monolayer) along the fracture face (see Figure 2.5); this case may not be too realistic due to the flowrate and turbulence effects in the fracture. The

proppants tend to move around and settle in time. In the case of a monolayer distribution embedment effect will be very significant due to stresses being applied on only one layer proppants, which will also cause a reduction in conductivity. Previous studies by Van Poolen et al., (1957) showed that the flow capacity of proppant packs increased with fracture width, or in other words, for a given proppant size, with increasing numbers of proppant layers. Since proppant distribution has significant effects on the conductivity and sustainability of the fracture, establishing an optimized distribution is important. Neither multilayer nor monolayer seems to be capable of being the most optimized distribution, thus another distribution possibility is a partial monolayer (see Figure 2.5). This distribution type is considered highly theoretical. Fracturing mechanics and design experts such as Economides and Nolte (1987) in their Reservoir Stimulation study stated that: "Although maximum conductivity can be obtained by placing proppant in a partial monolayer, placement of a partial monolayer in a vertical fracture is virtually impossible to achieve". Harrington and Hannah's (1975) reasoning for this was expressed as due to the inability to obtain uniform and complete coverage of the fracture with a partial monolayer, insufficient proppant strength to support the load, loss of fracture width due to proppant embedment and, potentially deleterious non-Darcy flow effects in the relatively narrow propped fracture.
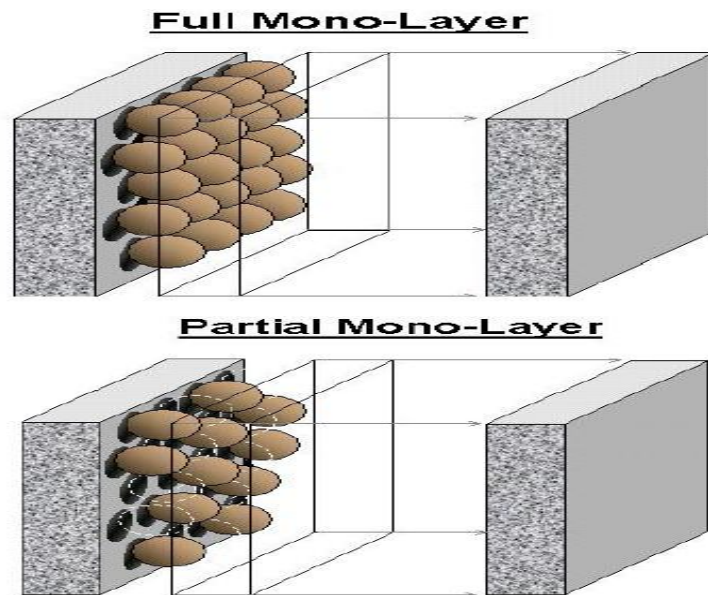
Figure 2.5: Representations of full monolayer and partial monolayer proppant distribution in fracture face (Brannon et al., 2004).

2.4 Conductivity

The primary goal of a hydraulic fracturing treatment is to create a highly conductive flow path to the wellbore that economically increases well production (Gillard et al., 2010). Fracture conductivity is the width of the fracture, w, multiplied by the apparent permeability of the proppant pack, kf. Brannon and Starks (2008) defined fracture conductivity as "the fracture conductivity defines the conductive path provided by the proppant material to enhance deliverability and provide economic benefit when the well is placed on production". This very important concept is calculated and estimated by the dimensionless fracture conductivity, F_{cd}, equation which dates back to the earliest days of hydraulic fracturing in 1950's. Dimensionless fracture conductivity is referred to as F_{cd} or C_{fd} is defined in Equation 2.1.

$$F_{cd} = \frac{k_f w}{k x_f} \qquad (2.1)$$

Where:
k = formation permeability, md
k_f = fracture permeability, md
w = fracture width, ft
X_f = fracture half length (wellbore to tip), ft

The dimensionless fracture conductivity is controlled and depicted both by the formation capacity to deliver fluids to the fracture and also the capacity of the fracture to produce the fluids into the wellbore. In other words, F_{cd} is a parameter that compares the capacity of the generated fracture to allow fluids to transport into the wellbore while also regarding the ability of the formation to deliver fluid into the fracture.

In addition to conductivity being related to permeability of the formation, it also is a very extrinsic parameter. It is highly dependent on and effected by the initial grain packing and grain distribution. Since conductivity is considered an extrinsic parameter of a fracture, it is affected by many different factors during and after a fracturing operation. Thus it is very important to design the fracture treatment to be as optimized and as efficient as possible for all producing stages. Some approaches and techniques for enhancing conductivity could be as follows:

- Selecting the proper proppant size and type that can withstand the maximum production and closure stress and minimize proppant embedment;

- Immobilizing fines derived from crushed proppants;

- Minimizing the invasion of formation fines into the proppant pack; and,

- Maximizing gel-residue removal by improving breaker efficiency.

This project focuses on the embedment issue in the prior list. The dimensionless fracture conductivity equation shows that width of proppant pack is critical. Embedment of proppants into the fracture face is a significant issue causing the width to decrease and thus also the conductivity.

2.5 Embedment

Embedment occurs when proppant grains are embedded into the fracture face due to the interaction between proppants and fracture surface in the condition of closure pressure which results in the fracture aperture and conductivity decrease (Li et. al., 2013). Embedment issues increase with the increase of production time, especially in the process of hydraulic fracturing, where the fluid can weaken the rock strength (Akrad et al., 2011 and Matthews et al., 2007). It can also occur through chemical reactions downhole such as diagenesis and degredation of proppants over time (Rayson and Weaver, 2012). Proppant embedment is an issue regarding fracture width and conductivity reduction, which ultimately is a threat to the overall success of hydraulic fracturing operations.

Proppants will embed due to high temperature and formation closure stress, and they can also be damaged by the cyclic stress. Throughout the life of wells, events such as shut-ins due to work-overs, introducing different stimulation techniques, connections to pipelines and pressure drawdown differences due to production occurs multiple times which all cause cyclic changes in fracture closure stress. Embedment also has an indirect effect on conductivity and proppant pack permeability. As downhole fracture closure stress increases, proppants can begin to crush and create fines. The chemical reactions between the proppant and formations can occur at substantial rates and affect the created fines, and

formation chemistry (Rayson and Weaver, 2012). The fines that are created through proppant crushing can accumulate on the fracture face causing additional loss of the fracture conductivity. Lacy et al., (1997) stated in their studies that proppant packs are significantly damaged due to formation fines caused by embedment. Figure 2.6 shows a representation of how proppants can be embedded into the formation downhole.
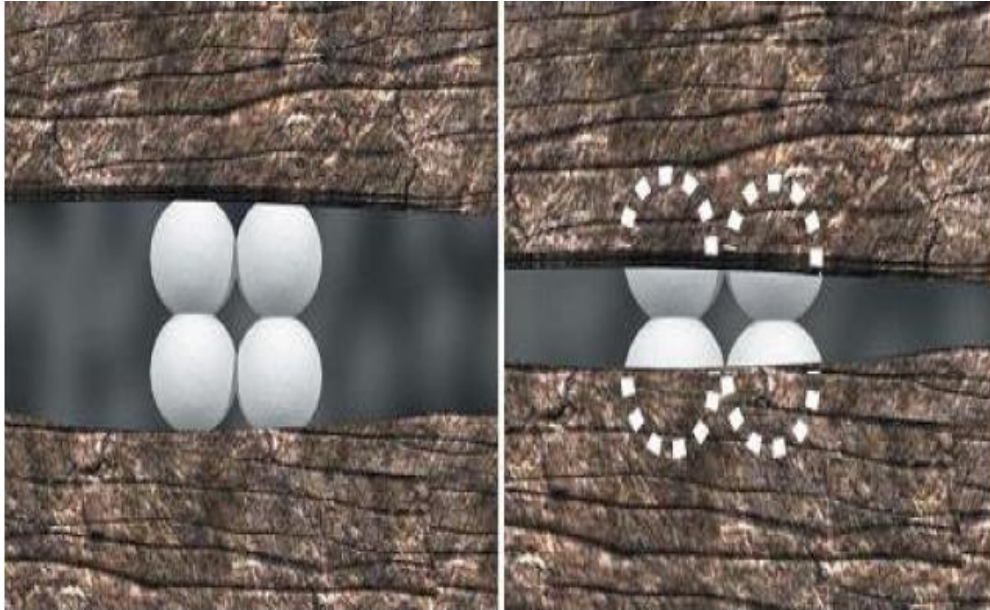
Figure 2.6: Showing the fracture width reduction caused by proppant embedment into the fracture face (Terracina et al., 2010).

Proppant embedment can be a more severe damage mechanism for certain types of formations than others. The shear weakening in carbonates due to fluid saturation also affects proppant embedment (Sharma et al., 2009) as seen in Figure 2.6. Embedment is most severe when hard proppant contacts a soft formation (Zhou et al., 2011). In general embedment is a greater issue for shale systems in comparison to sandstones or limestones. For formations with a Young's modulus value of less than 2×10^6psi, embedment becomes even a greater issues because a Young's modulus value that low represents a very ductile shale (Lacy et al., 1998). In ductile formations (high clay content formation) embedment may cause proppant pack width to reduce by up to several proppant diameters (Barree et al., 2003). This does not mean brittle formations will not experience proppant embedment. Fracturing fluids used during the hydraulic fracturing process can affect the strength of shale systems negatively. When shale systems are

exposed to fracturing fluids their Young's modulus can decrease immensely which makes even the strongest shale formation vulnerable to proppant embedment. Evidence of this behavior is discussed later in the thesis.

Figure 2.7 is taken from Cipolla et al., 2008 and it shows just how embedment is dependent on stress variation and also the Young's modulus of the subject formation. It is very evident that embedment inclines as the stress increases, however more importantly this figure shows that a formation with lower Young's modulus profile experiences a much more drastic decline in its embedment value in comparison to a higher Young's modulus formation.
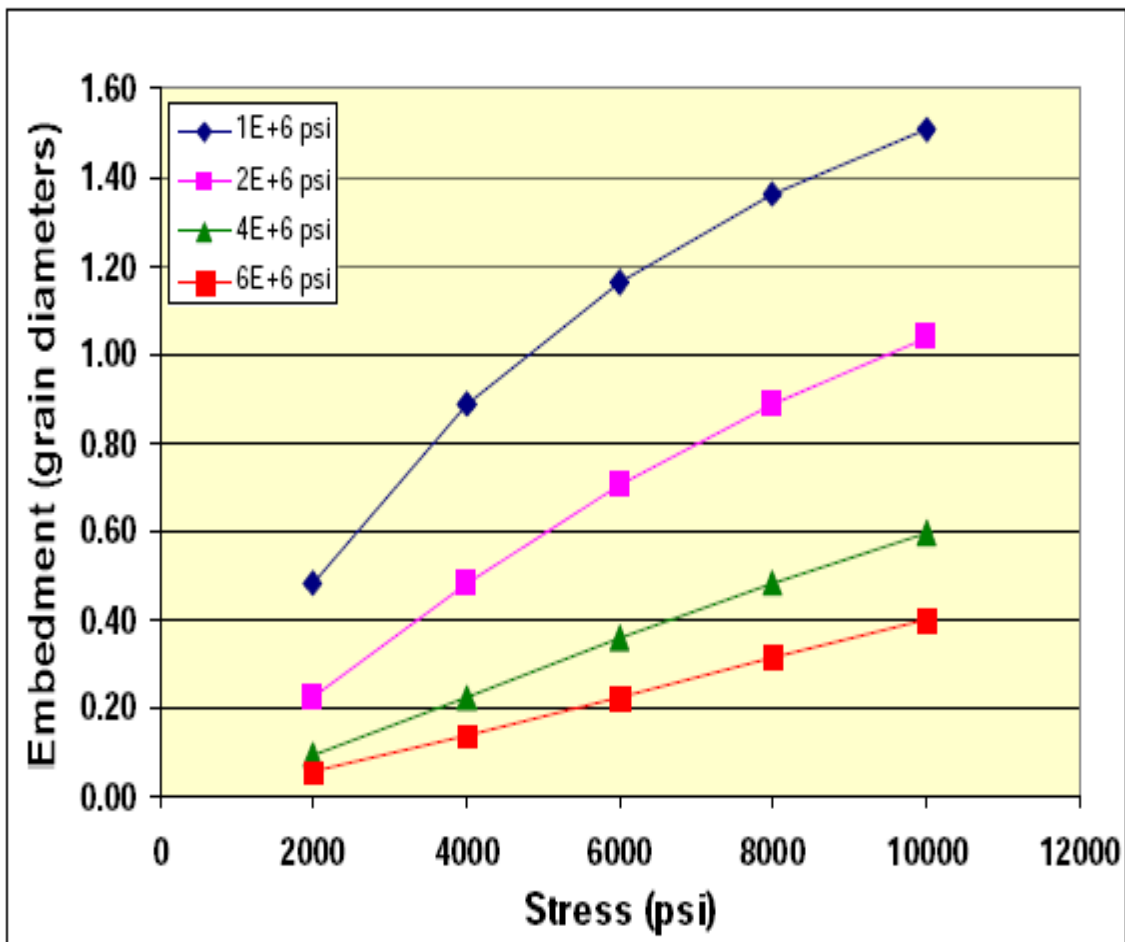
Figure 2.7: Plot represents proppant embedment versus stress for different Young's modulus values. It is very evident that lower Young's modulus can be associated with higher embedment, it also notable that as stress increases embedment also increases regardless of the Young's modulus values (Cipolla et al., 2008).

2.6 Mechanical Properties of Shales and Fracturing Fluids Effect on Them

Shale plays have completely different and unique geomechanical, geochemical and petrophysical attributes from each other. This dissimilarity between shale plays creates different reactions and responses when the same completions and stimulations designs are used in different plays. The two most influential mechanical properties on hydraulic fracturing and proppant embedment issues are Young's modulus and Poisson's ratio. Young's modulus, by definition, is the ratio of stress to corresponding strain for a material and it also referred to as the elasticity, whereas, Poisson's ratio is the ratio of transverse to axial strain. Young's modulus represents the ability of a rock to maintain initiated fractures (strength), and Poisson's ratio represents the deformation and failure of a rock under closure or overburden stress. "Brittleness" combines both of these properties and represents the "frackability" of a rock. Figure 2.8 shows how these properties can be related to each other using certain circumstances.
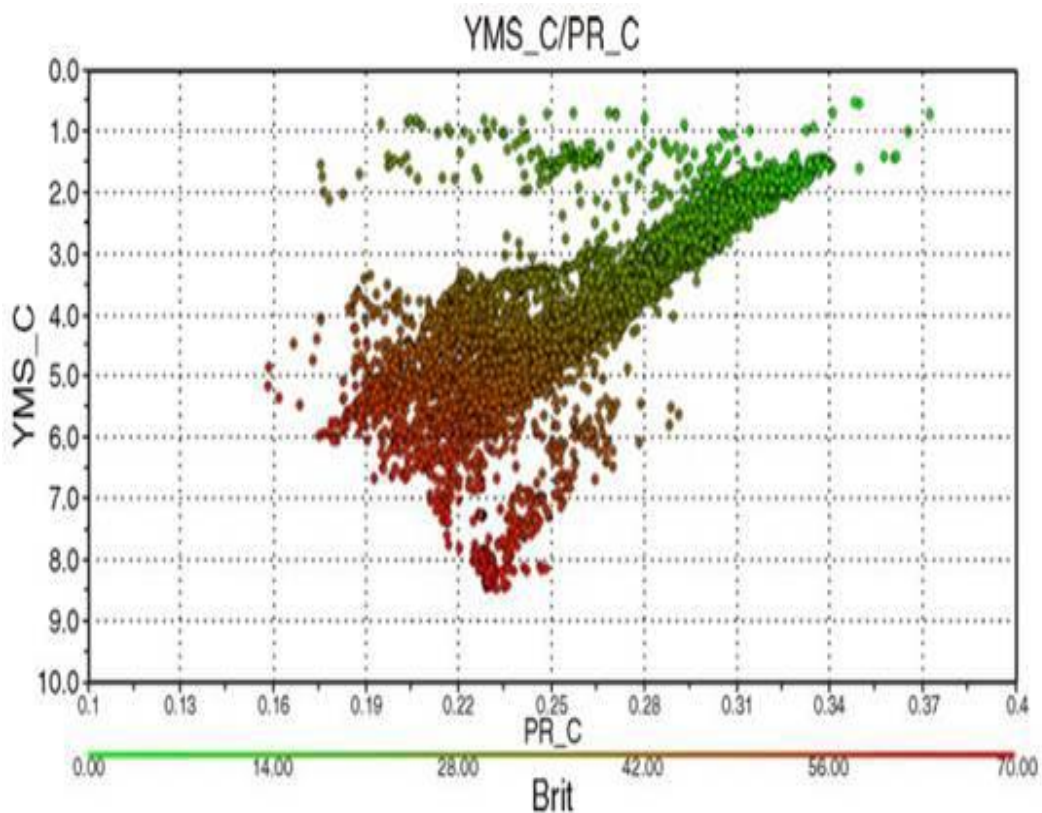
Figure 2.8: Cross plot of Young's Modulus and Poisson's Ratio showing the brittleness of shale increasing as Young's Modulus increases and Poisson's ratio decreases (Rickman et al., 2008).

25

Figure 2.8 shows that a higher Young's modulus combined with a lower Poisson's ratio represent more brittle shales which are color coded with red, whereas, low Young's modulus and higher Poisson's ratio represent more ductile and softer shales which are represented by the green color. Brittle and ductile shales have very different roles from a reservoir standpoint. Lacy et al., (1998) stated that ductile rocks (less stiff and low Young's modulus) have higher proppant embedment associated with them which makes them respond poorly to hydraulic fracturing.

Young's modulus is the major parameter that controls proppant embedment. Alramahi, (2012) stated that proppant embedment is largely controlled by Young's modulus. In the same paper they also stated that rocks with higher clay content (weaker and ductile) represent higher embedment. Lacy et al., (1998) stated that Young's modulus is the main factor in proppant embedment and any rock with a Young's modulus less than 2×10^6 psi will be affected more dramatically by proppant embedment. It is also known that fracturing fluids decrease Young's modulus and weaken the rock which essentially means what was once a brittle formation could behave as a ductile formation during and after the hydraulic fracturing process (Lacy et al., (1998). Even though Young's modulus is such an important factor, most studies to date regarding the geomechanical effects of fracturing fluids on embedment have been done by investigating and experimenting with Hardness and Brinell Hardness (BH) methods. Brinell Hardness (BH) can be defined as the resistance of the sample to plastic deformationas the sample is being indented using Brinell Hardness testing methods. Two of the most detailed and extensive studies done on the weakening of shales and proppants over time due to fluid and temperature effects are (LaFollette and Carman, 2010) and (LaFollette and Carman, 2011).

LaFollette and Carman, (2010) experimented with the Haynesville shale. The Haynesville cores were cut and proppants placed in between the shale samples. The shale samples with proppants in between were then put into broken high pH borate crosslinked gelled water and placed in a Teflon-lined pressure bomb that was heated up to 300˚F. The samples were not pressurized because approximately 80

psi of steam pressure was naturally generated. Experiments were run for a total of 240 days with retrieving before and after Brinell Hardness for shale, water chemistry and proppant strength on Days 30, 60, 90 and 240.

Water chemistry, proppant strength and Brinell Hardness all showed alterations at the end of the experiments. Different chemical characteristics of water, even after 30 days, indicated either the shale sample or the proppants or both dissolved because of the heated fluid and changed the chemistry of the water. This chemistry change increased and peaked at the end of 60 days and started showing a decreasing trend starting at the end of 120 days. At the end of 240 days, water composition looked similar to the initial properties at day 0 which indicates a healing trend after 120 days. At the end of 30 days, the proppant tensile strength had gone down by 31%. When the results from 60 days came in, proppant tensile strength showed a continuous decrease with having the 35% of its original strength. Just like the water chemistry, proppant strength values showed a changing trend starting at 120 days, the strength was decreased between 60 days and 120 days but with a less intensity, and proppant strength at 240 days seemed to have stabilized. Last but not least, the Brinell Hardness of the samples also showed interesting results. The 30 day sample exhibited a decline of 28% in BH compare to the original value. When the same sample was investigated after 60 days BH seemed to have lost 66% of its initial value. BH values at 120 day were slightly higher than the 60 day BH values. This ascending trend in BH values continued after 120 days and exhibited a substantial increase at the end of 240 days with BH values indicating that shale sample became harder than they were after 30 days but still lower than how they were initially. The Brinell Hardness change on the Haynesville sample over 240 days is shown in Figure 2.9.

These experiments by LaFollete and Carman proved that if the result could be repeatable that there is a time period where embedment is most severe, and by looking at the complete 240 day cycle there also is a time period where embedment starts decreasing due to stabilization of chemical and physical effects of fracturing fluid and heat on rocks, water and proppants (LaFollete and Carman, 2010).
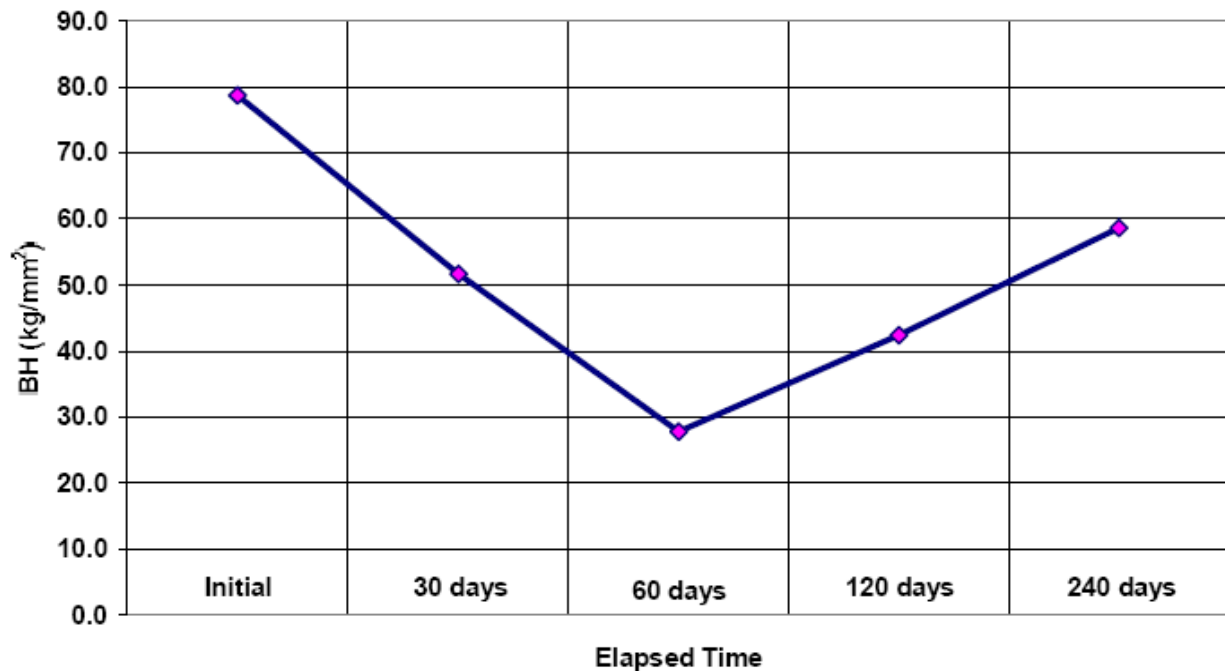
Figure 2.9: Brinell Hardness showing how hardness and strength of the Haynesville shale is changing when it is exposed to fluid for a duration of total 240 days. As seen Brinell Hardness decreases dramatically first 60 days but then starts hardening again (LaFollete and Carman, 2010).

Carman and Lant, (2010) also experimented with fracturing fluids and certain shale systems and investigated how Brinell Hardness of these shale systems changed. In this paper CST (capillary suction time), which is a technique that determines fluid and rock compatibility, was also utilized. Geologic age, formation temperature, mineralogy, Brinell Hardness and capillary suction time are among the parameters that were measured for eight different shale systems in this paper. Each sample was tested with different commonly used fracturing fluids under its expected reservoir temperature. Varying fluids also had different effects on the same system. The Bakken and Eagle Ford due to their mineralogy are the most similar systems to the Niobrara out of the eight that were tested. The Eagle Ford had a 48.2% BH reduction with the use of 7% KCl and a 32% reduction with the usage of 4% KCl. A major conclusion from this paper was that weakening of shales due to fracturing fluids is inevitable and all shale systems regardless of their mineralogy experience it. Also, having a different concentration of KCl did not make

too much of a difference in Brinell Hardness reductions. Thus higher concentrations of KCl may be unnecessary for clay control and preserving strength (Carman and Lant, 2010).

2.7 Shale Geology and the Niobrara System

Shales are the most frequently occurring sedimentary rocks that are composed of mostly mud, mixed flakes of clay minerals and small fragments of other minerals, especially quartz and calcite. They are usually colored in different tones and variations of gray and/or black but can also be present in different colors due to environment effects (Tare et al., 2001). They are known for their nanodarcy range permeability and very low porosity (Sone, 2012). They also are very challenging reservoirs to extract hydrocarbons from and are considered unconventional and tight reservoirs. These reservoirs, once known as impossible to produce due to technological and economical constraints, are now major producers in both oil and gas production. The technological advancements in geology, geophysics, drilling, completions, and production have made unconventional and tight shale formations the future of U.S production. The Niobrara shale system was selected for this project due to its new and emerging role in the energy industry.

The Niobrara is one of these new emerging shale plays and the currently productive area is mostly located in Colorado. Figure 2.10 shows the Niobrara's location and extent. The Niobrara has been long recognized as a hydrocarbon producer. Niobrara has been producing for a long time. However, it was not until the 1970s that the pace of development dramatically increased. In the last decade especially after 2009, the Niobrara became one of the largest hydrocarbon producing shale play in U.S through advances in technology, detailed and analytical investigations of reservoirs and successful multi-stage hydraulic fracturing treatments. The Niobrara as a new emerging play has very unique characteristics as do all of the other shale systems. It is being compared to the Bakken in North Dakota due to some similarities. Table 2.1 shows characteristics of the Niobrara and how they differ from other shale systems in the U.S.
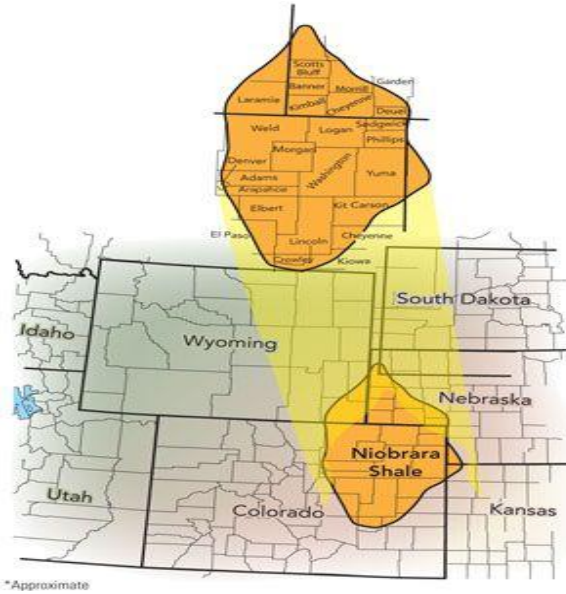
Figure 2.10: The Niobrara shale's approximated location and extent in between the four states that it is deposited in (http://www.coga.org/pdfs_facts/Niobrara_fastfacts.pdf).

Table 2.1: Reservoir and Geology Data for Popular Shale Plays in U.S (Polzin, 2012)

	Niobrara	Eagle Ford Oil Window	Bakken	Horn River	Barnett	Woodford	Fayetteville	Haynesville	Marcellus
Age	Cretaceous	Cretaceous	Upper Devonian	Devonian	Mississippian	Devonian	Mississippian	Jurassic	Devonian
Depth (TVD ft)	6,000-10,000	5,000-11,000	8,000-11,000	6,000-13,300	6,000-9,000	6,000-12,000	4,000-6,500	10,000-14,000	5,000-8,500
Thickness (ft)	150-500	80-175	<140	360-580	200-500	90-300	50-300	150-350	50-300
TOC (%)	1-8	3-6	8-10	3-7	3-8	4-10	2-4	2-3	4-6
In-Place (Bcfe/mi^2, MMBOE/mi^2)	20-50	50	5-15	150-318	150	135	50	200	100
IP (MMcfe/d, BOE/d)	400+	300-2000	300-2000	6-26	2-8	2-10	2-4	5-25	3-9
EUR (Bcfe, MBOE)	200+	200+	200-700	5-15	2.1	3.5	2.3	6.0	4.0
Royalty (%)	17%	25%	15-20	2-30%	20%	25%	20%	25%	16%
D&C ($MM)	3.5-6.5	4-7	4-6	7.6-11.8	3.5	4.5	4.0	7.5	4.5
F&D ($/Mcfe, $/BOE)	15-30	<20	10-25	2.05	2.08	1.71	2.17	1.67	1.34
Snapshot	Newest oil shale play; EOG and Noble have had a few good well results but too early to determine extent of high quality region	Emerging play with robust well results at moderate well costs; valuable liquids component	Huge region in the Williston Basin proving commercial for Bakken and in many areas the additional Three Forks reservoir; Operators push the envelope in terms of long laterals and no. of frac stages	Play still in early commercial stage; strong well results with continuous cost reductions	Technological proving ground for all US shale plays; economic geographical limits generally defined	Play generally defined; infill drilling primary focus with some laterals reaching >9,000'	Cost reductions and operational efficiencies ongoing	Highest IP wells of any shale play; cost reduction key to economics	Largest areal extent of any shale plays; core areas now emerging

The Niobrara formation is located in the Denver-Julesberg basin. The producing region runs through the Rocky Mountains to Southern Colorado extending into northwestern Kansas and southwestern Nebraska (cross-section shown in Figure 2.17). The Denver-Julesberg basin contains the most productive Niobrara section. The Niobrara formation was deposited approximately 90 million years ago during the Upper Cretaceous period of the Mesozoic era in the inland seaway that ran through all the way from present day Gulf of Mexico to the Arctic Ocean (see Figures 2.12a and 2.12b).
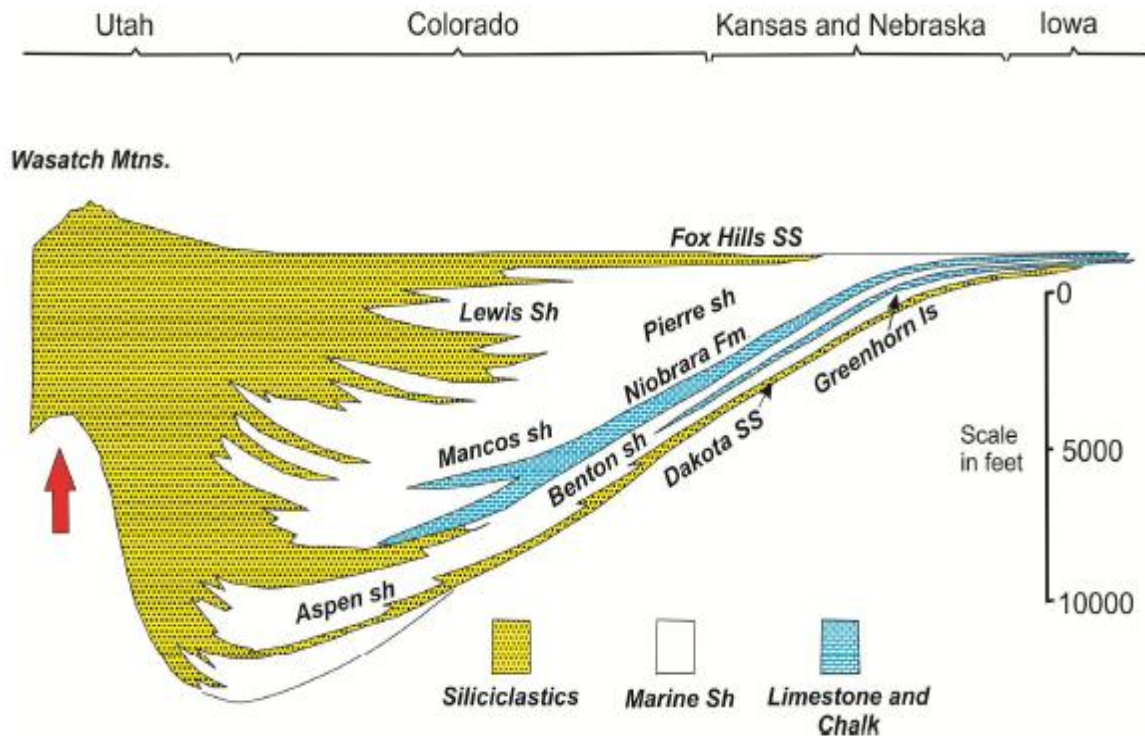
Figure 2.11: Generalized west to east cross section of Niobrara showing its lateral distribution through Utah, Colorado, Kansas, Nebraska and Iowa. It is noticeable that Niobrara is laterally equivalent to the Mancos Shale (Sonnenberg, 2012).

This seaway was limited to the west by the Cordilleran Orogenic belt, while to the East, the basin was a "broad, stable platform with little sudsidence" (Pollard and Schaella, 1986). Calcareous debris from algae and the remains of abundant marine life living in this seaway slowly accumulated, and when the sea finally withdrew, thick layers of clay, mixed clay and limestone, chalk and smaller amounts of slit and sand were left behind to form some of the sedimentary rocks we observe today on, and beneath, the surface of Colorado (Colorado Geological Survey, 2011). Due to interactions between cooler and warmer

waters during the withdrawal of sea and accumulations of sediments and asymmetry of the foreland basin, the Niobrara is interbedded and changes character from east to west along the basin. Figure 2.12 shows how the Niobrara was formed and its stratigraphy column for northeastern Colorado.
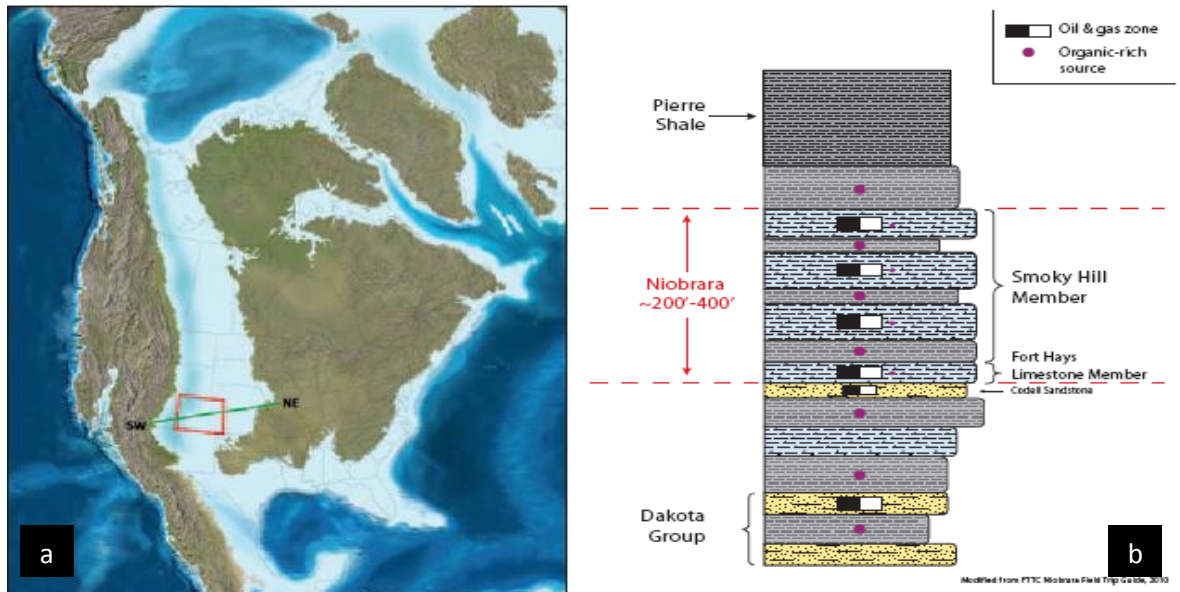
Figure 2.12: (a): Image of the inland seaway 90 million years ago that made Niobrara to be formed. (b): Image of Niobrara Formation stratigraphy for northeastern Colorado (Colorado Geological Survey, 2011).

There are many characteristic changes that occur from east to west including:

- Clay content gets higher towards the west side due to presence of mountains (terrigenous influx) (Longman et al., 1998 and Pollastro and Schoelle, 1986).

- Due to burial and subsidence of the basin, the chalk went through mechanical and chemical compaction as well as diagenetic changes. Chemical compaction caused reprecipitation of calcite grains (Longman et., 1998). This led to porosity loss, increase of brittleness and conversion of plastic, smectite clays to more brittle, illitic clays (Pollastro, 1992).

- Biogenic gas is produced from the east side of the basin and oil is produced on the west side.

The Niobrara is composed of alternating layers of organic-rich shales and limestones (chalk) as shown in Figure 2.12 (b). This changing vertical structure adds complexity to drilling, completion and production. The Niobrara deposits in eastern Colorado include chalk (made predominantly from algae-

derived carbonate plates known as coccoliths), carbonate mud, shale, and silt. Whereas in the western portion of the basin, deposits have more shale, silt and sand that were shed from the rising mountains.

The East section of the Niobrara is made up of two units; the Fort Hays Limestone Member and the Smoky Hill Member. The west section also has these two members but it is challenging to distinguish them. The Fort Hays ranges between 10 and 60 ft in thickness in eastern Colorado and it increases towards south. This member predominantly has chalk beds as seen in Figure 2.12 (b). The Smoky Hill member is made out of alternating layers of shale and limestone (chalk). This part of the Niobrara is the biggest contributor to hydrocarbon production, and its thickness varies from 200' to 1400' in the northwestern parts of Colorado. As stated before the Niobrara is very versatile in its production. The east portion produces gas from depths as shallow as 3000', and the west portion produces oil from depth as deep as 7000' to 12,000'.

Total Organic Carbon (TOC) of the Niobrara is varying through east and west portions. Most sedimentary rocks contain less than 1% TOC, where a high quality source rock contains more than a TOC of 5% (Colorado Geological Survey, 2011). Since the Niobrara is a highly complex geological structure and has interbedded layers of limestone and shales, the TOC content can vary significantly. In the west, where there is more chalk present the TOC level ranges from 5% to 8%. However in the northeastern portions where there is less chalk, the TOC level can be as high as 8%. The calcite percentage in the Niobrara can be as high as 95% which also indicates that Niobrara on an average has a TOC values ranging anywhere from 1.3% to 5%. This classifies Niobrara as a very good quality reservoir as far as its hydrocarbon content (Colorado Geological Survey, 2011). More detailed information on the Niobrara's mechanical and geological properties can be seen in Table 2.2.

The Niobrara has been producing hydrocarbons for over a hundred years. The first oil produced (found) was in 1860 near Canon City. This well produced approximately 1 BOPD. The first commercial oil well was established in 1881 and hit oil at a depth of 1445' (Sonnenberg, 2012). As years went by,

attempts to produce hydrocarbons from this formation increased, however due to limited technology and knowledge, most fields did not produce at profitable levels. In the 1970's, with evolving technology in the oil and gas industry, the Niobrara formation became of interest. In the mid 1970's, gas production started increasing in immensely high rates and is still increasing to this date. Throughout the years the Niobrara has mostly been a gas producing formation with some oil production in Weld County, Colorado, from vertical wells. However, after 2009, oil production in the Niobrara, especially in the Denver-Julesberg basin, has experienced a drastic increase with the introduction of horizontal drilling and multiple stage hydraulic fracturing.

Table 2.2: Mechanical, Geological and Reservoir Properties of the Niobrara Shale (Sonnenberg, 2012 and Maldonado, 2011)

Mechanical, Geological and Reservoir Properties of The Niobrara Shale	
Geological Age	Upper Cretaceous
Depth (ft)	5500-12000
Net Thickness (ft)	200-1400
Prospective Area (mi²)	14,000
Hydrocarbon Type	Oil & Gas
Natural Fractures	Locally abundant & highly fractured
Pressure Gradient (psi/ft)	0.41-0.67
TOC %	5.0-8.0
Porosity %	1.0-10.0
Young's Modulus (Mpsi)	6.1-9.0
Poisson's Ratio	0.18-0.27
Average Calcite Content %	89-95
Well Cost $	3.5MM

CHAPTER 3

RESEARCH METHODS AND EQUIPMENT

This project is a lab-based experimental project which involves cores and direct measurements from various equipments. Due to availability, Niobrara shale, a carbonate and calcite rich formation cores were tested to investigate the proppant embedment issue. All the cores received and used in this project are from the same well. The initial and most important step during this project was Young's Modulus (E) measurements. Young's Modulus and also Hardness (H) were measured using the MT'S Nanoindenter XP located in Material and Science Department. E and H for each core plug were measured before and after applying various frequently used fracturing fluids to them in order to determine how fracturing fluids altered the mechanical properties as time progressed. The values were checked on the 5th, 15th and 30th days. It is also very critical to know the mineralogy and porosity of the cores that are being used. Thus Quantitative Electron Microscope Scanner (QEMSCAN) was utilized on three pieces that were cut from the main cores for mineralogy and porosity identification. TOC data were provided along with the cores, thus experiments towards TOC measurements were not conducted. Upon completing Young's modulus measurements, the cores were from selected samples and pressurized with proppants in between them. Cores were then analyzed by Scanning Acoustic Microscope (SAM) and profilometer to observe and quantify proppant embedment.

3.1 Core and Sample Analysis

The following steps were taken and executed in order to successfully complete this project. The various machines and measurement techniques are discussed in Sections 3.2 – 3.6. A more detailed methodology explaining each step can be seen in supplemental file E:

1. Core plugs with 1.0 inch diameter and 1.5-2.0 inch length were first cut at Stimlab. Cores were cut with air in order to prevent them from being exposed to water which could have caused clay

swelling and Young's modulus reduction. Due to availability and also the need for repeatable experiments, coupled cores were retrieved from some depths. The orientations of cores were not considered to be important for this work.

2. After receiving the core plugs, three cores were picked from various depths considering their TOC and calcite percentage variation in order for results to represent the entire well.

3. Small chips were cut from the previously selected three samples and sent to the QEMSCAN imaging laboratory for mineralogy and porosity analysis.

4. After picking three different samples for the QEMSCAN imaging, ten samples including those to be imaged by QEMSCAN were picked for the remainder of the experiments to be saturated and heated for proppant embedment tests.

5. 1.0 inch diameter and 0.6 inch length pieces were cut from the ten samples for nanoindentation measurements before and after saturation and heat treatments by using diamond core cutter in.

6. These cut pieces were then polished down to 1.0 micron on one side by going through a vigorous polishing process (details explained in supplemental file E) with various fluids. The other ends of the cores were polished to 200 mesh to enable them to stand flat.

7. 1.0 inch diameter and 0.40 inch length pieces were cut from the ten samples once again for SAM and proppant embedment testing. Each sample produced at least 2 pieces of cores with these dimensions.

8. A piece representing each sample went through nanoindentation when they were dry after polishing.

9. These pieces were then saturated in four different fracturing fluids for five, 15, and 30 days. A nanoindentation measurement was performed at the end of each period. Four samples were originally completed. The second four samples were added later on as expansion samples.

10. The two remaining samples were saturated and also heated up to 180˚F in freshwater and KCl for five days.

11. Upon completing the nanoindentation process, cores cut for SAM and proppant testing were put in their associated fracturing fluids for 30 days to reach the same saturation level as the nanoindented cores, this made mechanical property data more relevant with the embedment results.

12. The Scanning Acoustic Microscope (SAM) was utilized on these cores to capture surface condition of cores prior to applying proppants under pressure.

13. Selected proppants were placed in between the saturated cores under high pressure (3030 psi).

14. The Scanning Acoustic Microscope (SAM) was utilized once again on the damaged cores to capture the proppant behavior and damage mechanisms on the cores surfaces.

15. As the final step, the profilometer was used to quantify the embedment depths and profiles.

3.2 Nanoindentation

Nanoindentation technology was developed in the mid-1970's and went through great developments in the 1990's. The technology has always been used for the material and science industry. It is now being used in the oil and gas industry to obtain mechanical property values. The nanoindentation tool is capable of generating two of the more important parameters required for hydraulic fracturing designs, Young's modulus and hardness. These values are generally calculated and generated through logs and acoustic measurements. However, due to the success of nano scale measurements in material science and motivation and interest in finding more direct ways to measure these critical mechanical properties, nanoindentation was introduced to the petroleum industry (Prasad et al., 2009 and Prasad, 2010). Nanoindentation was used in this project to investigate the Young's modulus (E) and hardness (H) changes in the Niobrara formation due to fracturing fluid exposure and to understand any associated embedment. The nanoindenter used is very similar to regular hardness tests, however, it does not require the measurement of a surface area. The data are obtained and recorded automatically from a complete cycle of loading and unloading. The biggest advantage this technology has for measurements is its sample

size capability. The rocks that are being indented can be as small as drill cutting chips, which is a major advantage for measuring rocks from reservoirs.

3.2.1 Nanoindentation Device and Technology

The nanoindentation device used in this work to measure Young's modulus and hardness values of the Niobrara cores is called the MT'S Nanoindenter XP (shown in Figure 3.1) and is located in the Colorado School of Mines' Material and Science Department. This specific device and the calculation methods that are built in the software are based on research done by Oliver and Pharr, (1992) and then reviewed and improved by Agee, (2009). The equations shown in this section are taken from both of these papers. The nanoindentation device is similar to a hardness test in that a rigid probe is pushed into the surface of a material. Traditional hardness tests return one value of hardness at a single penetration depth or force, and for most techniques, the calculation of this single value measurement requires the area of the residual hardness impression to be measured either optically or by microscopy (Agee, 2009). However, the Nanoindenter XP technology is very advantageous because it continuously records the force and displacement measurements through depth sensing as the force is being applied to the surface of the material through the tip, which is in this case a Berkovich (diamond) tip (Abousleiman et al., 2009). The tip can vary in its shape but the Nanoindenter XP uses the Berkovich (three-sided pyramid). Through the continuous and automatic force-displacement data, area is also obtained, therefore no physical measurement of the area is required (Oliver and Pharr, 1992).

The measurement process starts by placing and mounting the samples in the sample chamber. Then specific values for the displacement and force in addition to numerous other critical properties are assigned for experiments including number and location of indents to be run on each sample. The indent then approaches and penetrates the sample with a continuous force.
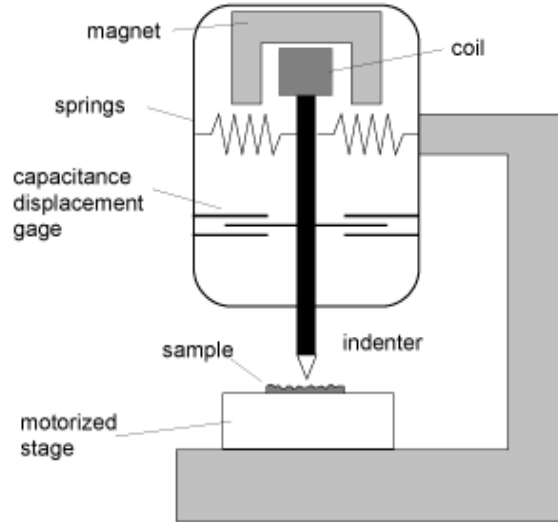
Figure 3.1: Image representing the nanoindenter used for the project. The main components are shown in the figure. The Indenter shown is a Berkovich tip which penetrates into the sample (Cornell University, 2010).

The penetration process continues until either the maximum assigned load or maximum penetration depth is reached. When either of these occurs, then the first cycle is claimed to be complete which is also known as the loading cycle. After the loading cycle, a constant force is applied to the sample for a short period of time which is determined and assigned by the user prior to starting the experiment. This time is called the dwell time which is implemented for materials that experience small amounts of creep (Agee, 2009). After this dwell time period, the indenter goes to the unloading cycle which happens at the same rate as the loading. For this entire loading and unloading process, the force and displacement are continuously recorded (Agee, 2009). These data are then used to derive Young's modulus, hardness and toughness values which are explained later in this section. Assumptions made to utilize this device are using a constant poisson's ratio for all the indentations and also same contact radius due to having the Berkovich tip.

Once a full loading and unloading cycle is complete, a graph similar to Figure 3.2 is plotted by the software for each indent. Since the instrument records all data during the loading and unloading cycle, both hardness and Young's modulus are automatically calculated (Agee, 2009). In addition to these two

properties, the software offers a wide range of different properties that can also be plotted using the same recorded data.
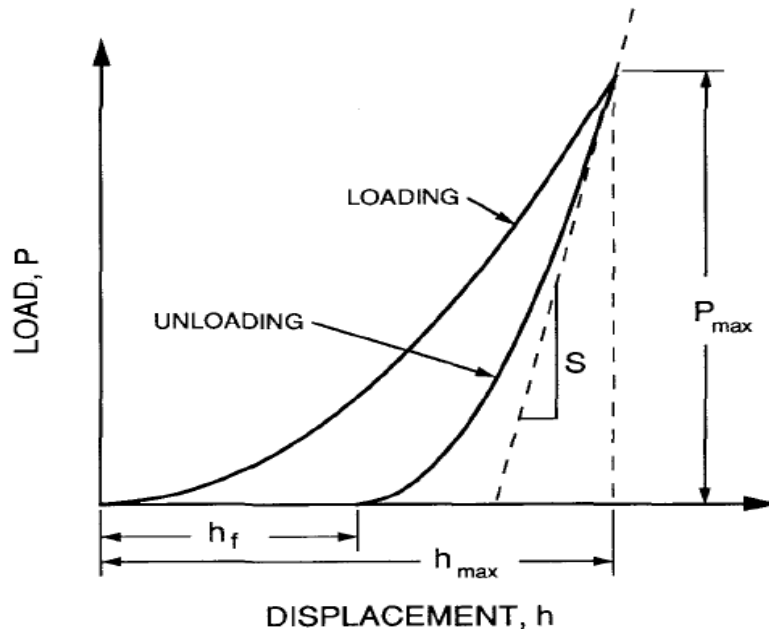
Figure 3.2: A schematic representation of load versus displacement data for an indentation experiment. The image can also be referred to as a typical displacement curve. The image shows the stiffness, the maximum load, and the maximum height can be obtained from the curve (Oliver and Pharr, 1992).

The analysis built in the software is based on a study done by Doerner and Nix, (1986) which then was extended and improved by Oliver and Pharr, (1992 and 2004). Contact stiffness (dP/dh), maximum load (P_{max}), maximum displacement (h_{max}) and the contact area are the main parameters that are used to calculate E and H. These values except the area are recorded and used to make the plot shown in Figure 3.2 and also can be obtained from the plot.

At the unloading stage when the indenter just begins to withdraw from the material, the relationship between force and displacement is quantified and called Stiffness (S). S represents the slope at the maximum displacement as shown in Figure 3.2 (Agee, 2009). Equation 3.1 expresses the relationship between the force (P) and displacement (h) for the unloading cycle only.

$$P(h) = \alpha(h - h_f)^m \qquad\qquad (3.1)$$

Where, $P(h)$= Load
                                            α = Power law fitting constant
                                            h = Total penetration depth
                                            h_f = Depth of residual impression after withdrawn of probe
                                            m = Power law fitting constant

Since S is the slope, it can be obtained by taking the derivative of P with respect to h. Thus it can

be expressed as shown in Equation 3.2.

$$S = \frac{dP}{dh} \int h = h_{max} = \alpha m (h_{max} - h_f)^{m-1} \qquad (3.2)$$

Where, S = Stiffness

In this equation, h_f represents the depth of residual impression after the probe has fully withdrawn

from the sample, and m and α are best fit constants found by fitting Equation 3.1 to the data in the

unloading segment of a DSI test on a reference material (Agee, 2009). After these constant parameters are

calculated, Equation 3.2 can be solved.

Since all these parameters are measured by the contact that the indenter is making with the

sample and all measurements are taken at the contact, the contact area becomes significantly critical and

essential to all measurements. The contact area can be calculated from contact depth and the geometry of

the indenter being used. The geometry can vary, but for this project the tip is a Berkovich geometry which

is a three-sided pyramid and its area can be defined as shown in Equation 3.3

$$A_c = 24.56 h_c^2 \qquad (3.3)$$

Where, A_c = Area of Berkovich indenter
                                            h_c = Contact Depth

The most difficult part in the area calculation is determining the height parameter due to the

indenters positioning and penetration status. Figure 3.3 gives an accurate representation of a sample and

indenter and their positioning. The h_c, which is the value used in the area calculation, is called the contact

depth (depth which the diamond makes contact with the material). h_c can also be explained as the

difference between the total penetration depth (h) and the displacement of the sample surface (h_s). The equation relating these parameters to one another is given with Equation 3.4.

$$h_c = h - h_s \qquad (3.4)$$

Where, h_s = Displacement of sample surface
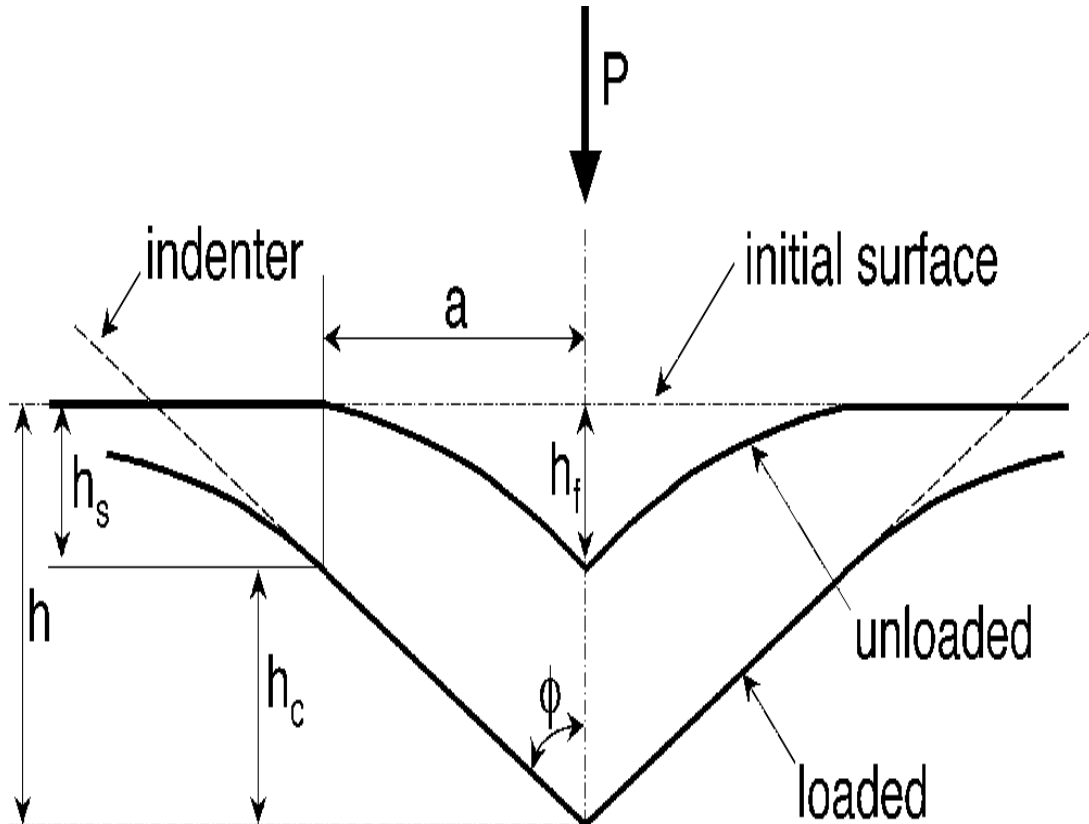
Figure 3.3: A schematic representation of sample's reaction to the load applied by the tip. All parameters from Equation 3.4 can be seen in this image. The image also shows the height associated with the positioning when the load is completely taken off the tip. φ will change depending on the geometry of the tip being used. This image also shows that once the tip penetrates into the sample, only a part of the tip is contacted with the sample. This contact area is the area calculated in Equation 3.3 (Oliver and Pharr, 1992).

After obtaining area, hardness can be calculated by using P_{max} and A_c as shown in Equation 3.5.

$$H = \frac{P_{max}}{A_c} \qquad (3.5)$$

Where, P_{max} = Maximum Load
                                H = Hardness

In order to calculate the Young's modulus (indentation modulus), a value called reducible modulus (E_r) which is related to S (contact stiffness) and area first needs to be calculated. E_r is defined by Equation 3.6.

$$E_r = \frac{\sqrt{\pi}}{2} \frac{S}{\sqrt{A}}$$ (3.6)

Where,
$\quad E_r$ = Reducible Modulus
$\quad$ A = Area

Taking the E_r originally defined by Oliver and Pharr, Equation 3.6 can be rearranged and it will yield to the indentation modulus (E_{IT}) which is can be described as shown in Equation 3.7.

$$E_{IT} = (1 - v_s^2) \left[\frac{1}{E_r} - \frac{1-v_i^2}{E_i} \right]^{-1}$$ (3.7)

Where,
$\quad E_{IT}$ = Indentation Modulus
$\quad v_s$ = Sample Poisson's ratio
$\quad E_i$ = Indenter Young's modulus
$\quad v_i$ = Indenter Poisson's ratio

Now substituting E_r in to Equation 3.7 will yield a new E_{IT} described as shown in Equation 3.8.

$$E_{IT} = (1 - v_s^2) \left[\frac{2}{S} \sqrt{\frac{A}{\pi}} - \frac{1-v_i^2}{E_i} \right]^{-1}$$ (3.8)

3.2.2 Determination of Nanoindentation Results

Nanoindentation in this project was used to measure the Young's modulus and hardness of Niobrara cores. 0.60 inch length cores were cut from the main cores for nanoindentation purposes. These pieces were polished to 1 micron on the nanoindented side and 200 mesh on the other side. In order for samples to be polished down to 1 micron, they went through a 5 step gradual polishing process (details given in supplemental file E). Nanoindentation measurements were taken when the cores were dry and also after they had been soaked for 5 days, 15 days and 30 days. The purpose for doing this was to investigate how the H and E changed with various fluids and as time progressed.

43

The polished cores were inserted into the nanoindentation chamber and glued to the aluminum sleeves for measurements. Figure 3.4 is an image taken before a nanoindentation run. The transparent sample is the silica which has to be run in every experiment for calibration and control purposes.
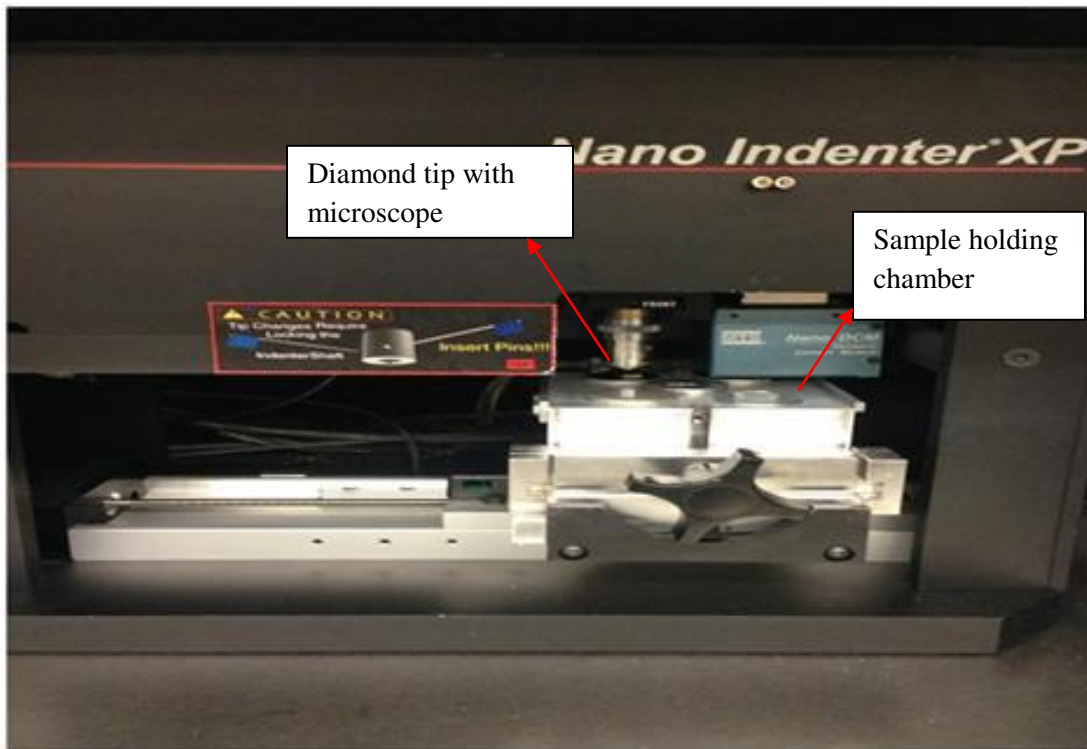
Figure 3.4: Image representing the nanoindenter located in the materials and metallurgy building. The rectangular chamber on the right side is where the samples are placed. The diamond tip which is attached to the microscope right above the chamber measures the mechanical properties of the samples.

Each sample is subjected to 25 indentation runs to eliminate possible erroneous values and heterogeneity effects and obtain more accurate, and representative values for H and E. 25 indents are achieved with a 5 X 5 array while also minimizing the space between indents in an attempt to obtain measurements within a more homogeneous zone while still preventing the indents from interfering with each other. Figure 3.5 is a representation of a core surface with all the spacing dimensions. All indentation depths are 500 nm into the core surface, and all indents are separated by 100 µm both in the x and y directions. 100 µm was picked for a spacing value, because a minimum of 50 µm spacing is required in between indents in order to prevent interference effects. The interference effect occurs when two created

indents make contact with each other at 500 nm. Any values that are above 100 µm were not selected due

to indentations not being able to stay in flat zones for spreading over a larger area.
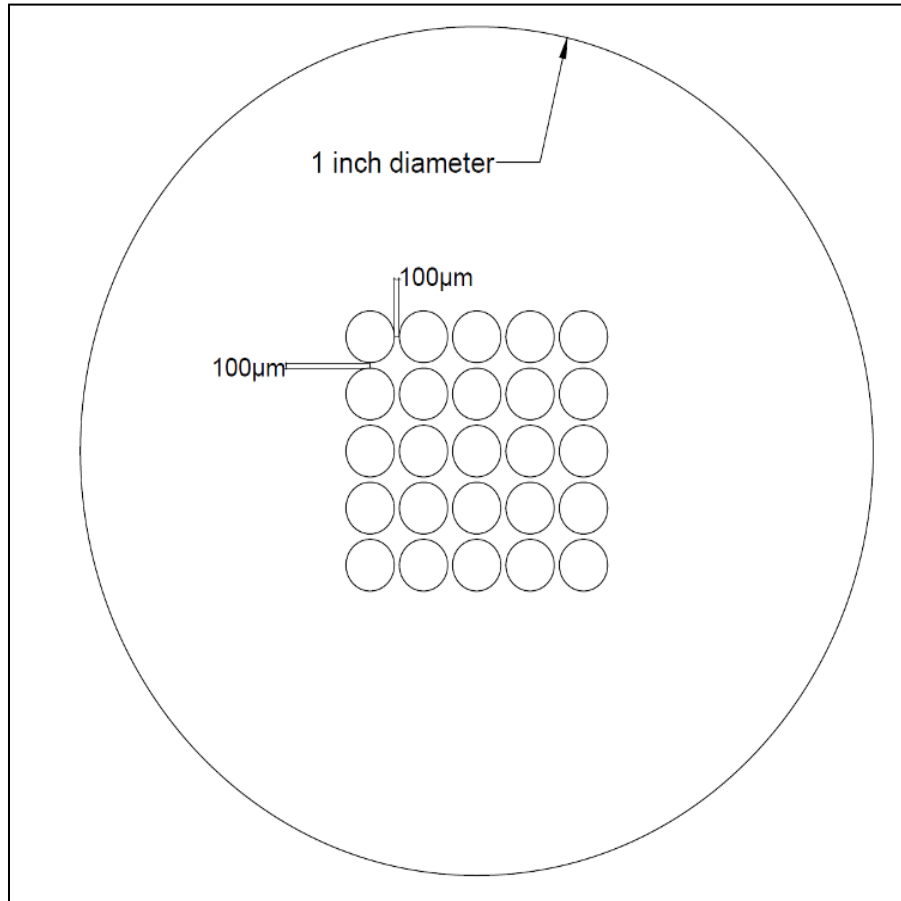
Figure 3.5: Image representing the nanoindentation area (5X5 array) on the core samples surface (1.0 inch). Each indent penetrates 500 nm in to the cores's surface. The core surface area is approximately 3.14 in^2 and the nanoindentation area is approximately 3.8E-10 in^2. Figure is not to scale.

These measurements were taken for a total of six different cores at different depths. Each core

was run through the nanoindentation process a total of four times and each time had 25 indentations, thus

each core was subjected to 100 indents. Since the dependence of Poisson's ratio is very weak on the

mechanical property measurements (Agee, 2009), a Poisson's ratio of 0.219 was used for all samples. The

value 0.219 was selected after looking at core data provided by CoreLab. Since the goal of this project is

to compare the mechanical properties of the Niobrara shale cores before and after saturating them with

fracturing fluids, the usage of the same Poisson's ratio for each sample is acceptable.

3.3 QEMSCAN

The quantitative electron Microscope Scanner (QEMSCAN) is a fully automated SEM based on a mineralogy and petrography electron beam image analysis tool. QEMSCAN performs and provides rapid and accurate quantitative analysis of minerals, rocks and man-made materials on the basis of an automated point counting. The associated iDiscover software allows for the automated stepping of the electron beam across samples at a user-defined pixel resolution (between 1-40 µm). By mapping the sample surface with high magnification, textural properties and contextual information such as particle and mineral grain size and shape, mineral associations, mineral liberation, elemental deportment, porosity and matrix density can be captured and reported numerically. The QEMSCAN system used in this work can be found in the EM (Electron Microscope) Laboratory which is located in the Department of Geology and Geological Engineering at the Colorado School of Mines.

3.3.1 QEMSCAN Device and Technology

The device contains a custom-built electron-beam platform equipped with four energy dispersive X-ray spectrometers (EDS) for mineral and compound identification within a wide range of sample types. After defining the user-desired pixel resolution for the scanning, at each pixel a low count EDS is generated to provide information on the elemental composition at each measurement point. In addition to EDS, the device also collects Back-Scattered Electrons (BSE) in order to differentiate between the epoxy being used and the minerals. From the acquired spectrum and data, elements are identified by comparing them to a library of reference spectra which is based on the combined information gathered from EDS, BSE and elemental intensities, then they are quantified and the minerals are identified. Once the minerals are identified, they each get assigned a color and this produces a false-colored image. QEMSCAN provides quantitative mineralogical and textural data, false-color mineral maps, and robust statistical data that can be used to quantify a variety of important variables. Some of these variables are as follows:

- Highly accurate mineral (phase) abundance maps

- Element X-ray mapping

- Particle and grain size

- Particle and grain shape

- Mineral associations

- Lithotyping

- Porosity quantifications

- Organic matter scans

- Mineral (phase) liberation

QEMSCAN has the ability to quantify and provide all the information above very accurately and precisely. It can provide these parameters from a diverse array of sample types which including:

- Standard thin sections (27 X 46 mm)

- 30mm and 25mm epoxy mounts

- Rough rocks and polished rock slabs (Max dimensions: 7.5 X 10 X 2 cm)

In order for QEMSCAN to deliver these parameters at a very high quality, accuracy and precision, it needs to be equipped with top of the line, components which contain exceptional features and specifications. These features include:

- Four Bruker X275HR silicon drift energy dispersive X-ray spectrometer (EDS)

- Carl Zeiss EVO50 platform (SEM)

- One four-quadrant semiconductor diode backscatter electron (BSE) detector

- One secondary electron detector

One of the most important things to remember while using the QEMSCAN mineralogy data is that the samples are being carbon-coated while being prepared for scanning. Thus carbon may be detected in samples even though the samples may not contain any carbon naturally. The QEMSCAN also assigns

colors due to chemical weights of the elements, thus heavier elements like pyrite or iron (Fe) originally get assigned brighter colors whereas calcite is represented with a very dark gray/black.

3.3.2 Determination of QEMSCAN Results

QEMSCAN'ing was the first step for this project. In order to save time and continue with the experiments more efficiently, small parts (0.2 inch length) were cut off from three different cores provided by one of the sponsor companies. These cores were picked based on their TOC content. The three cores that were picked had the lowest, highest and the median TOC values of the available samples. Thus data obtained by the QEMSCAN imaging represent a TOC and mineralogy variance for the cores that were used for the project. The parts that were cut were given to EM laboratory where they were epoxied, polished and carbon-coated.

Mineralogy and a porosity scans were run for the three samples. Mineralogy scans were run on an area of 1 x 5 mm and analyzed at a resolution at 2.5 µm. Porosity scans were run for an area of 10 x 10 mm and analyzed at a resolution at 2 µm. Detailed operating conditions, including technical specification for the samples, were provided by the EM lab as follows:

For the samples in this project, the QEMSCAN with four energy dispersive X-ray spectrometers (EDS) acquired spectra from each particle with a beam stepping interval (i.e., spacing between acquisition points) of 7 µm for the modal abundance and the organic matter scan, and of 2 µ for the porosity scan, an accelerating voltage of 25 keV (modal abundance and porosity scan) and of 15 keV (organic matter scan), and a beam current of 5nA. Interactions between the beam and the sample were modeled through Monte Carlo Simulation. The EDS spectra were compared with spectra held in a look-up table allowing an assignment to be made of a composition at each acquisition point. The assignment makes no distinction between mineral species and amorphous grains of similar composition. This procedure allows a compositional map of the particle to be generated. Results were output by the QEMSCAN software as a spreadsheet giving the area percent (wt.%) of each composition in the look-up table. These results are

semiquantitative because the area percent of each composition was calculated from the compositional assignments (rather than the original EDS spectra) using an approximate stoichiometry for each composition for rapid compositional identification rather than detailed compositional analysis (for which other techniques are more appropriate).

The dimensions for mineralogy and porosity were picked because they gave a great idea of the mineralogy and porosity of the samples at a detail that the project needs, while at the same time they are still time and cost effective.

3.4 Scanning Acoustic Microscope (SAM)

A SAM (Scanning Acoustic Microscope) is utilized in this research to capture core surface images before and after stress is applied on them while they were loaded with proppants. Tools similar to SAM have been used to identify lithology, pore space, interconnectivity of pores, grain size, and cementation which all control seismic wave velocity and attenuation. In addition to these properties, the SAM can also quantify microstructure as variations in acoustic impedance (Prasad, 2001). Via SAM the deformation on cores's surfaces and proppants as well as embedment can be investigated for each proppant type. SAM is a vital tool for investigating delaminations that are down to a micrometer thickness as well as any inhomogeneity in the subsurface (Prasad et al., 2009).

3.4.1 SAM Device and Technology

Ultrasonic waves are sensitive to local variations in elastic properties and therefore very suited for characterizing microstructural properties of reservoir rocks. Reflections from impedance boundaries in grains and between interfaces in the sample are used to construct the microstructural image. This section explains how the device and works. The specific SAM device that is used in this research is located in MZ 105 in Marquez Hall. The device's rights are held by SAM TEL and Kramer Scientific Instruments, and it operates with the WINSAM software.

Acoustic microscopy is very similar to seismology in its basic principles. The scanning acoustic microscope investigates the surface and subsurface of objects in the basis of the reflected acoustic waves, that is, on the impedance changes in the sample (Prasad, 2001). The sound waves are either transmitted through the sample or reflected back to the receiver. The resolution, penetration, frequency and other certain parameters can be controlled and adjusted for the desired quality of the image. A generalized representation of SAM is shown in Figure 3.6, and it consists of three main units:

1) The Acoustic and Scanning Unit:

- Transducer to generate and receive acoustic waves

- A sapphire rod that acts as a wave guide

- A sample stage that can move in x, y, and z direction

- A cavity at the bottom of the sapphire rod that focuses the waves though a coupling fluid (distilled water)

- Together the transducer, the sapphire rid, and the coupling fluid are referred to as the acoustic lens

2) The Pulse Generator and Receiver Unit:

- A high-frequency pulse generator that emits short pulses to excite the transducer and a receiver that amplifies and records the signals received by the transducer

- A switching device separating transmitted and received signals

3) The Image Handling and Storage Control Unit:

- Monitor

- Image storage that allows stage manipulation and transforms electrical signals from the transducer into a gray- or colored scaled image.
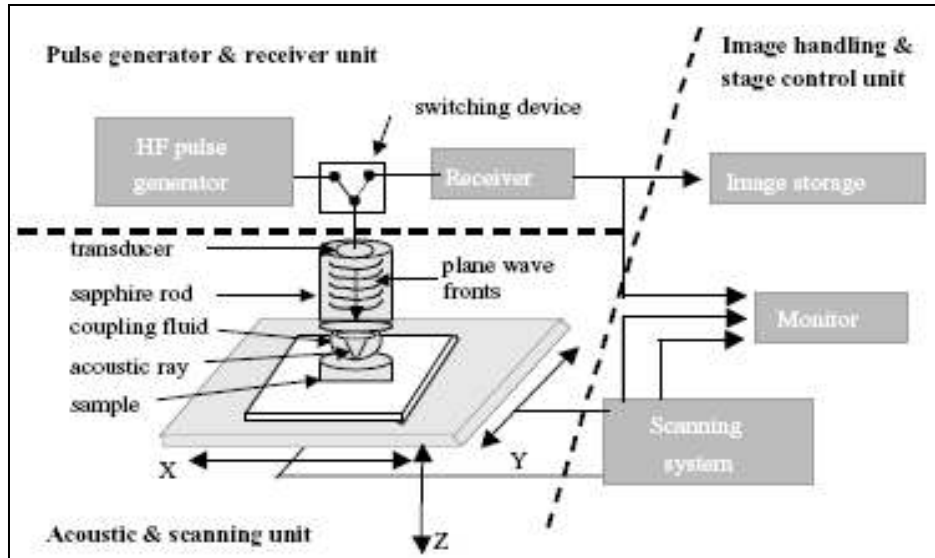
Figure 3.6: Image representing the three main units of SAM. The waves are generated from the transducer which then goes through the sapphire rod. Some of these waves get reflected and some of them get transmitted through the samples. Images are created by the waves that get reflected and return to the receiver where they are converted into electrical signals (Prasad, 2001).

Acoustic waves are either transmitted or reflected. The reflected waves get back to the sapphire rod and into the receiver located in the transducer. Here the acoustic waves are converted to electrical signals. Then the image handling and storage central unit transforms these electrical signals into gray or color scaled images based on their amplitudes (Prasad, 2001).

3.4.2 Determination of SAM Results

SAM was used to investigate the same cores that were saturated with certain fracturing fluids, which were also subjected to nanoindentation for Young's modulus measurements. In order for the cores to be successfully scanned, one side of the cores was polished to one micron and the other side to 200 mesh. The four fracturing fluids used in the project each had two sets of different samples submerged in them. Two 1.0 inch diameter and 0.40 inch length cores were cut from all these samples as seen in Table 3.1. In order to test the fracturing fluid effect, the samples that are saturated with the same fluids were combined, thus each fracturing fluid had a total of four cores (two from each sample) to be scanned and tested with proppants. This allowed two different types of proppants to be tested for each fluid. In addition, eight more cores were retrieved from Samples 9 and 10 shown below to test the heat effect on

the Niobrara shale Young's modulus alteration and proppant embedment. Table 3.1 shows all the cores and fracturing fluids used to saturate or heat these cores. There were abundant and undamaged core pieces available from depth 6742.25, so this depth provided enough cores for three different experiments.

Table 3.1: Important Mineralogy Characteristics of Chosen Samples

Ten Selected core depths from received cores and their important characteristics						
Sample #	Depth	Fracturing Fluid	TOC	Calcite	Porosity	Clay
	ft		%	%	%	%
1	6606.8	Freshwater	2.18	92.73	0.60	1.70
2	6742.25	Freshwater	2.89	88.85	1.00	7.90
3	6742.25A	2% KCl	2.89	88.85	1.00	7.90
4	6639.85	2% KCl	2.75	67.30	5.00	6.10
5	6742.25B	KCl+friction reducer	2.89	88.85	1.00	7.90
6	6772.25	KCl+friction reducer	1.33	84.00	6.00	4.40
7	6788.65	Freshwater+KCl substitute	2.82	87.70	1.00	4.30
8	6777.75	Freshwater+KCl substitute	2.70	87.90	5.50	3.30
9	6606.65	Heated with Freshwater @ 180°F	2.18	92.73	0.60	1.70
10	6764.2	Heated with KCl @ 180°F	1.28	92.63	0.70	3.50

A C-scan image was taken for each of these cores before and also after they were pressured up to 3030 psi with proppants placed in between them. This investigated how proppants affected and deformed the Niobrara shale's surface and how the deformation varied with changing fracturing fluids and proppant types.

Images of the cores that were saturated with H_2O and H_2O+KCl substitute were taken while the cores were submerged in water. The cores saturated with KCl and KCl+friction reducer were also taken while they were submerged in water, however, these cores were also coated with clear nail polish to prevent water invasion and alter the effects of KCl on cores. Properties such as frequency magnitude and sign, velocity, and depth of investigation can be adjusted and assigned in order to capture the best possible image.

For all samples four different images are taken. These are 125 positive, 125 negative, 1000 positive, 1000 negative, where the number represents the magnification and the sign represents frequency of the scan. The most clear and visible image out of these four images was selected for the use of proppant and fracture surface comparison before and after applying force on the cores (described in Section 3.5).

3.5 High Pressure Press

A high pressure press was targeted to be used in this research. This is one of the more vital parts of this research, as it helps to separate it from previous research in this area (Akrad et al., 2011). Akrad et al., (2011) only reached pressures up to 40 psi while testing proppants. The new press helped to reach higher pressures and allowed experimenting with more realistic stress profiles for testing the proppant embedment so that the results could be a better representation of actual fracturing treatments.

3.5.1 High Pressure Press Technology

This research uses the press located at MZ 103 in Marquez Hall. The machine is made by Carolina Tool and Equipment. The machine is built in an A-Shape steel form and is hydraulically operated. There are two main rods that control the hydraulics. These rods increase the pressure in the system which pushes down the main steel pipe attached to two springs (see Figure 3.7). It is via this steel pipe that the machine applies pressure values up to 50 tons.

The press is very user friendly and simple to operate. One of the necessary pieces of equipment is a big leveled steel frame that sits underneath the steel pipe which applies the load and attached to two springs. Once everything is in place, the rod on the left is cranked for a rapid increase in pressure. When the steel pipe is lowered enough to touch the experimental setup to be pressurized, then the rod on the right is used for more accurate and slowly applied pressure increase. Once the pressurizing the core chamber is completed, the valve by the rods is opened to release the pressure and the springs assist the steep pipe to return to its original position.

Figure 3.7: Image showing the high pressure press. The steel pipe moves down and applies pressure to any component that is placed on top of the rails. Rods on the right side are cranked, and the steel pipe moves down via the springs. The gauge shows the amount of pressure applied once the steel pipe makes contact with a surface.

3.5.2 Determination of High Pressure Machine Results

The same cores used for the SAM were used for the proppant testing in the press in order to obtain both before and after applied pressure SAM images. Each fluid sample was used to saturate four individual cores from two different depths. In order to simulate subjecting the proppants to high pressures in fractures, the cores from the same depth were paired up, which allowed two different types of proppant

54

to be tested for each fracturing fluid. In addition to saturated samples, a total of eight cores were saturated and heated with freshwater and KCl which also were subjected to pressure to test proppant embedment.

A unique set-up was designed and used in order to accurately and safely place and pressure the proppants in between the core halves (shown in Figure 3.8). A rectangular metal piece was placed on the bottom and a smaller square piece that contacts the steel pipe was used. The brass rod, which actually touches the core on the top and transfers the pressure, was shortened to three inches. The hollow steel pipe was cut to two inches in length and had its inside diameter reduced. The inside diameter of the pipe was reduced so that the two cores with proppants in between them as well as the brass rod fit comfortably inside it and applied the desired pressure. The inside diameter was cut to be large enough, so that samples would not get stuck after pressuring and small enough, so that the stress was contained in the vertical direction as much as possible.

Since the cores are pressured in confined stress. Pressure in the vicinity of 3000 psi was the goal to achieve given the depths of Niobrara samples are around 6500 ft. In order to achieve this pressure in the press, the isotropic stress equation is used. The equation and assumptions are shown below in Equation 3.9.

$$\sigma_h - \alpha\sigma_P = \frac{v}{1-v}(\sigma_v - \alpha\sigma_P) + Tectonic\ Stress \qquad (3.9)$$

Where,
σ_h = Horizontal stress
α = Biot's constant
σ_P = Pore Pressure
v = Poisson's ratio

Equation 3.9 is used to calculate how much of the applied stress through the press is actually transferred to the cores and proppants in between them. The pressuring chamber shown in Figure 3.8 is a closed but unconfined setup, thus there will be some stress generated in the perpendicular direction from the total stress applied. Tectonic stress was disregarded and the Biot's Constant was assumed to be one.

55

The goal was to obtain a pressure on cores, thus proppants of approximately 3000 psi. This number is picked due to the depth of the cores and the location of the field. Equations 3.10-3.12 show how the pressure is calculated.

Where,
$$\sigma_h = \frac{v}{1-v}(\sigma_v) \tag{3.10}$$

$$\sigma_v = \frac{Force\ Applied}{Area\ of\ Core} \tag{3.11}$$

$$Actual\ \sigma_v = (\sigma_v - \sigma_h) \tag{3.12}$$
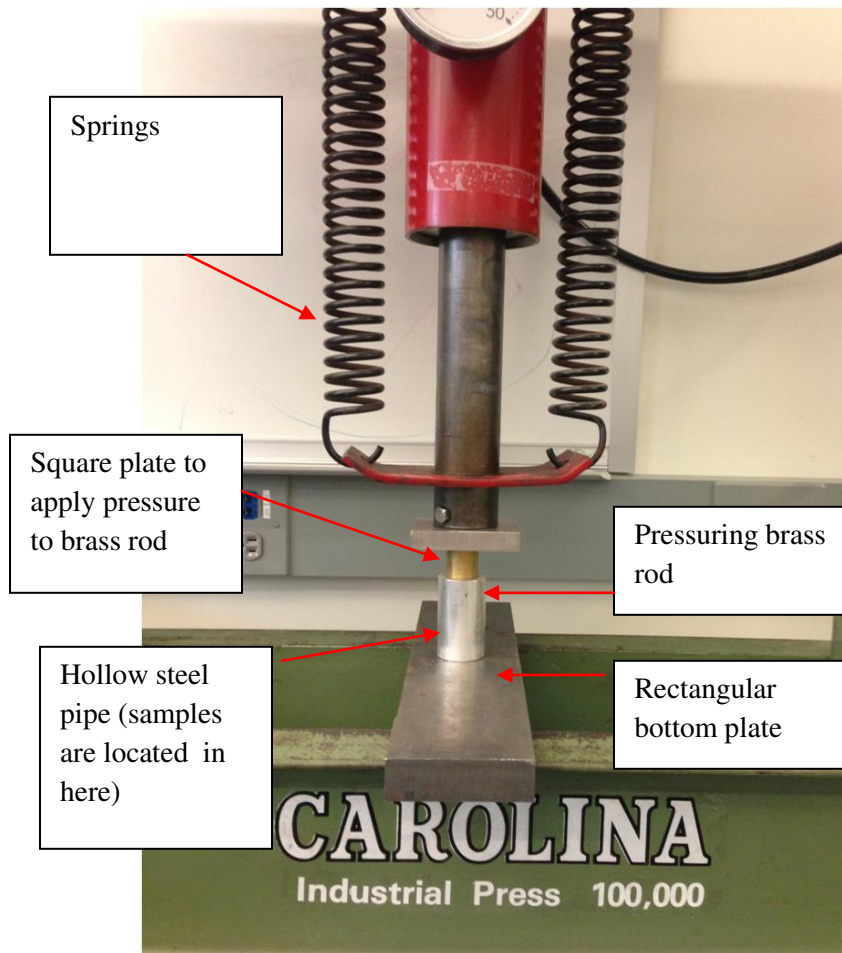
Figure 3.8: Image showing the setup for pressuring the cores. The cores are located inside of the metal pipe and pressured in between the brass road and the big rectangle metal piece.

The load applied is calculated with Equation 3.11. Given the area of each core being equal, load that had to be applied was 3307 pounds (1.5 tons since the press machine has units in tons) which yielded

4210 psi when it was distributed along the core surface area. Equations 3.10 and 3.12 show how the applied load is related to actual pressure values that affects the cores and proppants. The process was basically a back calculation by coming up with a field representative stress then calculating the load that had to be applied by incorporating the isotropic stress equation due to the unconfined chamber.

3.6 Profilometer

By definition, a profilometer is a tool that measures roughness and deformations of a given surface by looking at the topography of that surface. The profilometer in this research was specifically selected due to its accurate measurements on rocks, its ease of use and access. It was the best available tool for quantifying proppant embedment.

3.6.1 Profilometer Technology

The profilometer used in this research is a Tencor P10 and located at the Department of Physics at Colorado School of Mines. The profilometer consists of a closed box where the sample is set on a circular tray and a small micron scale range stylus tip which is attached to a motor. This tip is lowered until it makes contact with the sample. Once contact is made, the measuring process begins.

Prior to the tip starting to take the topography profile of the surface, the user defines various parameters such as load, velocity, resolution and, image quality. After these parameters are defined, the tray that holds the sample moves underneath the stylus tip as a constant load is applied on the sample. As the tip moves along the sample surface, it detects deformations and thus variations in vertical depth. This allows us to obtain embedment width in additional to embedment depth.

The camera attached to the stylus tip allows the user to see the surface in detail before the measurements is run. The user can also pick a designated length to be measured by isolating a specific spot on the sample surface by utilizing the camera. An image of a core surface representing grains and the embedded spot is shown in Figure 3.9 (a), and the graph representation of this embedded spot is shown in Figure 3.9 (b).
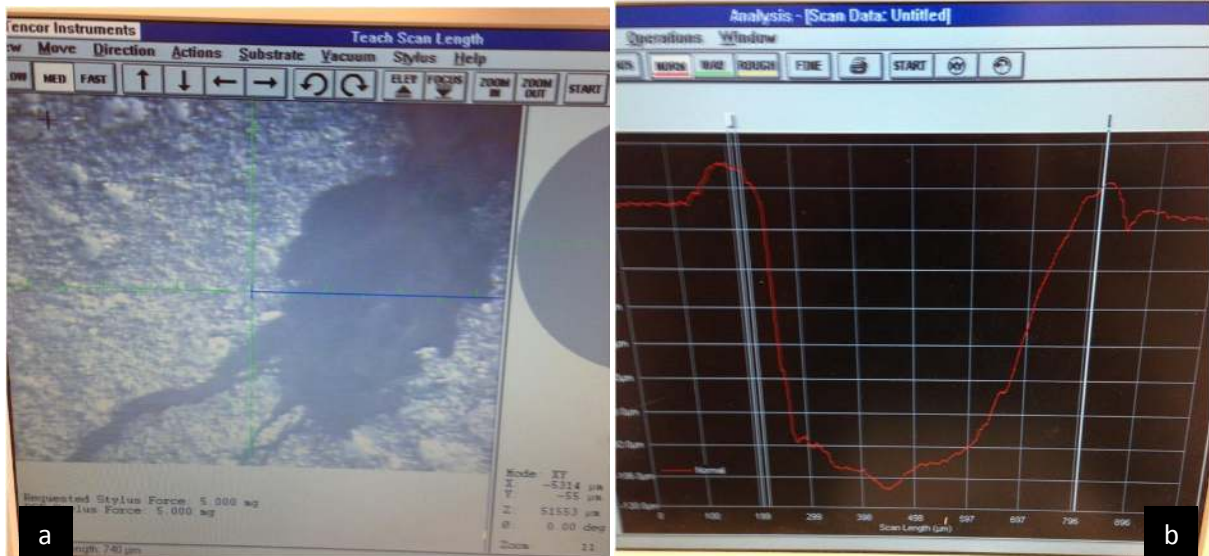
Figure 3.9: (a):Image of a core showing embedded and non-embedded parts on the core. (b): Graphical representation of the same embedded zone.

3.6.2 Determination of Profilometer Results

The profilometer was only used after the cores were subjected to pressure with proppants between them. Since two tests were assigned to each of the four fracturing fluids (samples 1-8) and the two heating experiments (samples 9 and 10), a total of 24 cores were tested under the profilometer after pressurizing. It is important to note that bottom and top cores for each sample that were named as Test #1 top core, etc. For example KCl+friction reducer Test #1 refers to embedment results for Sample #5 on the top half. In order to capture if top and bottom cores experience varying embedment profiles, cores were named as top and bottom and had individual measurements. Refer to Table 3.1 to see all the cores used in detail.

Proppant distribution along the surfaces were random, and due to not having a perfectly flat pressuring rod, the pressure distribution was not even on the core surfaces thus the proppant embedment on surfaces was also very varying even in one core. Taking this into consideration, 18 different embedment measurements were taken on each core at different spots. The readings were definitely varied for each core, however, the results showed a trend on the fracturing fluid and proppant type. These 18 different readings were than averaged to report a specific embedment value for each core. A detailed table of all embedment values is reported in Chapter 5.

CHAPTER 4

TEST RESULTS

As discussed, the Niobrara shale formation is located mostly in the Rocky Mountains and extends to northwestern Kansas and southwestern Nebraska. The major producing region of the Niobrara is located in the DJ-Basin and the Wattenberg field is the main producing area. The core samples used in this project all came from the Marathon Oil Company wildcat Crow Valley 7-62-32-1M well located in Weld County, Colorado, from a depth ranging from 6606.00' to 6834.50'. Ten cores from this depth range were selected for the research project. Eight (four original and four for expansion) cores were selected to be saturated with four fracturing fluids at room temperature and two additional sets of cores were heated to 180° and exposed to freshwater and KCl for five days. It is important to note that, due to lack of core samples, some of the cores used for different fracturing fluids are from the same depth.

Mineralogy contents and TOC values were provided by StimLab for all the cores and the initial selection of cores, for the experiments were made based on this data set. The core selection was made in such a manner that experiments could be conducted for samples with varying mineralogy. Maximum, minimum and median calcite percentages were picked first, and these samples were used for QEMSCAN imaging. Remaining of the samples were picked regarding their high calcite content and TOC values. Combining highest calcite content with a reasonable TOC range yielded the cores in Table 4.1 as the final selection for testing. Samples numbers 1, 3, 5, and 7 are the four original samples, Samples 2, 4, 6, and 8 are the expansion samples, and Samples 9 and 10 are the heated samples.

The mineralogy information given in Table 4.1 is a mixture of StimLab provided data and QEMSCAN results. Although all cores used in this project are from the same well, there are some variations in their mechanical properties and mineralogy as seen in Table 4.1. This variance in values and properties is due to the Niobrara's highly heterogeneous nature (especially vertically).

Table 4.1: Important Mineralogy and Mechanical Characteristics of Chosen Samples

Ten Selected core depths from received cores and their important characteristics								
							DRY	
Sample #	Depth	Fracturing Fluid	TOC	Calcite	Porosity	Clay	Young's Modulus	Hardness
	ft		%	%	%	%	Psi	Psi
1	6606.80	Freshwater	2.18	92.73	0.60	1.70	7.16E+06	1.61E+05
2	6742.25	Freshwater	2.89	88.85	1.00	7.90	6.83E+06	2.31E+05
3	6742.25A	2% KCl	2.89	88.85	1.00	7.90	7.72E+06	2.38E+05
4	6639.85	2% KCl	2.75	67.30	5.00	6.10	6.67E+06	2.40E+05
5	6742.25B	KCl+friction reducer	2.89	88.85	1.00	7.90	7.67E+06	2.44E+05
6	6772.25	KCl+friction reducer	1.33	84.00	6.00	4.40	6.42E+06	2.05E+05
7	6788.65	Freshwater+KCl substitute	2.82	87.70	1.00	4.30	6.94E+06	2.00E+05
8	6777.75	Freshwater+KCl substitute	2.70	87.90	5.50	3.30	6.89E+06	2.70E+05
9	6606.65	Heated with Freshwater @ 180˚F	2.18	92.73	0.60	1.70	5.46E+06	1.09E+05
10	6764.20	Heated with KCl @ 180˚F	1.28	92.63	0.70	3.50	6.05E+06	1.71E+05

One of the most important things to keep in mind is that all experiments are done on 1.0 inch diameter core plugs from a well which is one of thousands of wells within the Niobrara formation. Thus, some of the values of measurements and properties may not fall within the expected and known ranges in the industry, because these are small-scale measurements coming from only one set of cores.

Results discussed in this chapter include mechanical property changes of two samples (Samples 1 and 2), before and after their exposure to freshwater. The results of other three original (Samples 3, 5, and 7) samples and expansion (Samples 4, 6, and 8) samples are reported in supplemental files A, B, and C. The results obtained from the two samples that were exposed to five-day heat treatments (Samples 9 and 10) at 180°F in freshwater and 2% KCl are discussed in Section 5.4.

It is important to state that Poisson's ration is mechanical property that has a relationship to Young's modulus. However the nanoindentation results vary by such an insignificant factor, that the Poisson's ratio for all the samples are taken as the same value. Thus it is very important to note that all samples were assumed to have a Poisson's ratio of 0.219 which was provided by StimLab to be the Poisson's ratio of most of the samples given including Samples 1, 2, 4, 6, 7, and 10.

Mineralogy and porosity QEMSCAN images were done for three different samples including Sample 1 (6606.8'), Sample 2, 3, and 5 (6742.25') and Sample 10 (6764.2'). Mineralogy images cover an area of 1 X 5 mm at a 2.5-µm resolution and porosity images cover an area of 10 X 10 mm at a 2-µm resolution. QEMSCAN results show very similar results for all three cores.

Three parameters were studied from the obtained nanoindentation results and are discussed in Section 4.2: the effect of temperature, the effect of time, and the most importantly the effect of different fracturing fluids on the change of Young's modulus. This was done by using the following workflow:

- Measure Young's modulus (E) and Hardness (H) on a small piece taken from each sample without any fracturing fluid exposure;

- Measure E and H on small pieces taken from Samples 1, 3, 5, and 7 after wetting them in their associated fracturing fluids for five days at room temperature;

- Measure E and H on the same small pieces taken from Samples 1, 3, 5, and 7 after wetting them in their associated fracturing fluids for 15 (additional ten days) days at room temperature;

- Measure E and H on the same small pieces taken from Samples 1, 3, 5, and 7 after wetting them in their associated fracturing fluids for 30 days (additional 15 days) at room temperature;

- Measure E and H on the small piece taken from Sample 9 after heating it with freshwater at 180°F for five days;

- Measure E and H on the small piece taken from Sample 10 after heating it with 2% KCl at 180°F for five days;

- Measurements of E and H at 5, 15 and 30 days were then repeated on small pieces taken from Samples 2, 4, 6, and 8 for expansion; and,

- Between one and three, 1.0 inch diameter and 0.45 inch length rock pieces were cut from each sample, to run SAM (Scanning Acoustic Microscope) and prepare for proppant embedment testing.

Once the nanoindentation measurements were complete, scanning acoustic microscope measurements were taken on these rock pieces to capture a picture of their surface before proppants placed in between and subjected to high pressure. Proppant embedment quantification was then done through the profilometer and images of embedment were captured via the SAM. Since all the samples are from the same well and have similar characteristics, results are shown for each fracturing fluid not for sample depths or numbers. The results for samples saturated with freshwater are also reported in this chapter. However, due to the substantial amounts of graphs that are very similar to each other, the results for the other three fracturing fluids are located in supplemental files A, B, and C.

Before starting experiments with the Niobrara cores, a trial experiment was run to see the results and also to optimize the experimental procedure. This trial experiment was run with a shale formation from Canada. Young's modulus results for a 5-day saturation test of this Canadian shale core are discussed in Section 4.1.

4.1 Canada Shale Trial Experiment

This trial experiment was run to experiment and get familiar with the measurement equipment, as well as, to validate the results of Phase 1. The Young's modulus reduction result obtained from the trial experiment validated the general Young's modulus reduction trends in Phase #1. Trial experiment showed that Young's modulus decreases when the rock is exposed to a fracturing fluid regardless of its mineral content. Figure 4.1 shows the Young's modulus values of the Canadian shale before and after saturation plotted against the nanoindentation numbers.
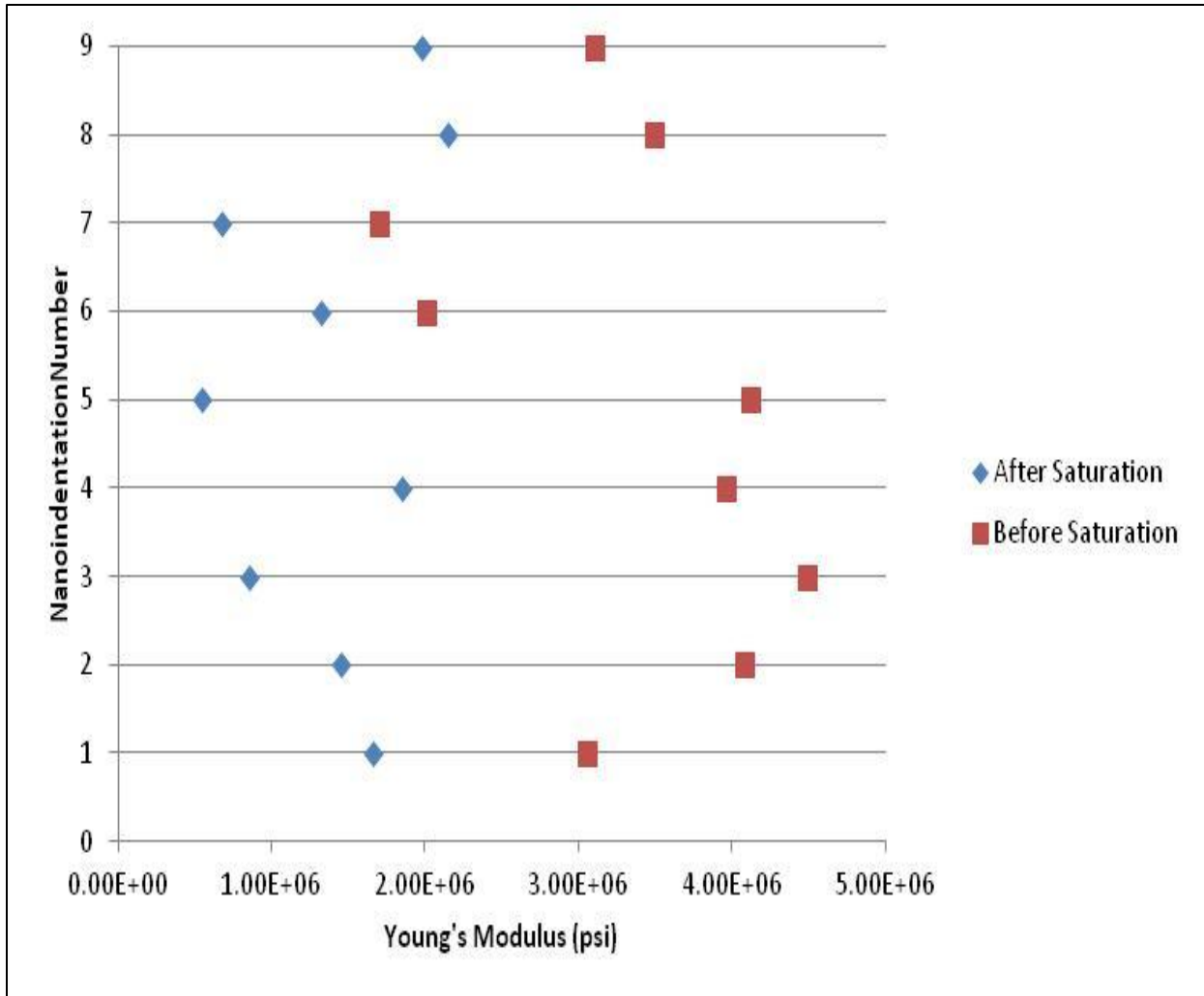
Figure 4.1: Nanoindentation results for the Canadian shale sample. Red dots represent the Young's modulus values before the sample was saturated with water for five days, and blue dots represent the results for the saturated version of the sample. It is very evident that there is drastic shift in the Young's modulus values due to saturation.

4.2 Nanoindentation Results of Freshwater Treated Cores (Samples 1 and2)

The first sets of samples are from 6606.8' (Sample 1) and 6742.25' (Sample 2). Sample 2 represents the expansion test for freshwater. The TOC of these samples are 2.18% and 2.89% respectively. Figure 4.2 shows the mineralogy of Sample 1 (6606.8'). It consists mainly of calcite at 92.73%. There are small amounts of pyrite (0.23%), quartz (0.18 %) and dolomite (0.04%) present. There is also a significant amount of mineral interphases which can be considered a combination minerals detected by the QEMSCAN.

Mineral Name	Volume %
Background	0.01
Calcite	92.73
Pyrite	0.23
Quartz	0.18
Chlorite	0.00
Alkali Feldspar (Na)	0.00
Plagioclase	0.20
Clay	0.01
Illite/Muscovite	0.02
Dolomite	0.04
Anhydrite/Gypsum	0.06
Rutile/Anatase	0.00
Apatite	0.03
Fe-sulphide-Carbonate boundary	3.65
Carbonate-Silicate interphase	0.58
Carbonate-Clay interphase	1.54
Carbonate-Illite/Muscovite interphase	0.15
Others	0.57

Figure 4.2: Mineralogy QEMSCAN image of the Sample 1 (6606.8'). This image shows that the core is predominantly made out of calcite (93%). It also contains various different minerals but all at very low percentages. Iron-carbonate and carbonate-clay interphase percentages have noticeable percentage values along with pyrite and quartz.

In addition to mineralogy QEMSCAN image, a porosity QEMSCAN image of Sample 1 was also obtained and can be seen as in Figure 4.3. Figure 4.4 shows the individual indents that were run on the surface of Sample 1 (6606.8'). There are only 17 indentation values available (18th is the average of the rest) on the figure as opposed to 25 which was the original number of indentations assigned to the machine for this sample as well as all other samples.

64

	Volume%
■ Porosity	0.08
■ Porosity+Mineral	0.47
■ Mineral	99.45

Figure 4.3: Porosity QEMSCAN image of the Sample 1 (6606.8'). QEMSCAN detects lighter minerals with darker beams. Thus the dark grey background color represents the calcite present in this core. The barely visible black and red dots represent porosity, this sample has a porosity of 0.6% which is very low.

The erroneous and inaccurate values due to surface roughness, polishing quality and surface angle were taken out from the initial 25 indents, thus there are 17 presentable indentation values available for interpretation. The nanoindenter machine produces some error. The error the machine itself generates is approximately 5% according to the user's manual. In addition to this 5% machine, standard deviation and coefficient of variation values were calculated for each sample at each saturation phase. This was done because, the Young's modulus values at each saturation phase of each sample is reported as an average value of all successful indentations made on that sample. Standard deviation and coefficient of variation of each data set that generated an average Young's modulus values are shown on each nanoindentation result figure. In addition to these values, hardness vs. Young's modulus figures have a R^2 (Regression Analysis) value. Table 4.2 lists all the average, standard deviation and coefficient of variation values for Samples 1 and 2.
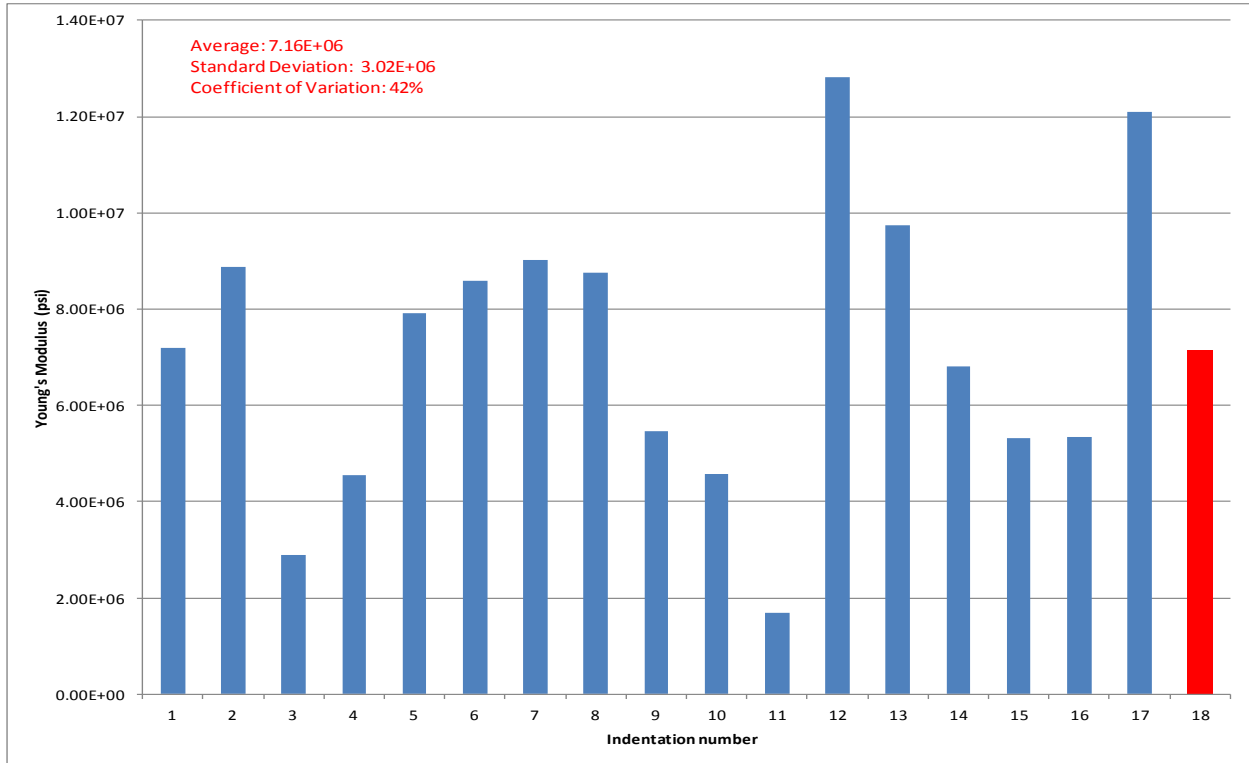
Figure 4.4: Nanoindentation results for the untreated Sample 1 (6606.8'), showing Young's modulus values of each indent done on the sample. Each point represents a Young's modulus value taken from the surface of the core. Red column represents the average Young's modulus of this sample (7.16E+6 psi).

Table 4.2: Error Analysis of the Measured Young's Modulus Values through Nanoindenter for Samples 1 and 2 at Each Saturation Phase

Error Analysis of Samples 1 and 2 at each saturation phase				
	Saturation Phase	Average	Standard Deviation	Coefficient of Variation %
Samples 1	Dry	7.16E+06	3.02E+06	42
	5-Days	4.75E+06	3.35E+06	71
	15-Days	4.27E+06	4.61E+06	108
	30-Days	4.45E+06	1.26E+06	28
Sample 2	Saturation Phase	Average	Standard Deviation	Coefficient of Variation %
	Dry	6.83E+06	1.25E+06	18
	5-Days	5.87E+06	9.00E+05	15
	15-Days	6.19E+06	5.31E+05	9
	30-Days	6.50E+06	1.63E+06	25

There is also a very visible variance in the values obtained. This variance seems like it may be an error in the measurements, however it represents the heterogeneity and the complex mineralogy of the samples. Figure 4.5 represents Young's modulus measurements of Sample 2 (6742.25') which is one of

66

the expansion samples when it is unaffected by fluids. The red column again represents the average value

of all the indentations taken on the surface.
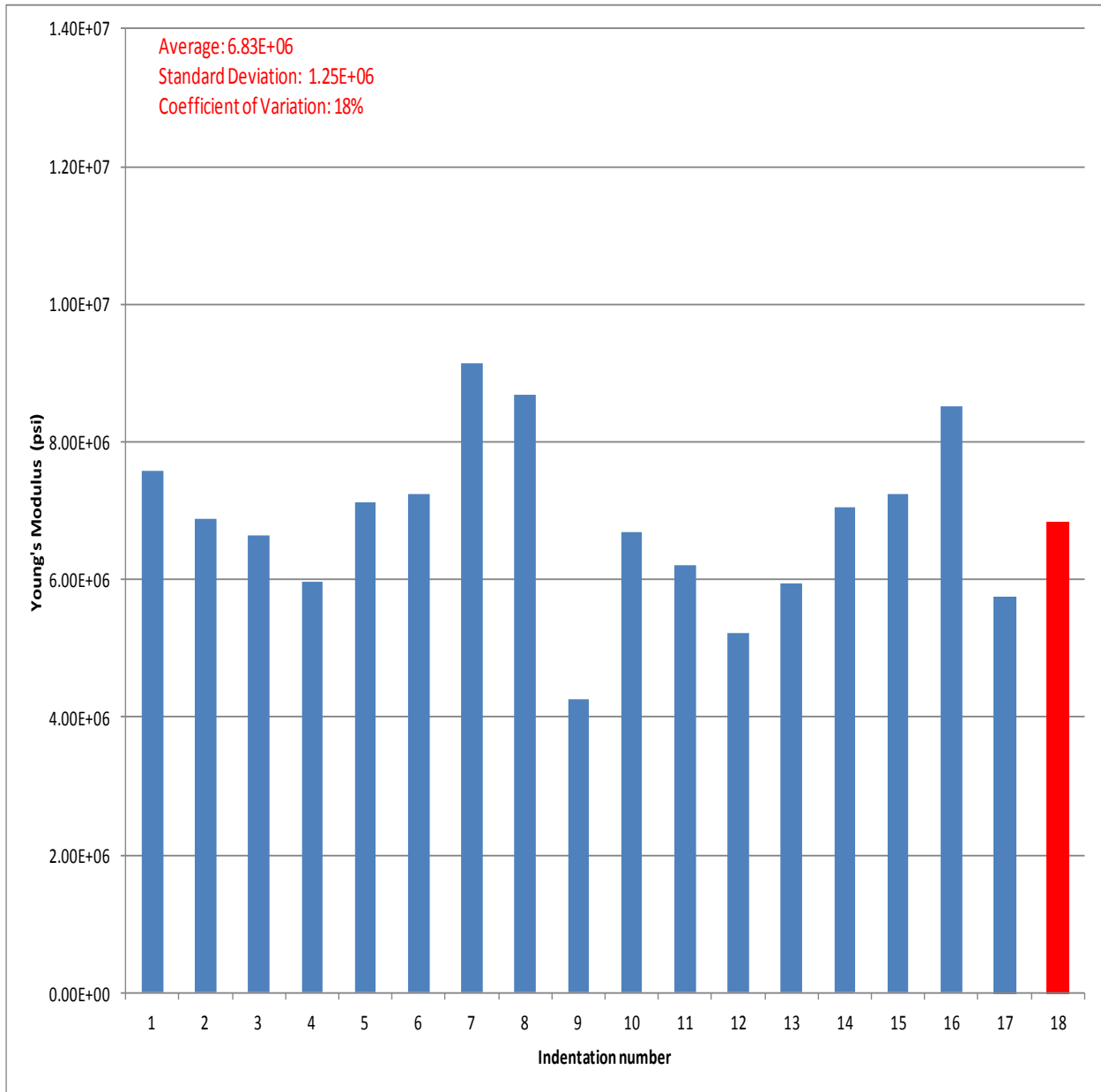
Figure 4.5: Nanoindentation results for the untreated Sample 2 (6742.25') sample showing Young's modulus values of each indent done on the sample. Each point represents a Young's modulus value taken from the surface of the core. Red column represents the average Young's modulus of this sample (6.83E+6 psi).

Figure 4.6 shows how hardness and Young's modulus of Sample 1 are related to each other.

Figure 4.7 shows the hardness and Young's modulus relation of the expansion sample, Sample 2.
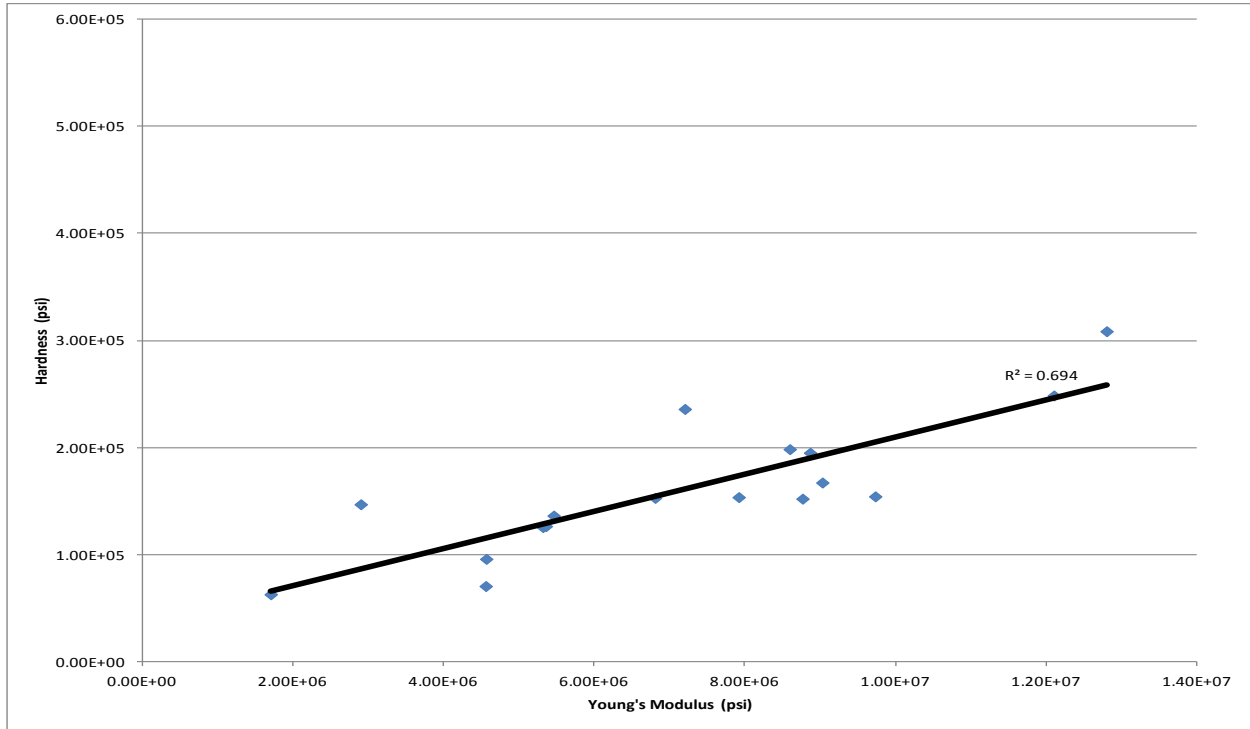
Figure 4.6: Results for the untreated Sample 1 (6606.8'), showing the relationship and trend between Young's modulus and hardness values obtained from the sample. Figure indicates a positive linear relationship between the two. As one increases the other also increases.
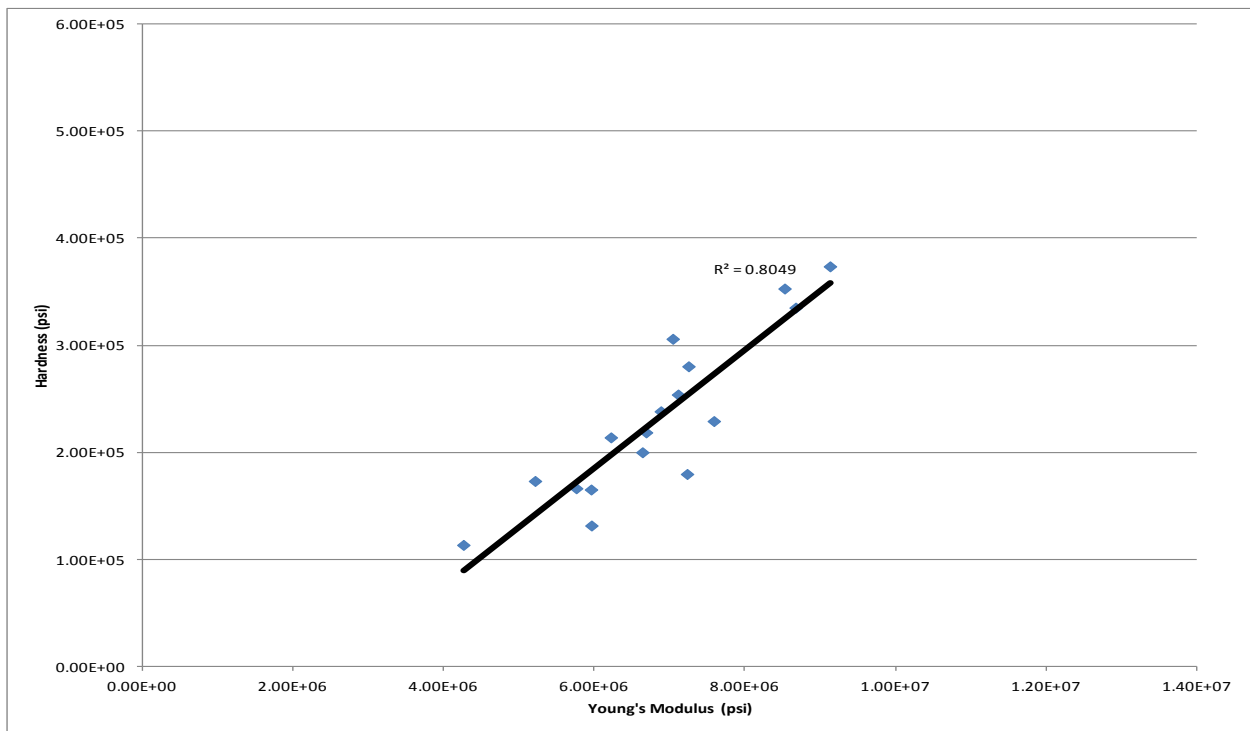
Figure 4.7: Results for the untreated Sample 2 (6742.25'), showing the relationship and trend between Young's modulus and hardness values obtained from the sample. Figure indicates a positive linear relationship between the two. As one increases the other also increases.

The same measurements were taken for the cores after they were saturated in freshwater for 5 days. Figure 4.8 and 4.9 show the Young's modulus values and how hardness relates to Young's modulus for Samples 1 and 2, respectively. Before Samples 1 and 2 were saturated, their average Young's modulus values (the red columns in Figures 4.4 and 4.5) were 7.16E+06 and 6.83E+06 psi. It is very obvious that both of these samples had tremendous reduction in their young's modulus values. Average Young's modulus values corresponding to the red columns after 5 days of saturation are 4.75E+06 and 5.87E+06 psi.
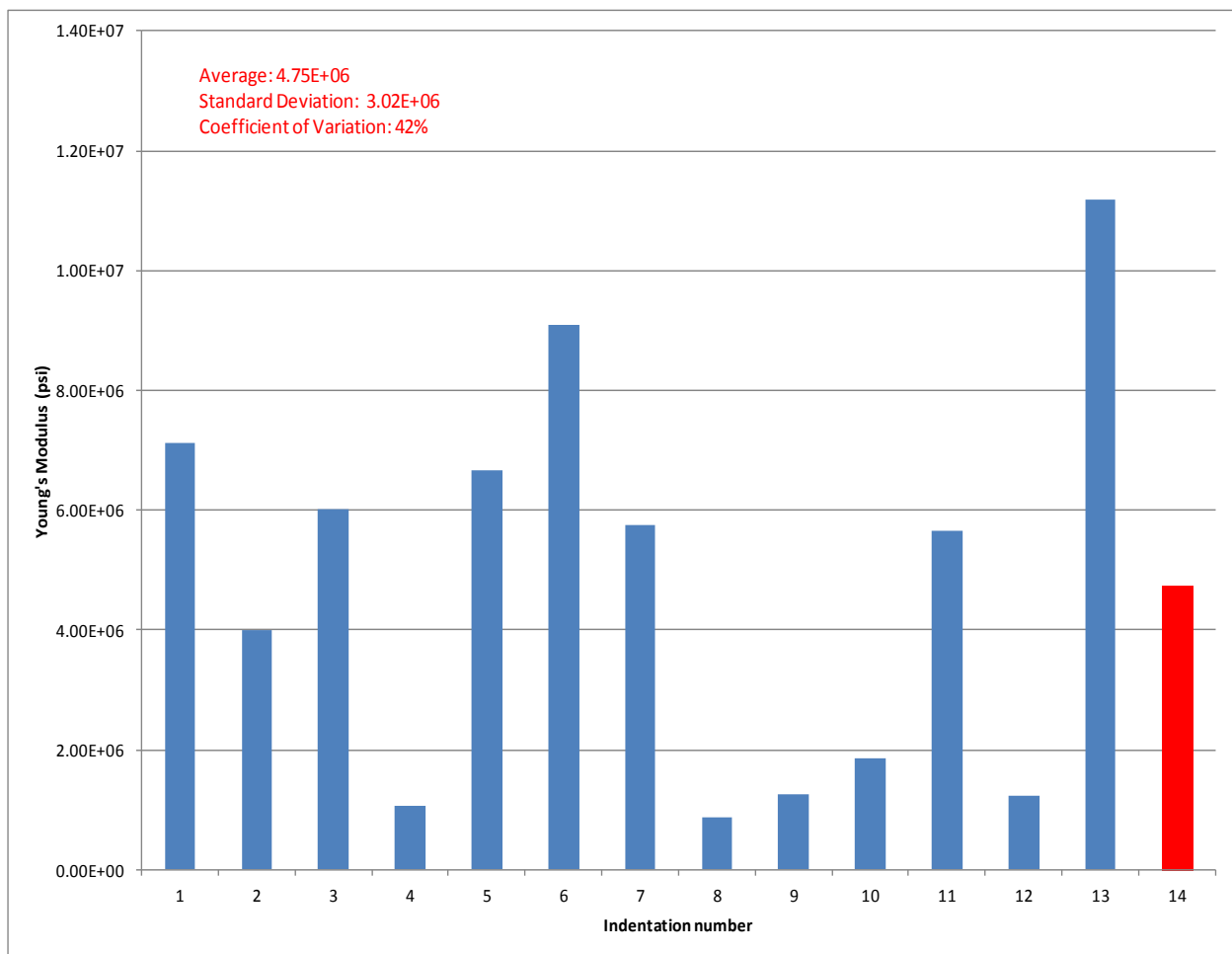
Figure 4.8: Nanoindentation results for the 5-Day saturated Sample 1 (6606.8'), showing Young's modulus values of each indent done on the sample. Each point represents a Young's modulus value taken from the surface of the core. Red column represents the average Young's modulus of this sample (4.75E+6 psi).
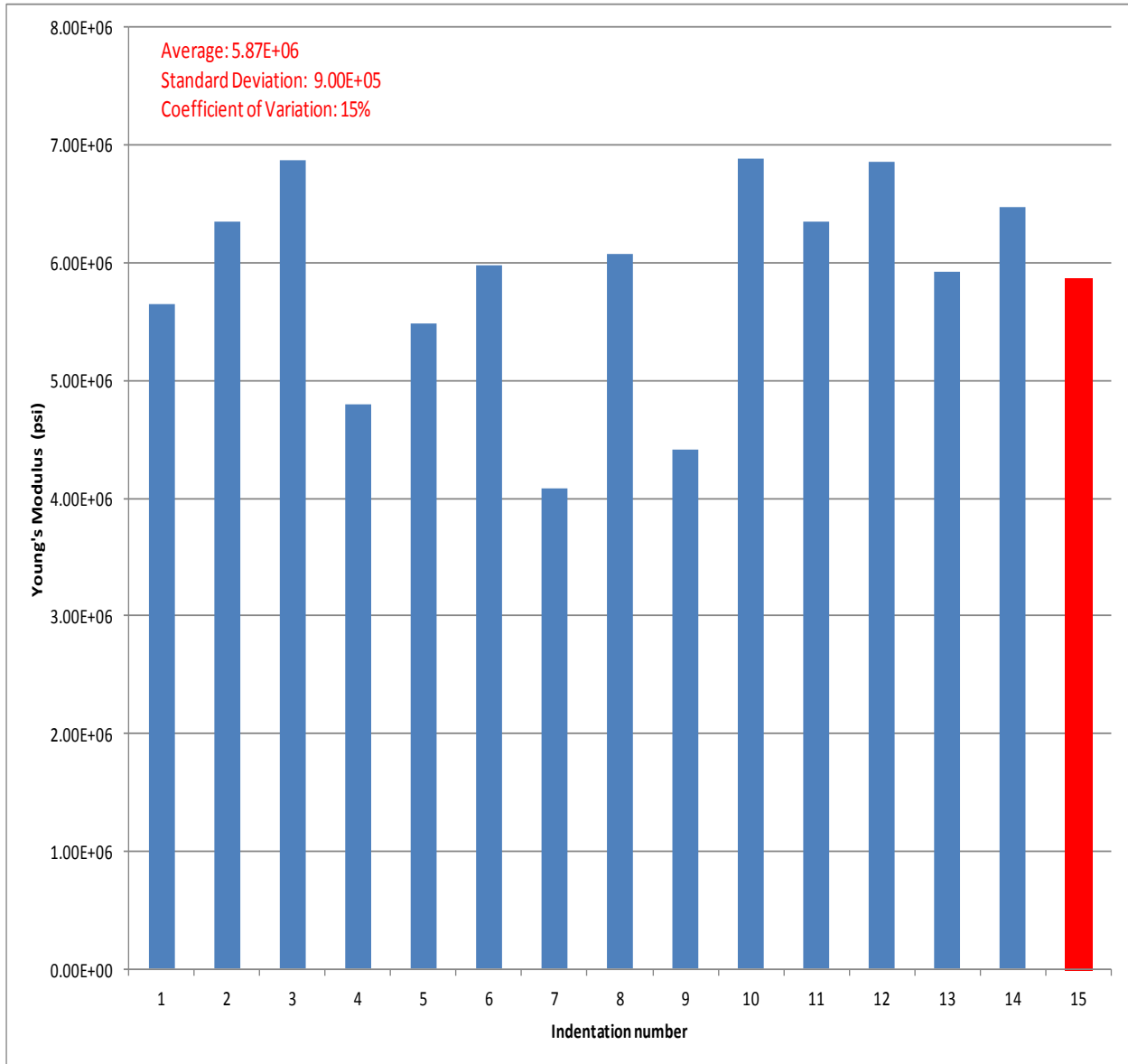
Figure 4.9: Nanoindentation results for the 5-Day saturated Sample 2 (6742.25'), showing Young's modulus values of each indent done on the sample. Each point represents a Young's modulus value taken from the surface of the core. Red column represents the average Young's modulus of this sample (5.87E+6 psi). Note the scale change in Young's modulus.

The hardness and Young's modulus relationship or Samples 1 and 2 after saturation for five days are shown in Figures 4.10 and 4.11. It is very evident that there is a trend between these properties after this saturation interval.
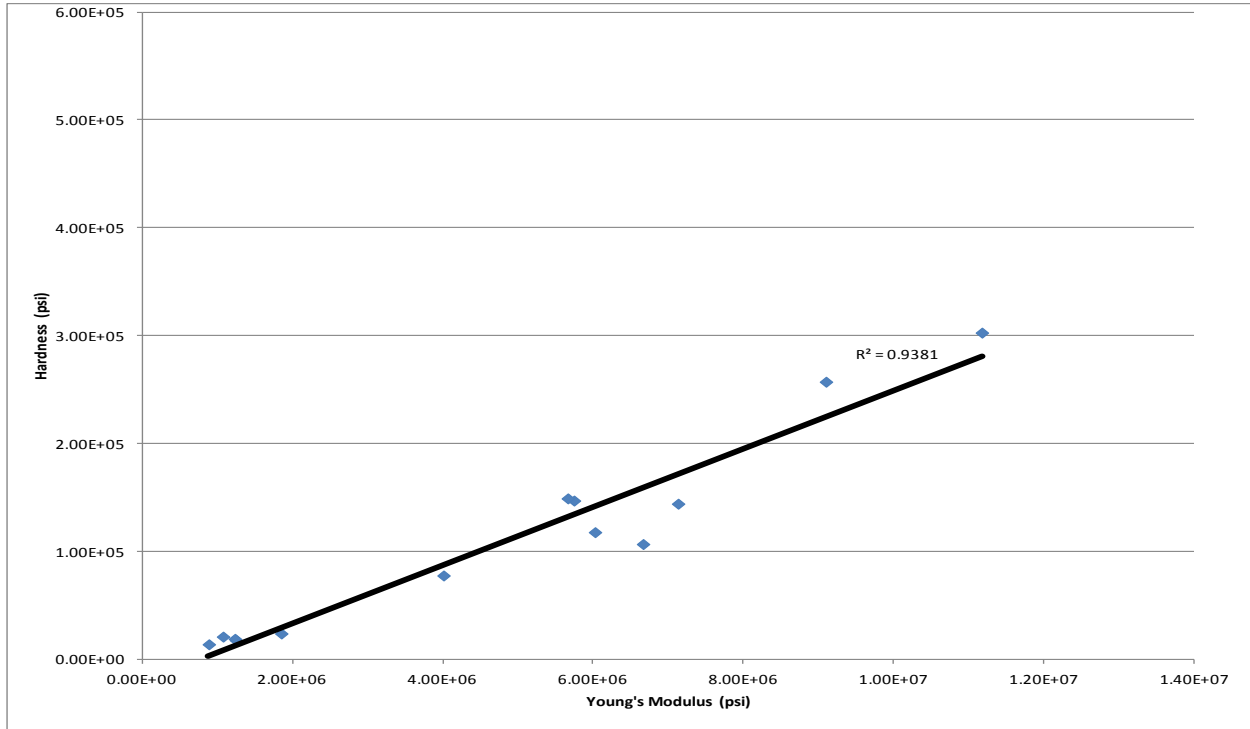
Figure 4.10: Results for the 5-Day saturated Sample 1 (6606.8'), showing the relationship and trend between Young's modulus and hardness values obtained from the sample. Figure indicates a positive linear relationship between the two. As one increases the other also increases.
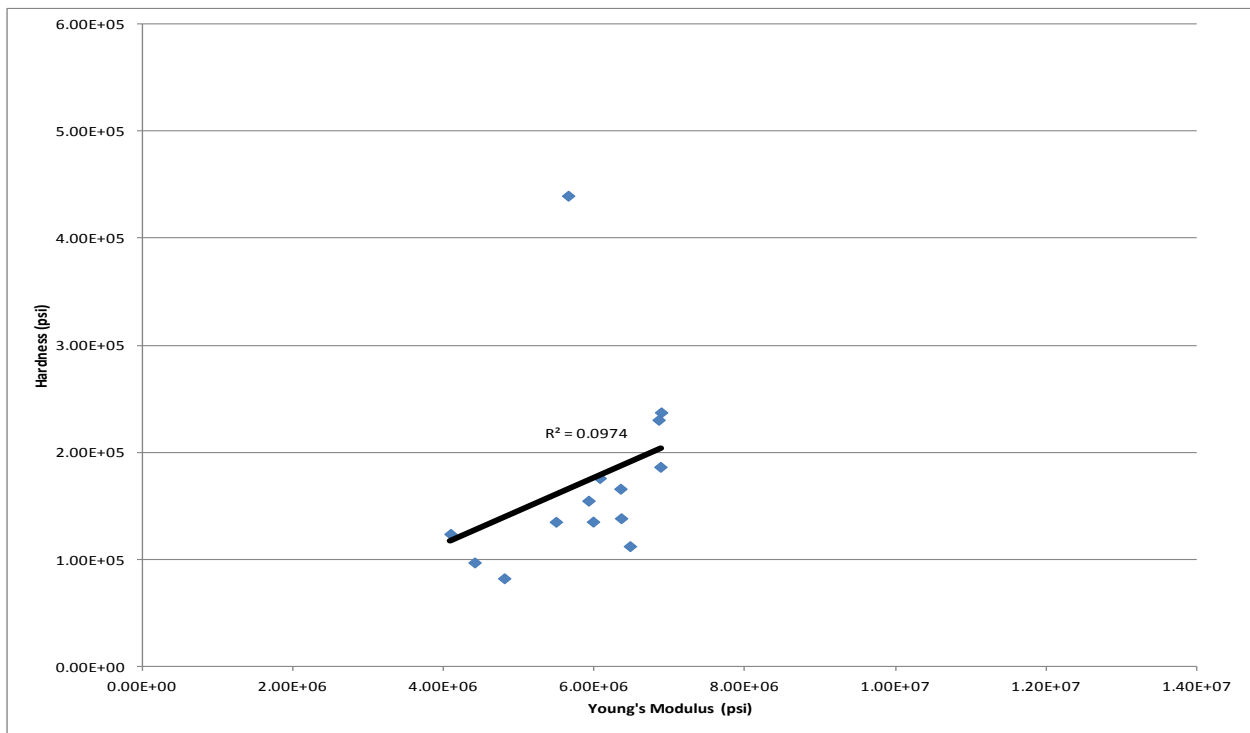
Figure 4.11: Results for the 5-Day saturated Sample 2 (6742.25'), showing the relationship and trend between Young's modulus and hardness values obtained from the sample. Figure indicates a positive linear relationship between the two. As one increases the other also increases.

Samples 1 and 2 pieces were saturated for an additional ten days after the five days measurements were taken. Sample 1 (6606.8') and most of the other samples that were saturated with different fluids experienced additional Young's modulus reduction. However, Sample 2 (6742.25') in this case showed a very insignificant increase in its Young's modulus value. The nanoindentation measurements for both Samples 1 and 2 are shown in Figures 4.12 and 4.13.
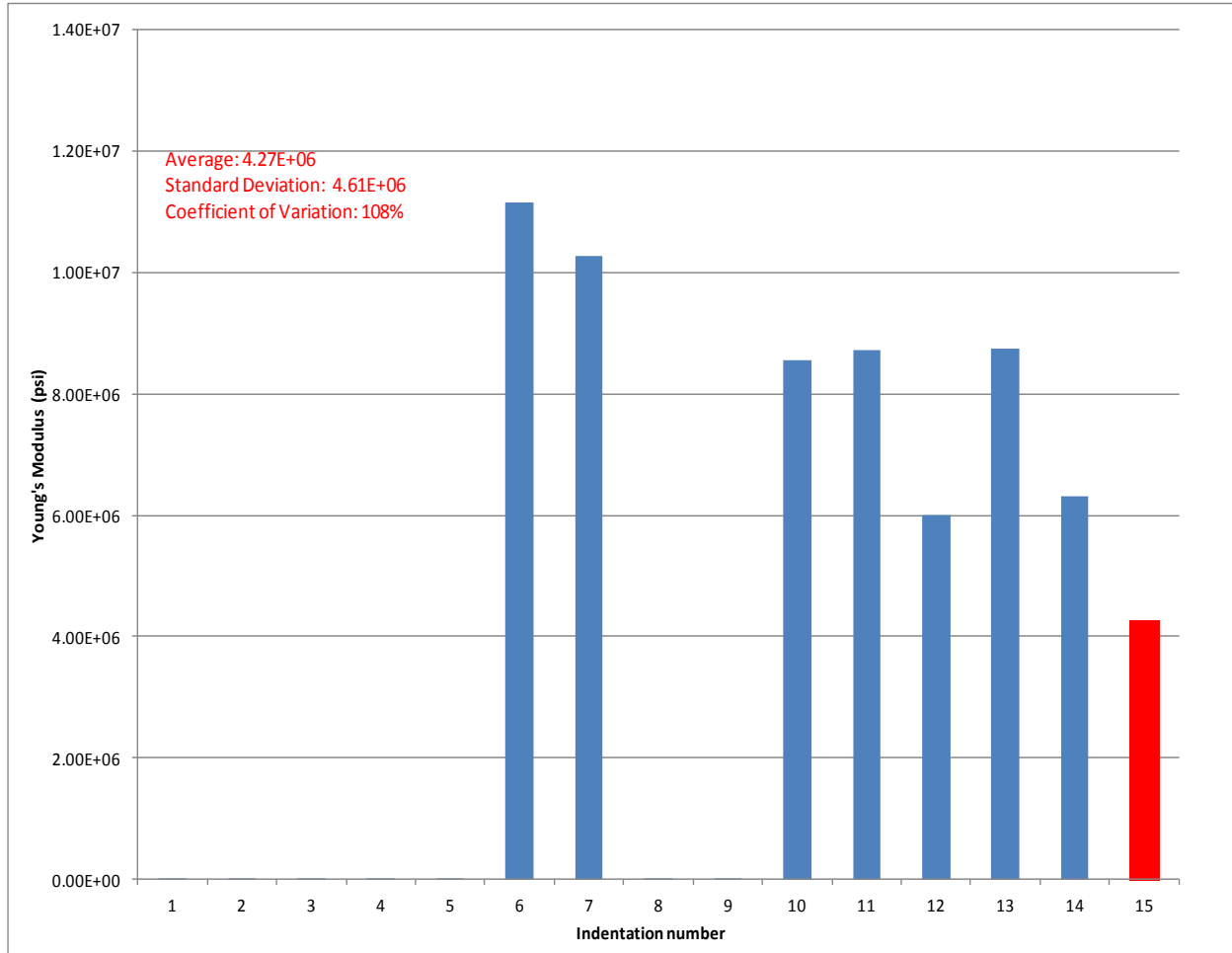
Figure 4.12: Nanoindentation results for the 15-Day saturated Sample 1 (6606.8'), showing Young's modulus values of each indent done on the sample. Each point represents a Young's modulus value taken from the surface of the core. Red column represents the average Young's modulus of this sample (4.27E+6 psi). Note the scale change in Young's modulus.

The low values in Figure 4.12 look as if they are missing, however these specific indentations have significantly low Young's modulus, they were recorded because they were within a reasonable range of values.
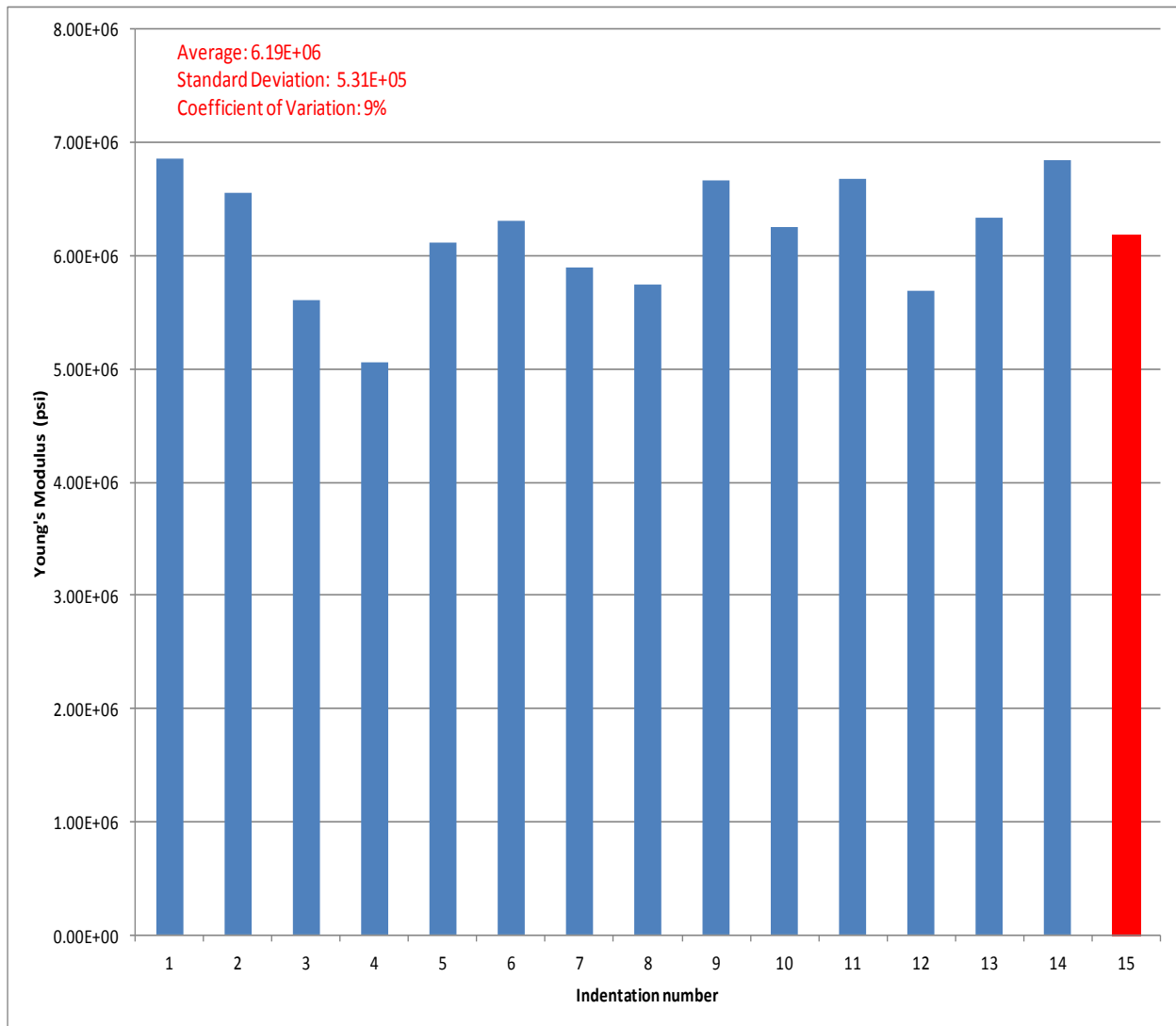
Figure 4.13: Nanoindentation results for the 15-Day saturated Sample 2 (6742.25'), showing Young's modulus values of each indent done on the sample. Each point represents a Young's modulus value taken from the surface of the core. Red column represents the average Young's modulus of this sample (6.19E+6 psi). Notice the scale change in Young's modulus.

Looking at Figure 4.12 we can see how beneficial it is to run 25 indentations. The values that are very low represent the soft and ductile minerals in the sample and there are some indentation values that have higher values which represent the hard minerals. The average value is within the reasonable range for the 15-Day wetting phase. The effects of each saturation phase on Young's modulus values are discussed in Chapter 5. Fifteen days saturation hardness and Young's modulus has the trend just like the previous saturation phases as seen in Figures 4.14 and 4.15.
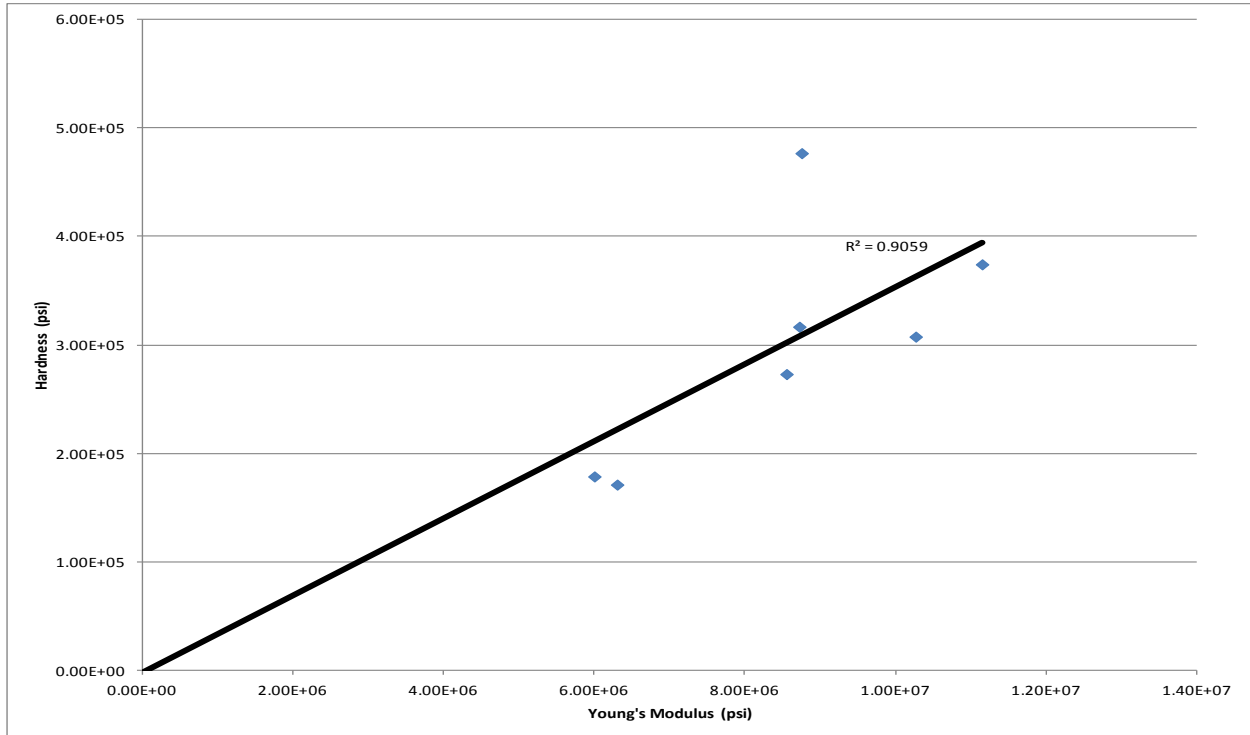
Figure 4.14: Results for the 15-Day saturated Sample 1 (6606.8'), showing the relationship and trend between Young's modulus and hardness values obtained from the sample. Figure indicates a positive linear relationship between the two. As one increases the other also increases.
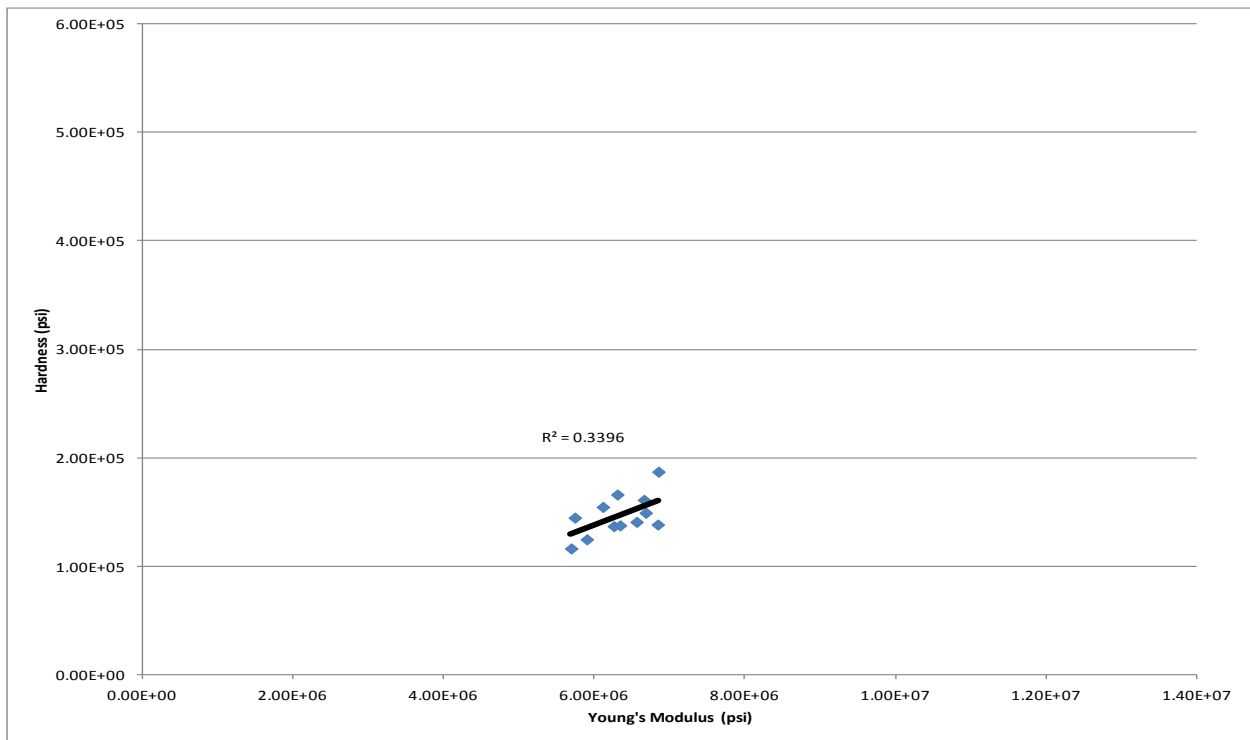
Figure 4.15: Results for the 15-Day saturated Sample 2 (6742.25'), showing the relationship and trend between Young's modulus and hardness values obtained from the sample.

The sample pieces were saturated once again but this time for an additional 15 days, which added up to a total of 30 days at the end. Figures 4.16 and 4.17 show the 30-days saturation measurements of Young's modulus and hardness. Sample 1 and 2 both experience an increase in Young's modulus after this additional 15 days. This is different result than for most of the samples, as it will be discussed more in depth in Chapter 5.
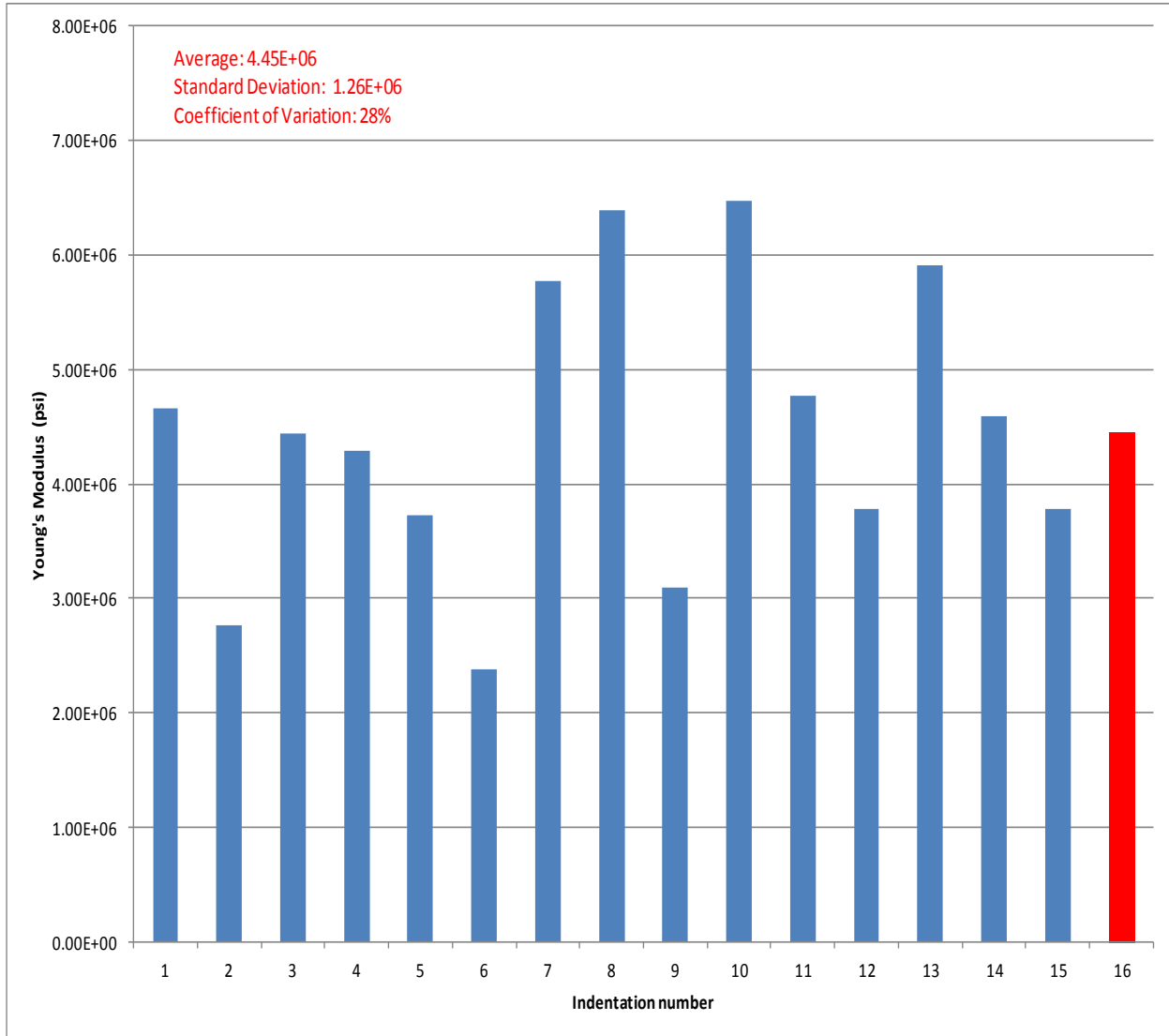
Figure 4.16: Nanoindentation results for the 30-Day saturated Sample 1 (6606.8'), showing Young's modulus values of each indent done on the sample. Each point represents a Young's modulus value taken from the surface of the core. Red column represents the average Young's modulus of this sample (4.45E+6 psi).
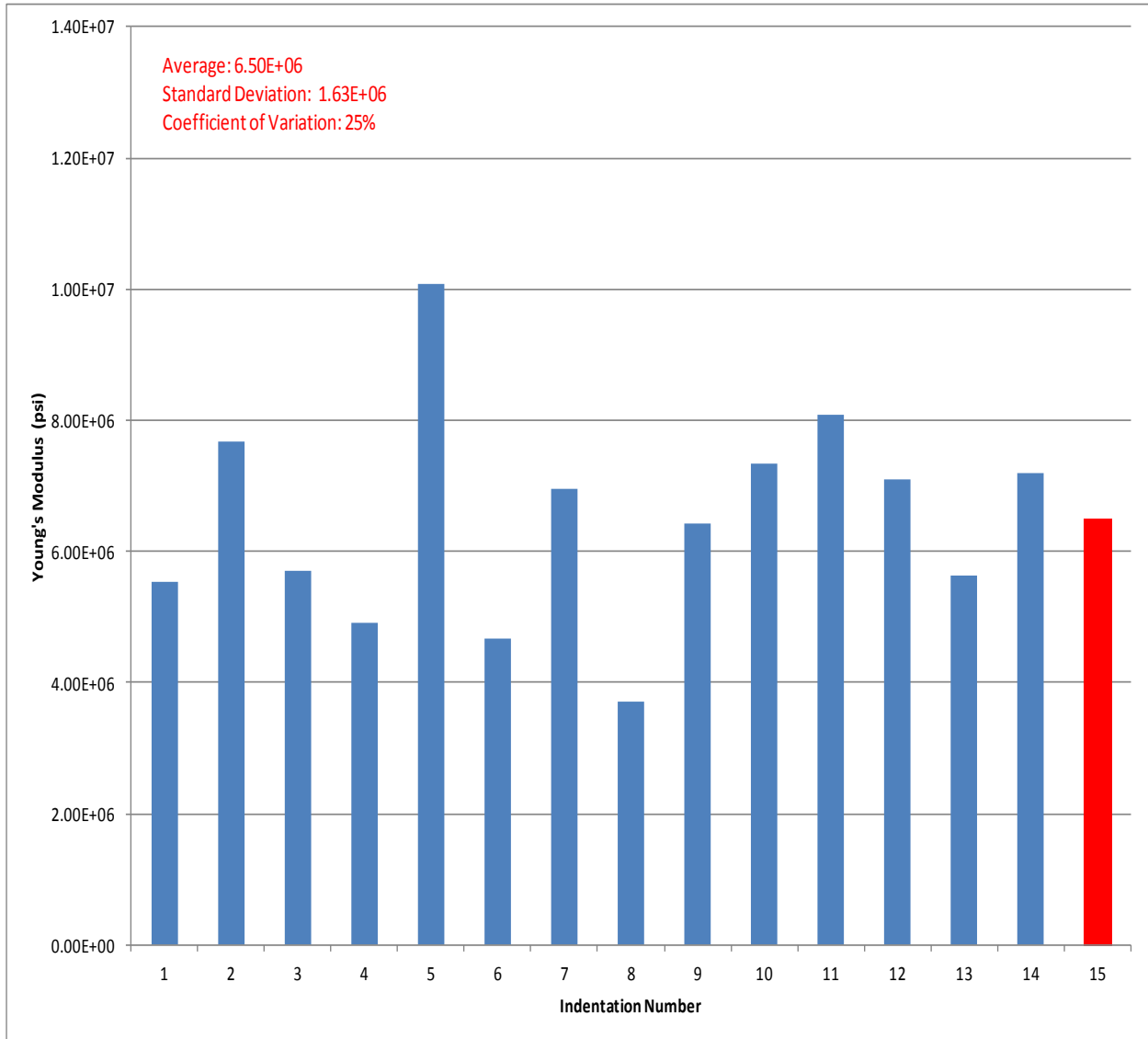
Figure 4.17: Nanoindentation results for the 30-Day saturated Sample 2 (6742.25'), showing Young's modulus values of each indent done on the sample. Each point represents a Young's modulus value taken from the surface of the core. Red column represents the average Young's modulus of this sample (6.50E+6 psi). Note the scale change in Young's modulus.

Both Sample 1 and 2 have reasonable 15 and 14 successful indentations respectively. It is very visible that with the exception of the 10-11 indentations that were disregarded, the remaining measurements have a more uniform distribution. Hardness and Young's modulus relationship is once again shown, this time after saturating the samples for a total of 30 days (Figures 4.18 and 4.19).
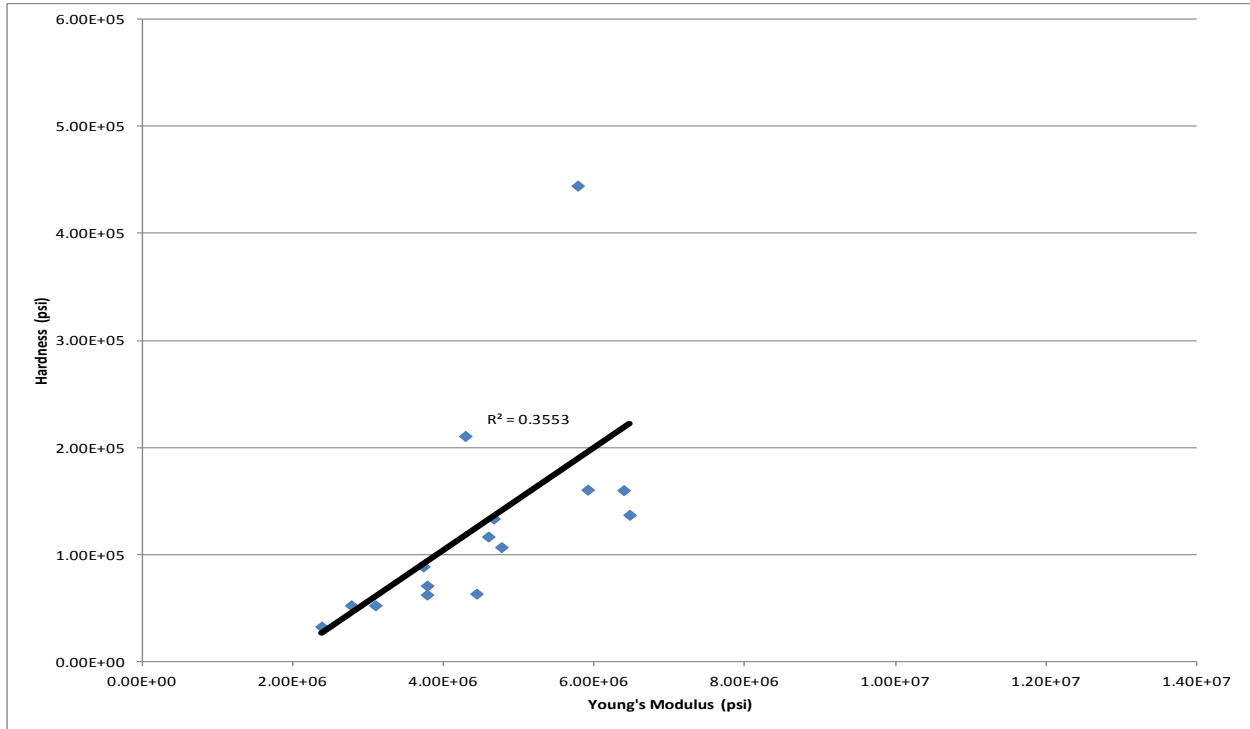
Figure 4.18: Results for the 30-Day saturated Sample 1 (6606.8'), showing the relationship and trend between Young's modulus and hardness values obtained from the sample. Figure indicates a positive linear relationship between the two. As one increases the other also increases.
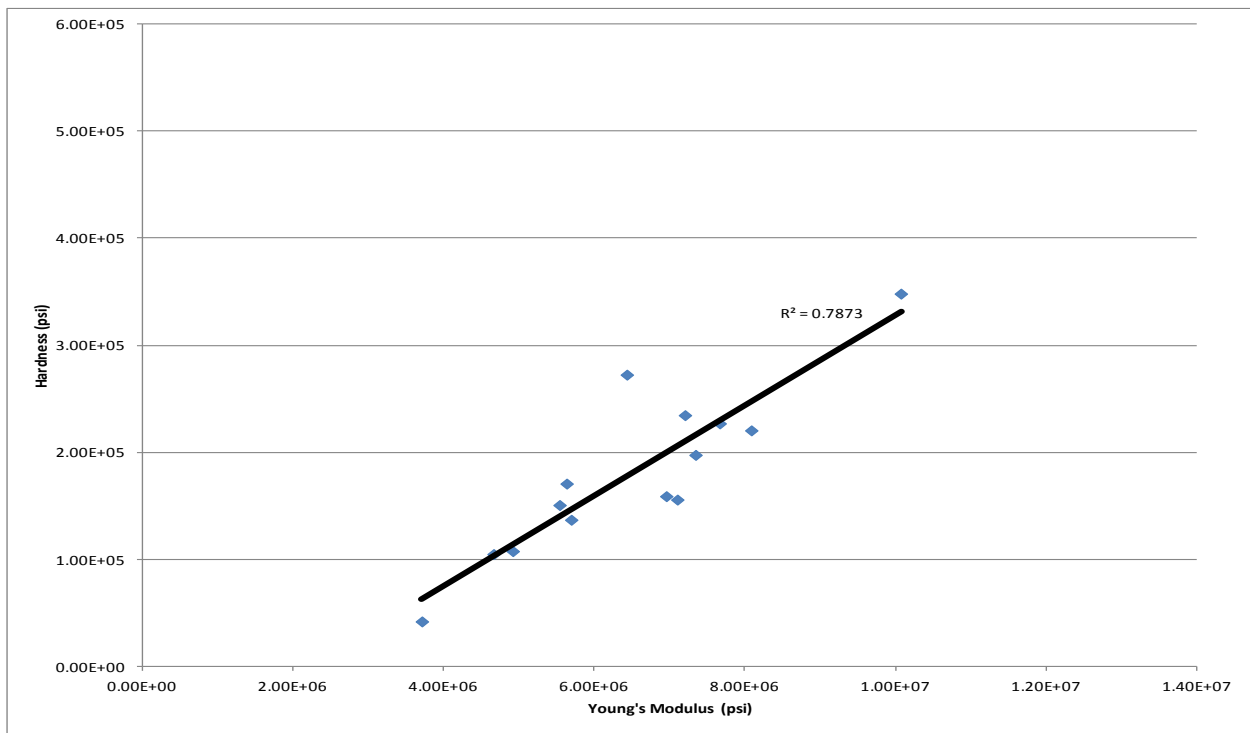
Figure 4.19: Results for the 30-Day saturated Sample 2 (6742.25'), showing the relationship and trend between Young's modulus and hardness values obtained from the sample. Figure indicates a positive linear relationship between the two. As one increases the other also increases.

Table 4.2 shows all the error analysis values for the nanoindentation results shown in Figures 4.4-4.19. Most of the samples have relatively high standard deviation values, and consequently high coefficient of variations. Normally this would mean that the data obtained and generated are not as accurate and representative of the actual values. However in this case, these large values were expected due to the heterogeneity of the samples. As mentioned, the nanoindenter has an approximately 5% error window. This amount of error is not large enough to make such drastic variations such as in Table 4.2. Therefore the large variations in Table 4.2 are due to the heterogeneity of samples. Another important point is the continuance of these large variations similar to each other as saturation time progresses. This indicates that the variations are not caused by the machine's error but they are related to changes in Young's modulus, and they stay similar to each other throughout the saturation process.

Figures 4.4-4.19 point to how the Young's modulus values of samples that are saturated with freshwater change on an individual basis for specific saturation periods. In the remainder of this chapter, results for the bigger picture in comprehending the time effect on mechanical properties of the Niobrara shale are provided. Individual nanoindentation measurements illustrate an obvious change in mechanical properties. Young's modulus definitely experiences a reduction when rocks are exposed to fracturing fluids, and this effect seems to increase as saturation time progresses. However, the same result can not necessarily be said for hardness, since hardness is an extrinsic property, and it represents mostly the measurements at specific spots. Therefore, hardness measurements shown in figures have more random and spontaneous values. Average Young's modulus values for Samples 1 and 2 for each saturation period are shown in Figures 4.20 and 4.21.
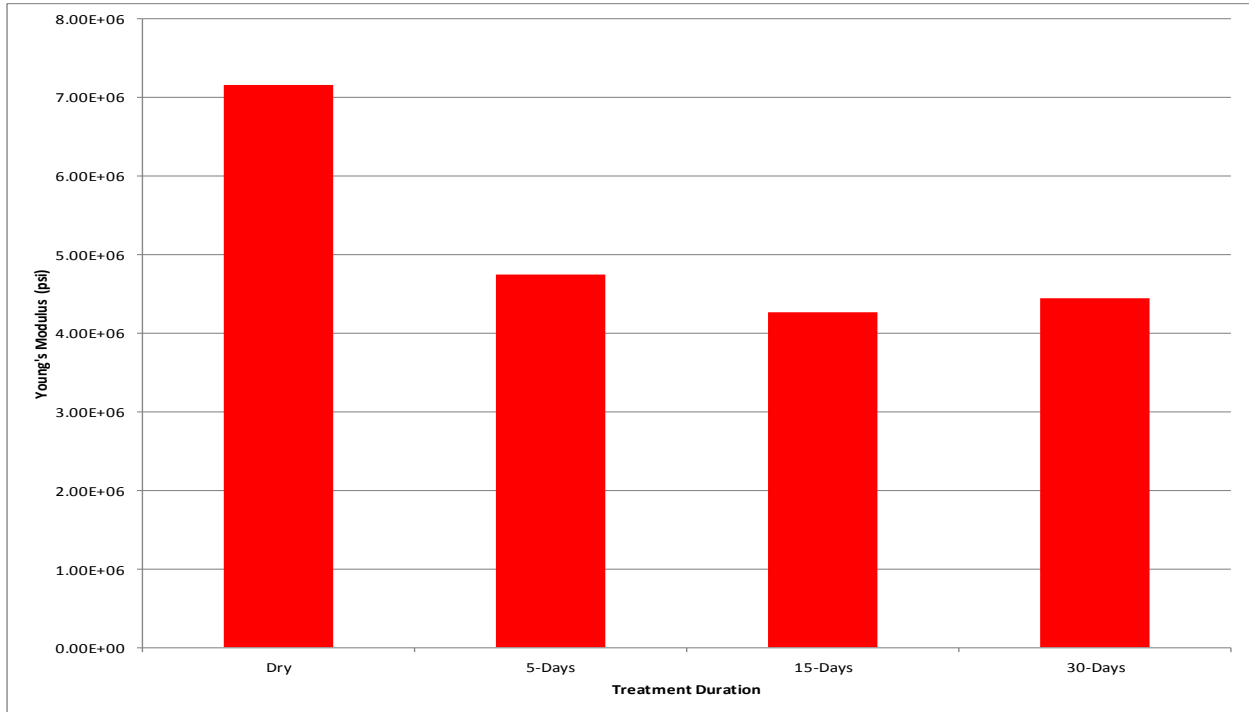
Figure 4.20: Average Young's modulus values of all treatment periods for Sample 1 (6606.8'). The y-axis shows Young's modulus in psi and x-axis shows the treatment periods. A reduction in Young's modulus values is very evident as time progresses and the largest reduction is between the dry and 5-Day period.
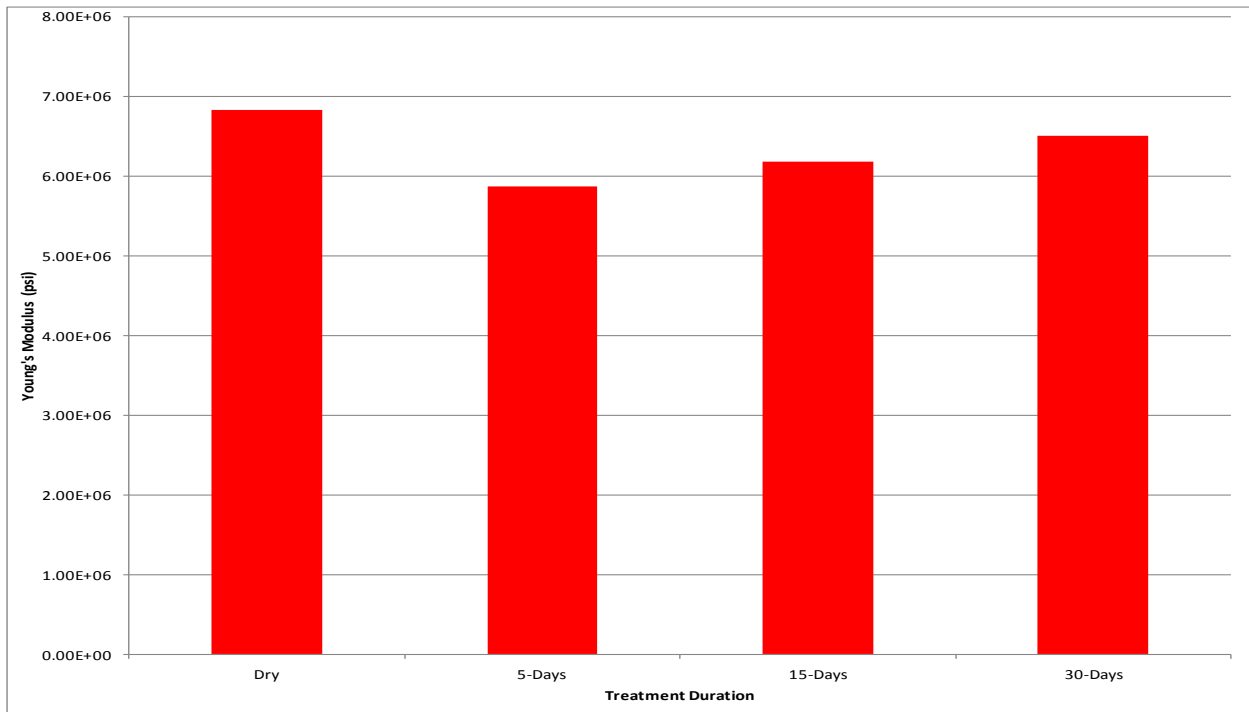
Figure 4.21: Average Young's modulus values of all treatment periods for Sample 2 (6742.25'). The y-axis shows Young's modulus in psi and x-axis shows the treatment periods. A reduction in Young's modulus values is very evident between dry stage and 5-days saturation.

It is very evident in Figure 4.20, that the Young's modulus decreases greatly in 30 days, and most of this reduction occurs within the first five days of fluid exposure. Between five and 15 days there is a noticeable decrease in Young's modulus. However, Young's modulus displays a slight increase between 15 days and 30 days. This doesn't necessarily mean that Young's modulus actually increased between these time frames, but rather that after 15 days, the reduction in Young's modulus starts diminishing and this slight increase could be due to the noise and small errors in the values. Although 15 days and 30 days values are mostly identical to each other, the heterogeneity of the sample could be the possible cause for this slight increase. Figure 4.21 is a great example for this heterogeneity problem in measurements. Young's modulus definitely has a severe reduction after saturation starts but it starts inclining after five days, Chapter 5 expand on this problem more in detail. Figure 4.22 and 4.23 show the hardness trend of the two samples as saturation time progresses.
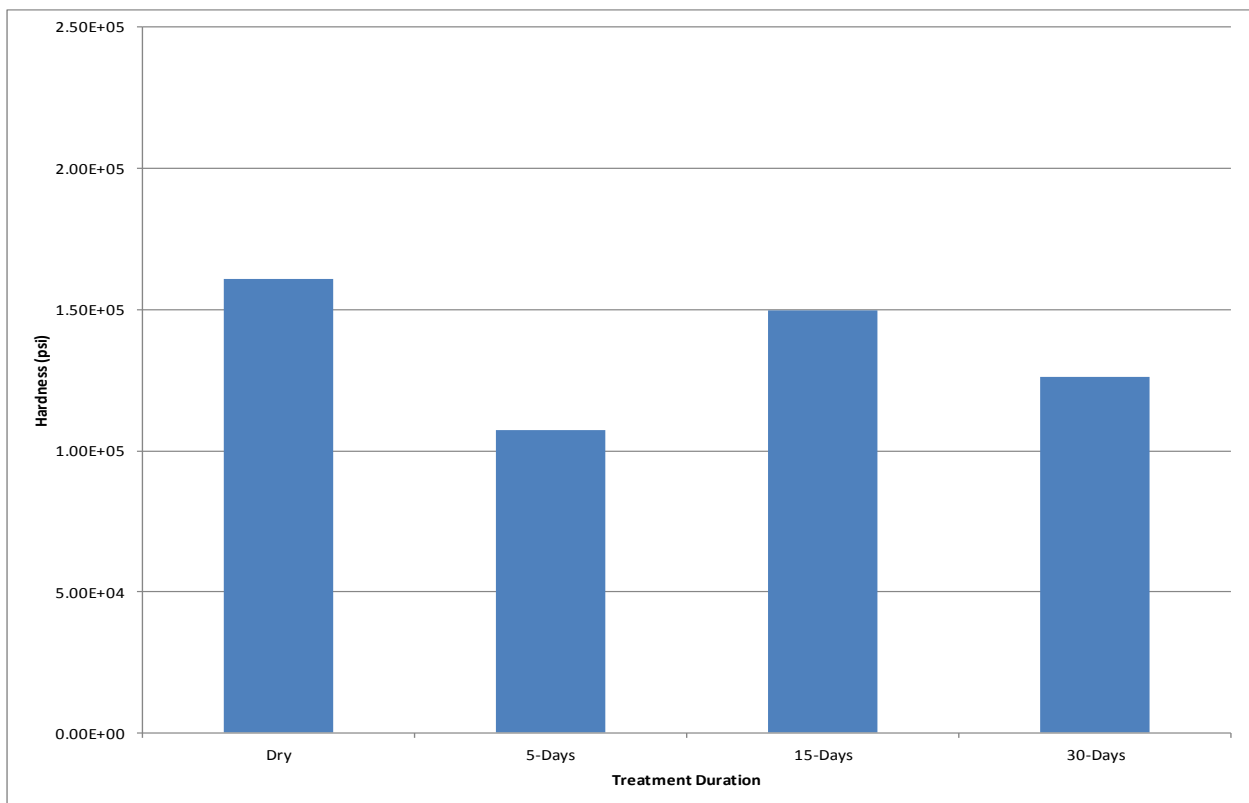
Figure 4.22: Average hardness values of all treatment periods for Sample 1 (6606.8'). The y-axis shows hardness in psi and x-axis shows the treatment periods. Hardness reduction is more spontaneous and random in comparison to Young's modulus due to being an extrinsic property of the core.
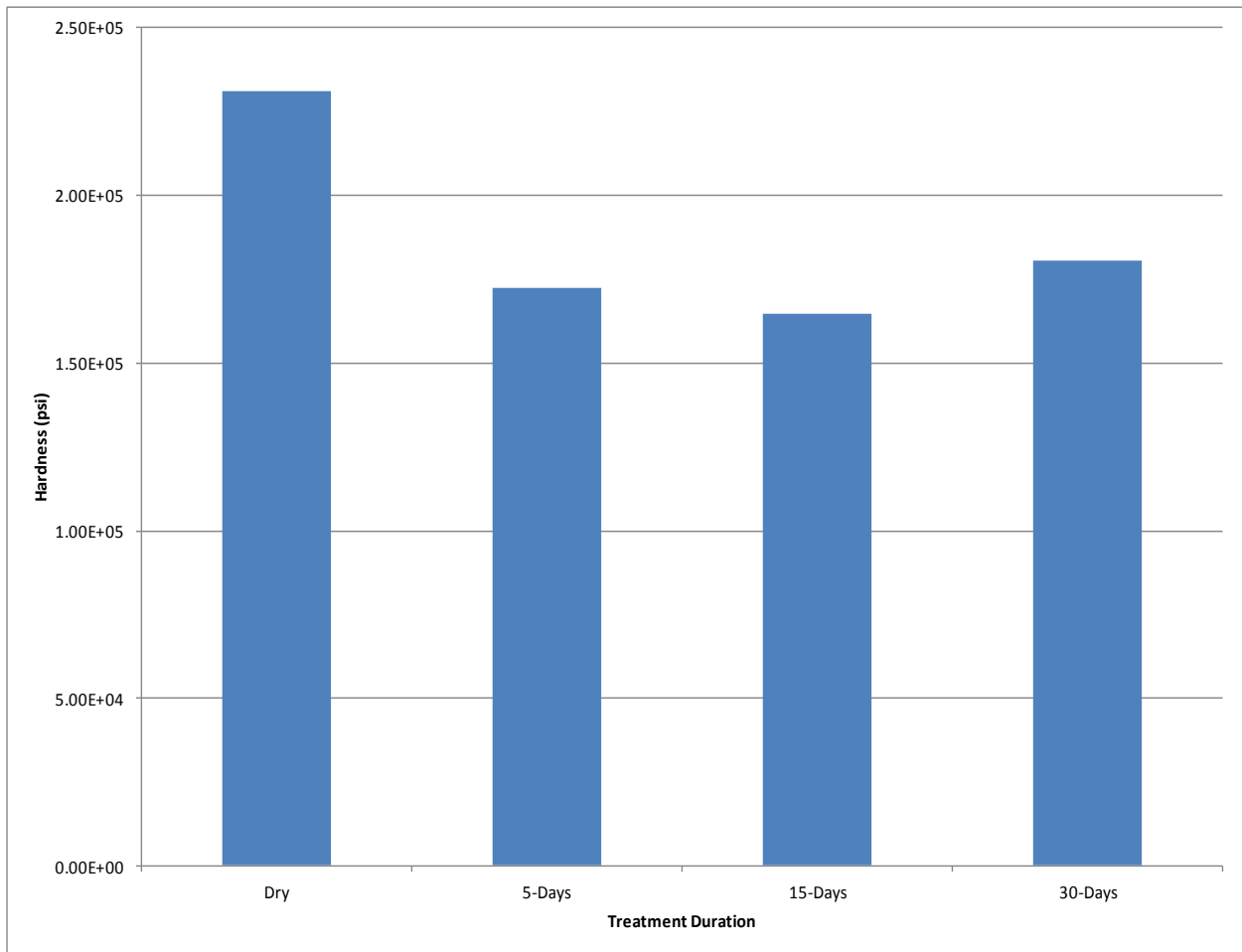
Figure 4.23: Average hardness values of all treatment periods for Sample 2 (6742.25'). The y-axis shows hardness in psi and x-axis shows the treatment periods. Hardness reduction is more spontaneous and random in comparison to Young's modulus due to being an extrinsic property of the core.

The expansion samples (Samples 2, 4, 6, and 8) were not originally a part of the project. However, they were added due to the need for more samples in order to expand to testing more proppants. However, the expansion tests validated the effects of four fracturing fluids on the Niobrara shale since the original results brought up some questions. The specific original and expansion results for the remaining three fracturing fluids are shown in supplemental files A, B, and C. However, the overall trend and how the original samples (Samples 1, 3, 5, and 7) and expansion samples (Samples 2, 4, 6, and 8) differ from each other are shown in Chapter 5. Figures 4.24 and 4.25 show the Young's modulus values for Samples 1 and 2 which were both saturated with freshwater. Table 3 shows the Young's modulus values of Samples 1 and 2 at different saturation stages.

81

Table 4.3: Young's Modulus Values of Two Sets of Samples (Original and Expansion Samples)

Original And Repeatability Young's Modulus Values of Freshwater Saturated Samples		
Saturation Phase	Freshwater-Sample #1 (psi)	Freshwater-Sample #2 (psi)
Dry	7.16E+06	6.83E+06
5-Days	4.75E+06	5.87E+06
15-Days	4.27E+06	6.19E+06
30-Days	4.45E+06	6.50E+06
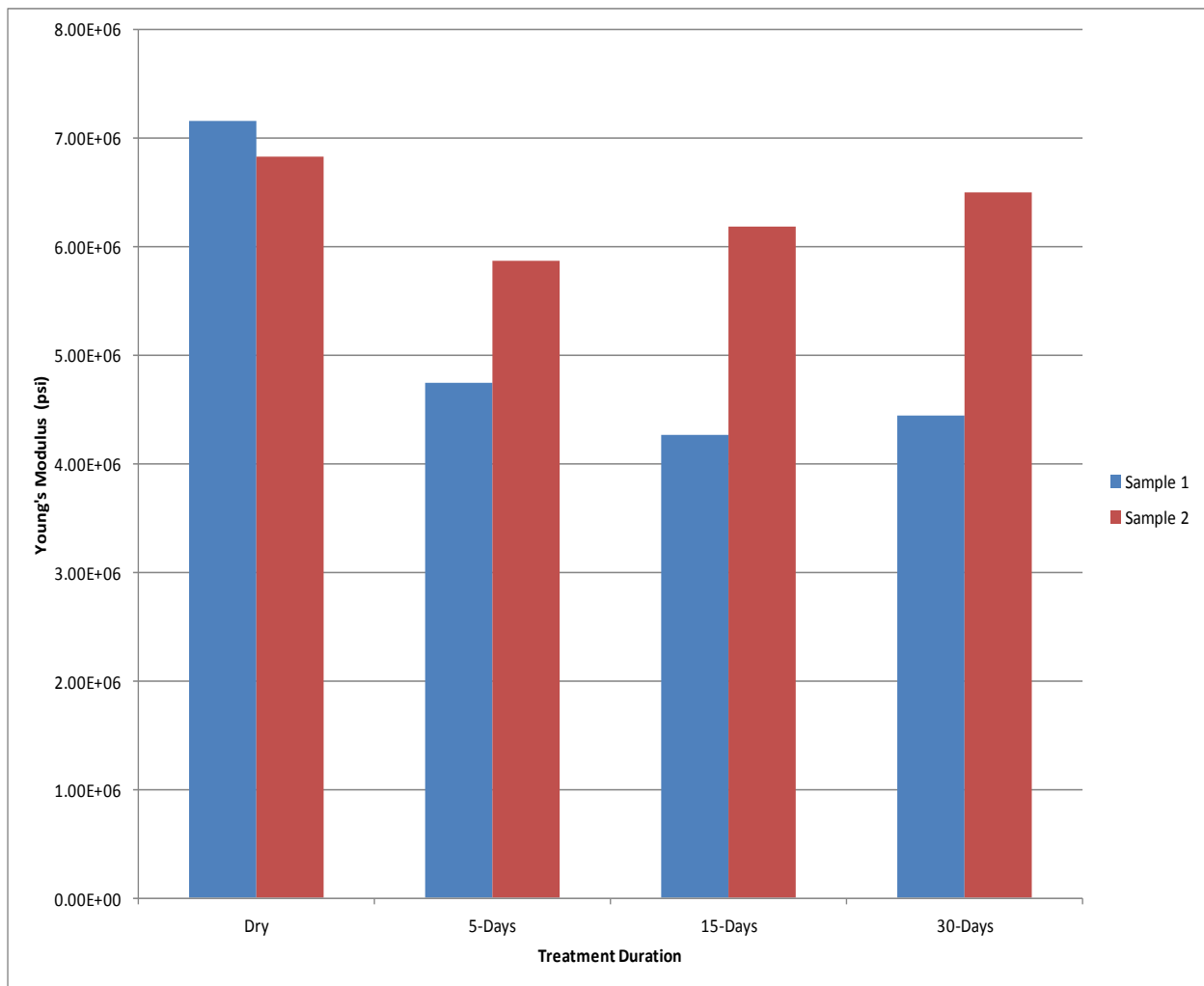
Figure 4.24: Young's modulus values of Sample 1 and 2 are shown at each saturation phase. The trend for Young's modulus reduction due to freshwater is displayed regardless of the core depth and test.
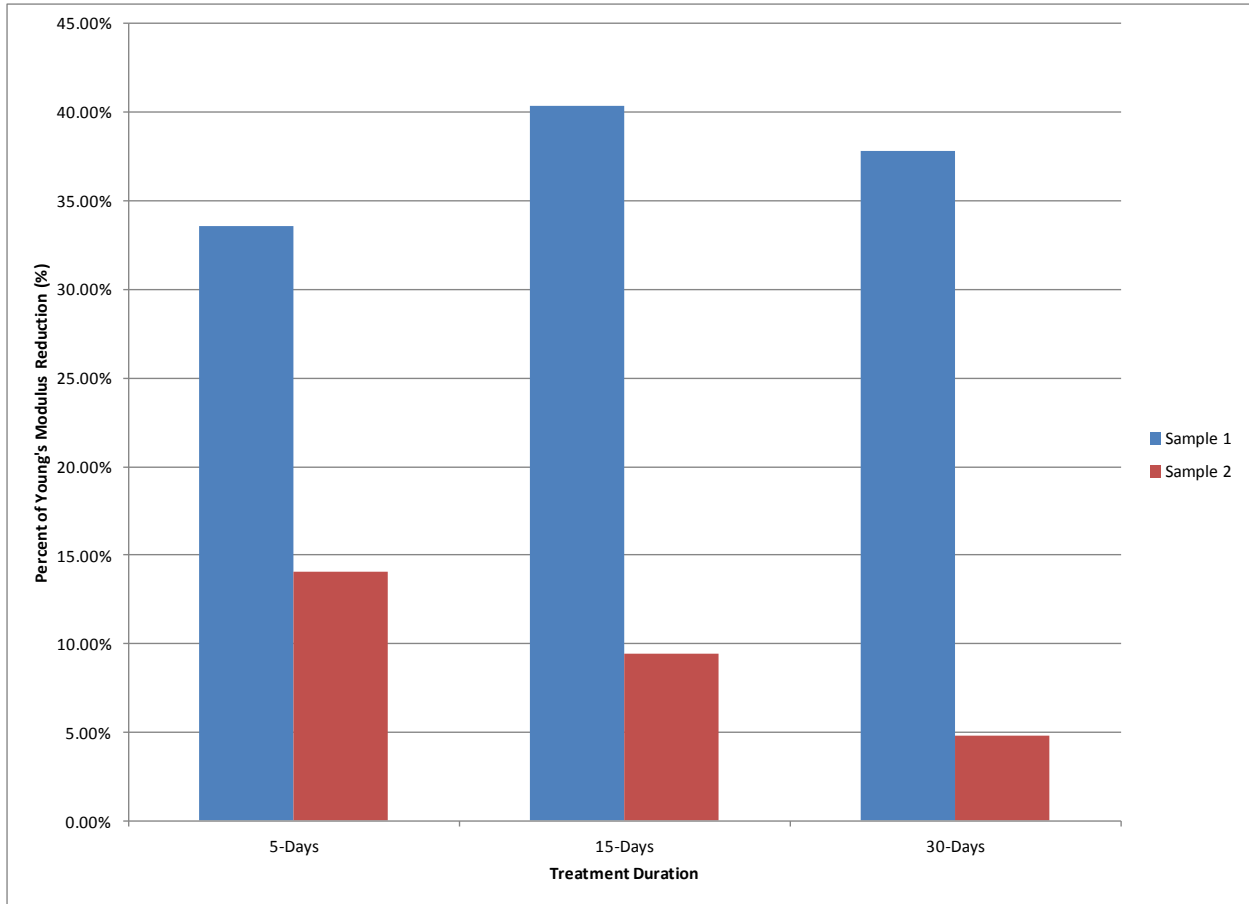
Figure 4.25: Young's modulus percentage reductions of Sample 1 and 2 are shown at each saturation phase. The trend for Young's modulus reduction due to freshwater is displayed regardless of the core depth and test.

Table 4.3 shows the Young's modulus values for Samples 1 and 2 at different saturation stages. As Figures 4.24 and 4.25 show, the magnitude of the Young's modulus change in the first five days is very drastic. Sample 2 (expansion) validates this extreme reduction. In general, the trend in Young's modulus change for all samples saturated with freshwater is similar. The first five days of saturation has the largest effect on mechanical properties of the samples.

The goal from running the expansion tests was to prove that the fracturing fluids could generate the same effect more than once on the Niobrara samples that are from different depths and possibly consists of different mineralogy. Figures 4.24 and 4.25 along with results for the other three fracturing fluids in supplemental files A, B, and C show that this goal is reached.

4.3 High Pressure Press and Scanning Acoustic Microscope Results of Freshwater Treated Cores

(Samples 1 and 2)

Capturing and quantifying proppant embedment in Samples 1-10 saturated with various fracturing fluids is the next step after nanoindentation. As explained before, each of the fracturing fluids were used on four samples. At least two pieces with dimensions of 1.0 inch diameter and 0.40 in length were cut from Samples 1-10. Four pieces with the least physical damage were selected to represent samples treated with fracturing fluids. For example, Sample 1 and 2 produced six different pieces. Four of these pieces were picked to be used for SAM imaging and testing proppant embedment for the Niobrara shale samples that are saturated with freshwater. Consequently, four pieces were selected from Samples 3-4, 5-6, 7-8, 9, and 10. Selecting four different pieces from each sample allowed two different types of proppants to be tested for each sample, thus fracturing fluid. Figure 4.26 shows the proppant test core set up. Proppants are placed between the bottom and top cores, these cores are then placed in the pressuring chamber and pressurized. The figures in this section shows the before and after pressurizing of different cores that were saturated with freshwater.

Figure 4.26: Image of proppant loading setup. Proppants are placed in between bottom and top cores.

Utilizing SAM (Scanning Acoustic Microscope) on the rock (core) surfaces before any pressure is applied is the first step following the nanoindentation measurements. SAM takes an image of the core surfaces while they are submerged in water. Since the proppant embedment quantification is expected to be dependent to the fracturing fluid type, cores saturated with KCl based fluids (KCl and KCl+Friction Reducer) had to be treated prior to being submerged in the water for SAM images. These cores were coated with clear nail polish in order to prevent the water from affecting them. The nail polish was removed after the initial images were captured so that the damages caused by pressure and proppants were not affected. Two different characteristic SAM images were taken for each core, one at 125X and one at 1000X magnification. All SAM images reported in this thesis are zoomed in versions of the 1000X images; since they produced the most clear and detailed images. These images really highlight the existence of natural fractures and already damaged zones. Capturing the existence of natural fractures and damaged zones prior to pressuring and testing for proppant embedment is critical from an embedment identifying and quantifying standpoint. Location and severity of these natural fractures drastically effects the proppant embedment. These natural fractures can be seen in pre-pressurized SAM images of Sample 1 and 2 which are saturated with freshwater (Figure 4.27). The four different images in Figures 4.27 and 4.28 show the four pieces cut from Samples 1 and 2.
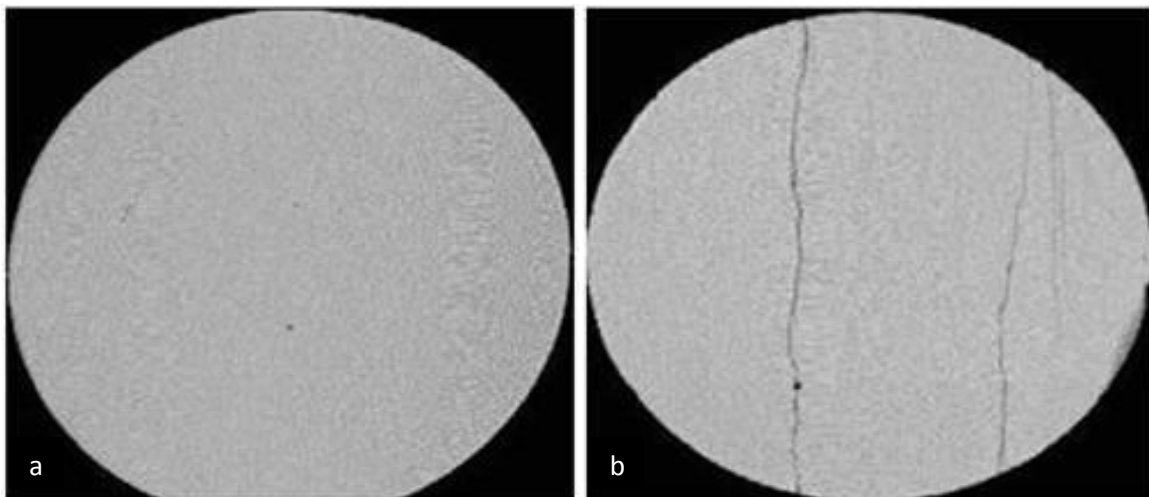
Figure 4.27: SAM images of bottom (a) and top (b) original cores for Freshwater Test #1. Core diameters are 1.0 inch.
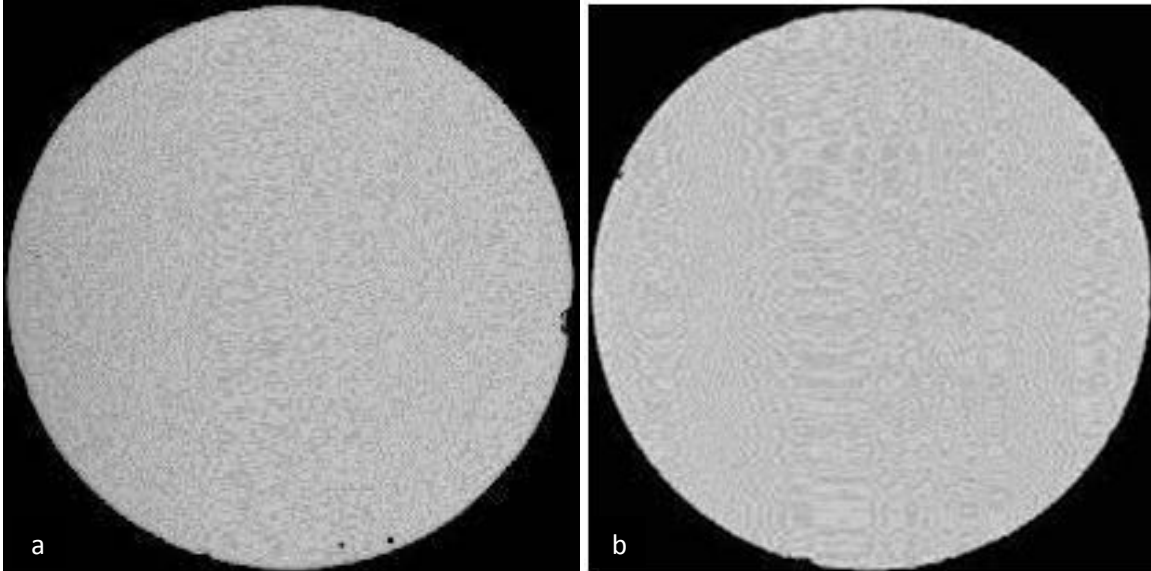
Figure 4.28: SAM images of bottom (a) and top (b) expansion cores for Freshwater Test #2. Core diameters are 1.0 inch.

The bottom core indicates the lower half of the core that the proppants were randomly distributed on, whereas the top core indicates the core that was placed above the proppants. In Chapter 3, Figure 3.8 shows the pressure loading setup, as the top and bottom cores shown in Figures 4.27 and 4.28 are both located in the chamber shown in Figure 3.8. Given the fact that samples used in this research are very fine-grained shales, SAM and optical pictures are not able to capture any of the grains on the core surfaces. However, images are taken to compare the condition of the cores before and after applying pressure to obtain the proppant embedment profiles.

Once all the cores were scanned with the SAM, they were prepared for pressurization with proppants in between them. A total of four different proppant types were used in all pressuring tests including the cores that were heated. The proppants used in the research are listed as:

- 16/30 Brady

- 20/40 Ottawa

- 20/40 Ceramic

- 20/40 RCS

Proppant selection was based on the fracturing fluids used. Each proppant was intended to be matched with a fracturing fluid that is also commonly paired with it in real fracturing jobs. Also, another main reason expansion tests were done was to test two similar proppant types with a set of cores that are saturated with the same fluid. This provided the embedment profile difference between these two proppant types at a given pressure for the Niobrara shale. Same proppants were also utilized in order to quantify which fracturing fluid would affect the proppant embedment more when cores were subjected under the same pressure while having same proppants between them. Therefore, 16/30 Brady and 20/40 Ottawa sand proppants are matched with cores that are saturated with freshwater and KCl, whereas 20/40 Ceramic and 20/40 RCS proppants are matched with cores that are saturated with KCl+Friction reducer and H_2O+KCl substitute. Sand proppants are matched with freshwater and KCl due to these fluids being less viscous, and the heavier proppants ceramic and RCS are matched with more viscous fluids. SAM was utilized again after pressurization of the cores with appropriate selected proppants. Figures 4.37a-b and 4.38a-b show the surfaces of the same cores shown in Figures 4.27 and 4.28 after pressurization.

The pressuring effect and embedment results of 16/30 Brady and 20/40 Ottawa on freshwater saturated cores are shown below, and the rest of the results for the other fracturing fluids can be seen in supplemental files A, B, C, and D. It is important to note that Figures 4.29 and 4.30 just like Figures 4.31 and 4.32, Figures 4.33 and 4.34, and Figures 4.35 and 4.36 are all corresponding to the SAM Figures 4.28a-b and 4.29a-b with the upper figure being Sample 1 and the lower one Sample 2.

Figures 4.29- 4.36 are optical images. Notice the white-clear coloring around the cores, especially the cores on the right sides. This coloring is due to white sticky food wrap that was used to prevent cores from breaking apart when they are under high pressure. A trial pressuring experiment was run without this wrap and the core ended up breaking into several pieces once it came out of the chamber, therefore all cores were wrapped with this material.

Figure 4.29: Images of bottom (left) and top (right) cores from Freshwater Test#1 without any pressure or proppant effect. Core diameters are 1.0 inch.

Figure 4.30: Images of bottom (left) and top (right) cores from Freshwater Test#2 without any pressure or proppant effect. Core diameters are 1.0 inch.

The bottom cores were loaded with proppants prior to placing them in the pressuring chamber. A proppant loading of 0.1 lb/ft^2 was achieved for each test. This loading may seem low from a real fracturing job stand point, however the profilometer requirement of having sufficient spacing in between embedded spots forced the loading to be low in the limited surface space available. 0.1 lb/ft^2 loading of 16/30 Brady sand is shown in Figure 4.31 prior to pressure being applied. Notice how inconsistent and poor the shape, roundness and size of this particular proppant is; whereas Figure 4.32 displays the Ottawa 20/40 sand proppant. Figure 4.32 also has a loading of 0.1 lb/ft^2. The quality difference in shape, size and roundness between the two proppants is noticeable.

Figure 4.31: Bottom and top cores from Freshwater Test#1 loaded with 16/30 Brady at 0.1 lb/ft^2 (no pressure). Core diameters are 1.0 inch.

Figure 4.32: Bottom and top cores from Freshwater Test#2 loaded with 20/40 Ottawa at 0.1 lb/ft^2 (no pressure). Core diameters are 1.0 inch.

As stated before, two similar but different sand proppants were picked to identify and capture embedment profile differences. As visible from Figures 4.31 and 4.32, where there is no pressure applied, one can make the assumption that embedment and rock damaging profiles of these two sand proppants will be different. This statement is made due to these two proppants displaying different physical characteristics such as shape and size. Once the proppants were successfully placed on the bottom core, both cores were placed in the steel chamber to be subjected to pressure via the brass rod. For each test, a pressure of 3030 psi was achieved and kept for almost an hour. 3030 psi may not seem like a high pressure for some shale formations, 3030 psi is enough for sand proppants to lose their conductivity. Proppant embedment and crushing of 16/30 Brady and 20/40 Ottawa sand proppants after 3030 psi was applied to Samples 1 and 2 are seen in Figures 4.33 and 4.34.
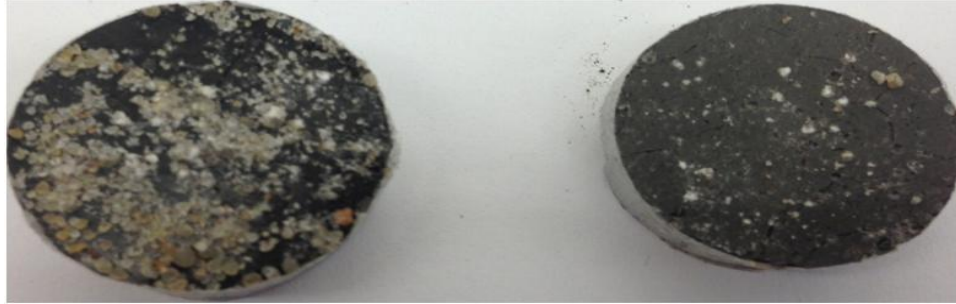
Figure 4.33: Bottom and top cores from Freshwater Test#1 loaded with 16/30 Brady at 0.1 lb/ft^2 after they were subjected 3030 psi for one hour. Core diameters are 1.0 inch.

Figure 4.34: Bottom and top cores from Freshwater Test#2 loaded with 20/40 Ottawa at 0.1 lb/ft^2 after they were subjected 3030 psi for one hour. Core diameters are 1.0 inch.

As expected the damage on sand proppants and proppant embedment are significant at 3030 psi. Sand proppants start losing a majority of their conductivity starting in the vicinity of 2000 psi. A load of 3030 psi on many sand proppants is sufficient enough to reduce hydraulic conductivity by 50-60% (Shah et al., 2010). Looking at the core surfaces, one can easily say that both the 16/30 Brady and 20/40 Ottawa were crushed. Most of the proppants that were crushed and embedded are occupying the bottom cores surface. This is mainly due to gravity, and doesn't imply that the top cores did not experience proppant embedment or damage. It is also very important to point out the distribution difference between the 16/30 Brady and 20/40 Ottawa sands. Figure 4.33 displays a more randomly packed damaged proppants, which will have a detrimental effect on proppant pack conductivity and flow in the fracture, whereas damaged 20/40 Ottawa sands have a more uniform and scattered distribution along the cores surface.

Figures 4.33 and 4.34 show some undamaged proppants along the edges of the cores. This is mainly due to the uneven surface of the brass rod that actually applies the pressure on cores. Since the surface is not completely flat, this disturbance on the surface effects the pressure distribution along the

cores. Thus some proppants along the edges remain undamaged. The strength difference between these two proppants also plays a significant role on how they are damaged. More of 16/30 Brady proppants ended up being crushed than the 20/40 Ottawa, also the amount of 20/40 Ottawa sands that penetrated through the core surfaces as a whole is higher than 16/30 Brady. This validates that 20/40 Ottawa sand is a stronger and a better shaped proppant than 16/30 Brady.

The core surfaces were damaged and fractured with the effect of pressure and proppants. Images of core surfaces (Figures 4.35 and 4.36) were taken once the proppants were scraped off in order to capture the damages on the core surfaces.

Figure 4.35: Bottom and top cores from Freshwater Test#1 (pressured to 3030 psi for 1 hour) after 16/30 Brady proppants are removed. Core diameters are 1.0 inch.

Figure 4.36: Bottom and top cores from Freshwater Test#2 (pressured to 3030 psi for 1 hour) after 20/40 Ottawa proppants are removed. Core diameters are 1.0 inch.

It is clear from Figures 4.35 and 4.36 that the cores themselves are damaged. In both cases, there are visible craters (holes) on the surfaces, with the bottom cores having more. These craters are due to proppant embedment. The embedment profiles are varying and different. As seen from Figures 4.35 and 4.36, there are a high number of embedded spots and they all vary in their shape, width, and depth. Embedment quantification of each core is presented in Chapter 5, and the embedment results for cores that are saturated with H_2O are shown in Section 4.4 along with images of how the embedment was measured. Figures 4.37 and 4.38 are SAM images of the two sets of cores after proppant tests. When

Figures 4.37 and 4.38 are compared to Figures 4.27 and 4.28 the fractures and embedded spots are very noticeable. There are also large damaged zones visible due to proppants forming packs and embedding the surface as a pack. Note that although there are not any fractures visible on optical images, however fractures can be easily seen in SAM images (Figures 4.37 and 4.38).
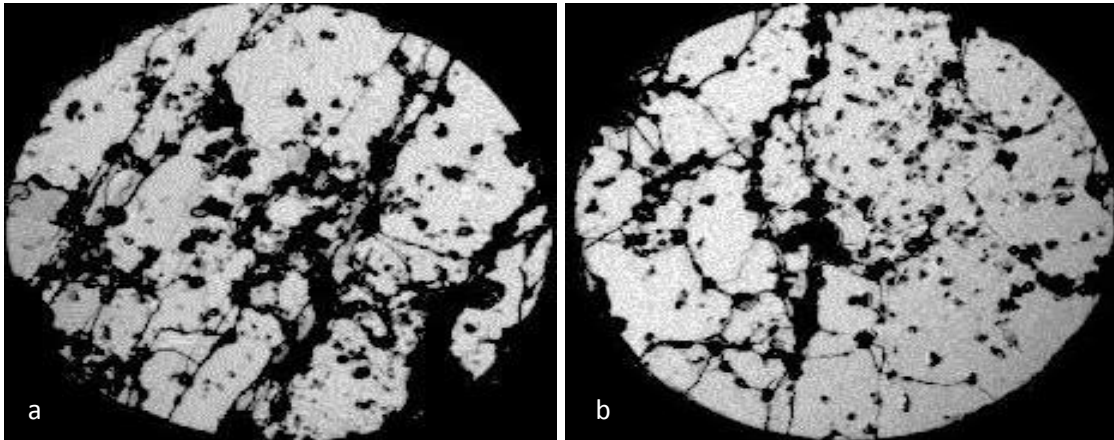
Figure 4.37: SAM images of bottom (a) and top (b) original cores for Freshwater Test #1 after proppant test with 16/30 Brady. Core diameters are 1.0 inch.
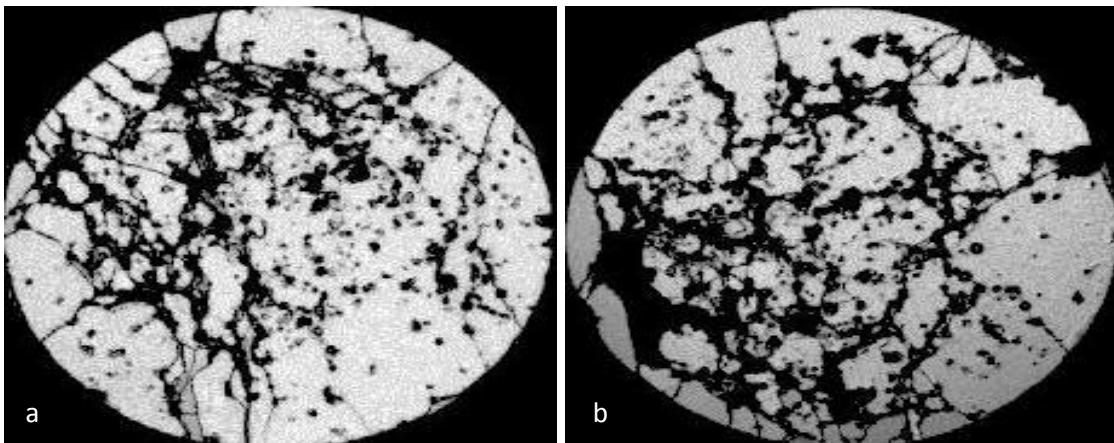
Figure 4.38: SAM images of bottom (a) and top (b) expansion cores for Freshwater Test #2 after pressure test with 20/40 Ottawa. Core diameters are 1.0 inch.

There are two distinguishable types of embedment present in these figures. The first one is where the created craters (holes) represent the proppants that got partially embedded and partially crushed or powdered. The other type is when the proppant is penetrated and embedded entirely in to the cores surface. This can be seen in Figures 4.35 and 4.36 where the sand proppants are still visible on the core

surfaces even after all the proppants were scraped off. As stated, the embedment of proppants as a whole was more severe when 20/40 Ottawa (Figure 4.36) was used due to its higher strength.

Another important result seen in Figures 4.35 and 4.36 is the generation and/or reactivation of natural fractures within these samples which were not visible before (Figures 4.29 and 4.30). Once the cores are subjected to 3030 psi when proppants are in between them, not only do core surfaces experience a high amount of embedment but also fractures are generated in various directions which creates a highly complex fracture network on the core surfaces. Although the cores are saturated and their brittleness has significantly reduced, the creation of these fractures suggests that the Niobrara cores will still be highly brittle even after a long duration of saturation.

4.4 Embedment Results of Freshwater Treated Cores (Samples 1 and 2)

As seen from Figures 4.27-4.36, proppant embedment and core damage occurring due to pressuring of the saturated and weakened cores are inevitable. Some cores are saturated with different fluids, and different proppants are used for each of these cores. Therefore embedment profile results for each test done with various fluids are different and unique. However, the results point out a trend and show different results for the different fluid and proppant effect. Proppant embedment results regarding only the freshwater saturated cores are shown in this section just like previous sections in this chapter. Overall results, including a comparison of all fluids and proppants, are reported in Chapter 5, and individual results for other fluids and heat treatments used in the research are reported in supplemental files A, B, C, and D.

In order to obtain accurate embedment results and approach the actual embedment profile created by specific proppants on chosen cores, a total of 18 different profilometer readings were obtained and recorded both for depth and width of the damaged areas. The average of 18 readings is reported and assigned as the actual embedment dimensions created by that fracturing fluid and proppant combination. Tables 4.4 through 4.7 show the individual 18 profilometer readings for depth and width along with the

average value for all freshwater-only cores. The cores were polished before pressurizing to make sure only damage mechanism effecting the proppant embedment was pressurizing the proppants.

Table 4.4: Proppant Embedment Depth and Width Results for H_2O Saturated Samples Test #1- Bottom Core

Profilometer Embedment Results for H20 Test #1 (Core#1---Core#3) Using Brady 16/30					
Embedment Results for Core #1 (Bottom Core while pressuring)					
	Width(µm)	Depth(µM)		Width(µm)	Depth(µM)
Scan #1	467	74	Scan #10	237	25
Scan #2	145	25	Scan #11	659	134
Scan #3	500	43	Scan #12	569	126
Scan #4	400	80	Scan #13	610	80
Scan #5	420	40	Scan #14	452	82
Scan #6	464	23	Scan #15	378	94
Scan #7	505	100	Scan #16	626	135
Scan #8	463	50	Scan #17	582	189
Scan #9	398	45	Scan #18	436	92
Average Depth(µm)		Range (µm)	Average Width(µm)		Range (µm)
80		23-189	462		145-659

Table 4.5: Proppant Embedment Depth and Width Results for H_2O Saturated Samples Test #1- Top Core

Profilometer Embedment Results for H20 Test #1 (Core#1---Core#3) Using Brady 16/30					
Embedment Results for Core #3 (Top Core while pressuring)					
	Width(µm)	Depth(µM)		Width(µm)	Depth(µM)
Scan #1	265	24	Scan #10	349	55
Scan #2	542	39	Scan #11	480	53
Scan #3	800	96	Scan #12	400	39
Scan #4	525	82	Scan #13	357	74
Scan #5	976	149	Scan #14	542	110
Scan #6	230	32	Scan #15	510	116
Scan #7	407	30	Scan #16	714	90
Scan #8	460	50	Scan #17	427	63
Scan #9	594	57	Scan #18	378	51
Average Depth(µm)		Range (µm)	Average Width(µm)		Range (µm)
67		24-149	498		230-976

Table 4.6: Proppant Embedment Depth and Width Results for H$_2$O Saturated Samples Test #2- Bottom Core

Profilometer Embedment Results for H20 Test #2 (Core#2---Core#4) Using Ottawa 20/40					
Embedment Results for Core #2 (Bottom Core while pressuring)					
	Width(μm)	Depth(μM)		Width(μm)	Depth(μM)
Scan #1	529	58	Scan #10	455	39
Scan #2	408	54	Scan #11	419	38
Scan #3	408	59	Scan #12	398	26
Scan #4	438	97	Scan #13	339	47
Scan #5	474	56	Scan #14	452	37
Scan #6	272	35	Scan #15	363	22
Scan #7	490	23	Scan #16	362	25
Scan #8	425	22	Scan #17	260	37
Scan #9	455	89	Scan #18	382	80
Average Depth(μm)		Range (μm)	Average Width(μm)		Range (μm)
47		22-97	407		260-529

Table 4.7: Proppant Embedment Depth and Width Results for H$_2$O Saturated Samples Test #2- Top Core

Profilometer Embedment Results for H20 Test #2 (Core#2---Core#4) Using Ottawa 20/40					
Embedment Results for Core #4 (Top Core while pressuring)					
	Width(μm)	Depth(μM)		Width(μm)	Depth(μM)
Scan #1	442	75	Scan #10	501	40
Scan #2	341	59	Scan #11	408	91
Scan #3	316	38	Scan #12	523	137
Scan #4	475	52	Scan #13	671	91
Scan #5	462	63	Scan #14	183	43
Scan #6	410	56	Scan #15	666	103
Scan #7	500	70	Scan #16	361	43
Scan #8	450	55	Scan #17	380	44
Scan #9	335	36	Scan #18	660	83
Average Depth(μm)		Range (μm)	Average Width(μm)		Range (μm)
66		36-137	449		183-671

The first thing to notice from Tables 4.4-4.7 is how much variation the profilometer readings have, even within one core. This validates the advantage and necessity of 18 different readings from each core for an accurate representation. Embedment values for the bottom core of the first test which are created with 16/30 Brady are 80 µm in depth and 462 µm in width whereas the values of depth and width

of top core are 67 µm and 498 µm. There is a very noticeable range between the top and bottom core values, and there are a couple reasons behind this variation. First of all, the cores used in this study are highly heterogeneous; therefore even if the pressure distribution is the same on two individual points, due to heterogeneity of the sample, the embedment profile could be different. The proppants are also randomly distributed along the core surfaces and unevenly pressured due to the non-flat surface of the pressuring rod, both of these factors add in changing the embedment profiles of proppants on the same core.

The images shown in Section 4.3 (Figures 4.33 and 4.34) show that more proppants remain on the bottom core after the top and bottom cores are separated. It is important to point out that the amount of proppants embedded and remaining on bottom cores does not mean that bottom core experiences a higher degree of embedment. This is simply due to gravity taking over once the pressuring is completed, and the cores are separated while the proppants are still placed in between them.

In each core the embedment depths are significantly lower than the width values. First of all, this is due to the depth values only representing one side of the embedment profile. The actual proppant embedment depth for Test #1 as a whole could actually be recorded as 147 µm (80+67 µm) which is the sum of the average embedment depth values for the bottom and top cores. However, since there is such separation between these values due to having random distribution and unknown orientation of cores, the depth values are reported individually. Since width values on each core represent only one specific value, they are higher and accordingly have a smaller range of variation. Another very important factor that affects the width measurements is the creation and possible regeneration of fractures on the core surfaces. Proppant embedment is most severe around the regions where there is a significant amount of fractures being created or natural fractures opening up. The proppant embedment width is greatly affected by these fractures. Depth values usually stay the same and do not get affected, however, the fractures cause the

width of embedded spots to expand and open up more. Therefore the width values are higher than the depth values.

There are significant differences in the embedment profiles of the 16/30 Brady and 20/40 Ottawa sands. Since the loads, cores, and saturating fluids are same, these differences can be compared and results can be drawn. The embedment values for 16/30 Brady from Tables 4.3 and 4.4 indicate that 16/30 Brady sand experienced more embedment and damage than the 20/40 Ottawa sand. This result can also be validated with Figures 4.33 through 4.36. Both the top and the bottom cores that had 20/40 Ottawa sand in between them experienced less embedment and showed significantly lower damage than the 16/30 Brady sands.

The embedment depth and width measurements on the core surfaces for the 16/30 Brady are significantly higher than for the 20/40 Ottawa. However, the embedment relevant to their size should also be investigated. Average sizes for 16/30 Brady and 20/40 Ottawa sands are 850 µm and 650 µm, respectively. When the bottom and top core embedment depth values are combined, the 16/30 Brady experiences a 17% loss in its depth due to embedment whereas 20/40 Ottawa's loss is 17%. The percentages are same due to the size difference of these proppants. When the sizes of the proppants are taken into account, the embedment difference does not seem too significant, especially if one thinks that 16/30 Brady should have more intact proppants remaining due to its larger size. However, looking at Figures 4.33 and 4.35, it is obvious that this is not the case. In addition to experiencing more embedment, the 16/30 Brady sand also experiences more crushing effects and damage on the remaining proppant pack. Therefore, as a main result, 20/40 Ottawa sand pressured with 3030 psi between cores saturated with freshwater yields less embedment, less overall damage on the proppant pack including crushing, thus provides better conductivity, permeability and flow in fractures compared to 16/30 Brady.

The profilometer has some error associated with it just like the nanoindenter. The error in this machine according to the user's guide is approximately 1%. Although this is a low value, it still affects

the results. As seen in Tables 4.4-4.7, the 18 profilometer readings obtained for each core have a wide range of values and each core generated significantly different averages than one another. This variation in the data cannot be linked to the 1% error the profilometer creates. The variation in values is dramatically larger than the impact of a 1% error. Therefore, the results obtained indicate and represent a data set for very heterogeneous set of cores. Also the variation in values comes from the unique and different effect each fracturing fluid had on the Niobrara shale samples.

In addition to the error values from the tool, error analysis from the data was also made, and the standard deviation and coefficient of variation were calculated and are shown in Table 4.8. These values were calculated from the 18 data points that the profilometer measured for the depth and width of proppant embedment profiles of each cores. As seen in Table 4.8, the standard deviation and coefficient of variation are relatively large. This is due to the significant variation in measurements obtained from the profilometer because of the heterogeneity of cores and varying fracturing fluid effect on cores. The proppant embedment error analyses for the samples that are saturated with other fracturing fluids and heated samples are shown in supplemental files A, B, C, and D.

Table 4.8: Error Analysis of the Depth and Width Proppant Embedment Measurement Obtained

	H20 Test #1 (Core#1---Core#3) Using Brady 16/30		H20 Test #1 (Core#1---Core#3) Using Brady 16/30	
	Bottom Core while pressuring		Top Core while pressuring	
	Depth	Width	Depth	Width
Standard Deviation	45.45	129.58	33.98	185.91
Coefficient of Variation %	56.93	28.06	50.55	37.37
	H20 Test #2 (Core#2---Core#4) Using Ottawa 20/40		H20 Test #2 (Core#2---Core#4) Using Ottawa 20/40	
	Bottom Core while pressuring		Top Core while pressuring	
	Depth	Width	Depth	Width
Standard Deviation	22.99	70.06	27.03	128.65
Coefficient of Variation %	49.04	17.21	41.26	28.65

CHAPTER 5

DISCUSSION OF RESULTS

Proppant embedment is an inevitable issue in hydraulic fracturing. Mechanical property alteration most importantly changes in Young's modulus during the fracturing process, are critical to understand in order to design and achieve a better fracture permeability and conductivity. A good understanding of Young's modulus behavior of a specific formation under various conditions will also dictate the fracturing fluid and proppant combination to be used in fracturing jobs. The experiments and measurements in this project show that Young's modulus starts decreasing as soon as rocks are exposed to fracturing fluids even in a five-day span. Measurements indicate that after a certain time Young's modulus values stop decreasing or even slowly start increasing. The Young's modulus reduction for the Niobrara cores occurred regardless of the fracturing fluid type. Sections 5.1-5.5 discuss the results of the testing described in Chapter 3 and 4.

5.1 Original and Expansion Samples Comparison

In the proposal stage, this work only had four samples that were going to be tested with four different fracturing fluids. However, the effects of some fracturing fluids on the Niobrara cores were not anticipated and were rather interesting. Therefore, four additional samples were added to the study to be saturated with the same fluids. These extra sets of samples expanded our data and showed that our results are representative of results in Chapter 4. The expansion sample tests proved critical, because they provided an extra set of experiments to validate the original results to check reliability and accuracy. They also make it possible to test embedment profiles of different proppants for the cores that were saturated with the same fracturing fluids. Both set of samples provide the same Young's modulus alterations in cores for the four fracturing fluids that were used. Table 5.1 shows the percentages of Young's modulus reductions and Young's modulus values of original and expansion samples that are saturated with the four fracturing fluids at each saturation phases. The fracturing fluid effect is the same on both sets of cores,

99

even though they show different magnitudes in their percentages. The sample numbers used in this chapter corresponds to Table 4.1, Samples 1, 3, 5, and 7 represent the original samples ,whereas Samples 2, 4, 6, and 8 represent the expansion samples.

Table 5.1: Young's Modulus Reduction Percentages and Young's Modulus Values for Samples 1-8 (Original and Expansion) at Each Saturation Phase

Saturation Duration	Fluids	Sample #	Young's Modulus % Reductions for Samples 1-3-5-7	Young's Modulus Values for Samples 1-3-5-7(psi)	Sample #	Young's Modulus % Reductions for Samples 2-4-6-8	Young's Modulus Values for Samples 2-4-6-8 (psi)
Dry	Freshwater	1	0.00	7.16E+06	2	0.00	6.83E+06
5 Days		1	33.58	4.75E+06	2	14.04	5.87E+06
15 Days		1	40.33	4.27E+06	2	9.42	6.19E+06
30 Days		1	37.78	4.45E+06	2	4.84	6.50E+06
Dry	KCl	3	0.00	7.72E+06	4	0.00	6.67E+06
5 Days		3	26.51	5.67E+06	4	19.18	5.39E+06
15 Days		3	53.68	3.58E+06	4	20.98	5.27E+06
30 Days		3	64.27	2.76E+06	4	5.06	6.33E+06
Dry	KCl+Friction Reducer	5	0.00	7.67E+06	6	0.00	6.42E+06
5 Days		5	43.75	4.31E+06	6	13.98	5.52E+06
15 Days		5	61.76	2.93E+06	6	47.89	3.35E+06
30 Days		5	78.65	1.64E+06	6	48.83	3.29E+06
Dry	Freshwater+KCl Substitute	7	0.00	6.94E+06	8	0.00	6.89E+06
5 Days		7	10.82	6.19E+06	8	9.54	6.24E+06
15 Days		7	17.16	5.75E+06	8	12.03	6.07E+06
30 Days		7	16.62	5.79E+06	8	1.78	6.77E+06

The largest reduction in Young's modulus occurred when the cores were saturated with KCl+friction reducer for both set of samples. KCl is the second most reducing fracturing fluid for both samples, which is followed by freshwater and freshwater+KCl substitute. All of the samples experience a significant reduction at the end of five days, which is followed by slightly more reduction until the end of the 15 days of saturation. However, once the saturation reaches 30 days, the Young's modulus reduction is either very insignificant or even in some cases starts to slightly increase. The same fluid effect that causes Young's modulus values to slightly increase after a long period of time is also supported by work done by LaFollete and Carman, (2010). Therefore, the 15-day saturation results are considered as the most influential and representable results for how much different fracturing fluids affect the Niobrara cores used in this work from a Young's modulus standpoint. Figure 5.1 shows the trend of Young's

modulus reduction percentage of both original (Samples 1, 3, 5, and 7) and expansion (Samples 2, 4, 6, and 8) samples with the four fracturing fluids at 15 days.
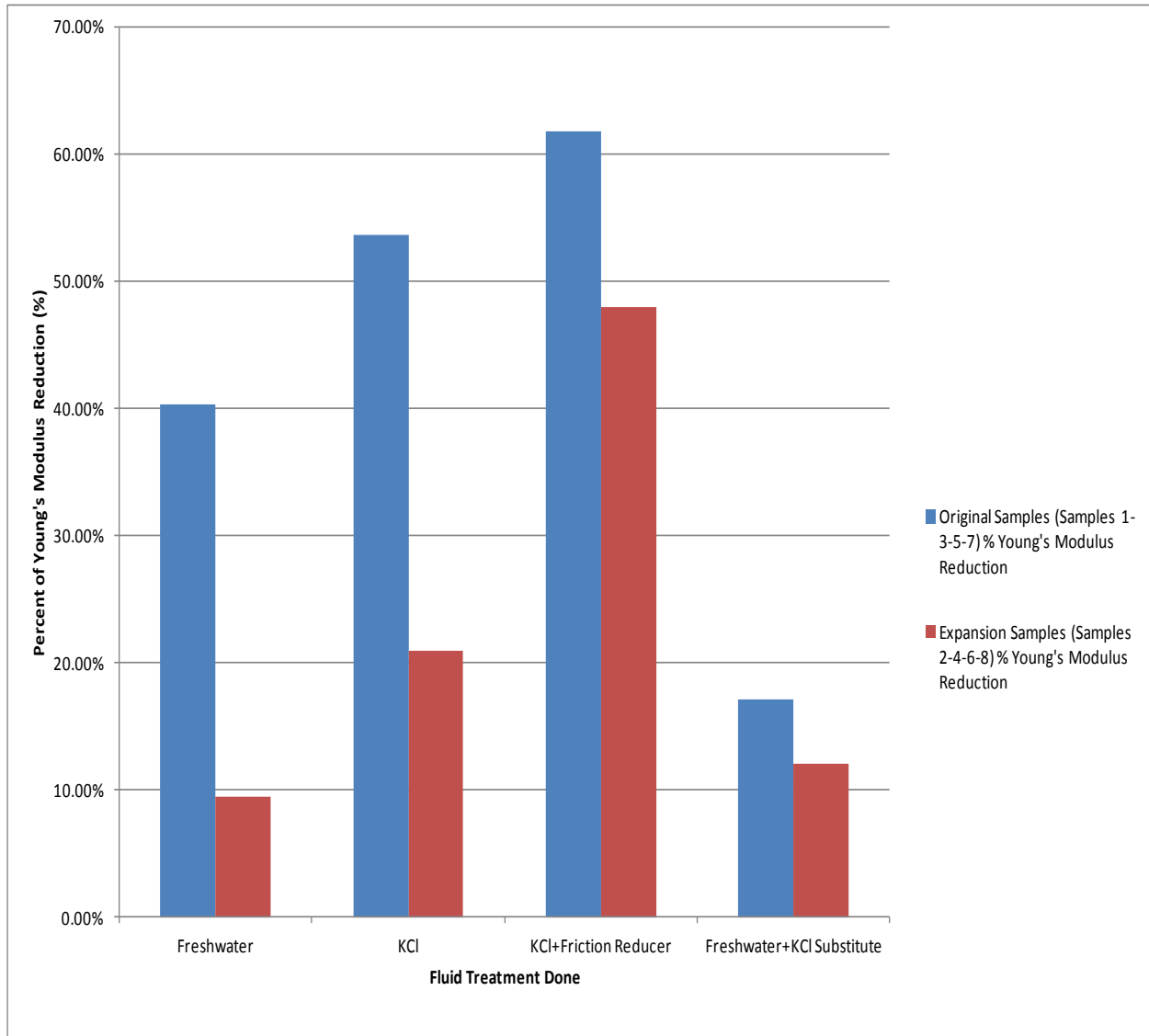
Figure 5.1: Young's modulus reduction percentages at 15 days saturation showing how original and expansion samples follow the same reduction trend.

Reduction due to KCl+friction reducer reaches 62% and 48%, whereas, the reduction effect by freshwater+KCl substitute is only at 17% and 12%. The reduction profiles of all fluids on both sets of samples are almost the same. These results show that KCl-based fracturing fluids reduce the Young's modulus of the Niobrara cores more than water-based fracturing fluids. This effect also directly effects the proppant embedment, thus KCl based fluids yield a higher proppant embedment issue when they are

used in formations similar to in this work (very high calcite and low clay). Figures 5.2 – 5.9 show the comparison of Young's modulus values and reduction percentages of original (Samples 1, 3, 5, and 7) and expansion (Samples 2, 4, 6, and 8) samples specifically for each fracturing fluid at all saturation phases.
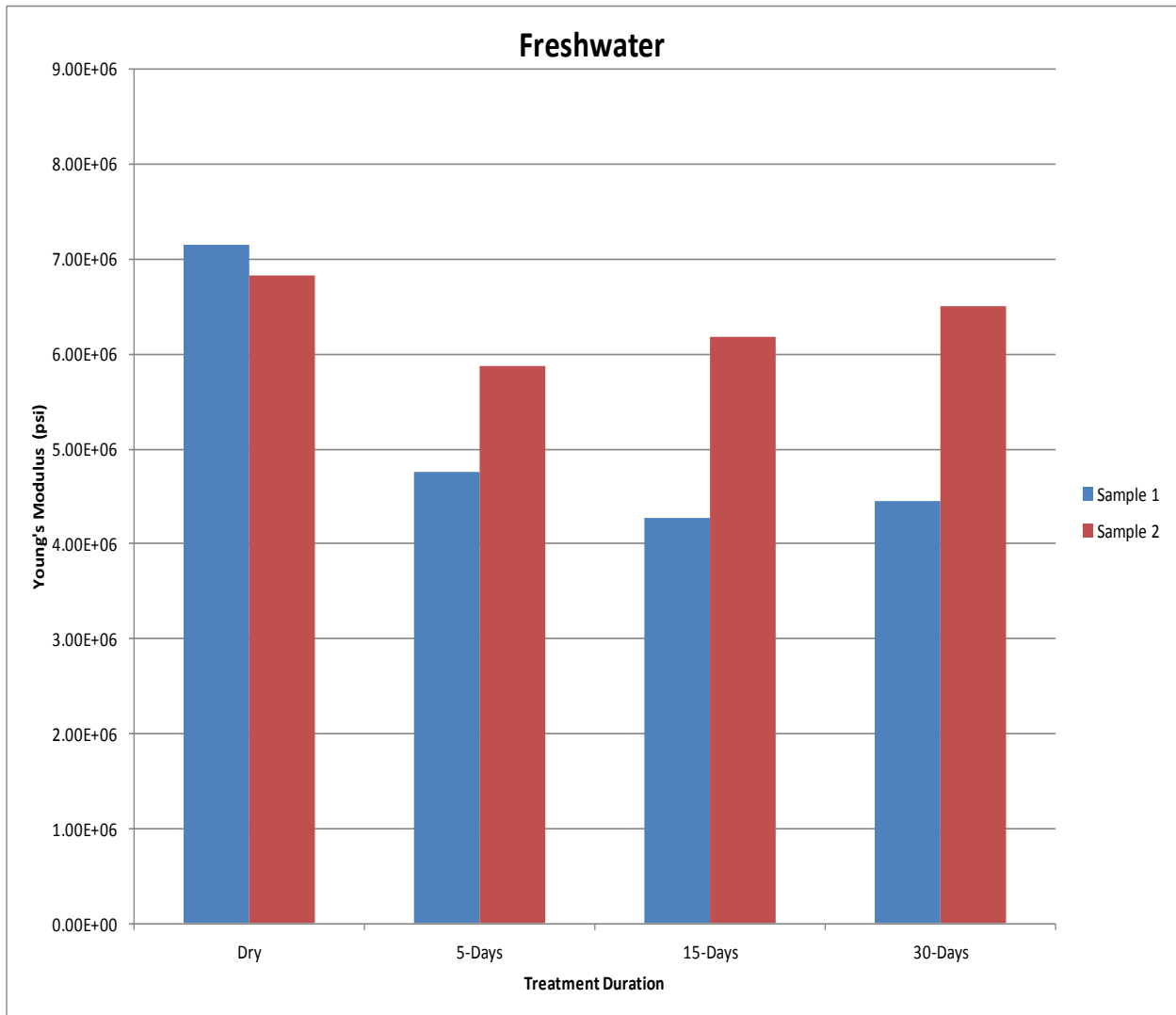
Figure 5.2: Young's modulus measurements of Sample 1 (6606.8') and Sample 2 (6742.25') prior to saturation and after 5, 15, and 30 days of saturation with freshwater. Reaction of both set of samples to freshwater is seen.

Sample 1 (6606.8') and Sample 2 (6742.25') both have initial Young's modulus values that are very close to 7.00E+06 psi. The Young's modulus values stop decreasing and start increasing at different freshwater saturation phases for these two samples. Sample 1 experiences this at 30 days, where as Sample 2 experiences this at 15 days.
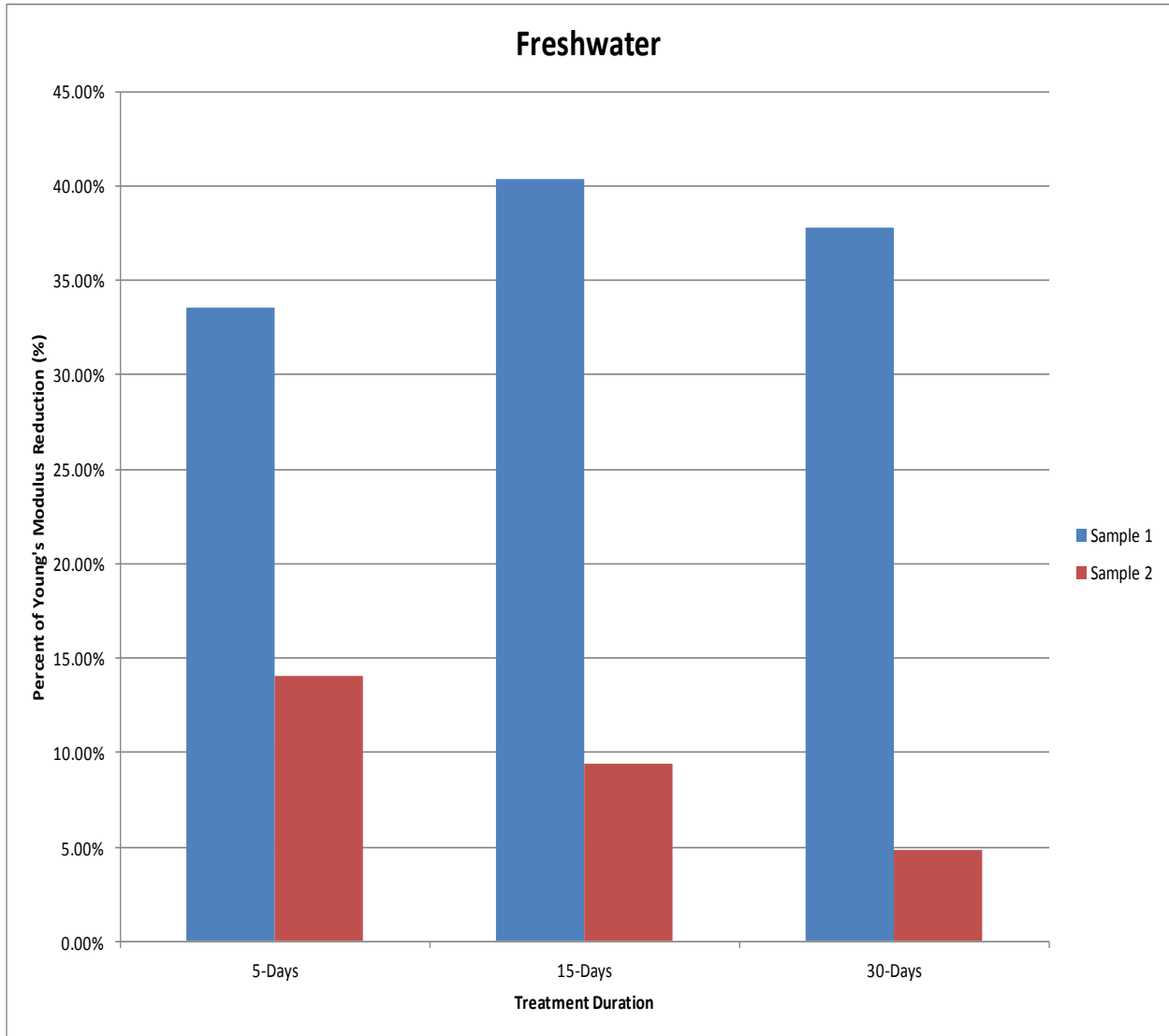
Figure 5.3: Percentage of Young's modulus reduction of Sample 1 (6606.8') and Sample 2 (6742.25' after 5, 15, and 30 days of saturation with freshwater. Reaction of both set of samples to freshwater is seen.

The reduction trend can be seen clearer in Figure 5.3. The shift in Young's modulus change was also noted in the LaFollete and Carman, (2010) study. However, there are also mechanical, experimental and logistical issues besides the natural reasons that can cause this shift in Young's modulus. Some of these causes include:

- Nanoindenter actually measuring harder minerals due to heterogeneity of cores;

- Measurements getting effected by fluid residue left on cores;

- Variation in polishing quality on cores surface; and,

- Operational issues and inconsistencies of the nanoindenter while measuring.
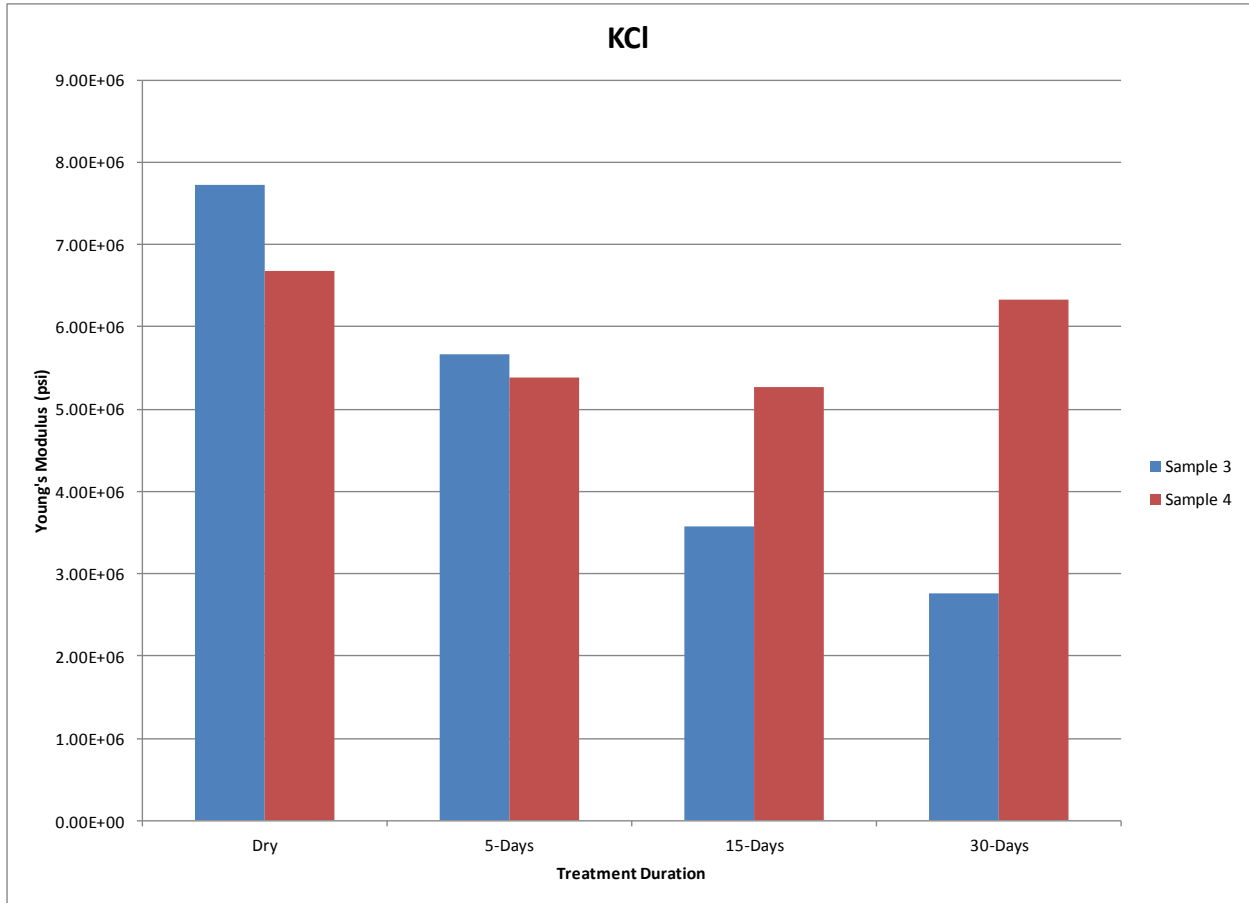
Figure 5.4: Young's modulus measurements of Sample 3 (6742.25'A) and Sample 4 (6639.8') prior to saturation and after 5, 15, and 30 days of saturation with KCl. Reaction of both set of samples to KCl is seen.

Figures 5.4 and 5.5 show the effects of KCl as a fracturing fluid on Young's modulus profiles of both samples. The initial Young's modulus values of Sample 3 (6742.25'A) and Sample 4 (6639.8') are close to Samples 1 and 2. The Young's modulus values and reduction trend is once again the same for both samples when these cores are saturated with KCl. The Young's modulus for Sample 3 does not stop decreasing or increase again for the KCl. However, Sample 4 experiences a more significant increase in its Young's modulus between 15 and 30 days; it goes from 5.27E+06 psi to 6.33E+06 psi.
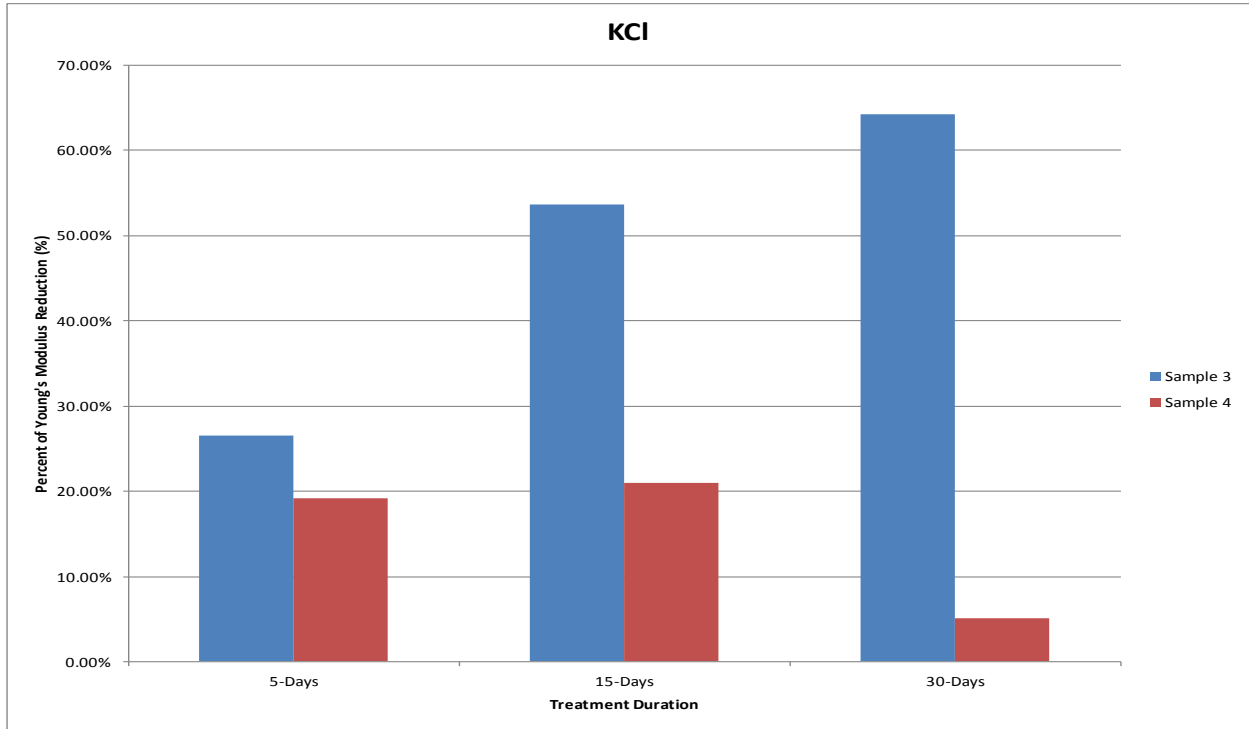
Figure 5.5: Percentage of Young's modulus reduction of Sample 3 (6742.25'A) and Sample 4 (6639.8') after 5, 15, and 30 days of saturation with KCl. Reaction of both set of samples to KCl is seen. Note the scale change in reduction percentage.
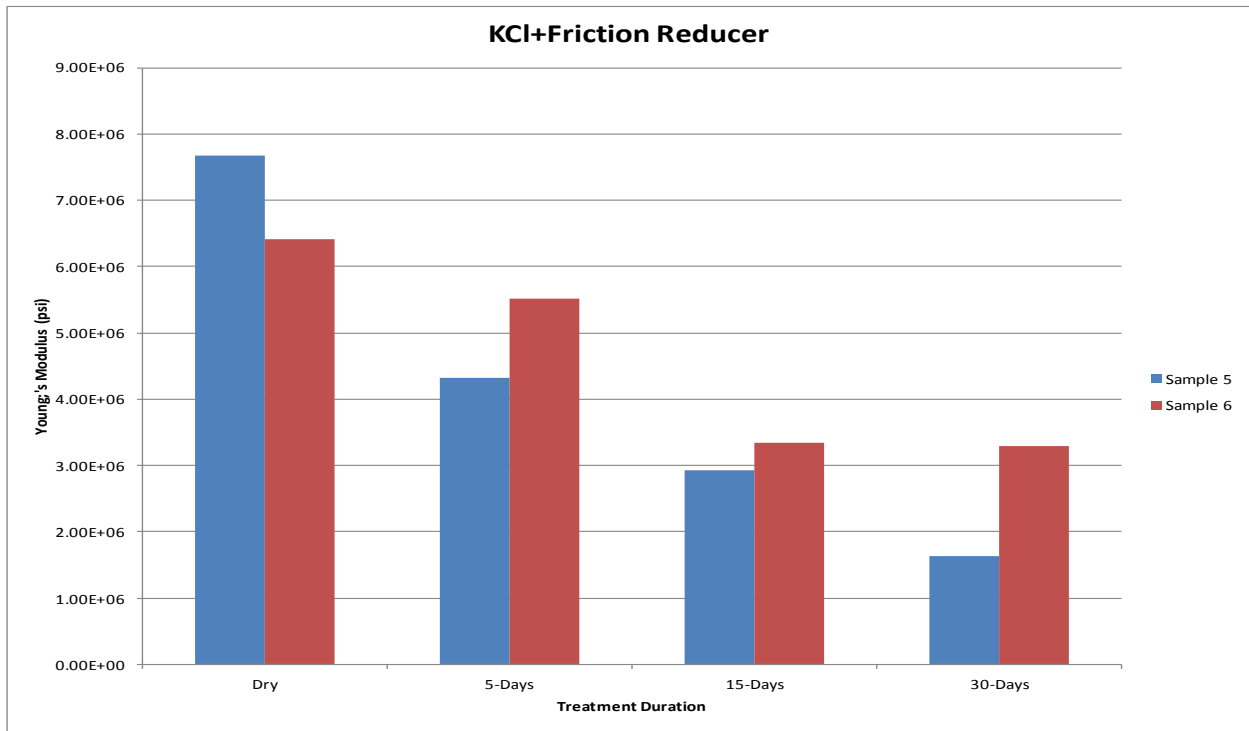
Figure 5.6: Young's modulus measurements of Sample 5 (6742.25'B) and Sample 6 (6772.25') prior to saturation and after 5, 15, and 30 days of saturation with KCl+Friction reducer. Reaction of both set of samples to KCl+friction reducer is seen.
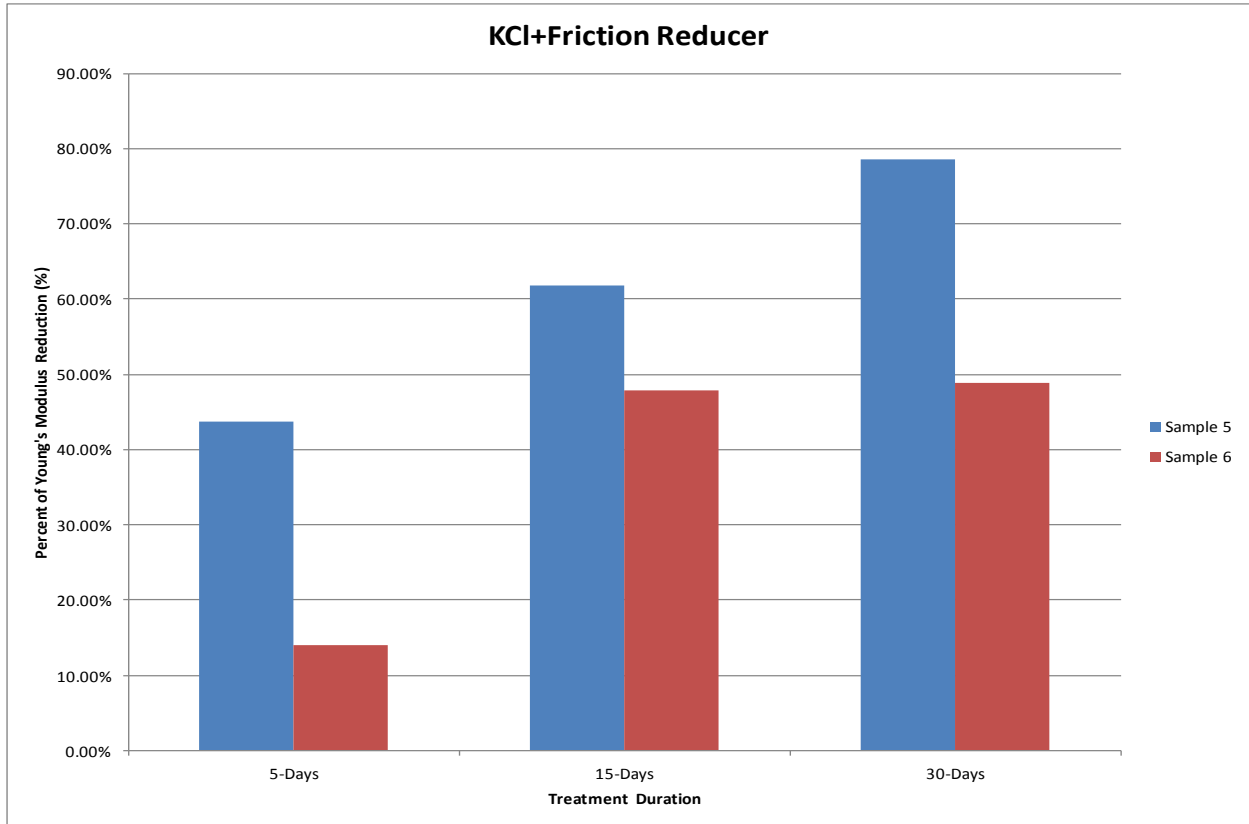
Figure 5.7: Percentage of Young's modulus reduction of Sample 5 (6742.25'B) and Sample 6 (6772.25') after 5, 15, and 30 days of saturation with KCl+friction reducer. Reaction of both set of samples to KCl+friction reducer is seen. Note the scale change in reduction percentage.

KCl+friction reducer fluid ended up being the most damaging fluid to Young's modulus in the experiments conducted for both samples. Figures 5.6 and 5.7 show the significant effect of this fracturing fluid on the Niobrara cores. Sample 5 (6742.25'B) at the end of 30 days experiences almost and 80% reduction in its Young's modulus, and Sample 6 (6772.25') experiences almost a 50% reduction. These numbers represent significant weakening in the samples' mechanical properties. Although the samples used in this work are highly carbonated and brittle samples that have natural fractures and can make the fractures more efficient due to their high strength, after experiencing reductions between 50-80% they will have no difference than ductile formations that are almost impossible to fracture and produce from. Cores that are saturated with the freshwater+KCl substitute also showed the most proppant embedment when both 20/40 Ceramic and 20/40 RCS were used. Embedment results are explained in more detail in Sections 5.6-5.7.
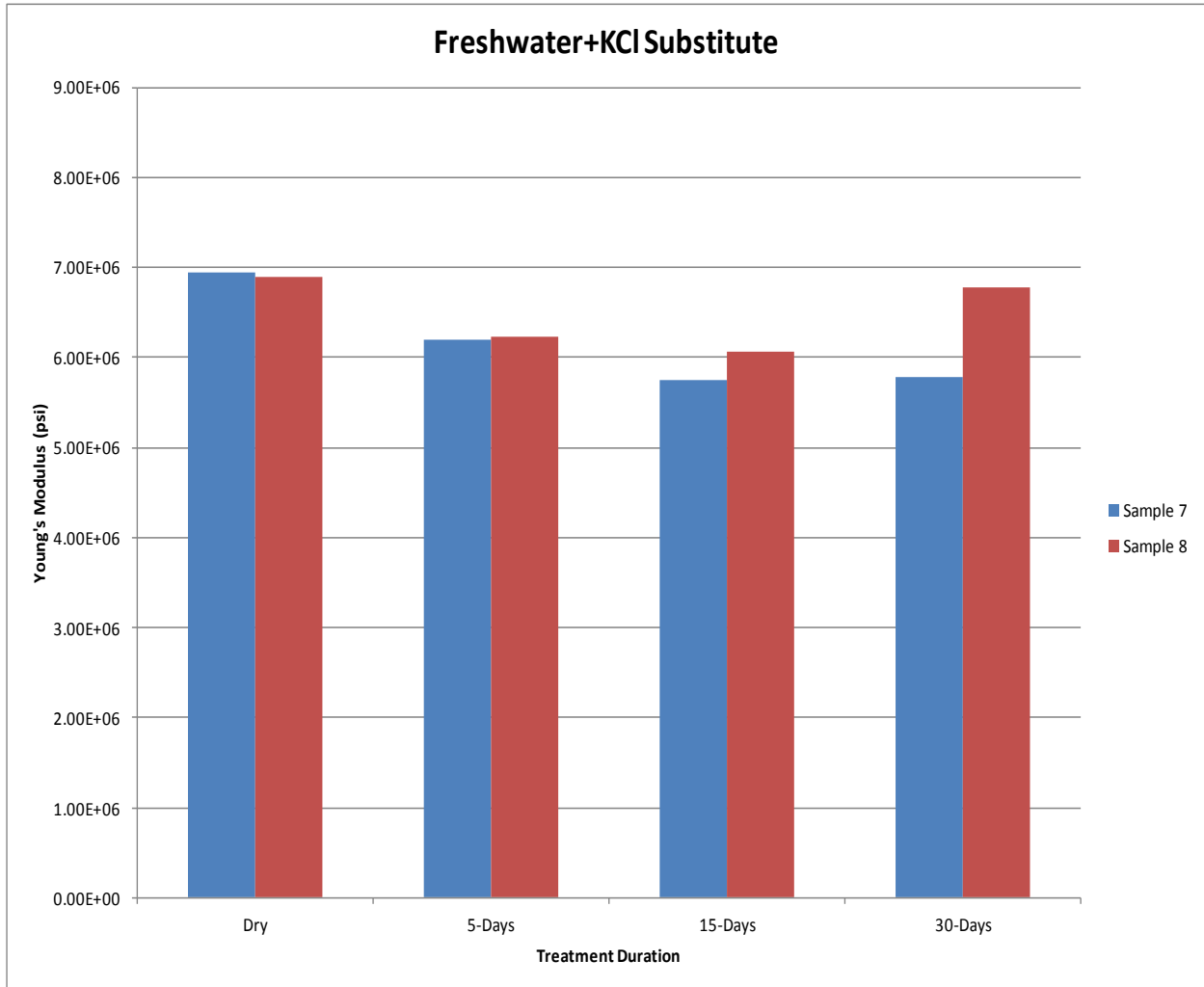
Figure 5.8: Young's modulus measurements of Sample 7 (6788.65') and Sample 8 (6777.75') prior to saturation and after 5, 15, and 30 days of saturation with Freshwater+KCl substitute. Reaction of both set of samples to Freshwater+KCl substitute is seen.

Figures 5.8 and 5.9 show how the Young's modulus profiles of Sample 7 (6788.65') and 8 (6777.75') vary when they are saturated with freshwater+KCl substitute. Freshwater+KCl substitute is the least damaging fluid to Young's modulus. As Figure 5.8 shows, the initial Young's modulus values are very close to the Young's modulus values at 15 and 30 days. Looking at Figure 5.9, it can be seen that both samples experience significantly lower reductions compared to the other fracturing fluids used in this work. However, they differ at the Young's modulus change after 15 days. Sample 7's experiences very insignificant, almost negligible Young's modulus change between 15 and 30 days, but Sample 8 shows almost a 10% increase in its Young's modulus value.

Freshwater+KCl Substitute
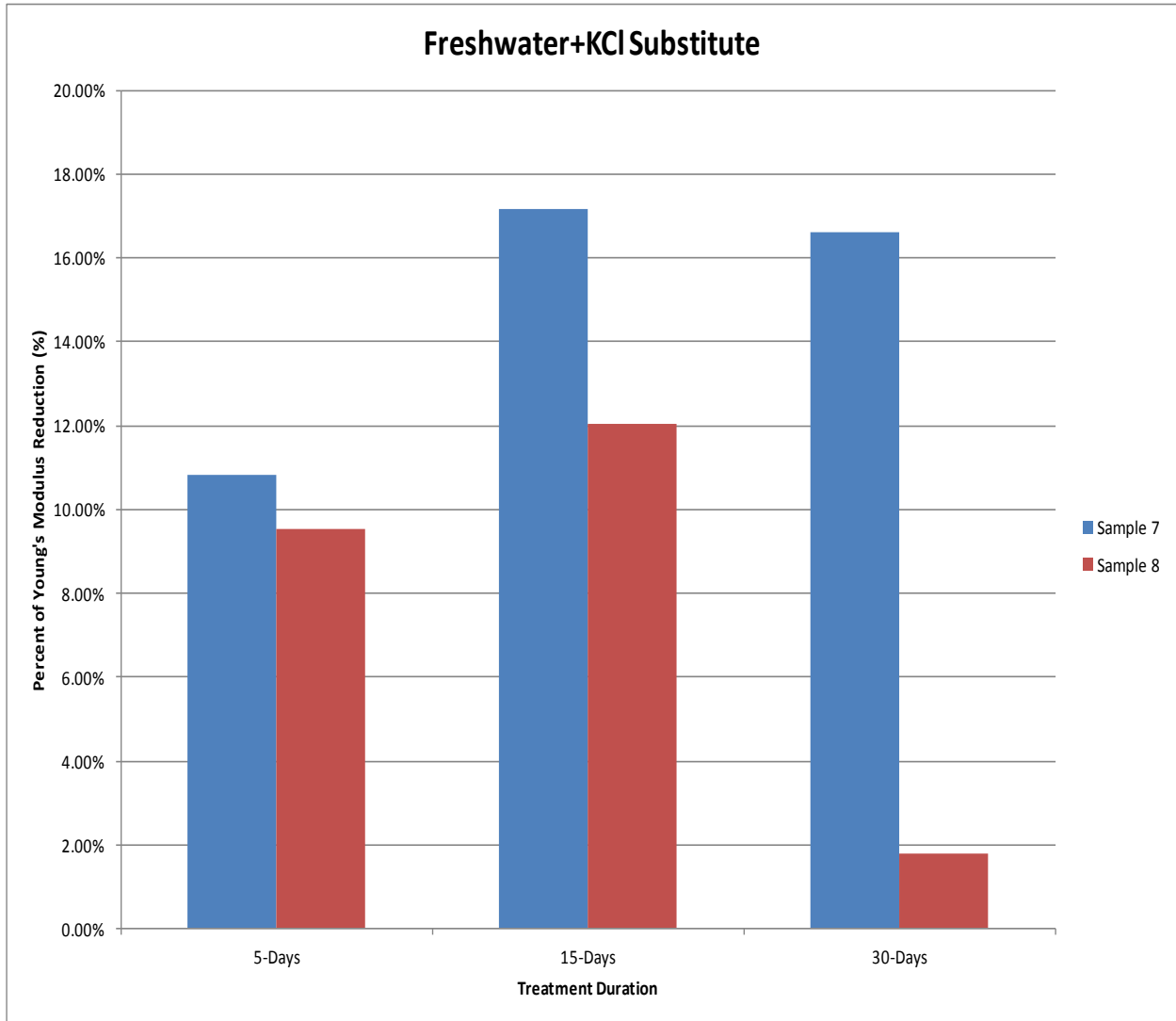
Figure 5.9: Percentage of Young's modulus reduction of Sample 7 (6788.65') and Sample 8 (6777.75') after 5, 15, and 30 days of saturation with Freshwater+KCl substitute. Reaction of both set of samples to Freshwater+KCl substitute is seen. Note the scale change in reduction percentage.

Running experiments on two sets of samples provided this work with more reliable and repeatable results. It also gave the opportunity to test more proppants in order to compare how different proppants embed when they are used with the same fluid. Results and figures in this section show that the four fracturing fluids used in this work have the same general effect on samples regardless of their variations in depth and mineralogy. Even though the magnitudes of the reactions are different, both sets of samples experienced the same reactions towards these four fracturing fluids.

5.2 Time Effect on Young's Modulus

While looking at these research results, it is also important to look at the Young's modulus alteration as something that is triggered not only by fluid selection but also time. Table 5.2 which is very similar to Table 5.1 shows the Young's modulus % reductions for each set of samples at each saturation phase. Figures 5.10-5.17 show how each of the fracturing fluids affect Young's modulus reduction specifically at saturation phases. This allows seeing more clearly how much effect saturation time has on Young's modulus alteration via certain fracturing fluids.

Table 5.2: Young's Modulus Reduction Percentages for Samples 1-8 (Original and Expansion) at Each Saturation Phase

Saturation Duration	Fluids	Sample #	Young's Modulus % Reductions for Samples 1-3-5-7	Sample #	Young's Modulus % Reductions for Samples 2-4-6-8
Dry	Freshwater	1	0.00	2	0.00
5 Days		1	33.58	2	14.04
15 Days		1	40.33	2	9.42
30 Days		1	37.78	2	4.84
Dry	KCl	3	0.00	4	0.00
5 Days		3	26.51	4	19.18
15 Days		3	53.68	4	20.98
30 Days		3	64.27	4	5.06
Dry	KCl+Friction Reducer	5	0.00	6	0.00
5 Days		5	43.75	6	13.98
15 Days		5	61.76	6	47.89
30 Days		5	78.65	6	48.83
Dry	Freshwater+KCl Substitute	7	0.00	8	0.00
5 Days		7	10.82	8	9.54
15 Days		7	17.16	8	12.03
30 Days		7	16.62	8	1.78

In Figures 5.10-5.17 each fluid is assigned a color. In each figure, blue represents freshwater, green represents KCl, purple represents KCl+friction reducer, and red represents freshwater+KCl substitute. These same colors are also used for Tables 5.1 and 5.2 as well as other figures shown in other sections in this thesis. Figure 5.10 shows how much each fracturing fluid reduced the Young's modulus values of the original samples (Samples 1, 3, 5, and 7) only after five days of saturation, which is then

follow by Figures 5.11 and 5.12 showing the same data at 15 days and 30 days saturation respectively. It is important to point out that the y-axis values (% reduction in Young's modulus) have different maximum values in each figure in order for the numbers to be clearly seen. Investigating the time effect saturation via different fluids on Young's modulus is beneficial, because different saturation phases may contain different and unique information in comparison to the result at the end of 30 days.

Figure 5.10, the five days saturation results indicate that the, freshwater+KCl substitute as the least damaging fluid with a 10.82% reduction and the KCl+friction reducer as the most damaging fluid with a 43.75% reduction. However, KCl shows a 26.51% reduction, which is lower than freshwater reduction at 33.58%. As stated before, KCl ended up being more damaging at the end of 15 and 30 days and yielded more embedment, but looking at the five days of saturation, freshwater seems to decrease the Young's modulus more than KCl does.
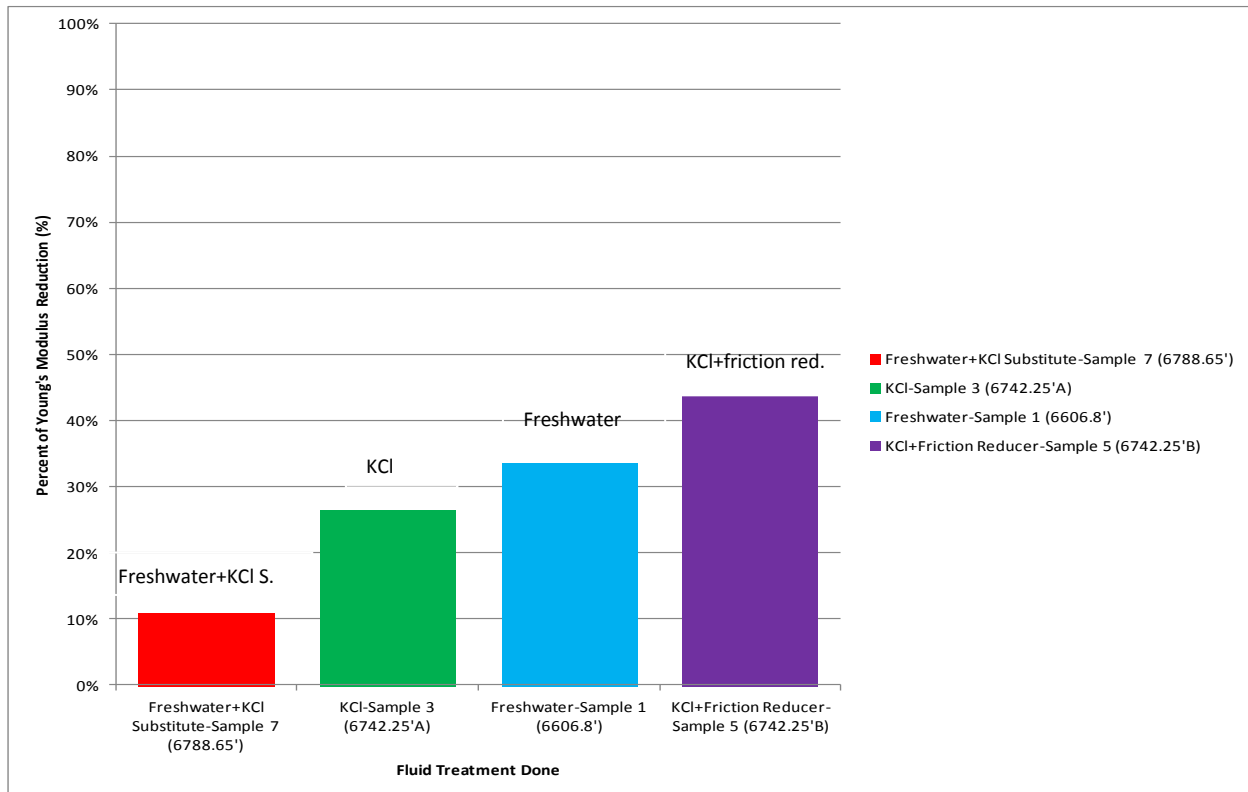
Figure 5.10: Young's modulus reduction percentage values for each fracturing fluid used on original samples (Samples 1, 3, 5, and 7) after 5 days of saturation.
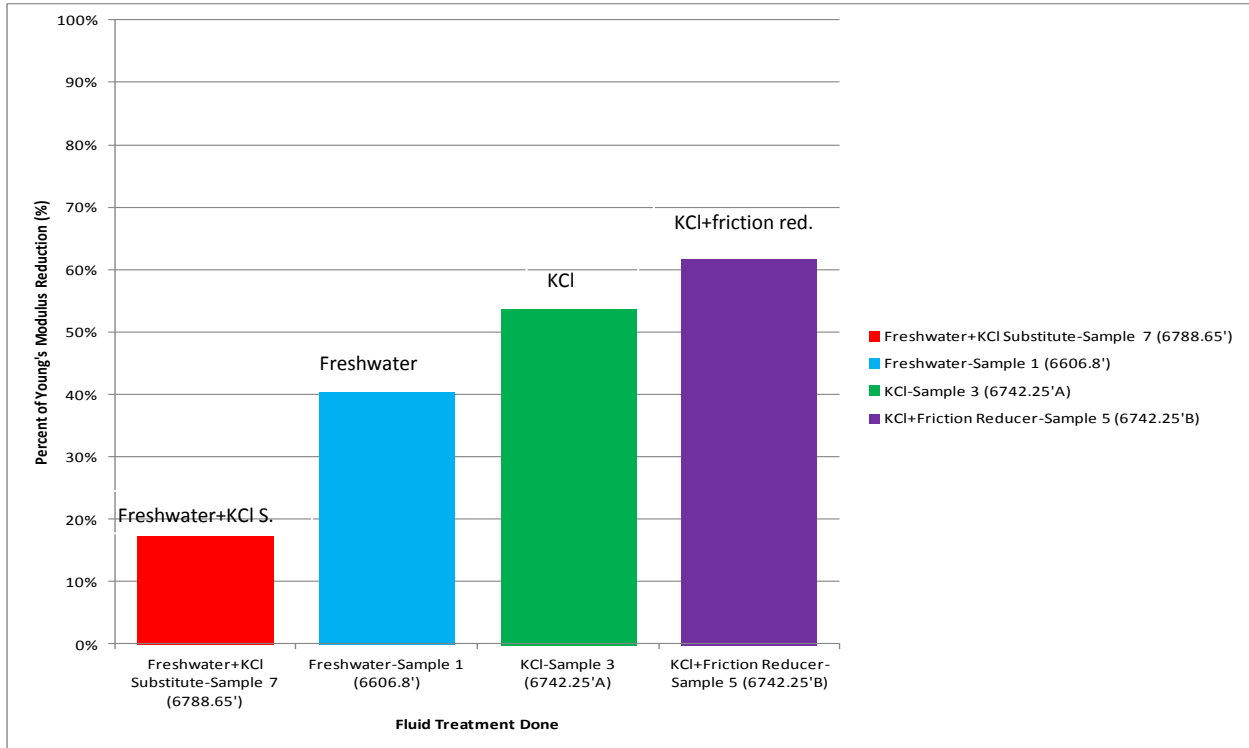
Figure 5.11: Young's modulus reduction percentage values for each fracturing fluid used on original samples (Samples 1, 3, 5, and 7) after 15 days of saturation.
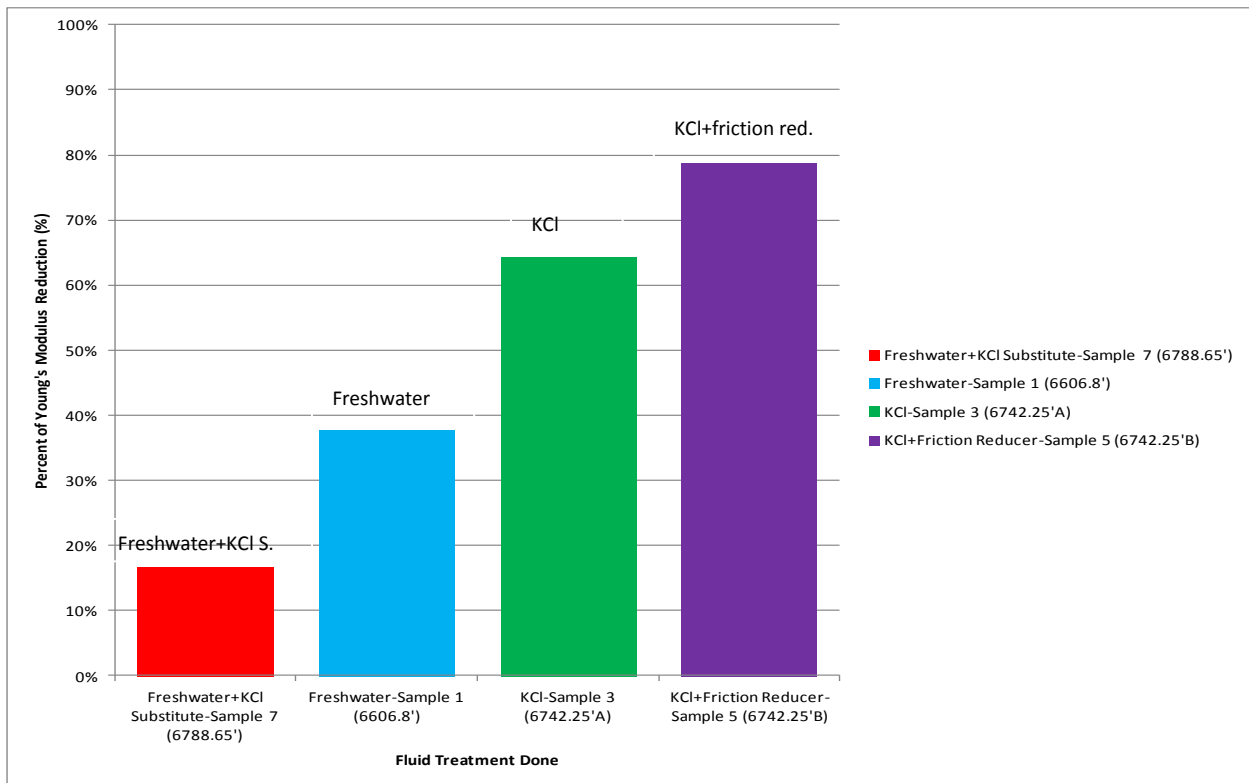
Figure 5.12: Young's modulus reduction percentage values for each fracturing fluid used on original samples (Samples 1, 3, 5, and 7) after 30 days of saturation.

Figures 5.10 through 5.12 are combined into one graph, Figure 5.13, in order for the saturation time effect on Young's modulus to be seen on all of the original samples.
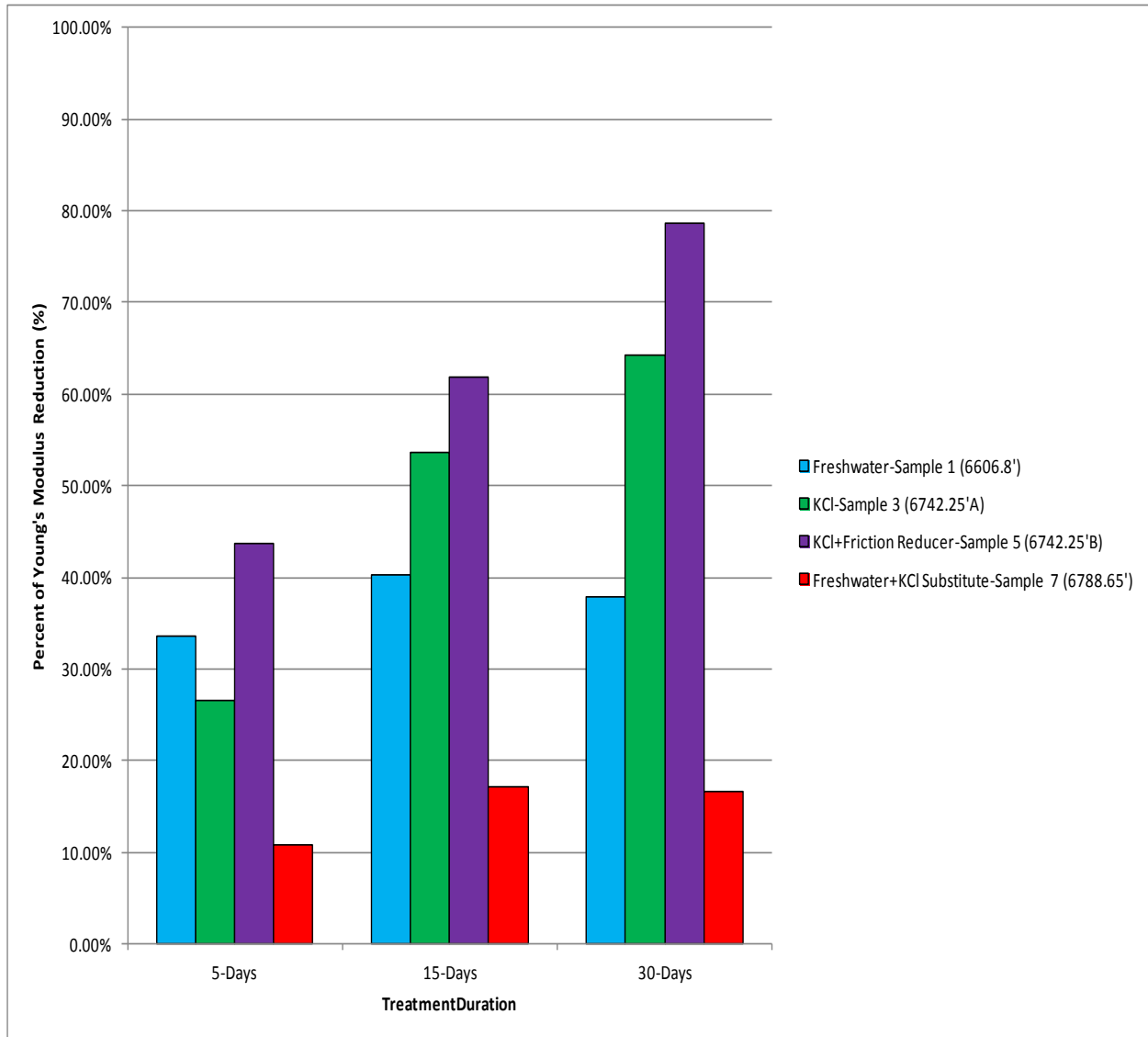
Figure 5.13: Young's modulus reduction percentage values for each fracturing fluid used on original samples (Samples 1, 3, 5, and 7) are shown. Values are grouped for each saturation phase to compare the fluid effects at different saturation phases.

Figure 5.13 shows the effects of each fracturing fluid next to each other at each saturation phase for a closer comparison. It is very clear that 30 days saturation has higher reductions caused by fluids. The most damaging fluid on Samples 1-3-5-7 is KCl+friction reducer with a 78.65% reduction, and the least damaging fluid is freshwater+KCl substitute as seen in red color with only a 16.62% reduction at the end of 30 days of saturation. Figure 5.13 shows Young's modulus alterations as a function of fluid type and

exposure time. Freshwater initially has a high reduction in Young's modulus (33.58%) at the end of five days. However, with prolonged exposure, the Young's modulus reduces only by 6.75% to reach a total reduction of 40.33%. After 30 days of exposure, Young's modulus actually experiences a recovery (37.78% of original value). Young's modulus reduction values related to freshwater+KCl substitute also display very similar behavior where five days saturation experiences a significant initial reduction, followed by an insignificant reduction between five days and 15 days, and a small increase in Young's modulus value at the end of 30 days. Looking at Figures 5.10-5.13, it is very reasonable to say that the initial Young's modulus reduction caused at the end of the first five days of saturation is very significant for each fracturing fluid, KCl+friction reducer being the most and freshwater+KCl substitute being the least. The weakening in Young's modulus values continues for every sample that is saturated by a different fluid after five days until the end of 30 days of saturation. Important results from these figures are, KCl saturated sample experiences more Young's modulus reduction within the first five days then freshwater saturated sample. Also samples saturated with freshwater and freshwater+KCl substitute do not experience any more Young's modulus reduction, instead their Young's modulus values start increasing.

The benefit of running expansion sample tests on the additional samples assisted the research project in looking at if the saturation time effect on Young's modulus values are repeatable when same fluids are used on different cores. Figures 5.14-5.17 show how much each fracturing fluid reduced the Young's modulus values on Samples 2, 4, 6, and 8. Figures for these samples show more unique and varying results in comparison to the general end result at the end of 30 days and the Samples 1, 3, 5, and 7 results. The effect of fracturing fluids do not necessarily follow a trend at the end of each saturation time instead, the sequence for reduction magnitude seems to change with each saturation time. The expanded sample set allowed us to evaluate the factors that affected the Young's modulus the most. Lithology turned out to be not as important as fluid type and exposure time.
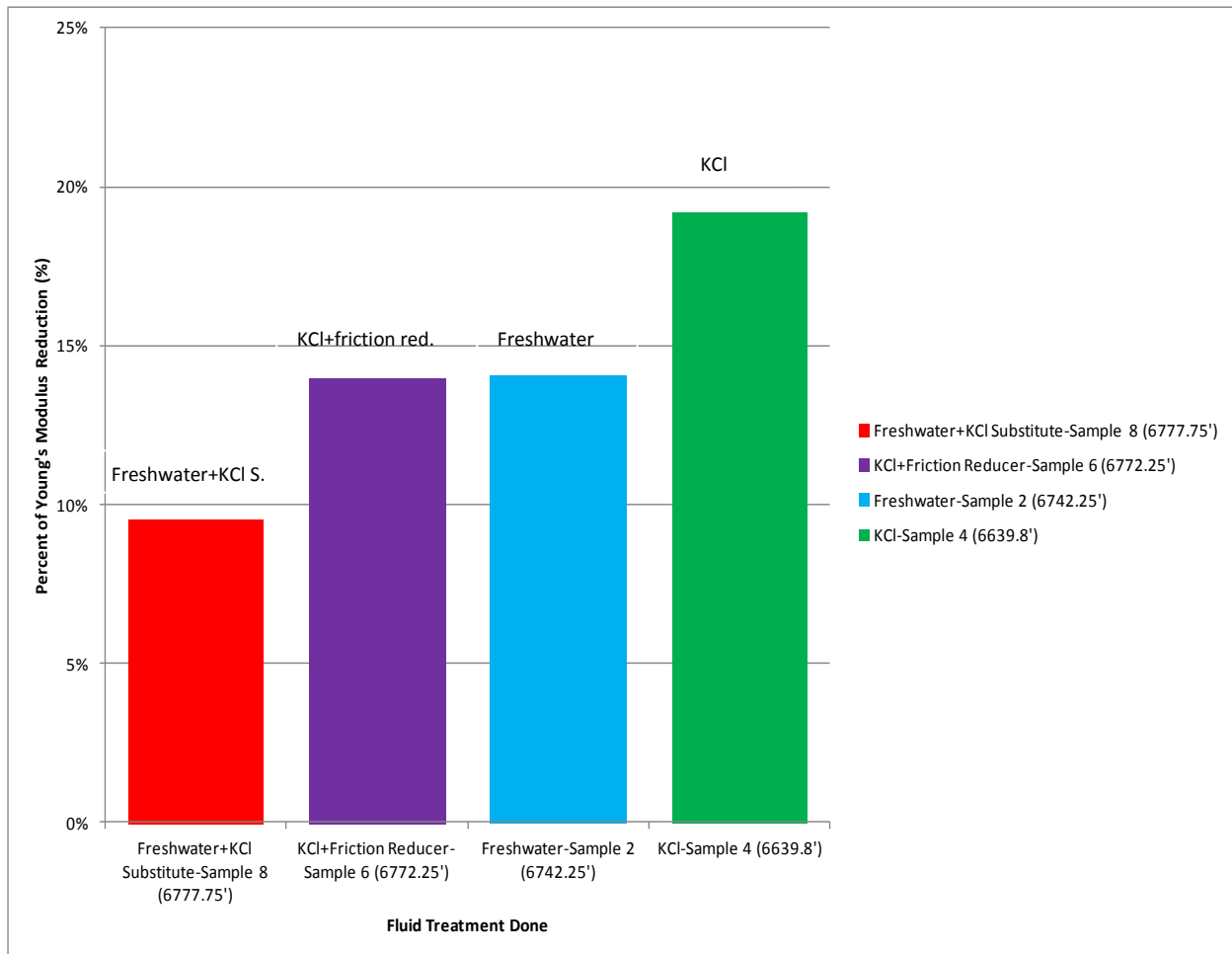
Figure 5.14: Young's modulus reduction percentage values for each fracturing fluid used on expansion samples (Samples 2, 4, 6, and 8) after 5 days of saturation. Note the scale change in reduction percentage.

Comparing Figure 5.14 with Figure 5.10, we can see that the most damaging fluid is KCl+friction reducer in each case for the Samples 1, 3, 5, and 7 and it is the second least damaging fluid for Samples 2, 4, 6, and 8,. Another important observation is the difference between the magnitudes of Young's modulus reductions in both sets of samples. Samples 1, 3, 5, and 7 reductions ranged 10% to 43%, whereas the Young's modulus reduction range of Samples 2, 4, 6 and 8 is 10% to 20%. This data shows that, initially after five days of saturating, Samples 1, 3, 5, and 7 experienced more weakening in their mechanical properties.
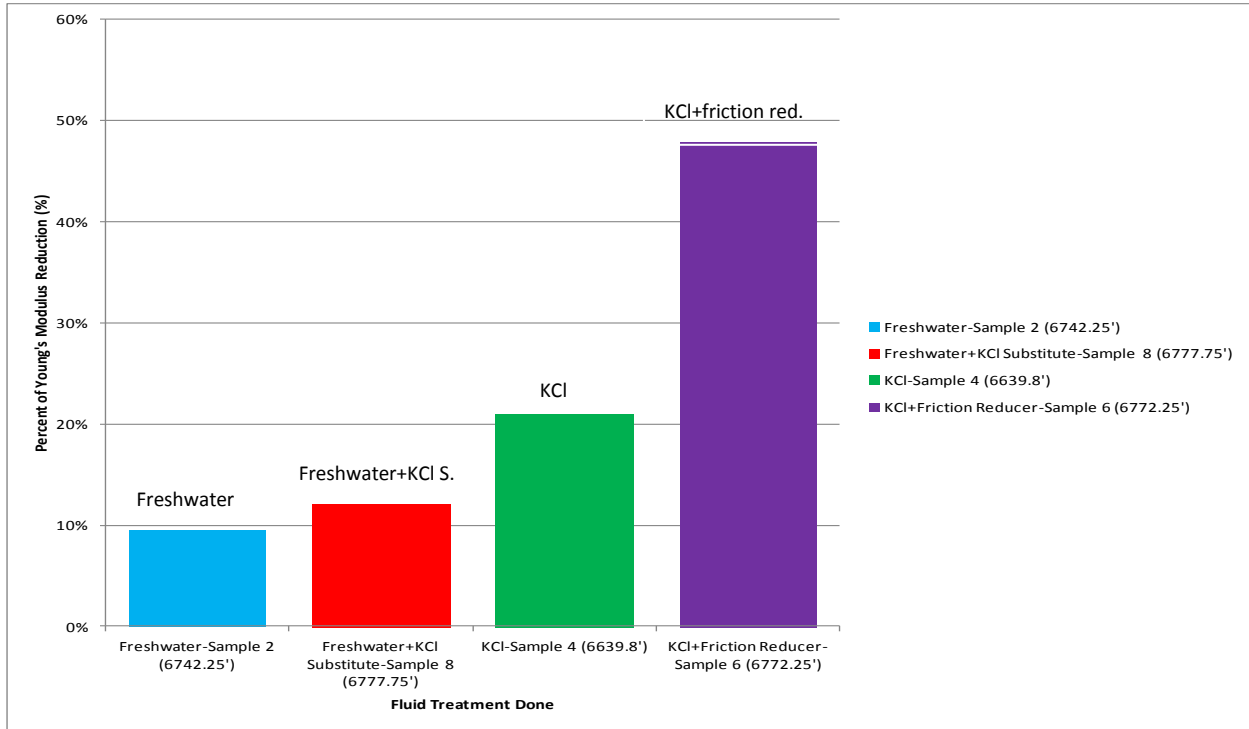
Figure 5.15: Young's modulus reduction percentage values for each fracturing fluid used on expansion samples (Samples 2, 4, 6, and 8) after 15 days of saturation. Note the scale change in reduction percentage.
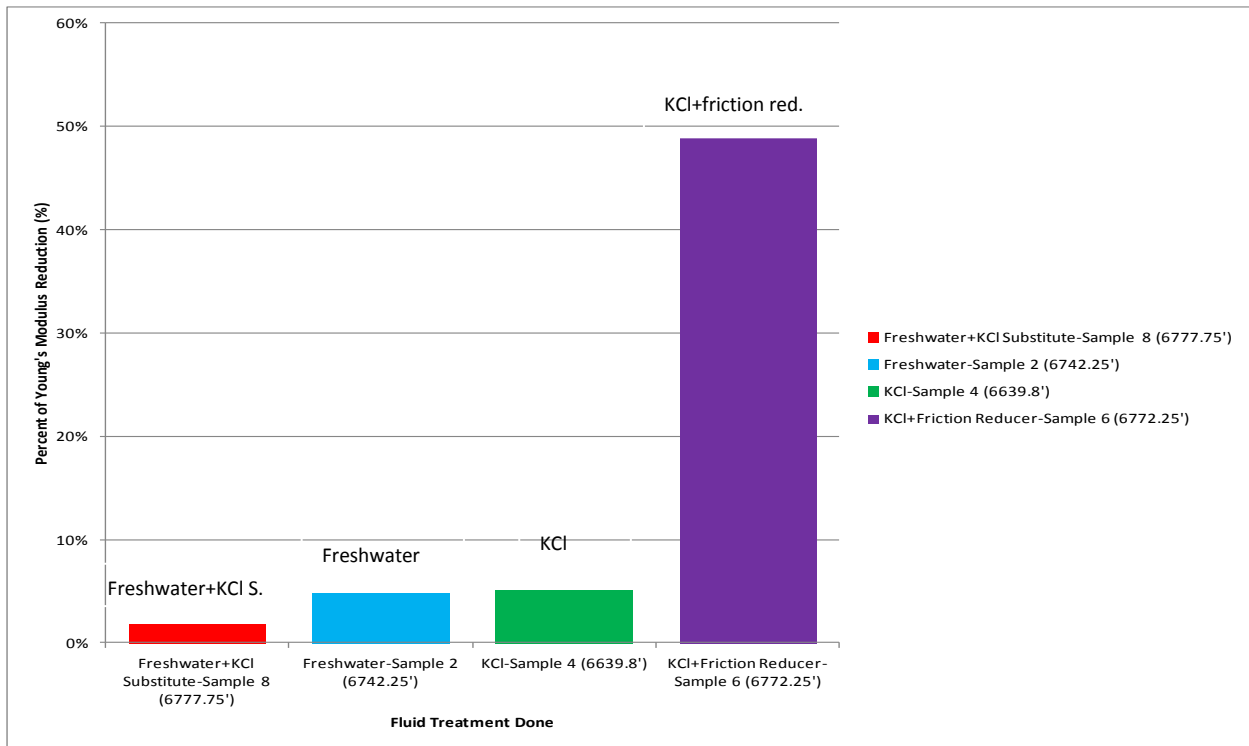
Figure 5.16: Young's modulus reduction percentage values for each fracturing fluid used on expansion samples (Samples 2, 4, 6, and 8) after 30 days of saturation.

Figures 5.15 and 5.16 show the Young's modulus reduction percentage values after Samples 2, 4, 6, and 8 were saturated for 15 and 30 days. Data shown in these figures also support the low Young's modulus reduction that was experienced after five days of saturation. The only fluid that affects the Young's modulus of samples drastically is the KCl+friction reducer but the Young's modulus reduction on Sample 6 is still approximately 30% less than Sample 5 at five days of exposure. Figure 5.15 also behaves differently than the original sample results. This set of data is where freshwater+KCl substitute is not the least damaging fluid for the first time, but instead freshwater is. Figure 5.16 displays very low reduction values for all fracturing fluids except KCl+friction reducer. Freshwater+KCl substitute, freshwater, and KCl all exhibit percentage reductions lower than 10%. Data shown in Figure 5.16 indicate very low Young's modulus reduction percentages caused by these three fluids, these reduction percentages are lower than the percentages shown in Figure 5.16, which also means all these samples experienced the Young's modulus increase at the 30 days saturation. Figure 5.17 shows the saturation time effect on Young's modulus on all of the expansion samples.
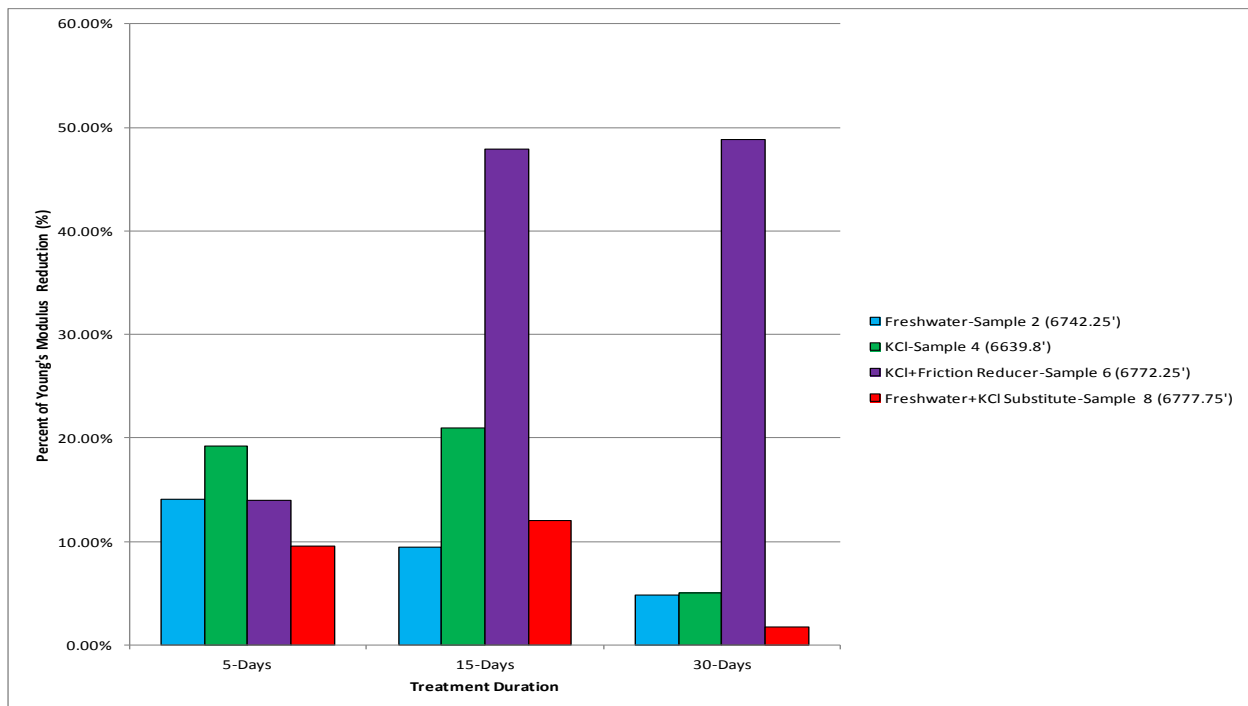
Figure 5.17: Young's modulus reduction percentage values for each fracturing fluid used on expansion samples (Samples 2, 4, 6, and 8) are shown. Values are grouped for each saturation phase to compare the fluid effects at different saturation phases.

116

Figure 5.17 is the same as Figure 5.13, except the data represent the effects of each fracturing fluid right next to each other for each saturation phase for Samples 2, 4, 6, and 8. When we look at Figure 5.17, KCl+friction reducer seems to be the most damaging fluid once again by a large margin. Young's modulus reduction values of Samples 2, 4, 6, and 8 are not on an increasing trend like the Samples 1, 3, 5, and 7 at five, 15 and 30 days (Figure 5.13). The most damaging to least damaging fracturing fluid sequence is the same if the averages of values are taken, or as stated before in Chapter 4, 15 days fluid exposure results are taken as a more representative set of results. Although each fluid exposure duration yielded different Young's modulus values for the two sample sets, all samples show a weakening effect due to fracturing fluids. In both sample sets, the KCl+friction reducer is the most damaging fluid for the Niobrara samples.

Our results show that, freshwater+KCl substitute has the least weakening effect on Young's modulus, followed by freshwater which is followed by KCl. The most damaging fluid used in this work is KCl+friction reducer. The treatment duration tests show that the maximum Young's modulus change occurs within five to 15 days fluid exposure. This result can directly be applied to the field and actual fracturing jobs. Formations that are being fractured with fracturing fluids will be very vulnerable to Young's modulus reduction and formation damage due to weakening through saturation. However, a longer treatment time at 30 days indicates some recovery of the Young's modulus values in most cases. This result can be due to measurements on different core spots containing different mineralogy, varying room and experiment conditions, variance in polishing quality, software and hardware issues caused by the nanoindenter. However, the same result occurs almost in every sample used. Therefore, there can be an optimized time for the formation, where after a fracturing treatment is pumped that the Young's modulus stops decreasing which causes the formation to gain or at least keep its strength. In this work, this optimized time started showing its existence after 30 days of saturation.

5.3 Fluid + Time Effect on Young's Modulus

So far, this work showed that Young's modulus reduction in the Niobrara sample is inevitable when they are saturated with certain fracturing fluids. Out of the four fracturing fluids used, freshwater+KCl substitute is the least damaging, freshwater is the second least damaging, KCl third, and KCl+friction reducer is the most damaging fluid to mechanical properties and Young's modulus in particular. This sequence is the same for both sets of samples (original and expansion). This work also shows that saturation time has great effect on Young's modulus, thus proppant embedment and fracture conductivity. There usually seems to be trend in Young's modulus reduction with time. As saturation time progresses, Young's modulus reduction continues and increases; however there are some exceptions to this. The strength regain of samples after 30 days of saturation is the main exception to Young's modulus values decreasing as time progresses

Results in this section capture the Young's modulus alteration results triggered by each fluid and combine them in same graphs. Therefore, the time effect on Young's modulus and fluid effect on Young's modulus can be seen clearly seen together. Tables 5.3 and 5.4 once again show the Young's modulus values and percentage reductions of each sample both the original and the expansion samples. All values are shown with the corresponding saturation time that they were obtained at.

Table 5.3: Young's Modulus Values of All Samples (Samples 1-8) at Each Saturation Phase

Young's Modulus Values of all Niobrara Samples at different durations										
		Treatment Duration					Treatment Duration			
Fluid Type	Sample #	0	5	15	30	Sample #	0	5	15	30
Freshwater	1	7.16E+06	4.75E+06	4.27E+06	4.45E+06	2	6.83E+06	5.87E+06	6.19E+06	6.50E+06
KCl	3	7.72E+06	5.67E+06	3.58E+06	2.76E+06	4	6.67E+06	5.39E+06	5.27E+06	6.33E+06
KCl+Friction Reducer	5	7.67E+06	4.31E+06	2.93E+06	1.64E+06	6	6.42E+06	5.52E+06	3.35E+06	3.29E+06
Freshwater+KCl Substitute	7	6.94E+06	6.19E+06	5.75E+06	5.79E+06	8	6.89E+06	6.24E+06	6.07E+06	6.77E+06

Figures 5.18-5.21 consist of four different clusters that each contains three or four columns depending on if they are showing Young's modulus values or reduction percentages. Each of these clusters represents a fracturing fluid as explained in the x-axis.

Table 5.4: Young's Modulus Reduction Percentage Values of All Samples (Samples 1-8) at Each Saturation Phase

Young's Modulus Reduction Percentage Values of all Niobrara Samples at different durations							
		Treatment Duration				Treatment Duration		
Fluid Type	Sample #	5	15	30	Sample #	5	15	30
Freshwater	1	33.58%	40.33%	37.78%	2	14.04%	9.42%	4.84%
KCl	3	26.51%	53.68%	64.27%	4	19.18%	20.98%	5.06%
KCl+Friction Reducer	5	43.75%	61.76%	78.65%	6	13.98%	47.89%	48.83%
Freshwater+KCl Substitute	7	10.82%	17.16%	16.62%	8	9.54%	12.03%	1.78%

Figures 5.19 and 5.21 have three columns for each cluster because the reduction in Young's modulus in the dry stage is always zero. The other three columns in these figures represent the saturation time (5-15-30 days). This same logic is applied to Figures 5.18 and 5.20, where the four columns in each cluster correspond to values at dry, 5 days, 15 days, and 30 days.
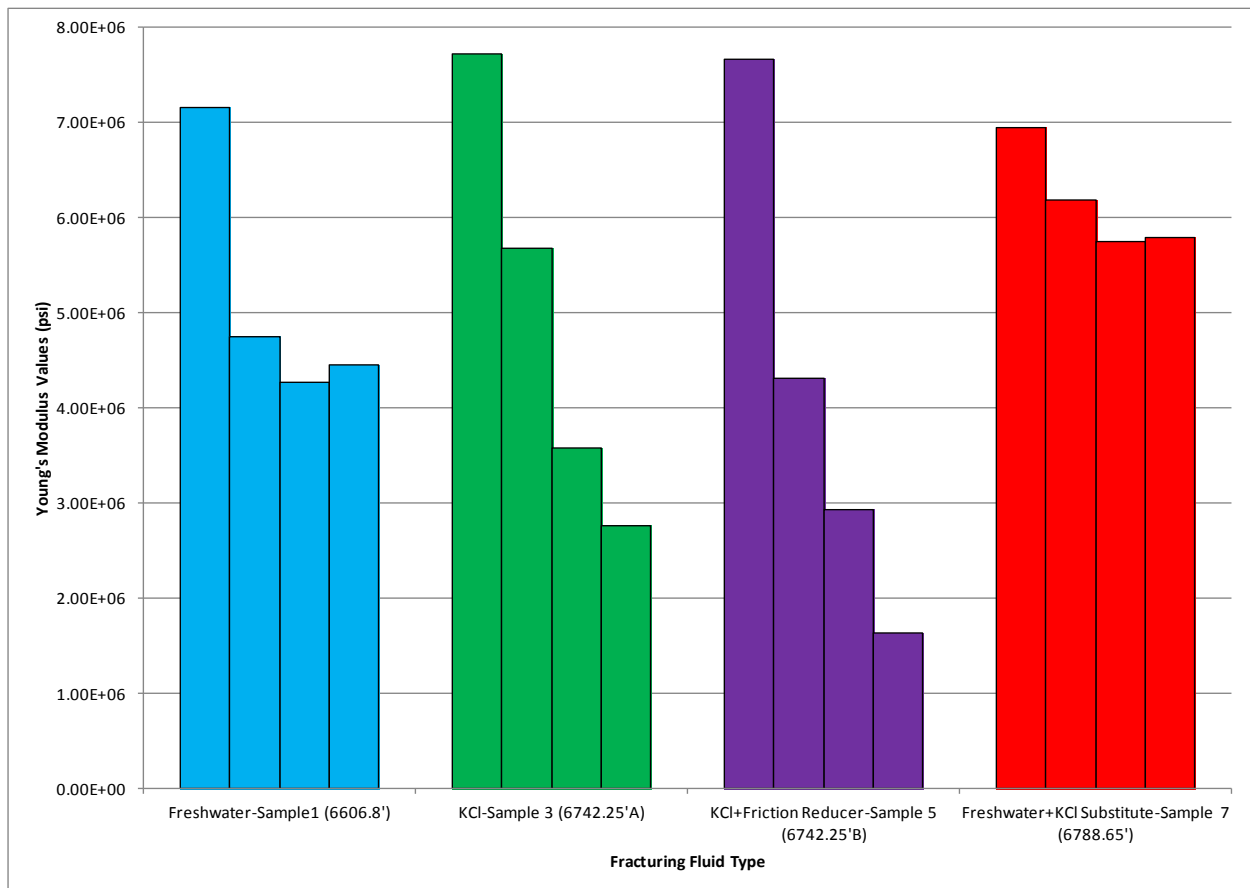
Figure 5.18: Young's modulus values of original samples (Samples 1, 3, 5, and7) for each fracturing fluid grouped together from dry stage to 30 days saturation stage. This grouping allows capturing the effect of time and fluid selection has on Young's modulus values more clear.

119

Figure 5.18 shows the Young's modulus values of cores at each saturation time. It is very clear here that freshwater+KCl substitute has the least weakening effect on Young's modulus. It is also very evident that KCl+friction reducer is the most damaging fluid to Young's modulus. Freshwater and KCl are the second and third most damaging fluids. The third (15 days) and fourth (30 days) columns in the freshwater and freshwater+KCl substitute clusters very clearly show the Young's modulus reduction diminishes and strength is regain after 15 and 30 days of saturation. The same results are provided and shown with Figure 5.19. KCl and KCl+friction reducer reduction percentage continues increasing, whereas the other fluid reductions stop increasing after 15 days. This figure also shows freshwater+KCl substitute is the least damaging and KCl+friction reducer is the most damaging fluid to Young's modulus.
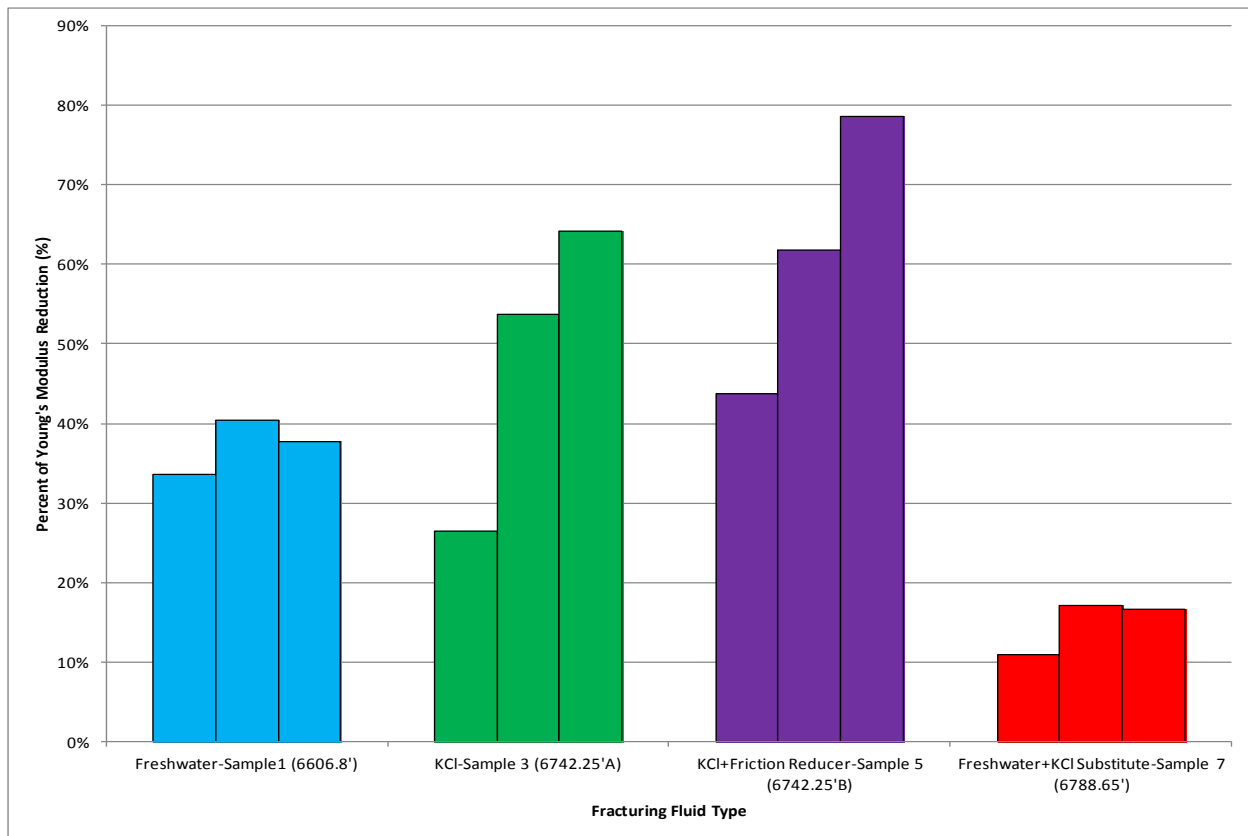
Figure 5.19: Young's modulus reduction percentage values of original samples (Samples 1, 3, 5, and7) for each fracturing fluid grouped together from dry stage to 30 days saturation stage. This grouping allows capturing the effect of time and fluid selection has on Young's modulus values more clear.

Figure 5.20 shows that the fluid effect on Young's modulus of Samples 2, 4, 6, and 8 is much less severe than Samples 1, 3, 5, and 7. Besides the most damaging fluid KCl+friction reducer, the other three fluids show a difference in Young's modulus values between their dry stages and saturated stages. This data set also shows freshwater as the second least damaging, and KCl as the third. However, the Young's modulus values obtained at different times when cores are saturated with these fluids are closer to each other, whereas the Samples 1, 3, 5, and 7 had significant separation in these values.
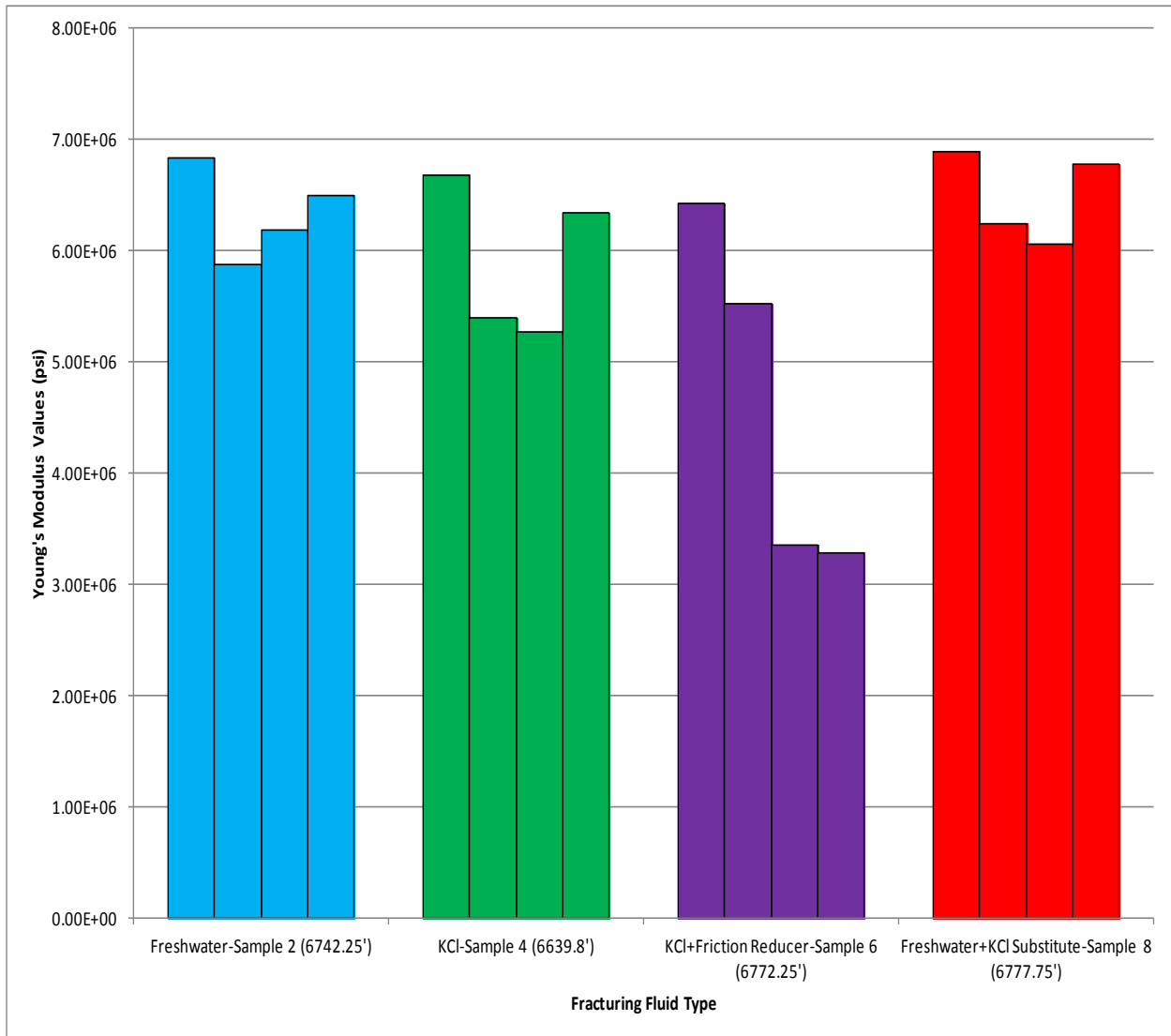
Figure 5.20: Young's modulus values of expansion samples (Samples 2, 4, 6, and 8) for each fracturing fluid grouped together from dry stage to 30 days saturation stage. This grouping allows capturing the effect of time and fluid selection has on Young's modulus values more clear.

Besides experiencing less Young's modulus reduction, these samples also exhibit the diminishing of Young's modulus reduction and strength regaining more severely. All three fracturing fluids besides KCl+friction reducer experience a significant increase in Young's modulus values between 15 and 30 days. Young's modulus values of these samples between five and 15 days are also either indifferent or 15 days values are very close to being higher. This can be due to heterogeneity of the samples or experimental differences like stated before, but one thing for sure can be said is that the Young's modulus alteration goes through a cycle where it first decreases and after samples are saturated for approximately 30 days, it stops decreasing and may eventually start increasing. Figure 5.21 shows the reduction percentages in all the expansion samples Young's modulus. It is easy to pick out the most and least damaging fluids.
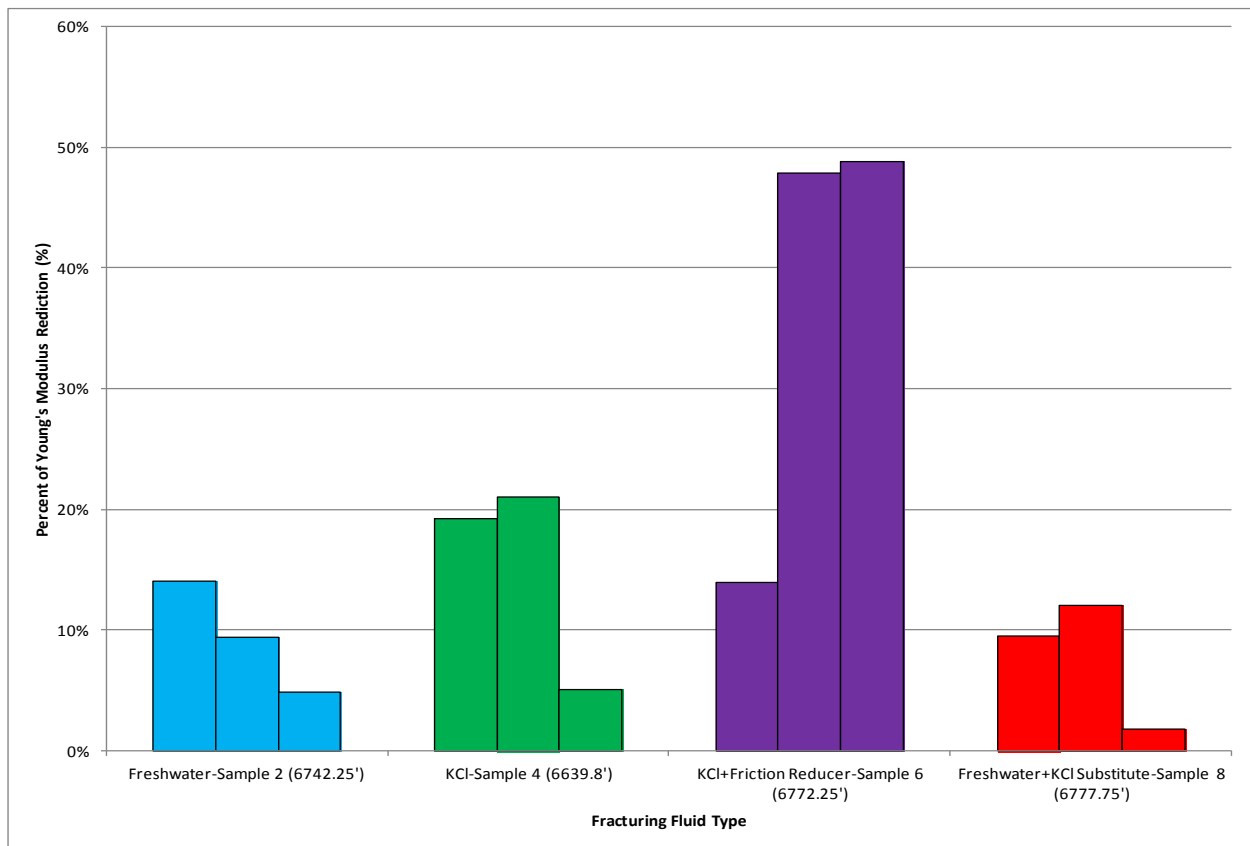
Figure 5.21: Young's modulus reduction percentage values of expansion samples (Samples 2, 4, 6, and8) for each fracturing fluid grouped together from dry stage to 30 days saturation stage. This grouping allows capturing the effect of time and fluid selection has on Young's modulus values more clear. Note the scale change in reduction percentage.

5.4 Heating Effect on Young's Modulus while saturated with H$_2$O and KCl

In addition to looking at Young's modulus changes and proppant embedment issue in cores that are saturated with fracturing fluids, this work also investigated the effects of heat as rocks are saturated on Young's modulus and proppant embedment. Two different samples as previously shown in Table 4.1 were picked to be heated while submerged in fracturing fluids. Just as the room temperature saturation experiments, four different pieces of cores were cut from Samples 9 and 10 and were used for each fluid to obtain two separate pressure and proppant embedment tests. This allowed two proppant types to be tested under the same conditions. The experimental procedure for the heat experiments was the same as the saturation experiments. Young's modulus values of two small chips from both samples were measured when they were dry, and after they were heated for five days. Four core pieces retrieved from Sample 9 were submerged in freshwater for five days at 180˚F and four core pieces retrieved from Sample 10 were submerged in KCl for five days at 180˚F. This section shows how Young's modulus of the Niobrara cores is affected when the cores are subjected to heat while being saturated for five days.

Table 5.5: Young's Modulus Values and Reduction Percentages of Samples 9 and 10 Before and After Heat Treatment

Young's Modulus Reductions of Niobrara Cores when they are heated for 5 Days at 180 F in H2O and KCl		
	Freshwater (6606.65') psi	KCl (6764.2') psi
Dry	5.46E+06	6.05E+06
5-Days Heating	3.53E+06	4.06E+06
Reduction %	35.32%	32.87%

Figures 5.22-5.26 show the nanoindentation results of Sample 9 (6606.65') when it is dry and also after it was heated at 180˚F for five days in freshwater. Figures 5.27-5.31 shows the results of Sample 10 (6764.2') before and after it was heated at 180˚F in KCl for five days. Figures 5.32 and 5.33 compare the effects of the two heated fracturing fluids on the Young's modulus of the samples. The initial Young's modulus values for these samples are significantly lower than the samples used for only saturation experiments. The freshwater and KCl samples have initial Young's modulus values of

5.46E+06 psi and 6.05E+06 psi, respectively. Since these values are significantly lower than other samples in this work, the Young's modulus reduction could be expected to be less severe; however the heat effect is expected to increase the effect of reduction. Figures 5.23, 5.25, 5.28 and 5.30 show the relationship between Young's modulus and hardness for these samples when they are dry and heated. For the heated samples, the relationship between the two mechanical properties is the same as Samples 1-8 that were only saturated. Young's modulus and hardness are positively related to each other.
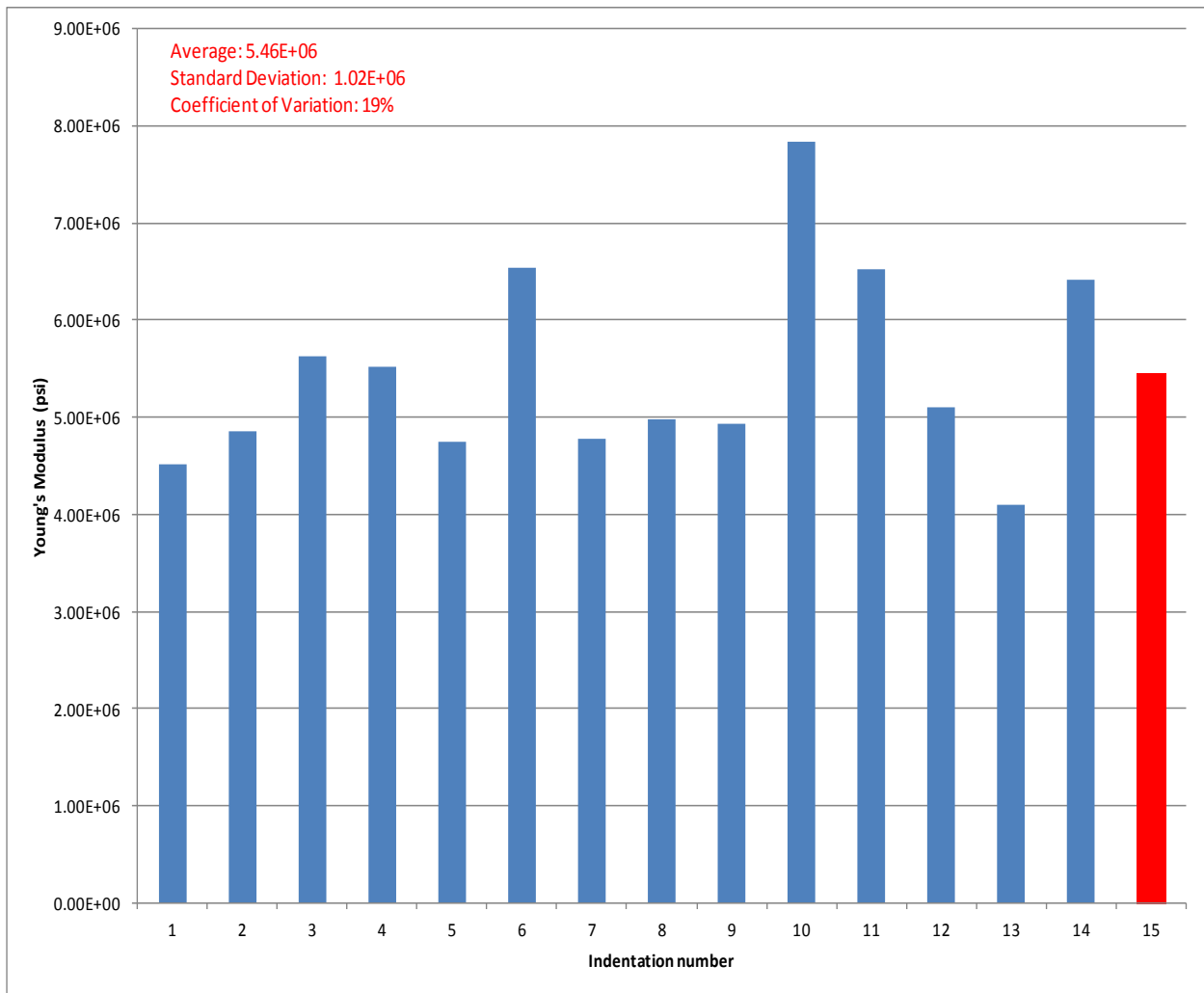
Figure 5.22: Nanoindentation results for Sample 9 (6606.65') when it is dry, showing Young's modulus values of each indent done on the sample. Each point represents a Young's modulus value taken from the surface of the core. Red column represents the average Young's modulus of this sample (5.46E+6 psi).

Looking at Figures 5.22 and 5.24, we can say that nanoindenter produced a decent amount of reliable data points for Young's modulus values, thus the data obtained for the freshwater heated samples

are considered accurate just like all other data in this work. Table 5.5 shows that sample that was heated at 180˚F in freshwater for five days has a Young's modulus reduction of 35.3%. This value is about 2% higher than the reduction freshwater caused for Sample 1 (6606.8)' and 21% higher than Sample 2 (6742.25') experienced after being saturated with freshwater for five days.
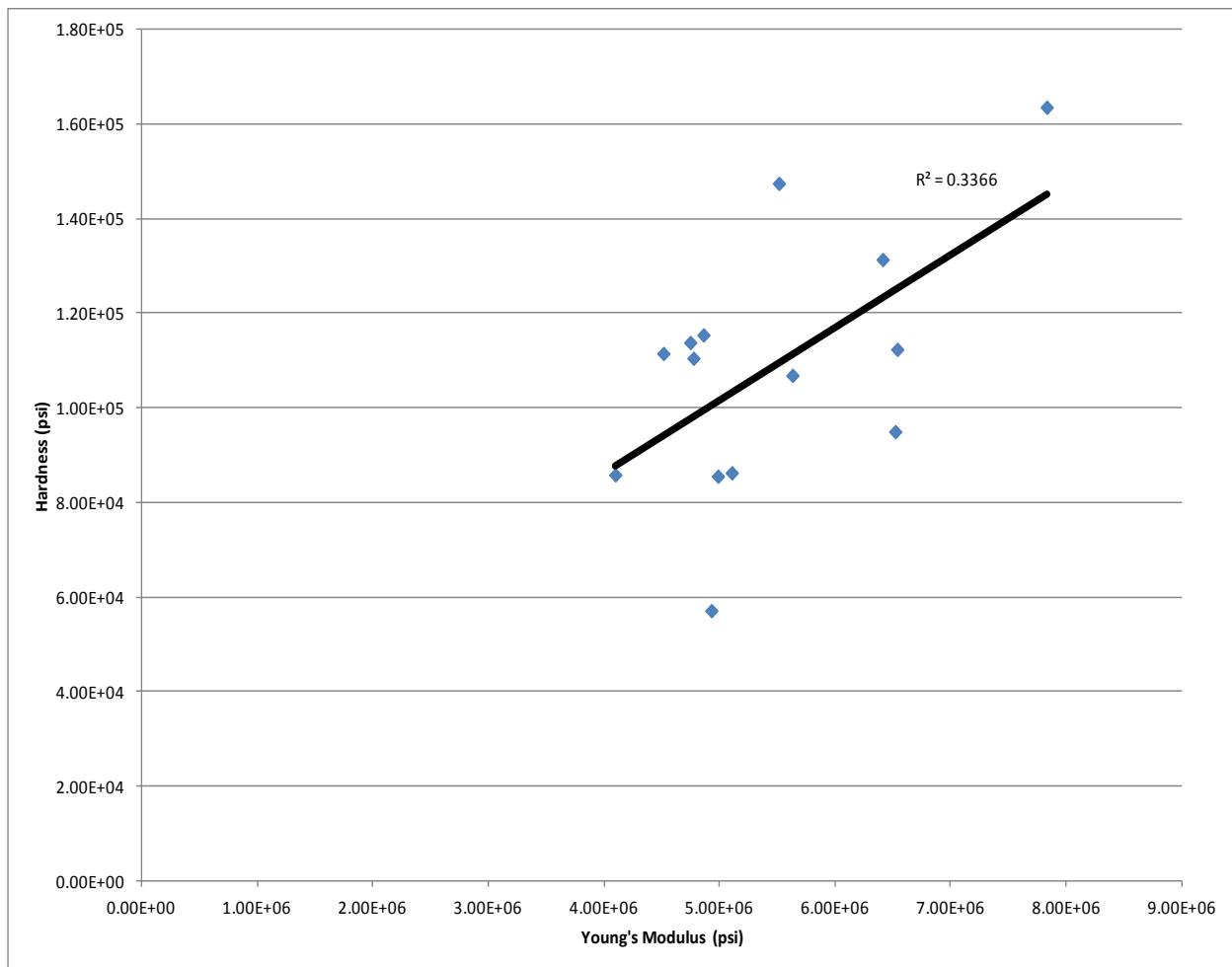
Figure 5.23: Young's modulus vs. hardness results for Sample 9 (6606.65') when it is dry. Figure shows the relationship and trend between Young's modulus and hardness values obtained from the sample. Figure indicates a positive linear relationship between the two. As one increases the other also increases.

Figure 5.26 shows this reduction in Young's modulus. 35.3% reduction in Young's modulus is a large reduction for a rock's Young's modulus. Since the original (Samples 1, 3, 5, and 7) and expansion (Samples 2, 4, 6, and 8) saturation samples generated very two different reduction percentages after the five days saturation, it was hard to anticipate the value of reduction percentage once the heating effect

was evaluated. Taking the results of Phase 1 into consideration, the only anticipation was that, heating the samples in fracturing fluids would increase the reduction in Young's modulus in comparison to only saturating them in fracturing fluids. Looking at all the reduction results, we can say that the anticipated result for the heat effect was obtained. The reduction percentage due to heat differs by 2% from Sample 1 and 21% from Sample 2. Heating the Niobrara core, Sample 9 at 180°F in freshwater for five days proved to have serious detrimental effects on Young's modulus, thus on proppant embedment and conductivity, even more so then only saturating the cores.
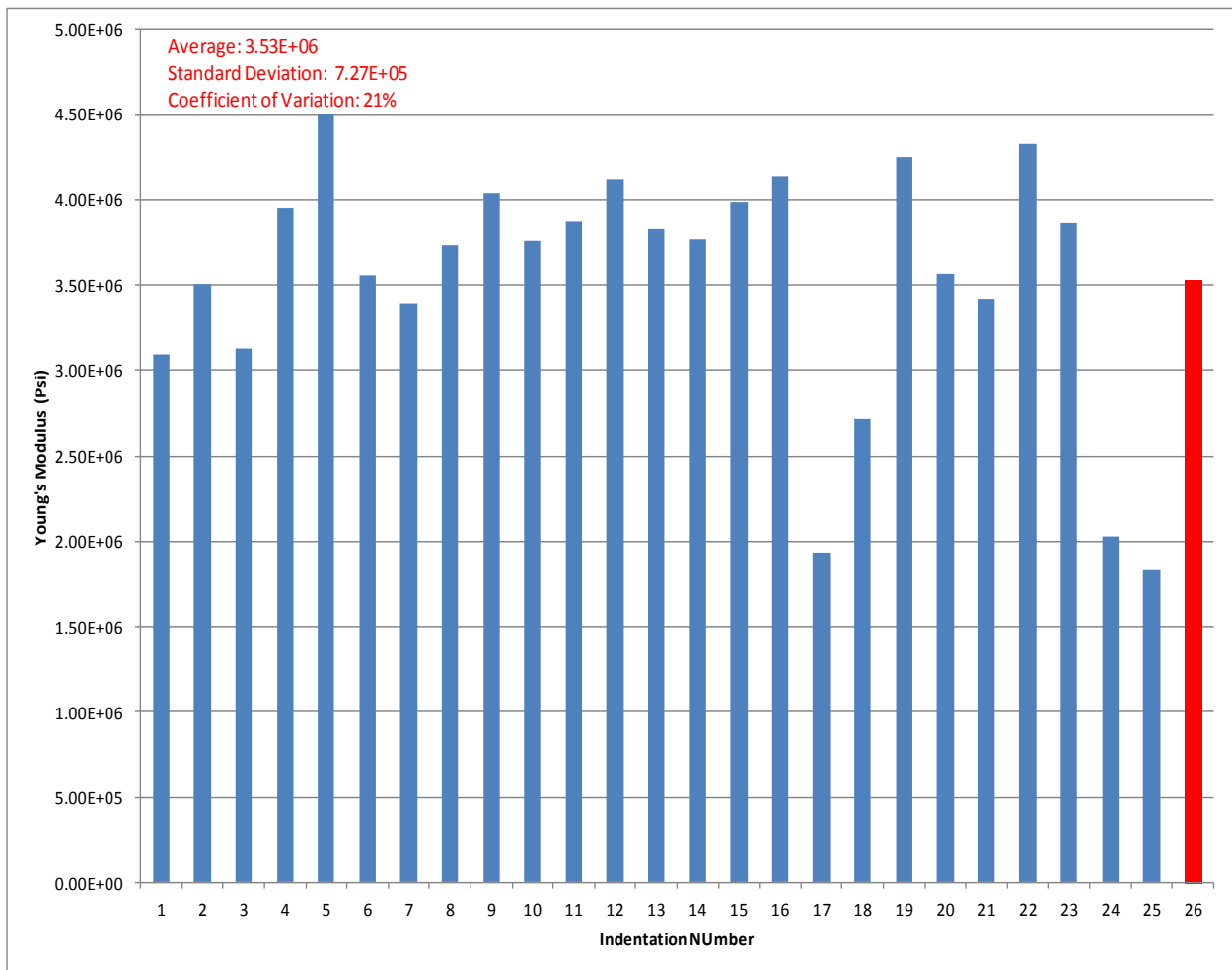
Figure 5.24: Nanoindentation results for Sample 9 (6606.65') when it is heated for 5 days showing Young's modulus values of each indent done on the sample. Each point represents a Young's modulus value taken from the surface of the core. Red column represents the average Young's modulus of this sample (3.53E+6 psi). Note the scale change in Young's modulus.
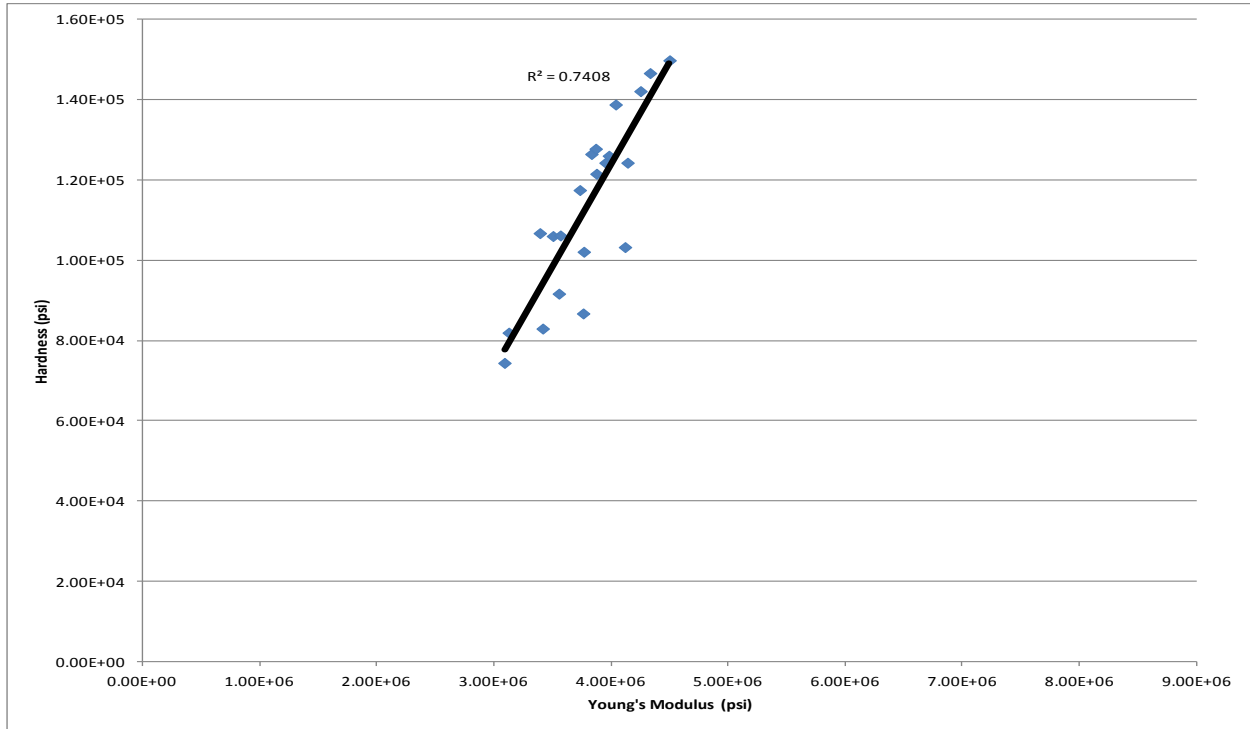
Figure 5.25: Young's modulus vs. hardness results for Sample 9 (6606.65') when it is heated for 5 days. Figure shows the relationship and trend between Young's modulus and hardness values obtained from the sample.
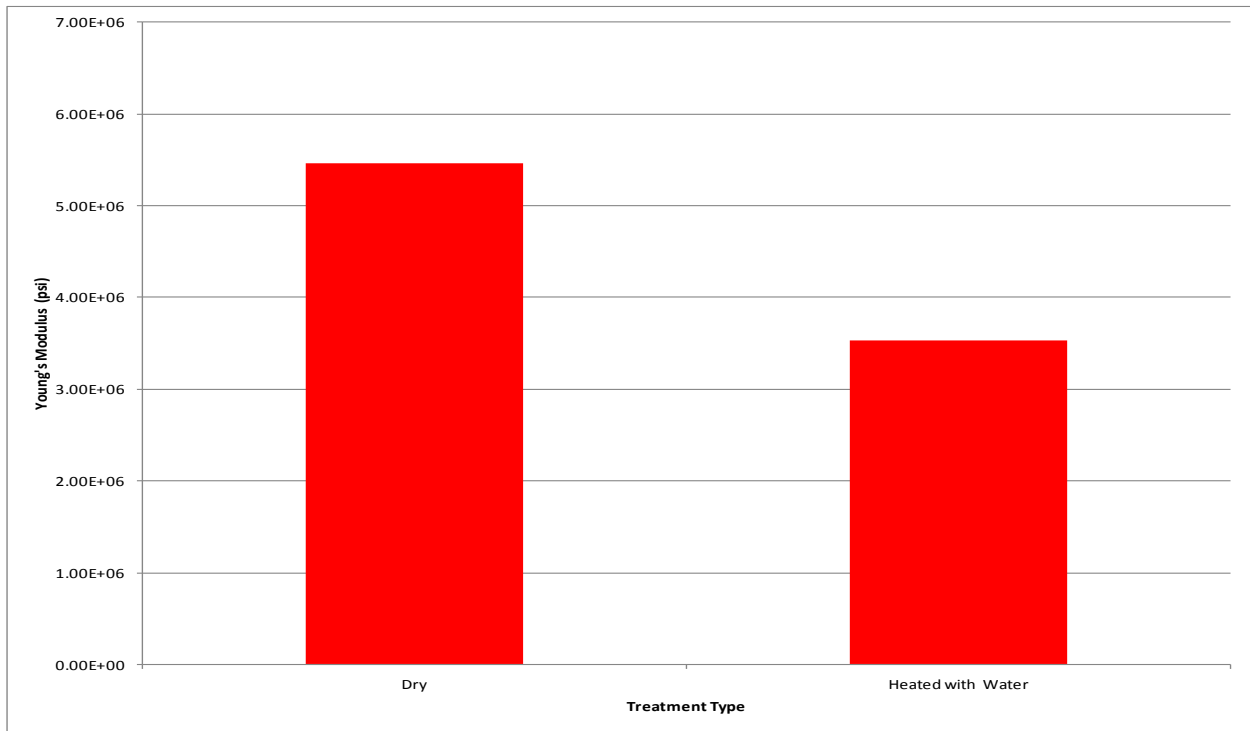
Figure 5.26: Average Young's modulus values of dry and heated cores shown in graph for Sample 9 (6606.65'). The y-axis shows Young's modulus in psi and x-axis shows the treatment periods. A reduction in Young's modulus values is very evident between dry stage and 5-day heat treatment.

Table 5.5 also shows the before and after Young's modulus values of the core that was saturated and heated with KCl. Heating Sample 10 (6764.2') in KCl at 180°F for five days caused a Young's modulus reduction of 32.87%. The nanoindentation data seen in Figures 5.27 and 5.29 indicate an evenly distributed set of values that are close to each other and do not vary too much both for the unaffected and heated sample. Again just like Sample 9, this sample also has a low initial Young's modulus value in comparison to samples that were used for the room temperature saturation experiments. This lower initial Young's modulus can also be the reason both of these samples are not responding to the heating effect with reduction values close to 50% or more as was observed with certain other Samples used in this study.
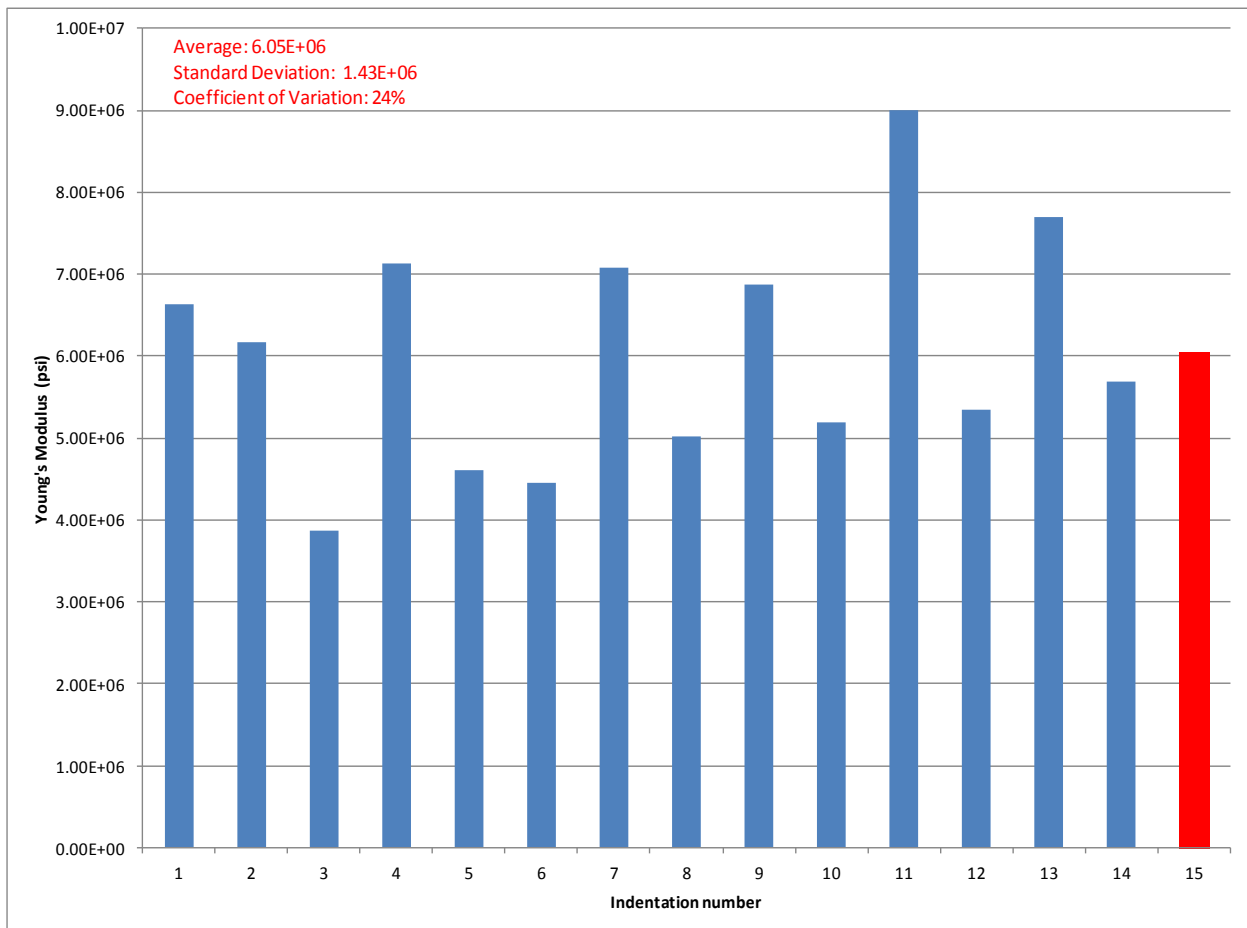
Figure 5.27: Nanoindentation results for Sample 10 (6764.2') when it is dry, showing Young's modulus values of each indent done on the sample. Each point represents a Young's modulus value taken from the surface of the core. Red column represents the average Young's modulus of this sample (6.05E+6 psi). Note the scale change in Young's modulus.

Figures 5.28 and 5.30 show the hardness and Young's modulus relationship for Sample 10. These figures indicate a positively related trend between two properties just like all the other samples. This relation is a non-changing trend between the two properties regardless of the sample condition and fracturing fluid used.
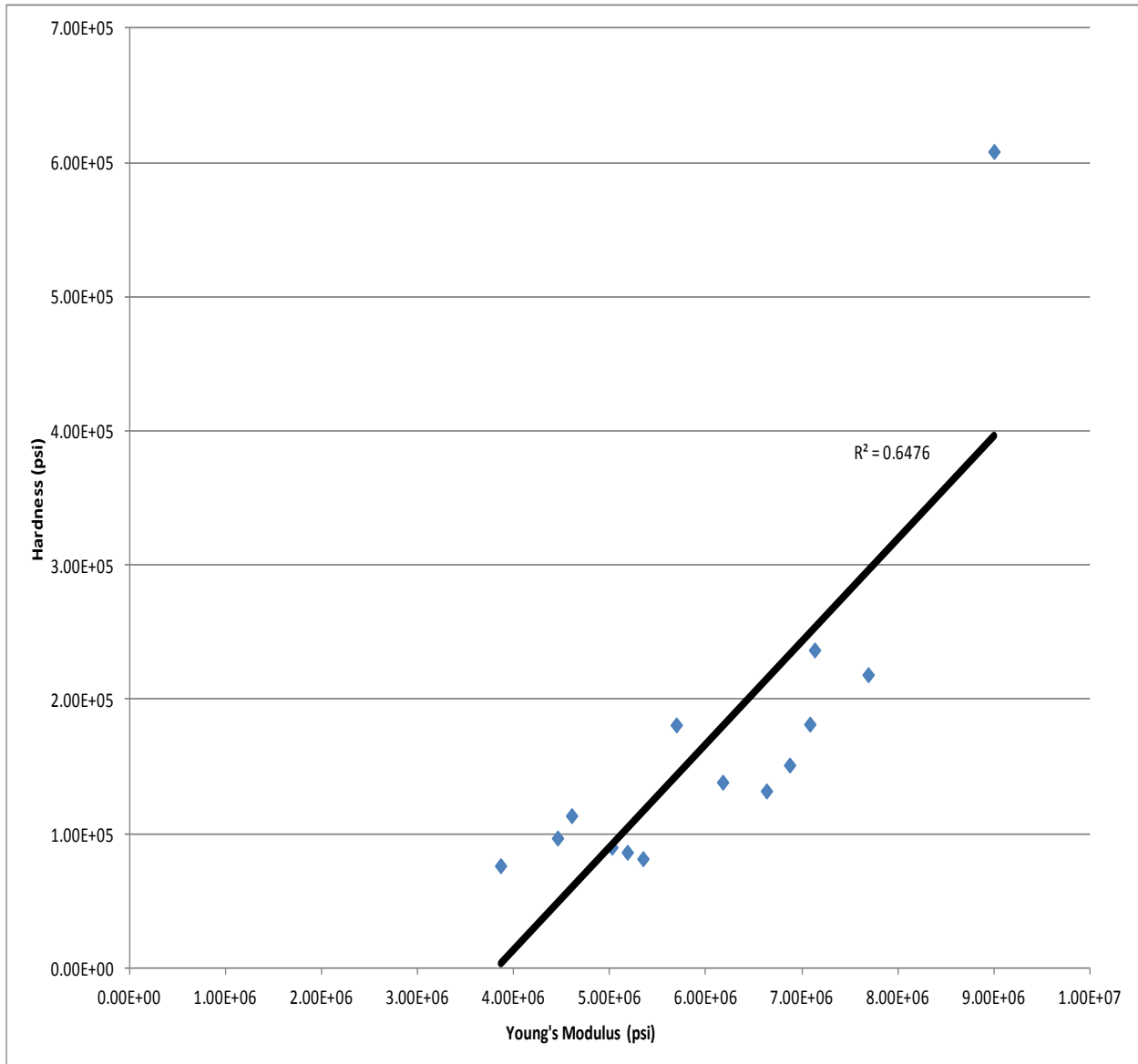
Figure 5.28: Young's modulus vs. hardness results for Sample 10 (6764.2') when it is dry. Figure shows the relationship and trend between Young's modulus and hardness values obtained from the sample. Figure indicates a positive linear relationship between the two. As one increases the other also increases.
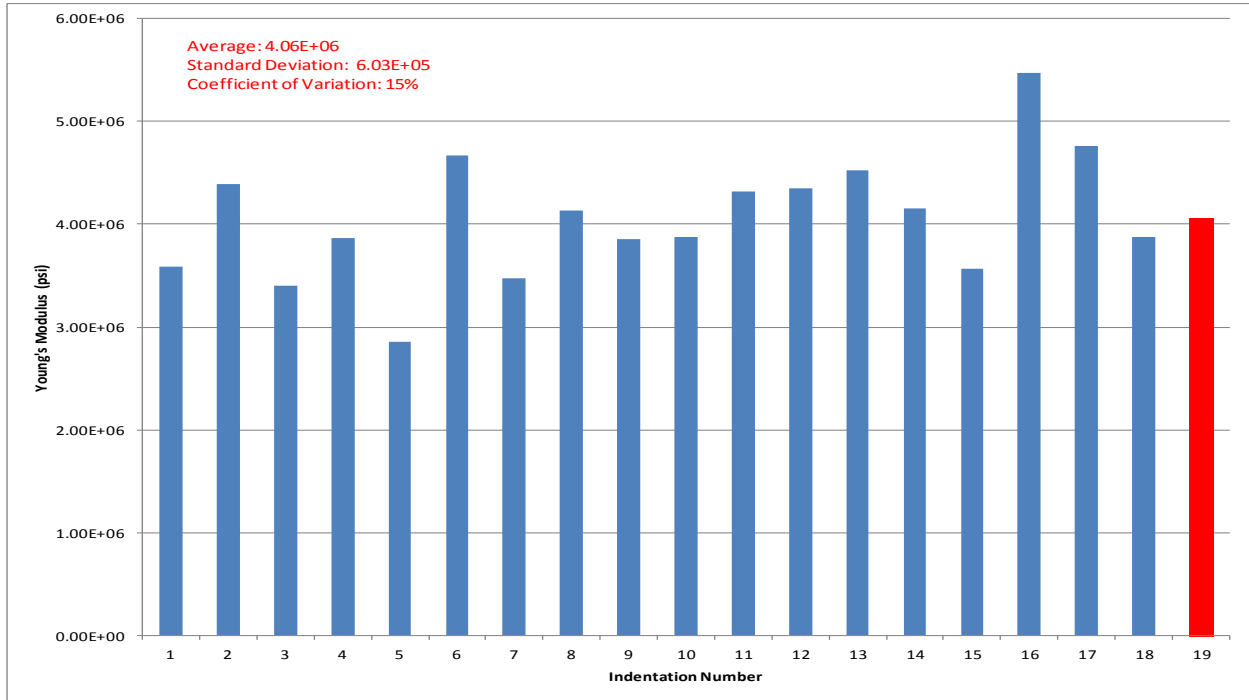
Figure 5.29: Nanoindentation results for Sample 10 (6764.2') when it is heated for 5 days showing Young's modulus values of each indent done on the sample. Each point represents a Young's modulus value taken from the surface of the core. Red column represents the average Young's modulus of this sample (4.06E+6 psi). Note the scale change in Young's modulus.
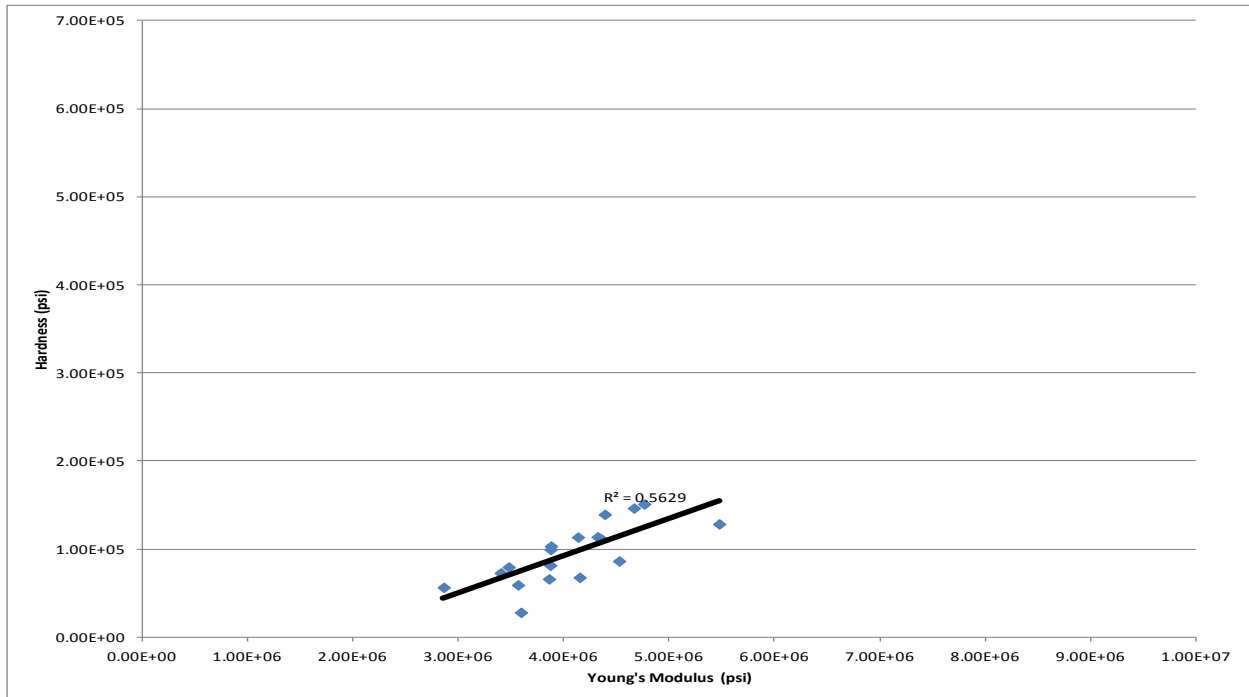
Figure 5.30: Young's modulus vs. hardness results for Sample 10 (6764.2') when it is heated for 5 days. Figure shows the relationship and trend between Young's modulus and hardness values obtained from the sample. Figure indicates a positive linear relationship between the two. As one increases the other also increases.

130

Figure 5.31 displays a graphical representation of Sample 10's Young's modulus value when it is dry and after it is heated with KCl. Heating the sample in KCl for five days at 180˚F reduces the Young's modulus from 6.05E+6 psi to 4.06E+6 psi. The reduction percentage caused by heating the sample with KCl is 32.87%. This value is a significant reduction in Young's modulus compared to Samples 3 and 4. Young's modulus reduction percentages of Samples 3 and 4 when they were saturated with KCl for five days are 26.5% and 19%. The reduction caused by heating the Sample 9 is significantly higher than Sample 4 (expansion sample) reduction value and slightly higher than Sample 3 (original sample) reduction value. Therefore, once again it is evident that heating the cores, even if the temperature is low, has a detrimental effect on the Niobrara shale's Young's modulus in comparison to just saturating them without any heat.
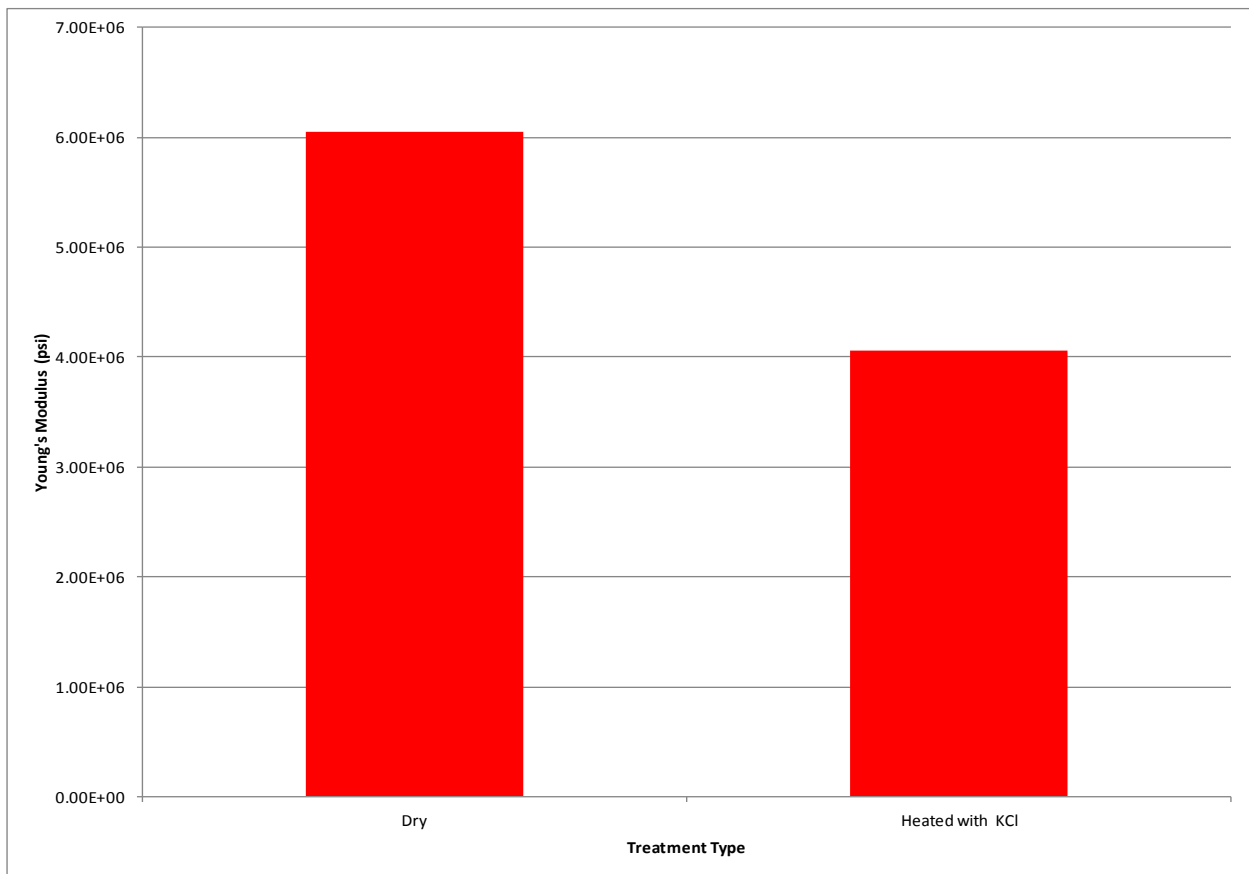
Figure 5.31: Average Young's modulus values of dry and heated cores shown in graph for Sample 10 (6764.2'). The y-axis shows Young's modulus in psi and x-axis shows the treatment periods. A reduction in Young's modulus values is very evident between dry stage and 5-day heat treatment.

The comparison of how the two fluids affected Young's modulus when heat also added as a damage mechanism is shown in Figures 5.32 and 5.33. The Young's modulus reductions caused in five days with the heated fluids both are very significant, and have highly damaging effects on proppant embedment (discussed in Section 5.5).

Previous experiments where the samples are only saturated with fracturing fluids show that at the end of 15 and 30 days, freshwater is the second least damaging fluid, which is followed by the more damaging fluid KCl. However, the effect at the end of five days points out the opposite result for the Samples 2, 4, 6, and 8 (expansion samples). Just like in that case, the sample heated with KCl has a slightly lower Young's modulus reduction than the sample heated with freshwater. This difference is about 3%, but it still indicates that KCl has less damage on the Niobrara shale when it is heated for five days at 180˚F.

The nanoindentation and hardness vs. Young's modulus graphs of Samples 9 and 10 have error analysis information attached to them just like the graphs in Chapter 4 for Samples 1 and 2. Table 5.6 compiles and reports the average, standard deviation and coefficient of variation values of Samples 9 and 10. A high standard deviation and coefficient of variation are also present for these samples. The reason for this is again due to variation in Young's modulus values since the Niobrara shale samples are so heterogeneous.

Table 5.6: Error Analysis of the Measured Young's Modulus Values through Nanoindenter for Samples 9 and 10 Before and After They are Heated

Error Analysis of Samples 9 and 10 before and after heating				
Sample 9	**Saturation Phase**	**Average**	**Standard Deviation**	**Coefficient of Variation %**
	Dry	5.46E+06	1.02E+06	19
	5-Day Heating at 180°F in H_2O	3.53E+06	7.27E+05	21
Sample 10	**Saturation Phase**	**Average**	**Standard Deviation**	**Coefficient of Variation %**
	Dry	6.05E+06	1.43E+06	24
	5-Day Heating at 180°F in KCl	4.06E+06	6.03E+05	15
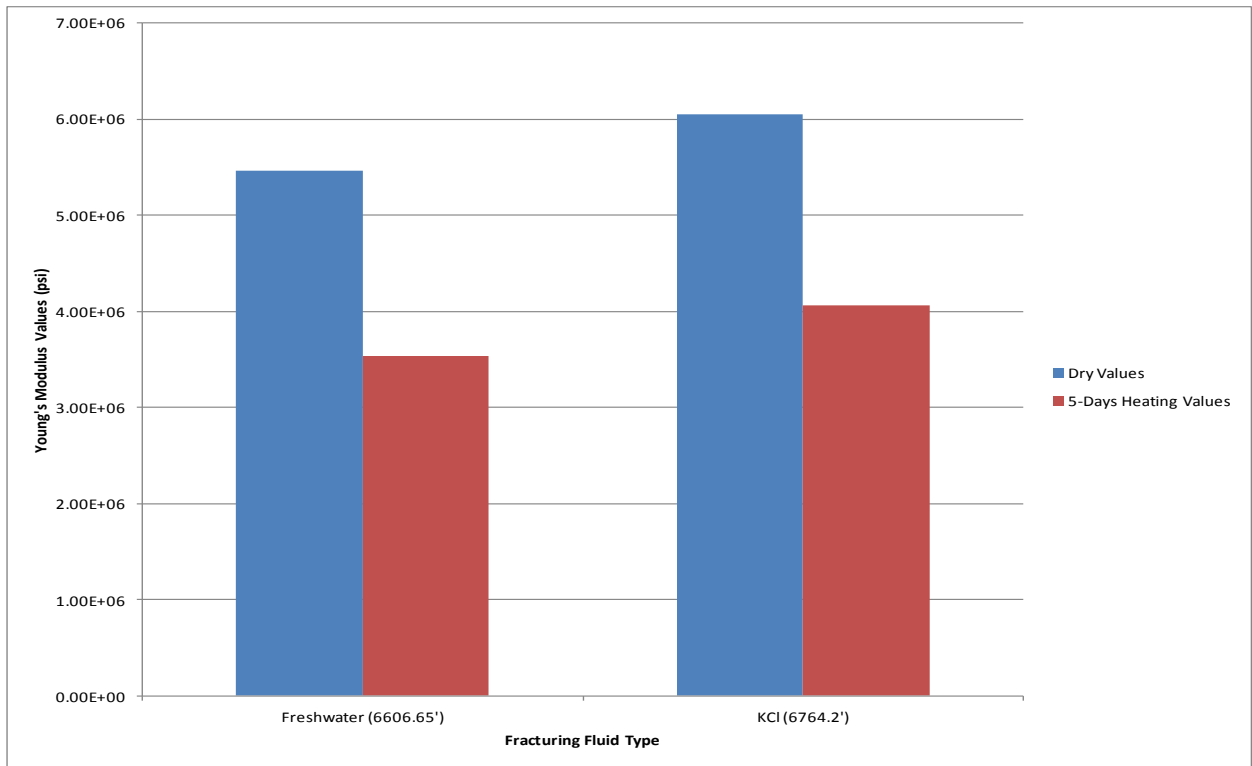
Figure 5.32: Young's modulus values of Samples 9 and 10 when they dry and when they are heated for five days at 180°F in H_2O and KCl.
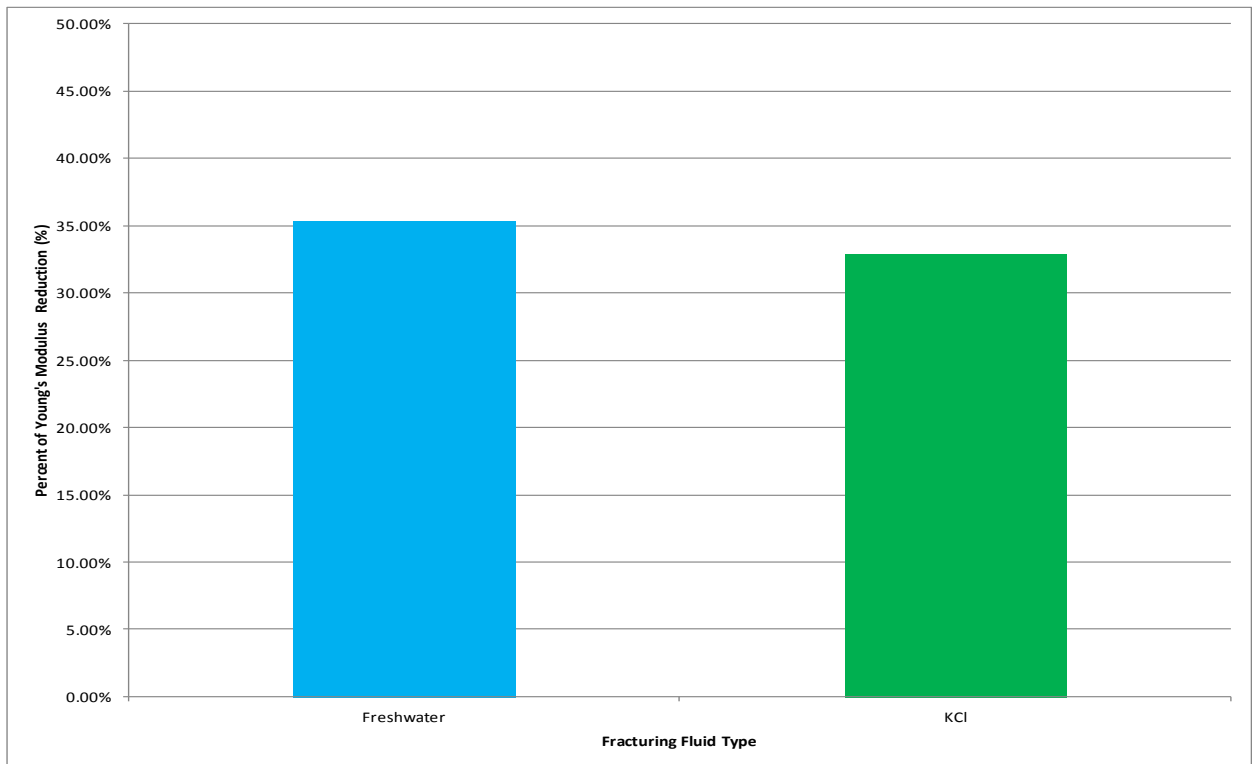
Figure 5.33: Young's modulus reduction percentage values for Sample 9 and 10 after they are exposed to heat in H_2O and KCl for five days at 180°F.

5.5 In-Situ Young's Modulus Values Using Gassmann's Equation

      After the Young's modulus values were measured at different stages of saturation in the lab environment, they were then compared to the saturated bulk modulus of the samples under in-situ conditions. This comparison was done by using the Gassmann fluid substitution equation. Gassmann's equation relates the saturated bulk modulus of the rock to its porosity, the bulk modulus of the porous rock, the bulk modulus of the mineral within the rock, and the bulk modulus of the pore-filling fluids, as shown in Equation 5.1.

$$K_{sat} = K_{dry} + \frac{(1-\frac{K_{dry}}{K_{min}})^2}{\frac{\emptyset}{K_{fluid}}+\frac{1-\emptyset}{K_{min}}-\frac{K_{dry}}{K_{min}^2}} \tag{5.1}$$

Where,
$\quad\quad\quad\quad\quad\quad$ K_{sat} = Saturated Bulk Modulus, psi
$\quad\quad\quad\quad\quad\quad$ K_{dry} = Dry Bulk Modulus, psi
$\quad\quad\quad\quad\quad\quad$ K_{min} = Mineral Bulk Modulus, psi
$\quad\quad\quad\quad\quad\quad$ K_{fluid} = Fluid Bulk Modulus, psi

      Gassmann's equation provides an understanding of the in-situ properties of samples and allows for modeling rocks that are being evaluated by changing the fluid and mineral type they consists of into other alternative circumstances. So in practice, available samples would be drained from initial pore fluid, and the bulk moduli calculated. Then the rock would be re-saturated with new pore fluid, and the new effective bulk modulus calculated. This theory was used in the project to calculate the in-situ saturated Young's modulus values of all the samples, which then represent the Young's modulus when the samples are assumed to be at 100% saturation with water and consist of calcite, i.e. under general reservoir conditions. In order to calculate the in-situ saturated Young's modulus, Equation 5.2 was used.

$$E_{sat} = 3K_{sat}(1 - 2v) \tag{5.2}$$

Where,
$\quad\quad\quad\quad\quad\quad$ E_{sat} = Saturated Young's Modulus, psi

The saturated Young's modulus was calculated for each of the study samples after calculating their saturated bulk modulus by using calcite as the mineral and water as the pore filling fluid. Bulk modulus of calcite was taken as 1.1E+07 psi (Mavko et al., 2009) and bulk modulus of water was taken as 3.2E+05 psi (Fjar et al., 2008). The in-situ saturated Young's modulus values were calculated to see how much Young's modulus reduction the samples experience when the cores are retrieved from their associated depths and phased in-to a dry stage in the lab. The saturated in-situ, dry and fracturing fluid saturated Young's modulus values of the eight samples are shown in Table 5.7.

Table 5.7: Saturated (In-Situ) and Measured Young's Modulus Values of All Samples (Samples 1-8)

Saturated (In-Situ) and Measured Young's Modulus Values of Niobrara Samples at different durations												
			Treatment Duration-Days						Treatment Duration-Days			
Fluid Type	Sample #	Sat. (In-Situ)	0	5	15	30	Sample #	Sat. (In-Situ)	0	5	15	30
Freshwater	1	1.47E+07	7.16E+06	4.75E+06	4.27E+06	4.45E+06	2	1.47E+07	6.83E+06	5.87E+06	6.19E+06	6.50E+06
KCl	3	1.25E+07	7.72E+06	5.67E+06	3.58E+06	2.76E+06	4	1.47E+07	6.67E+06	5.39E+06	5.27E+06	6.33E+06
KCl+Friction Reducer	5	1.48E+07	7.67E+06	4.31E+06	2.93E+06	1.64E+06	6	1.46E+07	6.42E+06	5.52E+06	3.35E+06	3.29E+06
Freshwater+KCl Substitute	7	1.47E+07	6.94E+06	6.19E+06	5.75E+06	5.79E+06	8	1.47E+07	6.89E+06	6.24E+06	6.07E+06	6.77E+06

As expected the saturated in-situ Young's modulus values are significantly higher than the Young's modulus values measured before the samples were treated any type of fracturing fluid. Table 5.8 shows the Young's modulus reduction percentage between the new in-situ Young's modulus and all Young's modulus values calculated with the nanoindenter.

Table 5.8: Saturated (In-Situ) and Measured Young's Modulus Reduction Percentage Values of All Samples (Samples 1-8)

Saturated (In-Situ) and Measured Young's Modulus Reduction Percentage Values of Niobrara Samples at different durations										
			Treatment Duration-Days					Treatment Duration-Days		
Fluid Type	Sample #	In-Situ-Dry	InSitu-5	InSitu-15	InSitu-30	Sample #	In-Situ-Dry	InSitu-5	InSitu-15	InSitu-30
Freshwater	1	51.40%	67.72%	71.00%	69.76%	2	53.50%	60.02%	57.88%	55.75%
KCl	3	38.28%	54.64%	71.41%	77.94%	4	54.52%	63.24%	64.06%	56.82%
KCl+Friction Reducer	5	48.14%	70.83%	80.17%	88.93%	6	56.14%	62.27%	77.15%	77.56%
Freshwater+KCl Substitute	7	52.77%	57.89%	60.88%	60.62%	8	53.09%	57.56%	58.73%	53.92%

As seen in Figure 5.8, the difference between the saturated in-situ and measured Young's modulus when the rocks were not damaged with the fracturing fluids vary between 38% to 56%. This means and also shows that the differences between values become even greater as the rocks are damaged by the fracturing fluids. Figures 5.34 and 5.35 show the Young's modulus values for the original samples and the Young's modulus reduction percentage between the previously measured values and calculated saturated in-situ Young's modulus. The columns on the left side of each group in Figures 5.34 and 5.36 represent the calculated in-situ saturated Young's modulus values for those samples.
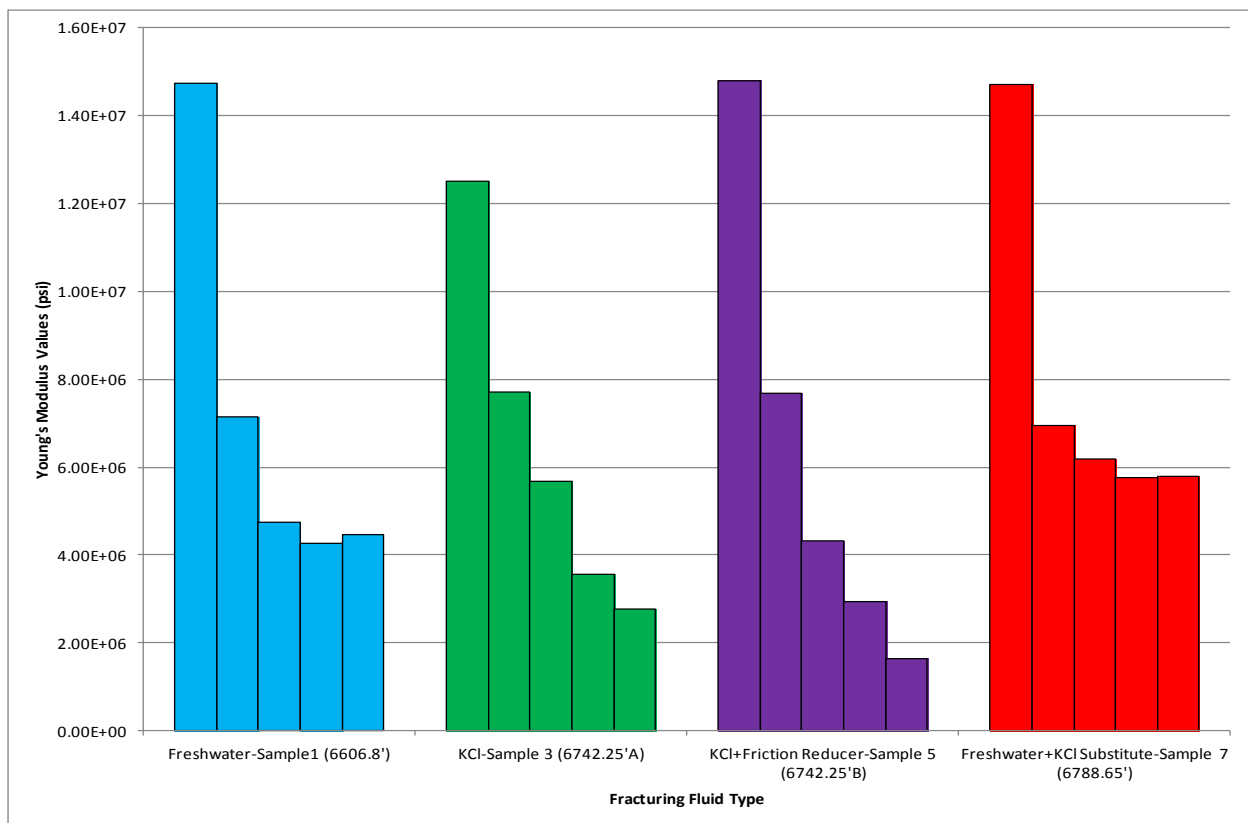
Figure 5.34: Measured Young's modulus and saturated in-situ Young's modulus values of original samples (Samples 1, 3, 5, and 7) for each fracturing fluid. This grouping shows how the saturation in-situ Young's modulus values are substantially higher than measured Young's modulus values.

The percentage reduction between the in-situ saturation Young's modulus and measured Young's modulus can be clearly seen in this graph. Figures 5.36 and 5.37 show the same two graphs for the expansion set samples.
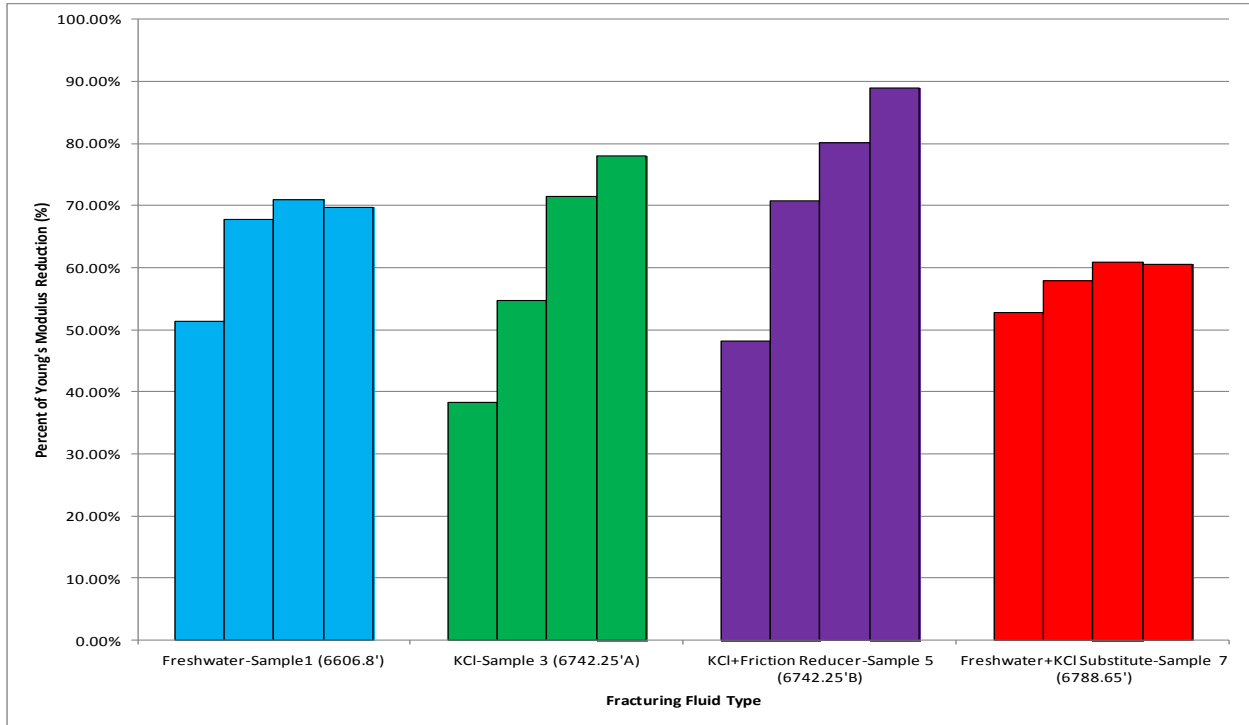
Figure 5.35: Measured Young's modulus and saturated in-situ Young's modulus reduction percentage values of original samples (Samples 1, 3, 5, and 7) for each fracturing fluid. This grouping shows how the saturation in-situ Young's modulus values are substantially higher than measured Young's modulus values.
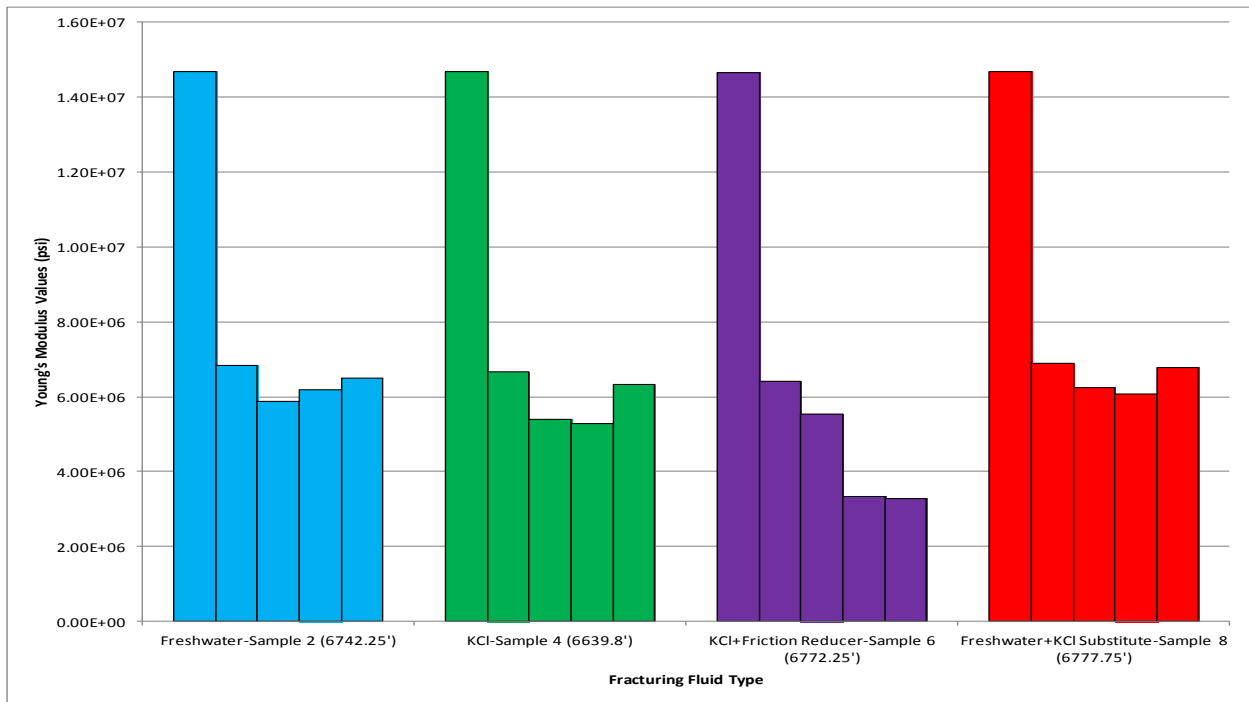
Figure 5.36: Measured Young's modulus and saturated in-situ Young's modulus values of expansion samples (Samples 2, 4, 6, and 8) for each fracturing fluid. This grouping shows how the saturation in-situ Young's modulus values are substantially higher than measured Young's modulus values.
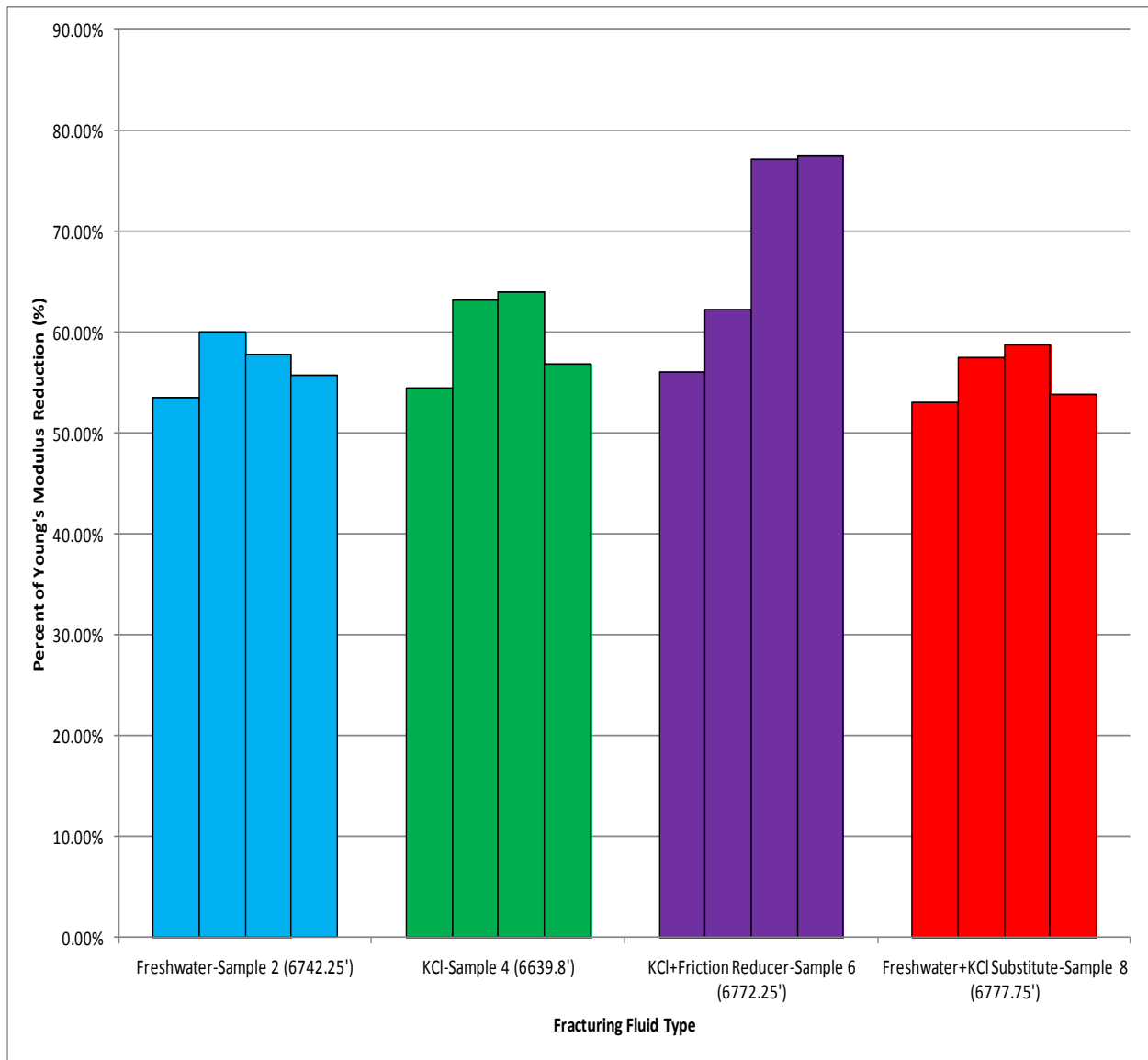
Figure 5.37: Measured Young's modulus and saturated in-situ Young's modulus reduction percentage values of original samples (Samples 1, 3, 5, and 7) for each fracturing fluid. This grouping shows how the saturation in-situ Young's modulus values are substantially higher than measured Young's modulus values.

The calculation of the in-situ saturated Young's modulus values by the Gassmann equation showed that rocks go through a dramatic change and experience high Young's modulus reductions when taken through various saturation and pressure conditions. This reduction was even higher than the fracturing fluid effects on dry core Young's modulus values after 15 and 30 days of exposure.

5.6 Proppant Embedment Results

The results reported and explained in Sections 5.1-5.4 represent the effects of four fracturing fluids (H_2O, KCl, KCl+friction reducer, H_2O+KCl substitute) on Young's modulus changes of the Niobrara shale. This work is proposed to take the cores that are saturated and heated in these fracturing fluids and pressure them while various proppants are placed in between them in order to capture and quantify the proppant embedment issue in specific fracturing fluid and proppant combinations. This section delivers the results of the proppant embedment tests.

A total of six different scenarios are used to experiment with the proppant embedment issue. Four of these are saturating the samples in fracturing fluids, and two are heating the samples in two of the selected fracturing fluids. Two different proppant types were used for each scenario. However, the same proppants were used multiple times for different fluids in order to compare the fluid effect on proppant embedment. Table 5.9 shows the combinations of proppants and treated samples, specifying the fluid.

Table 5.9: Fracturing Fluid and Heating Treatment Matchups with Proppant Types

Fracturing Fluid Used	Proppant Used	Fracturing Fluid Used	Proppant Used
Freshwater-Samples 1-2 (6606.8' & 6742.25')	16/30 Brady	**KCl-Samples 3-4 (6742.25'A & 6639.8')**	16/30 Brady
	20/40 Ottawa		20/40 Ottawa
KCl+Friction Reducer-Samples 5-6 (6742.25'B & 6772.25')	20/40 Ceramic	**Freshwater+KCl Substitute-Samples 7-8 (6788.65' & 6777.75')**	20/40 Ceramic
	20/40 RCS		20/40 RCS
Heated with Freshwater @ 180˚F-Sample 9 (6606.65')	20/40 Ottawa	**Heated with KCl @ 180˚F-Sample 10 (6764.20')**	20/40 Ottawa
	20/40 Ceramic		20/40 Ceramic

The combinations shown in Table 5.9 allow four very common proppants that are used in the industry today to be tested with four common fracturing fluids. The proppants were placed in between

two separate cores to be pressured that were previously saturated or heated. Therefore each proppant test yielded two different results, one being the bottom core where the proppants were put on and the other one being the top core which got placed on the proppants. Figures 5.38 and 5.39 display proppant test #1 done on the KCl+friction reducer saturated sample with 20/40 Ceramic proppant. Figures show how the bottom and top cores surfaces and proppants look like before and after pressurizing them. These figures are used here to demonstrate how proppants and cores look like after pressuring. Chapter 4 shows all the results including proppant embedment results for cores that are saturated with freshwater and supplemental files A, B, C, and D show the results of cores that are saturated with other three fracturing fluids and samples that are heated. As seen in these figures, the proppants are randomly distributed along the core surfaces at a concentration of 0.1 lb/ft^2.

Figure 5.38: Bottom and top cores from KCl+friction reducer Test#1 loaded with 20/40 Ceramic at 0.1 lb/ft^2 (no pressure). Core diameters are 1.0 inch.

Figure 5.39: Bottom and top cores from KCl+friction reducer Test#1 loaded with 20/40 Brady at 0.1 lb/ft^2 after they were subjected 3030 psi for one hour. Core diameters are 1.0 inch.

A total of 18 different embedment measurements were taken on the core surfaces in order to eliminate inaccurate values, and the average of these values represents the reported embedment profile for each core. Table 5.10 shows the average proppant embedment profiles of each test and each core within that test. The embedment profiles are reports in µm (micrometers).

Table 5.10: Average Proppant Embedment Profiles for Each Core That Was Treated with Fracturing Fluid and/or Heat

	Freshwater-Sample 1-2 (6606.8' & 6742.25')				KCl-Samples 3-4 (6742.25'A & 6639.8')			
Average Embedment Values	Test #1-Core #1 (Bottom Core)	Test #1-Core #3 (Top Core)	Test #2-Core #2 (Bottom Core)	Test #2-Core #4 (Top Core)	Test #1-Core #1 (Bottom Core)	Test #1-Core #3 (Top Core)	Test #2-Core #2 (Bottom Core)	Test #2-Core #4 (Top Core)
Proppant Type	16/30 Brady		20/40 Ottawa		16/30 Brady		20/40 Ottawa	
Depth(μm)	80	67	47	66	86	106	92	91
Width(μm)	462	498	407	449	518	747	693	520
	KCl+Friction Reducer-Sample 5-6 (6742.25'B & 6772.25')				Freshwater+KCl Substitute-Samples 7-8 (6788.65' & 6777.75')			
Average Embedment Values	Test #1-Core #1 (Bottom Core)	Test #1-Core #3 (Top Core)	Test #2-Core #2 (Bottom Core)	Test #2-Core #4 (Top Core)	Test #1-Core #4 (Bottom Core)	Test #1-Core #5 (Top Core)	Test #2-Core #6 (Bottom Core)	Test #2-Core #7 (Top Core)
Proppant Type	20/40 Ceramic		20/40 RCS		20/40 Ceramic		20/40 RCS	
Depth(μm)	70	106	107	97	62	74	67	64
Width(μm)	497	520	556	596	390	442	397	425
	Heated with Freshwater @ 180°F-Sample 9 (6606.65')				Heated with KCl 180°F-Sample 10 (6764.20')			
Average Embedment Values	Test #1-Core #2 (Bottom Core)	Test #1-Core #1 (Top Core)	Test #2-Core #4 (Bottom Core)	Test #2-Core #3 (Top Core)	Test #1-Core #1 (Bottom Core)	Test #1-Core #2 (Top Core)	Test #2-Core #3 (Bottom Core)	Test #2-Core #4 (Top Core)
Proppant Type	20/40 Ottawa		20/40 Ceramic		20/40 Ottawa		20/40 Ceramic	
Depth(μm)	65	75	57	59	103	101	88	85
Width(μm)	489	562	370	395	619	630	541	480

In table 5.10, the depth value of the embedment is more critical and has more influence on the conductivity and permeability of the fracture then the width value. Thus the sequence of least embedment to highest embedment is primarily based on the depth value of the embedments. Table 5.11 lists all the embedment profiles from lowest to highest. The embedment depths of bottom and top cores are added for each test in order to report the total embedment affecting the space between the two cores since this space in reality represents a fracture. The width values reported in this table are the average width values for the top and bottom cores for each test since the embedment width will only affect one side. Table 5.11 also reports the total percentage of proppant depth lost due to embedment. This value is calculated by dividing the total proppant embedment depth experienced to an average proppant diameter for the proppant type used in that test. Even though the depth values of the embedment profiles are used as the primary identification data set in figuring out which proppant and fracturing fluid combination type yielded the lowest and highest embedment, the width values also follow the same sequence with the exception of the couple values. This indicates that the depth and width of embedments on core surfaces are positively related to each other even though width values are significantly higher than the depth values.

The actual reasons behind why the width values are significantly higher than the depth values are not specifically investigated in this work. However it can be speculated that, the severe embedment damage is initially triggered by the high rapid pressure that is applied on the core and this initial force causes the embedment width to be high, since the core surfaces are the weakest points because they were in contact with the fracturing fluids. It takes higher pressures and longer time durations to embed the proppants in to the cores surface. Therefore the depth values are significantly lower than the width values. Table 5.11 lists the least embedment to most embedment values by looking at the embedment depth only. Consequently, the total embedment % (% of proppants lost) fall in the same sequence, except the 16/30 Brady used with cores saturated in freshwater and KCl. This occurs because the diameter of 16/30 Brady is larger than the other proppants used. So even though the embedment values of these proppants are large, the remaining portion can be larger due to their initial large size.

Table 5.11: Average Proppant Embedment Profiles for Each Core Used From Samples 1-10

Fluid Type+ Test#	Proppant Used	Proppant Diameter (μm)	Embedment Width (μm)	Embedment Depth (μm)	Total Embedment %
H_2O Test #2	20/40 Ottawa	650	428	113	17%
Heated H_2O Test #2	20/40 Ceramic	650	382	116	18%
H_2O+KCl Substitute Test #2	20/40 RCS	650	411	131	20%
H_2O+KCl Substitute Test #1	20/40 Ceramic	650	416	136	21%
Heated H_2O Test #1	20/40 Ottawa	650	526	140	22%
H_2O Test #1	16/30 Brady	850	480	147	17%
Heated KCl Test #2	20/40 Ceramic	650	511	173	27%
KCl+Friction reducer Test #1	20/40 Ceramic	650	508	176	27%
KCl Test #2	20/40 Ottawa	650	607	183	28%
KCl Test #1	16/30 Brady	850	633	192	23%
KCl+Friction reducer Test #2	20/40 RCS	650	576	204	31%
Heated KCl Test #1	20/40 Ottawa	650	625	204	31%

Looking at the results in Table 5.11, the 20/40 Ottawa pressurized between cores saturated with freshwater and the 20/40 Ceramic pressurized between cores that are heated and saturated with freshwater yielded the least proppant embedment. The third and fourth in the list are both cores that were saturated with freshwater+KCl substitute that had 20/40 RCS and 20/40 Ceramic in between them. As the list continues towards the highest embedment profile, it is visible that the fracturing fluids are KCl based. This trend could have been anticipated from the Young's modulus results each fracturing fluid yielded.

The freshwater and KCl heated samples have very similar values in Young's modulus reductions to those values freshwater and KCl values have at the end of five days. However, the heat had a very significant effect on the proppant embedment profiles. The second least proppant embedment is experienced when the Niobrara shale is heated and saturated with freshwater for five days, and this embedment value is very close to the embedment result obtained from the core that was saturated with freshwater for 30 days. This indicates that the additional heat treatment applied on the core for five days has the same effect on proppant embedment as submerging the core in the fluid for another 25 days. The core that is heated with KCl for five days experienced the highest embedment profile. This result proves two things; first, adding heat for five days to the core causes it to experience greater embedment profiles then when it is saturated with KCl+friction reducer for 30 days which was shown as the highest damaging fluid. Second, is that KCl based fluids are much more detrimental and damaging on the Niobrara shales mechanical properties and proppant embedment since the heated freshwater sample has one of the least embedment profiles and the heated KCl has the highest embedment recorded.

The different proppant types used in between cores that are saturated with various fracturing fluids also have an influence on the proppant embedment profiles. The heated freshwater and heated KCl samples are compared since they represent the opposite sides of the spectra. Saturating the sample with KCl in addition to heating definitely increases the Young's modulus reduction, and with that more proppant embedment should be expected. However the reason there is such a significant difference between these embedment profiles is also due to different proppant types being tested. 20/40 Ceramic

144

proppants are rounder, more spherical, uniform and stronger then 20/40 Ottawa proppants. This difference in proppants make 20/40 Ottawa sand more prone to proppant embedment and any other damage mechanism caused by mechanical and chemical factors in fractures. It is also important to point out that proppant embedment is only one of the several damage mechanisms that effects the general effectiveness of proppants just as explained by work done by Terracina et al., in page 17. During and after the pressuring and profilometer (measuring embedments) process, many observations were made regarding the cores reactions to being pressured with proppant being between them. Observations varied depending on the saturation types and proppants used. These observations can be summarized by the following:

- There were very few undamaged or crushed proppants remaining after pressurizing the cores. The uneven pressure distribution is believed to be the cause for the undamaged proppants, since most of the remaining proppants were on the edges of cores, where the pressuring brass rod is uneven;

- Proppants were either entirely embedded into core or partially embedded with the remainder being crushed. Significant amounts of proppant pieces were scraped off to make the core surfaces visible;

- It was very clear and evident that 16/30 Brady and 20/40 Ottawa proppants were mostly crushed if they were not embedded, whereas 20/40 Ceramic and 20/40 RCS were shattered;

- The poor shape, size, and distribution of 20/40 Ottawa and especially 16/30 Brady were very evident when they were placed on the cores, this suggests that these proppants are not able to bare the load and share it equally amongst the proppant pack;

- The low Young's modulus reduction caused by H_2O+KCl substitute on the core and using the stronger and better shaped 20/40 Ceramic proppant while pressuring this core showed visible differences in embedment profiles and damages done on the core. This core substantially and drastically had less damage and higher amounts of undamaged proppants;

- The cores were all extremely damaged, after high pressure was applied while proppants were placed in between them. The damage was not only caused because of proppant damage but also due to mechanical damage saturation and heating;

- Cores visibly had significant amounts of fractures in addition to craters (holes) due to proppant embedment;

- Cores that had visible natural fractures initially resulted in extremely complex fractures and highly damaged surface. These fractures also visibly connected the embedded spots and generated clusters of embedded zones, which looked like the core was grated;

- The Young's modulus effect of fracturing fluids on cores was definitely observed in how the cores were affected from pressuring. It was visible that the core saturated with the most damaging fluid had the highest amount of damage on its surface; and,

- There was significantly more visible proppant embedment occurring in the vicinity of the fractures that were created.

5.7 F3 Embedment Factor and Permeability Loss due to Young's Modulus Reduction

The Stimlab Proppant Consortium has some correction factors (F-values) that can be applied to the conductivity calculations when proppants are being tested. Correction factor F1 takes the effect of time, temperature and stress on proppant pack permeability, F2 takes the effect of fracturing fluids on proppant pack permeability, and F3 takes embedment into account (Miskimins, 2008). For this work only the F3 proppant embedment factor is calculated to determine the embedment conductivity correction factor using the affected and unaffected Young's modulus values. Since each sample will have a before and after F3 value the difference in between these two values represent a percent reduction caused by Young's modulus reduction which will have direct effect on effective permeability calculations if F1 and F2 factors are also factored in, thus this percentage in Table 5.13 is called the percent of permeability loss due to Young's modulus reduction. A conductivity loss percentage was also desired to be calculated; however the width change between the cores is almost impossible to accurately calculate. This problem is

due to the non-consistent and spontaneous embedment of the proppants and also the proppants being crushed and shattered after they are embedded to the core surfaces. Inability in calculating and accurately measuring the width change due to proppant embedment led the project to use only the F3 factor. Therefore the difference between Young's modulus changes which were calculated the F3 factor differences represents the deformation in these samples which causes more embedment, thus effecting the effective permeability calculations.

Thus the percent of permeability loss column in Table 5.13 represents the possible percentage embedment factor which would be caused by Young's modulus reduction due to fracturing fluids which then would be used to calculate the effective permeability of the fracture. In addition to this calculation, since the width reduction cannot be calculated from the actual physical cores, the actual proppant embedment values for each proppant and the fluid that were used with are shown in Section 5.6 by quantifying and reporting the total depth (height) value of proppants lost strictly due to embedment.

Table 5.12 is a summary table that has all the samples used in this work. It shows the main mineralogical characteristics of the samples, and which type of treatment was done on them along with the Young's modulus values at each stage of treatment.

The percentage of permeability loss values are calculated at each of the treatment time durations of each sample from the F3 factors. Table 5.13 shows the data set and the associated permeability loss. Young's modulus values are recorded before the samples are treated (E before), and after the samples are exposed to fracturing fluids and/or heated (E after). These values are then used to calculate the F3 values for before and after exposure to fracturing fluids and heat with Equation 5.3

$$F3 = e^{\frac{-S_c}{3E}}$$ (5.3)

Where,   F3 = Embedment Correction
S_c = Stress
E = Young's Modulus

Table 5.12: Summary of the Niobrara Shale Young's Modulus Results Treated with Various Fluids

Mineralogy	Sample #	Depth	Core Characteristics				Treatment Done	Young's Modulus Values at different saturation times						
		ft	Porosity %	Calcite %	Clay %	TOC %	Saturation/ Heat	Dry (ppi)	5-Days (psi)	15-Days (psi)	30-Days (psi)	Total Reduction (5 Days) %	Total Reduction (15 Days) %	Total Reduction (30 Days) %
Calcite-Rich	1	6606.80	0.60	92.73	1.70	2.18	H_2O	7.16E+06	4.75E+06	4.27E+06	4.45E+06	33.58	40.33	37.78
Calcite-Rich	2	6742.25	1.00	88.85	7.90	2.89	H_2O	6.83E+06	5.87E+06	6.19E+06	6.50E+06	14.04	9.42	4.84
Calcite-Rich	3	6742.25A	1.00	88.85	7.90	2.89	2% KCl	7.72E+06	5.67E+06	3.58E+06	2.76E+06	26.51	53.68	64.27
Calcite-Rich	4	6639.85	5.00	67.30	6.10	2.75	2% KCl	6.67E+06	5.39E+06	5.27E+06	6.33E+06	19.18	20.98	5.06
Calcite-Rich	5	6742.25B	1.00	88.85	7.90	2.89	KCl+Friction Reducer	7.67E+06	4.31E+06	2.93E+06	1.64E+06	43.75	61.76	78.65
Calcite-Rich	6	6772.25	6.00	84.00	4.40	1.33	KCl+Friction Reducer	6.42E+06	5.52E+06	3.35E+06	3.29E+06	13.98	47.89	48.83
Calcite-Rich	7	6788.65	1.00	87.70	4.30	2.82	H_2O+KCl Substitute	6.94E+06	6.19E+06	5.75E+06	5.79E+06	10.82	17.16	16.62
Calcite-Rich	8	6777.75	5.50	87.90	3.30	2.70	H_2O+KCl Substitute	6.89E+06	6.24E+06	6.07E+06	6.77E+06	9.54	12.03	1.78
Calcite-Rich	9	6606.65	0.60	92.73	1.70	2.18	Heated with H_2O @ 180°F	5.46E+06	3.53E+06			35.32		
Calcite-Rich	10	6764.20	0.70	92.63	3.50	1.28	Heated with KCl @ 180°F	6.05E+06	4.06E+06			32.87		

Equation is initially applied to the E (before) values in Table 5.13, and then it is applied to the E (after) values. The two F3 factor values are then subtracted from each other in order to calculate the how much embedment would be effected from the Young's modulus reduction which has an effect on the permeability loss within the fracture. This difference is then reported on the last column as the percent of permeability loss due to Young's modulus reduction.

In Table 5.12, there are two cases for the total Young's modulus reduction, one of them is reported after 15 days of saturation and the other after 30 days of saturation for the samples that were only saturated with fracturing fluids. Looking at the core characteristics, it is very evident that calcite is the dominating mineral in these samples. The negligible amounts of other minerals in the samples do not appear to have significant effects on the Young's modulus changes, thus no correlations were found between the three main results; change in Young's modulus, permeability loss and embedment; and core mineralogy and TOC values.

The last column in Table 5.13 shows the permeability loss due to the Young's modulus changes by using only the F3 factor. These values are directly related to the Young's modulus values measured for those specific cores, which means a larger reduction in the Young's modulus values between the saturation stages cause a larger permeability reduction, since the core gets weaker and becomes more prone to proppant embedment. Taking this correlation between Young's modulus reduction and the F3 embedment factor which represents the permeability loss that would change the effective permeability and also Table 5.13, it is very evident that, the cores that are saturated with freshwater+KCl substitute and freshwater experience the least amount of permeability loss.

Table 5.13: Permeability Loss Due to Young's modulus

Sample #	Sample Depth	Treatment Type	Treatment Duration	E (Before)	E (After)	F3 (Before)	F3 (after)	F3 (Before)-F3 (After)	Percent of Permeability Loss (Reduction) due to Young's Modulus Reduction
	ft			(psi)	(psi)	dec.	dec.	dec.	%
1	6606.80	Saturated with H_2O	5 Days	7.16E+06	4.75E+06	0.8656	0.8046	0.0704	7.04
			15 Days	7.16E+06	4.27E+06	0.8656	0.7851	0.0930	9.30
			30 Days	7.16E+06	4.45E+06	0.8656	0.7929	0.0839	8.39
2	6742.25	Saturated with H_2O	5 Days	6.83E+06	5.87E+06	0.8596	0.8386	0.0244	2.44
			15 Days	6.83E+06	6.19E+06	0.8596	0.8462	0.0156	1.56
			30 Days	6.83E+06	6.50E+06	0.8596	0.8530	0.0077	0.77
3	6742.25A	Saturated with KCl	5 Days	7.72E+06	5.67E+06	0.8747	0.8335	0.0471	4.71
			15 Days	7.72E+06	3.58E+06	0.8747	0.7490	0.1437	14.37
			30 Days	7.72E+06	2.76E+06	0.8747	0.6875	0.2140	21.40
4	6639.85	Saturated with KCl	5 Days	6.67E+06	5.39E+06	0.8565	0.8256	0.0361	3.61
			15 Days	6.67E+06	5.27E+06	0.8565	0.8220	0.0403	4.03
			30 Days	6.67E+06	6.33E+06	0.8565	0.8495	0.0082	0.82
5	6742.25B	Saturated with KCl+Frcition Reducer	5 Days	7.67E+06	4.31E+06	0.8740	0.7870	0.0995	9.95
			15 Days	7.67E+06	2.93E+06	0.8740	0.7031	0.1956	19.56
			30 Days	7.67E+06	1.64E+06	0.8740	0.5321	0.3912	39.12
6	6772.25	Saturated with KCl+Frcition Reducer	5 Days	6.42E+06	5.52E+06	0.8514	0.8294	0.0258	2.58
			15 Days	6.42E+06	3.35E+06	0.8514	0.7343	0.1375	13.75
			30 Days	6.42E+06	3.29E+06	0.8514	0.7302	0.1423	14.23
7	6788.65	Saturated with H_2O+KCl Substitute	5 Days	6.94E+06	6.19E+06	0.8617	0.8463	0.0179	1.79
			15 Days	6.94E+06	5.75E+06	0.8617	0.8356	0.0304	3.04
			30 Days	6.94E+06	5.79E+06	0.8617	0.8365	0.0292	2.92
8	6777.75	Saturated with H_2O+KCl Substitute	5 Days	6.89E+06	6.24E+06	0.8608	0.8473	0.0157	1.57
			15 Days	6.89E+06	6.07E+06	0.8608	0.8433	0.0203	2.03
			30 Days	6.89E+06	6.77E+06	0.8608	0.8585	0.0027	0.27
9	6606.65	Heated with H_2O @ 180˚F	5 Days	5.46E+06	3.53E+06	0.8276	0.7464	0.0982	9.82
10	6764.20	Heated with KCl @ 180˚F	5 Days	6.05E+06	4.06E+06	0.8431	0.7755	0.0802	8.02

Out of six different cases when freshwater+KCl substitute was the fracturing fluid, the highest permeability loss turned out to be 3%, and the minimum permeability loss was 0.27%, which is negligible. For the cores that are saturated with freshwater, the highest permeability percentage loss is almost 10%. When KCl is used as the fracturing fluid, the percentage of permeability loss can be as high as 21%. As shown earlier to be the most damaging fracturing fluid used in this work, KCl+friction reducer can cause the cores to have an extremely high percentage of permeability loss at 39%. The samples that were heated with freshwater and KCl showed similar permeability losses. When the core is heated with freshwater at 180°F for five days, the permeability loss is almost 10%, under same conditions with the exception of changing the fluid from freshwater to KCl, the last core has 8% permeability loss.

For this work, it is very hard to draw correlations and conclusions from a mineralogical standpoint. Therefore, this work focused on various fracturing fluid and proppant combinations while assuming that all cores had the same mineralogy, or similar enough that differences were negligent to all the results reported. The main observation made regarding the fluids is, fracturing fluids are detrimental to Young's modulus of the Niobrara shale regardless of what they are, especially fluids containing water. Based on a paper by Birkle et al., (2006), carbonate such as calcite and dolomite are sensitive to water and have temperature-dependent solubility. Their conclusion was that water causes precipitate of minerals, especially calcite, which causes formation plugging. The same observations are made in this work regarding the fluid effect. However, the damaging effect is more severe when KCl and friction reducer additives are used in water-based fluids. The Young's modulus reduction values are significantly higher for the cores that are saturated with KCl and KCl+friction reducer. The actual reason for this effect is not investigated in this work. However, it is speculated that the potassium chloride increases and/or initially speeds up the solubility of calcite in the fracturing fluids. This causes more precipitate of minerals and salt residue on the cores, and which consequently decreases the Young's modulus of the samples more severely in comparison to when they are saturated only with freshwater.

Looking at the permeability loss results, it is evident that they are positively related to the proppant embedment results shown in Section 5.6. By looking at these results, it can definitely be said that Young's modulus reduction dictates proppant embedment and permeability loss with in a fracture, and they are negatively related to each other.

CHAPTER 6

CONCLUSIONS AND RECOMMENDATIONS

The experimental work done in this research showed that the Young's modulus of the Niobrara shale decreases once the rocks are exposed to certain fracturing fluids and/or heat. This reduction occurs regardless of the fracturing fluid type and saturation time. However, modulus reductions vary with changing fracturing fluid type and saturation time. Due to modulus reduction, proppant embedment is shown to be inevitable and varying depending on the saturation type, time on formation, and proppant type used.

6.1 Conclusions

Upon completing all the laboratory work and experiments, the objectives of this project were met and the conclusions were drawn, these conclusions can be summarized by the following:

- The Niobrara Shale samples used in this work showed Young's modulus decreased after being exposed to fracturing fluids, and heat, which caused proppant embedment, therefore decreasing the fracture permeability and conductivity;

- Mineral reaction caused by the fracturing fluid is thought to be the main cause for the Young's modulus reduction in samples. The calcite in the studied samples is thought to be partially dissolving due to the exposure of fracturing fluids which then reduces the Young's modulus values;

- KCl+Friction Reducer was shown to have the most reduction in Young's modulus of the two Niobrara shale samples it saturated. Reductions were 61.76% and 47.89% at the end of 15 days of saturation and 78.65% and 48.83% at the end of 30 days of saturation;

- H_2O+KCl substitute was shown to have the least reduction in Young's modulus of the two Niobrara shale samples it saturated. Reductions were 17.16% and 12.03% at the end of 15 days of saturation and 16.62% and 1.78% at the end of 30 days of saturation;

153

- Freshwater showed Young's modulus reductions of 40.33% and 9.42% at the end of 15 days of saturation and 37.78% and 4.84% at the end of 30 days of saturation for the two samples it saturated; whereas KCl showed reductions of 53.68% and 20.98% at the end of 15 days of saturation and 64.27% and 5.06% at the end of 30 days of saturation, putting KCl as a more damaging fracturing fluid to the Niobrara shale samples used.

- The higher Young's modulus reduction caused by the KCl based fluids is thought to be occurring due to a chemical reaction between the KCl and calcite minerals in the samples which dissolves larger amounts of calcite in comparison to freshwater based fluids. The larger reduction experienced by KCl based fluids could also be due to nanoindenter measuring the salt precipitates or the actual friction reducer residue on these samples;

- The Young's modulus value regains are possibly due to fracturing fluids losing their initial effective chemical composition after some period of time. After this period, the calcite minerals adopting to the treatment system they are in, may be re-precipitating and reaching an equilibrium stage which may aid in regaining some of their strength back;

- The Gassmann fluid substitution equation showed that Niobrara samples, when they were assumed to be saturated with water and consist of calcite, had higher Young's modulus values under in-situ conditions than dry laboratory conditions. There is approximately 50% reduction in samples Young's modulus when they are removed from in-situ to lab conditions.

- Heating the Niobrara shale samples at 180°F for five days in freshwater and KCl reduced their Young's modulus by 35.32% and 32.87% respectively which are higher than the samples exposed to room temperature in these fluids for five days;

- 16/30 Brady showed more embedment and crushing in comparison to 20/40 Ottawa and sand proppants experience more of a crushing deformation, whereas RCS and Ceramic proppants show either shattering or embedment as a whole piece;

- The force applied and the resulting stress distribution on cores which affect the proppants is very important. This uneven distribution of force among the proppants causes variation in proppant embedment and crushing. The point effect of the applied force dictates how proppant crushing profiles;

- Rocks fractured more and generated microcracks where natural fractures were present which caused proppants to migrate towards these microcracks and further embed in packs. This could be detrimental for the proppant pack conductivity in the main fracture since the amount of proppants supporting the main fracture decreases substantially;

- The largest embedment was experienced when 20/40 Ottawa was pressured between two cores that were heated at 180°F with KCl for five days. The total embedment depth calculated was 204 μm which means the 20/40 Ottawa lost 31% of its volume to proppant embedment and decreased the fracture permeability by 8.02%;

- Results from this research show that the three combinations that caused the least proppant embedment and Young's modulus reduction are: H_2O with 20/40 Ottawa, 5 days at 180°F heated in H_2O with 20/40 Ceramic, and H_2O+KCl substitute with 20/40 RCS.

6.2 Recommendations for Future Work

Some beneficial ideas that could not be done, but thought to be worth investigating were generated while this work was in progress. They are:

- Utilizing the same wide selection of fracturing fluids and proppants on different shale plays that consists of different mineralogies;

- Increasing the saturation time from 30 days to 60 and 90 days to further investigate the Young's modulus reductions stopping and gaining the strength back. Also running water and fluid analysis on the fracturing fluids after each saturation phase to investigate the changes in fluid chemistry;

155

- Heating the samples, without submerging them in fracturing fluids and observing the modulus change;

- Calculating the dynamic Young's modulus and comparing them with the static Young's modulus values obtained from nanoindentation;

- Using larger cores in order to increase the proppant concentration and experiment with proppant distribution;

- Investigating the "humps" formed during proppant embedment on core surfaces and seen on the profilometer measurements and correlating this behavior to the proppant type that is being used;

- Testing different proppant types with at different pressures by referring to "API Standard Recommended Practice 19";

- Combining the Young's modulus reduction findings and proppant embedment values with production data and develop correlations between these results and decline curves; and,

- Developing a model to calculate the conductivity loss, and Young's modulus reduction as saturation type and duration and proppant types being inputs.

NOMENCLATURE

A …………………………………………………………………….......Area, nm

A_c ………………………………………………………………Contact Area, nm

BH …………………………………………………………………Brinell Hardness, GPa

BSE…….…..……………………………………………………….Back-Scattered Electron

CRCS …….…..…………………………………………………...Curable Resin Coated Sand

CST …….…..…………………………………………………….capillary suction time, sec

D & C…………………………………………………………….Drilling and Completion, \$MM

E……….…..…………………………………………………….......Youngs Modulus, psi

E_i……….…………………………………………………..Indenter Young's Modulus, psi

E_{IT}……….…..……………………………………………….Indentation Modulus, psi

E_r ….…..……………………………………………………..Reducible Modulus, psi

EDS …..…..…………………………………………………..Energy Dispersive X-ray Spectrometers

EUR……….…..……………………………………………....Estimated Ultimate Recovery, Bcfe, MBOE

F1……….…..……………………………………………Time, Temperature and Stress Correction Factor

F2……….…..…………………………………………………..Fracturing Fluids Correction Factor

F3……….…..…………………………………………………..Proppant Embedment Correction Factor

F_{cd}……….…..……………………………………………….Dimensionless Fracture Conductivity, Dimensionless

F & D…..…..…………………………………………….………...Finding and Development, \$MM

H ……….…..………………………………………………………….......Hardness, psi

h……….…..…………………………………………………….Depth of Total Penetration, nm

h_c ………..…..…………………………………………………..Depth of Contact, nm

h_f……….…..…………………………………………………..Depth of Residual Impression, nm

h_{max}……….……………………………………………………Maximum Displacement, nm

h_s……….…………………………………………………….Displacement of Sample Surface, nm

IP………..……………………………………………………..Initial Production, MMcfe/d, BOE/d

k ………………………………………………………………Formation Permeability, mD

k_f ……………………………………………………………Fracture Permeability, mD

K_{dry}………………………………………………….…..Dry Bulk Modulus, psi

K_{fluid}………………………………………………….....Fluid Bulk Modulus, psi

K_{min}……………………………………………………...Mineral Bulk Modulus, psi

Ksat……………………………………………………….Saturated Bulk Modulus, psi

ls…..…………………………………………………………………….…………Limestone

lb…....…………………………………………………………………………….Pounds

m…..………………………………………………………………Power Law (Best Fit Constant)

nm.………………………………………………………………………………….Nanometer

P(h) ………………………………………………………………………….…………Load, lb

P_{max}………………………………………………………….……………….Maximum Load, lb

RCS……...…………………………………………………………….……………….Resin Coated Sand

S.…………………...………………………………………………………..Contact Stifness, lb/inch

SAM ………………………………………………………………Scanning Acoustic Microscope

S_c ………………………………………………………………..Closure Stress, thousands of psi

Sh………………...…………………………………………………………………..Shale

SS……………………………………………………………………………..Sandstone

TOC……....…...………………………………………………….Total Organic Carbon, Percent

w ……………......……………………………………………….……………Fracture Width, ft

x_f……………………………………………………….…………………Fracture Half Length, ft

α…………………………………………………………………Power Law (Best Fit Constant)

α ………………………………………………………………….……Biot's Constant

μm ………………………………………………………………………………….Micrometer

$σ_h$.…………………………………………………………………Horizontal Stress, thousands of psi

σ_p …..………………...…………………………………………..Pore Pressure, thousands of psi

v …………....………………………………………………Poisson's Ratio, Dimensionless

v_i …………….………………………………………….Indenter Poisson's Ratio, Dimensionless

v_s …………….…..………………………………………….Sample Poisson's Ration, Dimensionless

$\emptyset$………………...……………………………………………………….Porosity, Percent

REFERENCE CITED

Abousleiman, Y., Tran, M., Hoang, S., Ortega, A., and Ulm, F. J. (2009, October). Geomechanics field characterization of the two prolific US Mid-West gas plays with advanced wire-line logging tools. *SPE Paper 124428 SPE Annual Technical Conference and Exhibition.*

Agee, Phillip. (2009). Instrumented Indentation Testing with Agilent Nano Indenter G200. *Agilent Technologies.*

Akrad, O., Miskimins, J., and Prasad, M. (2011, October). The effects of fracturing fluids on shale rock mechanical properties and proppant embedment. *SPE Paper 146658 in SPE Annual Technical Conference and Exhibition.*

Alrahami, B., Sundberg, M.I. (2012, June). Proppant Embedment and Conductivity of Hydraulic Fractures in Shales. *ARMA Paper 2012-291 in 46th U.S. Rock Mechanics/Geomechanics Symposium.*

American Petroleum Institute. (2013). Hydraulic *Fracturing Q and A's (Retrieved on 02, 10, 2013).* http://www.api.org/oil-and-natural-gas-overview/exploration-and-production/hydraulic-fracturing/hydraulic-fracturing-qa.aspx.

Anderson, H., Bratrud, T., and Delorey, J. (1982). A Logical Approach to Fracture Fluid Selection. *Journal of Canadian Petroleum Technology*, *21*(6).

Arthur, J., Bohm, B., Coughlin, B. J., Layne, M., and Cornue, D. (2009, March). Evaluating the environmental implications of hydraulic fracturing in shale gas reservoirs. *SPE Paper 121038 in SPE Americas E&P Environmental and Safety Conference.*

Barree, R. D., Cox, S. A., Barree, V. L., and Conway, M. W. (2003, October). Realistic assessment of proppant pack conductivity for material selection. *SPE Paper 84306 in SPE Annual Technical Conference and Exhibition.*

Birkle, P., Pruess, K., Xu, T., Contreras-Lopez, E., and Diaz-Lopez, M. (2006, August). Using Laboratory Flow Experiments and Reactive Chemical Transport Modeling for Designing Waterflooding of the Agua Fría Reservoir, Poza Rica-Altamira Field, Mexico. *SPE Paper 103869 In SPE First International Oil Conference and Exhibition in Mexico.*

Brannon, H., Malone, M., Rickards, A., Wood, W., Edgeman, J., and Bryant, J. (2004, September). Maximizing fracture conductivity with proppant partial monolayers: theoretical curiosity or highly productive reality?. *SPE Paper 90698 in SPE Annual Technical Conference and Exhibition.*

Brannon, H., and Starks, T. (2008, September). The Effects of Effective Fracture Area and Conductivity on Fracture Deliverability and Stimulation Value. *SPE Paper 116057 in SPE Annual Technical Conference and Exhibition.*

Britt, L., and Schoeffler, J. (2009, September). The geomechanics of a shale play: what makes a shale prospective. *SPE Paper 125525 in SPE Eastern Regional Meeting.*

Carman, P., and Lant, K. (2010, October). Making the Case for Shale Clay Stabilization. *SPE Paper 139030 in SPE Eastern Regional Meeting*.

Cipolla, C., Warpinski, N., Mayerhofer, M., Lolon, E., and Vincent, M. (2008, September). The relationship between fracture complexity, reservoir properties, and fracture treatment design. *SPE Paper 115769 in SPE Annual Technical Conference and Exhibition*.

Colorado Geological Survey. (2001). *Colorado Geological Survey Rocktalk (Vol. 13, No.1) (Retrieved on 10,14,2012).* http://geosurvey.state.co.us/pubs/Documents/rtv13n1%204-15-11%20B.pdf.

Colorado Oil and Gas Association. (2012). *COGA Fast Facts, Niobrara*. http://www.coga.org/pdfs_facts/Niobrara_fastfacts.pdf.

Cornell University. (2010). *Nanoindentation (Retrieved on 9,14, 2011*). Nanoindentation.cornell.edu.

Daneshy, Ali. (2005). Pressure Variations Inside the Hydraulic Fracture and Its Impact on Fracture Propagation, Conductivity, and Screen-out. *SPE Paper 95355 in SPE Annual Technical Conference and Exhibition.*

Darin, S. R., and Huitt, J. L. (1960). Effect of a partial monolayer of propping agent on fracture flow capacity. *Trans., AIME*, *219*, 31.

Doerner, M. F., and Nix, W. D. (1986). A method for interpreting the data from depth-sensing indentation instruments. *J. Mater. Res*, *1*(4).

Economides, M. J., andNolte, K. G. (1987). Reservoir Stimulation. *In Schlumberger Reservoir Stimulation 1987.*

Energy Information Agency. (2013, June). *Analysis and Projections (Retrieved on 07, 20, 2013).* http://www.eia.gov/analysis/studies/worldshalegas/.

Etherington, J., and Ritter, J. (2007, April). The 2007 SPE/AAPG/WPC/SPEE Reserves and Resources Classification, Definitions and Guidelines. Defining the Standard!. *SPE Paper 107693 In SPE Hydrocarbon Economics and Evaluation Symposium.*

Fjar, E., Holt, R. M., Raaen, A. M., Risnes, R., and Horsrud, P. (2008).*Petroleum related rock mechanics* (Vol. 53). Elsevier.

Gillard, M., Medvedev, O., Hosein, P., Medvedev, A., Peacorada, F., and d'Huteau, E. (2010, September). A New Approach to Generating Fracture Conductivity. *SPE Paper 135034 in SPE Annual Technical Conference and Exhibition.*

Harrington, L., and Hannah, R. (1975, September). Fracturing design using perfect support fluids for selected fracture proppant concentrations in vertical fractures. *SPE Paper 5642 in Fall Meeting of the Society of Petroleum Engineers of AIME.*

John Kullam, Carbo Ceramics. (2011). *The Complicated World of Proppant Selection (Retrieved on 10, 16, 2011).* http://images.sdsmt.edu/learn/speakerpresentations/Kullman.pdf.

Kundert, D., and Mullen, M. (2009, April). Proper evaluation of shale gas reservoirs leads to a more effective hydraulic-fracture stimulation. *SPE Paper 123586 in SPE Rocky Mountain Petroleum Technology Conference.*

Lacy, L., Rickards, A., and Ali, S. (1997, October). Embedment and fracture conductivity in soft formations associated with HEC, borate and water-based fracture designs. *SPE Paper 38590 in SPE Annual Technical Conference and Exhibition.*

Lacy, L. L., Rickards, A. R., and Bilden, D. M. (1998). Fracture width and embedment testing in soft reservoir sandstone. *SPE drilling and completion,13*(1), 25-29.

LaFollette, R., and Carman, P. (2010, February). Proppant Diagenesis: Results So Far. *SPE Paper 131782 in SPE Unconventional Gas Conference.*

LaFollette, R., and Carman, P. (2011, January). Long Term Stability of Proppants Exposed to Harsh Shale Reservoir Conditions. *SPE Paper 140110 in SPE Hydraulic Fracturing Technology Conference.*

Li, K., Wang, M., Gao, Y., and Lv, Y. (2013, March). New Mathematical Models for Calculating the Proppant Embedment and Conductivity. *IPTC Paper 16410 In 6th International Petroleum Technology Conference*.

Longman, M. W., Luneau, B. A., and Landon, S. M. (1998). Nature and Distribution of Niobrara Lithologies in the Cretaceous Western Interior Seaway of the Rocky Mountain Region. *The Mountain Geologist*.

Maldonado, A. C. (2011). *Elastic and Mechanical Properties of the Niobrara Formation with Application to Hydraulic Fracture Design* (Doctoral dissertation, Colorado School of Mines).

Matthews, H., Schein, G., and Malone, M. (2007, January). Stimulation of Gas Shales: They're All the Same? Right?. *SPE Paper 106070 in SPE Hydraulic Fracturing Technology Conference*.

Mavko, G., Mukerji, T., and Dvorkin, J. (2009). *The rock physics handbook: Tools for seismic analysis of porous media*. Cambridge University Press.

Mayerhofer, M., Lolon, E., Warpinski, N., Cipolla, C., Walser, D., and Rightmire, C. (2008, November). What is stimulated rock volume?. *SPE Paper 119890 in SPE Shale Gas Production Conference*.

Miskimins, J.L. (2008). *Well Completions and Stimulation Course Notes*. Colorado School of Mines.

Miskimins, J.L. (2008, February). Design and Life Cycle Considerations for Unconventional Reservoir Wells. *SPE Paper 114170 in SPE Unconventional Reservoirs Conference*.

Momentive Fracline. (2011). *A Brief History of Proppants (Retrieved on 10, 20, 2011).* http://momentivefracline.com/a-brief-history-of-proppants.

Nguyen, P., Weaver, J., Dewprashad, B., Parker, M., and Terracina, J. (1998, February). Enhancing fracture conductivity through surface modification of proppant. *Paper SPE 39428 in SPE Formation Damage Control Conference.*

Oliver, W. C., and Pharr, G. M. (1992). Improved technique for determining hardness and elastic modulus using load and displacement sensing indentation experiments. *Journal of materials research*, *7*(6), 1564-1583.

Oliver, W. C., and Pharr, G. M. (2004). Measurement of hardness and elastic modulus by instrumented indentation: Advances in understanding and refinements to methodology. *Journal of materials research*, *19*(01), 3-20.

Pollastro, R. M. (1992). Clay minerals as geothermometers--Indicators of thermal maturity for hydrocarbon exploration. *The petroleum system--Status of research and methods*, 61-66.

Pollastro, R. M., and Scholle, P. A. (1986). Diagenetic relationships in a hydrocarbon-productive-chalk—The Cretaceous Niobrara Formation. *Studies in Diagenesis: US Geological Survey Bulletin*, *1578*, 219-236.

Polzin, Ward. (2012). Niobrara *Multi-Basin Oil Shale (Retrieved on 10, 14, 2012)*. http://www.springsgov.com/units/boardscomm/OilGas/CO%20Springs%20TPH%20Niobrara.pdf.

Prasad, M. (2001). Mapping impedance microstructures in rocks with acoustic microscopy. *The Leading Edge*, *20*(2), 172-179.

Prasad, M., Mukerji, T., Reinstaedler, M., and Arnold, W. (2009, October). Acoustic Signatures, Impedance Microstructure, Textural Scales, and Anisotropy of Kerogen-Rich Shales. *SPE Paper 124840 in SPE Annual Technical Conference and Exhibition.*

Rayson, N., and Weaver, J. (2012, April). Improved Understanding of Proppant-Formation Interactions for Sustaining Fracture Conductivity. *SPE Paper 160885 in SPE Saudi Arabia Section Technical Symposium and Exhibition.*

Rickman, R., Mullen, M., Petre, J., Grieser, W., and Kundert, D. (2008, September). A practical use of shale petrophysics for stimulation design optimization: All shale plays are not clones of the Barnett Shale. *SPE Paper 115258 in SPE Annual Technical Conference and Exhibition.*

Sahai, R. (2012). *Laboratory Evaluation of Proppant Transport in Complex Fracture Systems* (Doctoral dissertation, Colorado School of Mines).

Shah, S., Vincent, M., Rodriquez, R., and Palisch, T. (2010, January). Fracture orientation and proppant selection for optimizing production in horizontal wells. *SPE Paper 128612 in SPE Oil and Gas India Conference and Exhibition.*

Sharma, R., Ludmila, A., and Prasad, M. (2009, October). Effects of Fluid, Frequency, and Heterogeneity on Elastic Properties of Carbonate Rocks. *SPE Paper 125102 in SPE Annual Technical Conference and Exhibition.*

Sone, H.. (2011). Mechanical Properties of Shale Gas Reservoir Rocks and Its Relation to the IN-Situ Stress Variation Observed in Shale Gas (Doctoral dissertation, Stanford University).

Sonnenberg, S. A., Underwood, D. (2012). *Polygonal Fault Systems: A New Structural Style for the Niobrara Formation, Denver Basin, CO. (Retrieved on 10, 13, 2012)*. http://www.searchanddiscovery.com/documents/2012/50624sonnenberg/ndx_sonnenberg.pdf.

Tare, U. A., Mody, E. K., and Mese, A. I. (2001, July). Time dependent impact of water-based drilling fluids on shale properties. In *DC Rocks 2001, The 38th US Symposium on Rock Mechanics (USRMS)*.

Terracina, J., Turner, J., Collins, D., and Spillars, S. (2010, September). Proppant selection and its effect on the results of fracturing treatments performed in shale formations. *SPE Paper 135502 in SPE Annual Technical Conference and Exhibition.*

Van Poollen, H. K. (1957). Do Fracture Fluids Damage Productivity?. *Oil and Gas J.(May, 1957)*, 120-124.

Vincent, M. C., Miller, H. B., Milton-Tayler, D., and Kaufman, P. B. (2004, September). Erosion by proppant: a comparison of the erosivity of sand and ceramic proppants during slurry injection and flowback of proppant.*SPE Paper 90604 in SPE Annual Technical Conference and Exhibition*.

Walsh, J. B. (1981, October). Effect of pore pressure and confining pressure on fracture permeability. In *International Journal of Rock Mechanics and Mining Sciences and Geomechanics Abstracts* (Vol. 18, No. 5, pp. 429-435). Pergamon.

Wang, Y., and Miskimins, J. (2010, November). Experimental Investigations of Hydraulic Fracture Growth Complexity in Slickwater Fracturing Treatments. *SPE Paper 137515 inTight Gas Completions Conference.*

Warpinski, N. R., Mayerhofer, M. J., Vincent, M. C., Cipolla, C. L., and Lolon, E. P. (2009). Stimulating unconventional reservoirs: Maximizing network growth while optimizing fracture conductivity. *Journal of Canadian Petroleum Technology*, *48*(10), 39-51.

Weaver, J., Nguyen, P., Parker, M., and van Batenburg, D. (2005, May). Sustaining fracture conductivity. *SPE Paper 94666 in SPE European Formation Damage Conference*.

Zhou, D., Zhang, G., Ruan, M., He, A., and Wei, D. (2011, November). Comparison of Fracture Conductivities from Field and Lab. In *International Petroleum Technology Conference*.

APPENDIX – SUPPLEMENTAL FILES PROVIDED

Supplemental files are provided for additional images and graphs containing results for different fracturing fluids used in the project. Step-by-step methodology explains everything done during the cores of this project.

GUIDE TO SUPPLEMENTAL FILES.docx	File explaining the content of supplemental files
SUPPLEMENTAL FILE A.docx	KCL SATURATED SAMPLES
SUPPLEMENTAL FILE B.docx	KCL+FRICTION REDUCER SATURATED SAMPLES
SUPPLEMENTAL FILE C.docx	FRESHWATER+KCL SUBSTITUTE SATURATED SAMPLES
SUPPLEMENTAL FILE D.docx	FRESHWATER AND KCL SATURATED SAMPLES
SUPPLEMENTAL FILE E.docx	STEP-BY-STEP METHODOLOGY